JOHANNES GUTENBERG UNIVERSITÄT MAINZ

MAX-PLANCK-INSTITUT FÜR POLYMERFORSCHUNG

# Fluid Gels

## Rheology, Tribology and Thermal Properties of Hydrocolloid Systems

Kumulative Dissertation zur Erlangung des Grades „Doktor der Naturwissenschaften“

am Fachbereich Chemie, Pharmazie und Geowissenschaften

der Johannes Gutenberg-Universität Mainz

von

Marta Ghebremedhin

Mainz, 2025

1. Gutachter: [redacted]

2. Gutachter: [redacted]

Tag der mündlichen Prüfung:

# Abstract

This work investigates the underlying gelation mechanism of hydrocolloid systems, with particular emphasis on agarose gelation under shear. The focus is directed at the physico-chemical properties of agarose fluid gels and their rheological, mechanical, and tribological behaviour. Fluid gels, based on gelling polysaccharides like agarose, undergo gelation at defined shear rates, resulting in suspensions of gel particles with controlled microstructures. These systems exhibit viscoelastic behaviour, characterised by the coexistence of solid and fluid-like properties over different time scales. Agarose, a strong gelling polysaccharide, typically forms firm, brittle gels through double-helix aggregation via hydrogen bonding while cooling. However, applying shear during gelation modifies this behaviour. The resulting agarose fluid gels display elastic, solid-like behaviour at rest that transitions to a fluid-like state upon exceeding a critical stress – attributed to the "hairy" microstructure of gels particles, which plays a role in the rheological, mechanical and tribological properties. A range of agarose concentrations (0.5 wt%, 1 wt% and 2 wt%) was investigated. Rheological measurements revealed that increasing agarose concentration resulted in higher storage moduli of the microgel particles. Notably, 1 wt% agarose fluid gels exhibit the lowest viscosity at low shear rates and the shortest linear viscoelastic range. Microstructure and particle size analysis indicated a decrease in particle size and unordered chains at the particle surfaces with decreasing agarose concentration. Based on these findings, we propose models to elucidate the effects of particle size, concentration, and "hairy" surface structure on the rheological and tribological behaviour of fluid gels. Atomic force microscopy revealed the inner network structure of gel particles, showing a dense core that decreases in density towards the periphery, emphasising structural gradients that affect elasticity and, consequently, bulk properties. The addition of co-solutes, such as sucrose, strongly influences interactions between agarose, water, and sucrose molecules during shear, impacting structure formation and network behaviour. Increasing sucrose concentration resulted in the formation of microgel particles with different sizes, shapes, and interconnected network structures. These microstructural changes arise from the dynamic competition between gelation and shear-induced disruption, directly impacting the rheological and tribological properties of fluid gels. The findings enhance our understanding of the structure-property relationship in fluid gels and broaden their potential in food applications – particularly in designing tailored textures for products targeting conditions such as dysphagia. This work contributes to advancing the functional design of agarose-based fluid gels by elucidating the molecular mechanisms underlying their formation and behaviour under shear

# Zusammenfassung

Diese Arbeit untersucht die zugrundeliegenden Gelierungsmechanismen von Hydrokolloidsystemen, mit besonderem Schwerpunkt auf der Gelierung von Agarose unter Scherung. Der Fokus liegt dabei auf den physikalisch-chemischen Eigenschaften von Agarose Fluid-Gelen sowie deren rheologischem, mechanischem und tribologischem Verhalten. Fluid-Gele, basierend auf gelierenden Polysacchariden wie Agarose, gelieren bei definierten Scherraten und bilden dabei Suspensionen von Gelpartikeln mit kontrollierter Mikrostruktur. Diese Systeme zeigen ein viskoelastisches Verhalten, das durch das gleichzeitige Vorliegen fester und flüssigkeitsähnlichen Eigenschaften auf verschiedenen Zeitskalen hinweg gekennzeichnet ist. Agarose, ein stark gelierendes Polysaccharid, bildet typischerweise durch die Aggregation von Doppelhelices über Wasserstoffbrückenbindung beim Abkühlen, feste, spröde Gele. Dieses Verhalten ändert sich jedoch, wenn während der Gelierung Scherkräfte angewendet werden. Die resultierenden Agarose-Fluidgele zeigen im Ruhezustand ein elastisches, festkörperähnliches Verhalten, das bei Überschreiten einer kritischen Spannung in einen flüssigkeitsähnlichen Zustand übergeht. Dieses Verhalten wird auf die “hairy“ Mikrostruktur der Gelpartikel zurückgeführt wir, die das rheologische, mechanische und tribologische Verhalten maßgeblich beeinflusst. Es wurden verschiedene Agarosekonzentrationen (0,5 Gew.-%, 1 Gew.-% und 2 Gew.-%) untersucht. Rheologische Messungen zeigten, dass eine steigende Agarosekonzentration zu höheren Speichermodulen der Mikropartikel führte. Auffallend war, dass das 1 Gew.-% Agarose Fluid-Gel die niedrigste Viskosität bei niedrigen Scharrten sowie den kürzesten linear-viskoelastischen Bereich aufwies. Mikrostrukturanalysen und Partikelgrößenbestimmungen ergaben, dass mit abnehmender Agarosekonzentration sowohl die Partikelgröße als auch ungeordnete aggregierte Kettenstrukturen auf der Partikeloberflächen abnahmen. Auf der Grundlage dieser Ergebnisse schlagen wir spezifische Modelle vor, um den Einfluss der Partikelgröße, der Konzentration und der “hairy“ Oberflächenstruktur auf das rheologische und tribologische Verhalten verschiedener Fluidgele zu erklären. Mithilfe der Rasterkraftmikroskopie konnte die innere Netzwerkstruktur der Gelpartikel sichtbar gemacht werden. Diese zeigt einen dichten Kern, dessen Dichte zur Peripherie hin abnimmt, wodurch strukturelle Gradienten entstehen, die die Elastizität und damit die makroskopischen Eigenschaften beeinflussen. Die Zugabe von Co-Soluten wie Saccharose beeinflusst deutlich die Wechselwirkung zwischen Agarose-, Wasser- und Saccharosemolekülen unter Scherbedingungen und wirkt sich auf die Strukturbildung und das Vernetzungsverhalten aus. Eine Erhöhung der Saccharosekonzentration führte zur Bildung von Mikrogelpartikeln unterschiedlicher Größe, Form und Netzwerkstruktur. Diese mikrostrukturellen Veränderungen resultieren aus der dynamischen Konkurrenz zwischen Gelierung und scherinduziertem Bruch und haben einen direkten Einfluss auf die rheologischen und tribologischen Eigenschaften der Fluid-Gele. Die Ergebnisse dieser Studie verbessern das Verständnis der Struktur-Eigenschafts-Beziehungen in Fluid-Gelen und erweitern ihr Anwendungspotenzial in der Lebensmitteltechnologie, insbesondere bei der Entwicklung

maßgeschneiderter Texturen für Produkte, die auf Erkrankungen wie Dysphagie abzielen. Diese Arbeit leistet einen Beitrag zur Weiterentwicklung des funktionellen Designs agarosebasierter Fluid-Gele, indem sie die molekularen Mechanismen aufklärt, die ihrer Bildung und ihrem Verhalten unter Scherung zugrunde liegen.

# Table of contents

# List of figures

# 1 Introduction

## 1.1 Motivation and background

Functional foods based on structured soft materials are in growing demand as they address critical health, demographic, and environmental challenges. This drives global market growth and significant research into new processes, materials and products. Biopolymers and hydrocolloids, like polysaccharides for instance, are widely used as thickeners and gelling agents in the food and cosmetic industries to improve quality and textures. They have a broad range of functional properties [1]–[3]. However, they often fail to fully meet the industry and consumer-driven demands for healthy, convenient, and high quality formulated products.

Fluid gels have addressed this gap by enabling the customisation of materials to meet increasingly diverse structural and functional requirements. These soft, viscoelastic materials are based on gelling biopolymers, where application of shear results in particulate gel suspensions with controlled microstructures. A proven method to produce fluid gels is to apply a shear field to a polysaccharide solution during gelation. This induces a competing mechanism between physical cross-linking, which promotes network formation, and shear forces, which disrupt it [4], [5]. Ultimately, the result are discrete microgel particles suspended in a continuous liquid phase with the ability to maintain solid-like elasticity at rest while exhibiting fluid-like behaviour under stress. The unique texture of these gel suspensions enables novel material designs across applications ranging from food technology and dysphagia management to pharmaceutical and biomedical delivery systems. In the food sector, in particularly they serve as effective fat replacers in low calorie products while offering precisely tuneable texture properties. Their pharmaceutical applications include controlled drug delivery and release systems, while their distinct elasticity and lubrication properties make them suitable for developing specialised food systems for individuals with swallowing disorders (dysphagia) [6]–[8].

Agarose is well suited to fluid gel research because of its well-characterised gelation mechanism. As a strongly gelling polysaccharide extracted from seaweed, it is an ideal model for studying the structure-function relationship in fluid gels [4], [9]. Its molecular structure and physicochemical properties allow agarose to form a tight three-dimensional network of cross-links upon cooling. The formation of double helices from single chains via hydrogen bonding and their subsequent aggregation is central to its gelling mechanism. Furthermore, the resulting dense network and fast gelation kinetics lead to firm, brittle and highly elastic gels, features that typically result in poor mouthfeel by conventional preparation [10], [11].

Here, the preparation as a fluid gel allows to achieve completely different textural properties. When an agarose solution is subjected to controlled shear during gelation, it forms soft microgel particles with

tuneable properties. By adjusting the agarose concentration, cooling rate and shear rate, these particles can be precisely tailored, as is shown in this work. The applied shear disrupts the rapid gelation kinetics that would otherwise form a continuous network and instead produces dispersed particles with controllable size, morphology and surface structure.

Despite numerous studies on fluid gels, the exact gelation mechanism under shear and its impact on viscoelasticity, texture, and lubrication remain poorly understood. A fundamental physical understanding of these processes is still lacking, particularly regarding how shear forces and molecular modifiers (e.g. sugars) influence microstructure formation and macroscopic behaviour. Of particular interest are two aspects: First, the relationship between internal particle microstructure and bulk rheological, mechanical, and tribological properties. And second, how the particle microstructure is influenced by processing conditions including temperature rate, concentration, and applied shear rate. Although research interest is growing, the missing comprehensive understanding hinders the targeted design of fluid gels for specific functional applications and limits their broader application potential.

Moreover, adding low molecular weight co-solvents, such as sugars, significantly alters the mechanical and rheological properties of fluid gels [12]. This in turn indicates how interactions at molecular level causes changes in the macroscopic structure. These co-solvents influence the gelation process of the biopolymers by competing for hydration water, interfering with hydrogen bonding, and thus altering the thermodynamic conditions [13]–[16]. Sucrose, for example, is known to shift the temperature of the agarose sol-gel transition with changing concentration, which is associated with an effect on the viscoelastic properties and gel strength [15], [17]. However, its role in fluid gel systems, particularly during gelation under shear, remains largely unexplored. Therefore, a deeper understanding of these molecular level interactions of agarose competing with additives such as sugar for hydration water and hydrogen bonding is essential to explain the behaviour of fluid gel systems.

## 1.1 Aims and scope of this thesis

The work presented in this dissertation is motivated by the need to establish a fundamental understanding of fluid gel formation by linking gelation conditions, particle microstructure, and macroscopic performance. It raises the question of how internal structure and interfacial properties govern the mechanical and sensory behaviour of these materials. A deeper understanding of the physical principles underlying soft materials in model food systems – such as fluid gels – beyond application-driven food engineering will not only enrich the field of soft matter physics but also enable the tailored design of materials for applications ranging from food technology to biomedical innovations.

This study aims to understand the precise gelling mechanism under shear that governs microgel formation. The focus is on how agarose concentration determines the particle size and shapes, and thus

the physical behaviour of the fluid gels. By combining versatile characterisation methods like rheology, tribology, light scattering, light microscopy, and atomic force microscopy, this work advances the fundamental understanding of fluid gel formation. These systems serve as simple models for structurally complex, water-rich food materials, providing insights relevant to both soft matter physics and applied food science.

After a review of the main concepts, methods and literature body in the following chapter, the above stated research objectives are addressed through three publications that form the central part of this dissertation:

The first publication, "*Physics of agarose fluid gels: Rheological properties and microstructure"* (2021), systematically investigates the physicochemical properties of fluid gels using agarose, with particular focus on their rheological, mechanical and tribological behaviour. It examines how agarose concentration and gelation under shear affect the particle morphology, including shape and size, which are revealed by microscopy and particle size measurements. The work introduces the concept of "hairy" gel particles, consisting of a dense core and soft, loosely aggregated chains protruding from the particle surface. These irregular particles with heterogeneous shapes were found to be directly related to the viscoelastic, textural and lubrication behaviour. Moreover, a schematic model was proposed to illustrate this structure-function relationship.

The second publication, "*Molecular behaviour of fluid gels – the crucial role of edges and particle surface in macroscopic properties*" (2022), continues the investigation of the relationship between microscopic structure and macroscopic properties by using atomic force microscopy. A key objective of this study is to establish a fundamental correlation between the network meshes of the gel particles and their bulk behaviour. The results show that the dense network structure of the core region decreases towards the periphery of the gel particles. These network structure gradients also change with agarose concentration, which in turn affects the viscoelastic and lubricating behaviour. The work highlights how molecular-scale properties such as surface chain mobility during gelation under shear and network density control macroscopic behaviour, providing new insights into polymer dynamics in soft matter systems such as fluid gels. It relates the irregular particle structures and their heterogenous shape to the experimental observation of the fist paper.

The third publication, "*Effects of sugar molecules on the rheological and tribological properties and on the microstructure of agarose-based fluid gels*" (2024), introduces sucrose as a co-solvent to modify the solvent composition and investigate its impact on the fluid gel formation. This study of the co-solute-water-agarose interaction shows that changing the sucrose concentration significantly affects the size, shape, and aggregation behaviour of the microgel particles. A model was proposed to describe the interplay between gelation and breakup during shear in the presence of sucrose, suggesting that sucrose interferes with agarose gelation by competing for hydration water. Consequently, these structural

changes were found to be critical in affecting the behaviour of the resulting fluid gels, particularly their rheological and tribological behaviour.

# 2 Literature review

This chapter provides an overview of the relevant literature on hydrocolloids, polysaccharide structures, and their interactions in aqueous solutions. It examines the functional properties of polysaccharides and their impact on forming microstructures in edible soft matter, focusing on their influence on viscosity and gelation. Agarose is discussed in detail as a model gelling biopolymer. The chapter also introduces fluid gels, outlining their formation mechanisms, key properties, and interactions with low molecular weight co-solvents such as sucrose. Additionally, basic theories of rheology, tribology, and texture analysis applicable to viscoelastic materials, including particulate fluid gels, are discussed. Further characterisation methods for microgel particles are presented to complement and support the study of viscoelastic and lubricating behaviour.

## 2.1 Biopolymer and hydrocolloid systems

Hydrocolloids, such as biopolymers, are versatile thickening and gelling agents with wide applications in the food, cosmetic and pharmaceutical industries [18]. They act as emulsifiers, stabilizers, and improve the texture and quality of various products [19]. Natural biopolymers, like polysaccharides, exhibit thickening and gelling effects when hydrated in water above a critical concentration and subjected to physico-chemical processes. These biopolymers play an important role as structural additives in the food industry. However, there is a growing demand for an expanded application of hydrocolloid systems beyond their conventional role as gelling and thickening agents. This shift aims to fulfil the industries and consumers desires for healthier, more convenient, and high-quality products. As a result, fluid gels have been developed to meet a broader range of structural requirements. This thesis will focus only on polysaccharides as they are relevant to the research being undertaken. In fact, the interest in using polysaccharides in food applications is due to their ability to modify and enhance the rheological and textural properties, resulting in a better mouth feeling by precisely controlling the texture and viscoelastic properties [18], [20].

Polysaccharides are complex carbohydrates composed of monosaccharide chains linked by glycosidic bonds. These macromolecules exhibit diverse molecular weights, often comprising thousands of repeating monomers units, and are derived from plants, algae and micro fermentation sources. Depending on the polysaccharide, its molecular structure varies, exhibiting either linear or branched configurations. This diversity influence physical properties such as water solubility, viscosity, and gelling behaviour, which changes as the degree of branching increases [21]. The increase in viscosity of liquids and the formation of viscous dispersions and gels due to the solubility in water results from the presence of numerous hydroxyl groups capable of forming hydrogen bonds with surrounding water

molecules [19]. These hydroxyl groups a primary component, can be partially derivatized by esterification, resulting in their existence as acetate, sulphate, phosphate, or etherified forms. Consequently, polysaccharide solutions can be highly viscous to varying degrees, a property influenced by, among other factors, the size, shape and conformation of the molecule, which can also lead to gel formation [21]. However, the demand for polysaccharides with unique properties are constantly increasing. Therefore, the molecular structure of available polysaccharides is modified chemically, physically, or enzymatically so that their novel properties meet the functional requirements [22].

## 2.2 Hydrocolloids as thickeners and gelling agents

### 2.2.1 Mechanisms of thickening

The utilization of polysaccharides in food is based on their capacity to improve and alter rheological properties, enabling precise control of viscoelastic characteristics. As thickeners, they are used, in various culinary applications such as soups, sauces and salad dressing, with examples including xanthan, guar gum, Locust bean, and konjac glucomannan [19], [23], [24]. Their incorporation into food formulations is a common practice to achieve specific texture, viscoelasticity and mouth feel by thickening the food [25]. Additionally, they serve as gelling agent in products such as jams, jellies, and sugar or calorie reduced foods, using ingredients such as agar, carrageenan, gellan gum, or alginate. However, the optimal application of hydrocolloids as thickeners requires a thorough understanding of thickening processes.

The extent of viscosity change varies depending on the type of hydrocolloid and is determined by the interaction between disordered and non-specific entanglements of the polymer chains. This interaction rises with concentration, with the critical concentration c* being the overlap concentration (see Fig. 1). Below this concentration, the polymers can move freely, do not influence each other, and consequently exhibit Newtonian flow behaviour [19].

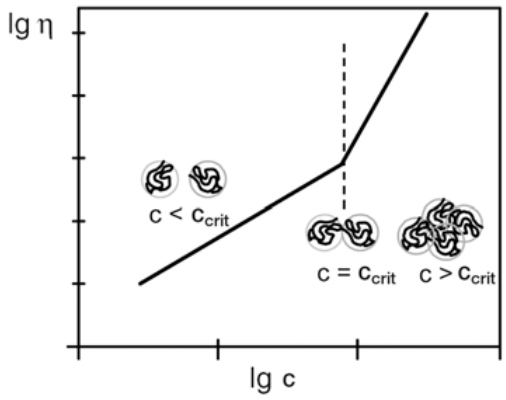


*Fig. 1. Low shear viscosity as a function of polymer concentration of a polymer solution (with critical concentration $c_{crit}$)* [26].

Above this concentration, however, the polysaccharides come into contact with each other, leading to mutual restriction of their movement and resulting in entanglement. These polymer chains can no longer move freely in the solution, but are entangled in a kind of network and thus exhibit non-Newtonian flow behaviour [22], [27], [28]. The rheological properties of hydrocolloids depend on their chemical structure and the intra- and intermolecular interactions through hydrogen bonding, electrostatic interactions, hydrophobic interactions, and steric exclusion. These interactions can be affected by processing and conditions such as temperature, ionic strength, shear, pH and the solvent [25]. Accordingly, in the absence of enthalpic interactions between the polymer chains, the thickening property results from the molecular weight and concentration of the hydrocolloids [19].

The intrinsic viscosity of a polymer solute quantifies its influence on the solution viscosity. This parameter is useful for comparing the viscosity of different hydrocolloid dispersions. According to the Mark-Houwink equation, the intrinsic viscosity is directly related to the molecular weight of the hydrocolloid (see Eq. 1).

$$\eta = \mathrm{K}\,\mathrm{M}^{\alpha} \tag{1}$$

With M as molecular weight and K and α as Mark-Houwink parameters.

As the molecular weight of the polysaccharide increases, the concentration at which c* is exceeded decreases. Above this concentration, dispersions with network-like entanglements now exhibit shear-thinning behaviour, which shows a decreasing viscosity with increasing force (shear rate) [19], [27]. However, at low shear rates, the irreversible deformation of this network is slower than or equal to the formation of new entanglements and thus exhibits Newtonian behaviour. The viscosity during this process is known as zero shear viscosity. If the shear rate is increased, the destruction of the network increases and exceeds the formation of new entanglements. From this point, the viscosity decreases as a function of the shear rate and is referred to as shear thinning [27].

### 2.2.2 Mechanisms of gelation

Although most hydrocolloids tend to thicken, only a few are capable of forming gels. Gelation is a molecular process in which polymer molecules rearrange and associate to form a continuous three-dimensional network. This transition from sol to gel involves a thermodynamic change, where the loss of conformational entropy and hydration energy is compensated by energetically favourable enthalpy interactions between polymer chains [29]. Unlike chemically cross-linked networks, primarily characterised by single covalent bonds, biopolymer gels typically feature extended ordered junction zones formed through physical associations between polymer chains. These junction zones can result from single point cross-links, extended cross-links involving at least two chains, or the formation of multiple associated chain structures [30]. They are usually stabilised by non-covalent bonds, such as ionic, hydrophobic, or hydrogen bonds [18]. Furthermore, the remaining disordered polymer chain segments connect these ordered arrays and contribute to the overall gel network structure [31]. The molecular structure of the polymer, which affects the gel strength and the occupied volume in solution, as well as the solvent that forms the gelling system, all contribute to the formation of these types of networks. Understanding the conditions that govern the gelling mechanism is therefore crucial for the development of food formulations, as gels exhibit significant variations in modulus, fracture properties and texture.

The gelling property arises from the association and cross-linking of polymer chains, leading to an ordered conformation and creating of a three-dimensional network that immobilises water. This stable structure exhibits viscoelastic properties, exhibiting characteristics of both solids and liquids, allowing the structure to flow under applied force or energy, such as a change in temperature. Cross-links, formed by associated regions of two or more polymers, play a crucial role in the gelling process, with various mechanisms involved, for example, double or triple helices in agarose or gelatine and ionic linkages through divalent cations in alginate [22]. However, the structural attributes of the gel, including elasticity, brittleness, viscosity, and creaminess, vary considerably depending on the specific hydrocolloid employed [22].

The strength of the gel structure depends on the intermolecular interaction of the bonds and the extent of the cross-linking. A firmer gel strength is achieved with longer junction zones, a higher number of molecules in these zones, and a smaller intermolecular mesh size of the network (Fig. 2). For permanently cross-linked gels, de Gennes et al. (1979) [32] report a relationship between the mesh size $\xi$ and the gel strength, or elastic modulus (see Eq. 2) [32], [33]. Beyond this, the flexibility originating from the non-aggregating intermediate segments is important for the gel strength property.

$$G \simeq \frac{k_B T}{\xi^3} \tag{2}$$

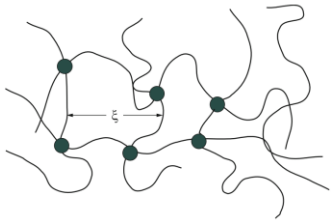


*Fig. 2. Schematic representation of a crosslinked polymer gel network. Dark circles denote junction points where polymer chains form crosslinks, determining the average mesh size (ξ) The mesh size is inversely proportional to crosslink density, which depends on polymer concentration* [33].

In addition, the properties of gels depend on the hydrocolloid concentration. Gelation does not take place below a certain minimum concentration, known as the critical gelling concentration $c_g$, which varies for different gelling systems. This variation is attributed to the degree of space occupancy by the polymer molecules in the systems. Consequently, gel formation requires that the polymer chains are sufficiently close to each other to form junction zones. This condition is reached at the coil overlap concentration [31]. Once the critical gelling concentration is exceeded, the gel-like properties increase rapidly with increasing concentration, and the concentration dependence of the gel stiffness follows a power law correlation.

The physical arrangement of the cross-links within the network can be influenced by various parameters such as temperature and the presence of ions. Three main mechanisms have been proposed for the gelation of hydrocolloids: ionic gelation, cold-set gelation, and heat-set gelation (see Fig. 3). Ionic gelation occurs through the cross-linking of charged polymer chains by ions. It is typically a cation-mediated gelation process of negatively charged polysaccharides (e.g. alginate). In cold-set gelation, the hydrocolloids are dissolved in hot water to form a dispersion. On cooling, this dispersion turns into a solid gel, resulting in a three-dimensional network due to the enthalpically stabilised helical structures of the individual chains or double helices (e.g. agarose, carrageenan or gelatine). Heat-set gelation involves the heating of hydrocolloids to induce gelation. The application of heat causes the unfolding of the biopolymer and their subsequent rearrangement into a network (e.g. methylcellulose and globular proteins such as whey) [19], [34]. During these sol-gel transitions, the randomly distributed polymer coils adopt an increasingly ordered conformation. These ordered structures can aggregate to form a continuous network, trapping the solvent within their interconnected spaces.

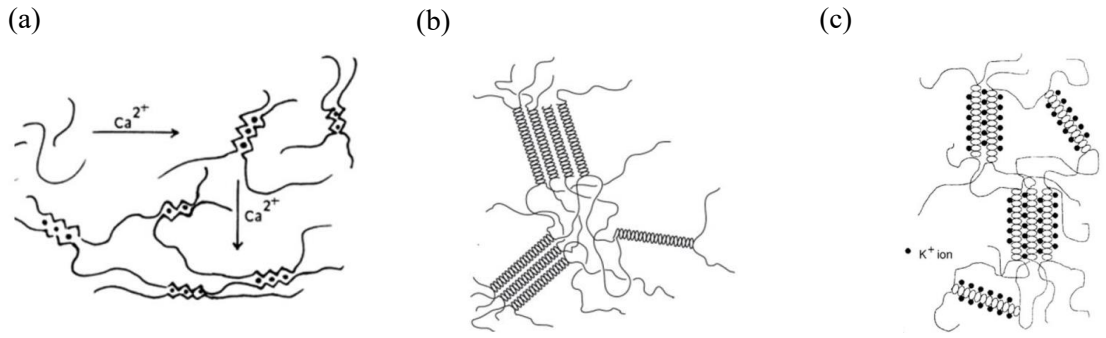


*Fig. 3. Schematic representation of different gelling mechanisms. (a) Cation-mediated formation of an alginate network illustrated by the egg-box model. (b) Network formation thorough aggregated double helices of agarose. (c) Cross-linked double helix of κ-carrageenan* [1], [10], [35].

The relatively weak interactions in polysaccharide gels, as compared to covalent bonds, allow for the formation of thermo-reversible gels. As the temperature increases or decreases, a transition from gel to sol or from sol to gel occurs. Indeed, the extent of the temperature difference between the gelation and melting gives indications of the strength of the interactions underlying the gelation [36]. This difference, known as thermal hysteresis, highlights the discrepancy between the temperature of gel formation and the increased temperature required for re-melting. Given the diverse physicochemical properties and unique molecular structure of different polysaccharides, the extent of thermal hysteresis varies accordingly. This can further be influenced by external factors such as the addition of low molecular weight co-solutes or salt [30]. Thermal hysteresis is particularly pronounced in agarose, with a significant temperature difference between its gelation and melting points. This suggests that the double helices forming the three-dimensional agarose network requires substantially more energy to dissolve than to assemble [36], [37].

## 2.3 Agarose

Because of its molecular structure and significance in biotechnological, pharmaceutical and food applications, agarose is extensively used as a model for studying the gelation mechanism of polysaccharides with gelling properties. Consequently, the forthcoming chapter provides a comprehensive overview of the current understanding of agarose, including its properties and gelation behaviour.

Agarose, the primary gelling agent in agar, is a neutral polysaccharide that forms firm and brittle gels. Agar also contains as a minor component agaropectin as a minor, a charged polymer that forms weaker gels. Agaropectin is composed of agarobiose with varying percentages of pyruvic and methyl acid groups, as well as sulphate groups. These substituents inhibit its gelling capacity, distinguishing it from agarose. It is assumed that some agaropectin may serve as a precursor molecule for agarose, potentially polymerised and de-sulphated enzymatically during algal cell metabolism [9].

Agar, commercially extracted from red algae (*Rhodophyceae*) – mainly from the seaweed species *Gelidium* and *Gracilaria* – is embedded as an amorphous matrix within the algal cell wall and has been extensively studied by Japanese scientists over several decades. Originating in Japan in the mid-seventeenth century, agar as a seaweed hydrocolloid has a long history of, serving as a gelling, thickening, and stabilizing food additive.

Prior to the extraction of agar from seaweed using hot water, often under pressure, a pre-treatment step, such as alkali hydrolysis, is undertaken to enhance the extraction efficiency and to impart the desired gelling properties to the final product. The agar production process then includes subsequent steps such as filtration, gelation and concentration through a freeze-thaw or gel press method, followed by drying and milling. The concentration step is pivotal to the functional characteristics of the final product and can be achieved either by removing water from the spongy frozen gel structure via thawing or through dewatering the gel under pressure through syneresis [9]. However, the quality of agar, and therefore agarose, can vary considerably due to the different species of algae used, residual impurities, and varying extraction conditions. These influencing factors require precise specifications for the produced agar or agarose to ensure its appropriate use in scientific applications and the manufacturing of functional food additives [9].

### 2.3.1 Molecular structure and gelation mechanism of agarose

Agarose the main gelling fraction in agar is a linear polymer, consisting of (1-3)-linked agarobiose units, where β-D-galactopyranose is (1-4)-linked to 3,6-anhydro-α-L-galactopyranose (Fig. 4) [9].

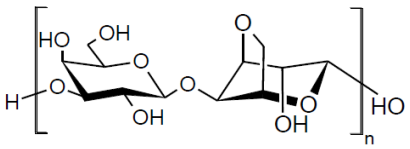


[β-D- galactopyranan-(1-4)-3,6-Anhydro- α-L- galactopyranosyl]

*Fig. 4. Backbone structure of agarose, consisting of repeating agarobiose unit composed of (1-3)-linked β- D-galactopyranose and (1-4) linked 3,6-anhydro-α-L-galactopyranose.*

Agarose chains form inter- and intramolecular hydrogen bonds, resulting in solute-solute and solute-solvent interactions. Initially, intramolecular hydrogen bonding occurs at temperatures below 60 °C, inducing conformational ordering within the polymer chains. On further cooling below 40 °C, intermolecular hydrogen bonding with water molecules and adjacent polymer chains promotes the formation of a three-dimensional network, resulting in gelation. This mechanism also explains the

insolubility of agarose in cold water due to the hydrophobic carbon and hydrogen atoms at their periphery as the agarose polymers are tightly bound. Above 90°C, increased kinetic energy and Brownian motion cause complete hydration and dissociation. Therefore, agarose exhibits thermal hysteresis as a characteristic feature, with gel setting below 40°C and melting above 90°C [38] [39].

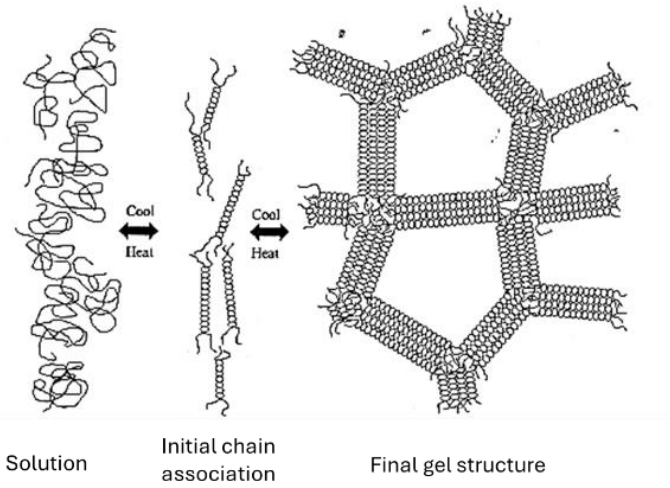


*Fig. 5. Formation of agarose gel structure. Randomly distributed polymer coils initially associate to form helices on cooling, which then aggregate to form a network on further cooling* [9].

Fig. 5 shows the gelation mechanism of agarose. Agarose solution undergoes a very rapid sol-gel transition on cooling, forming a three-dimensional network due to its molecular structure and physicochemical properties [40]. Above 60 °C, the agarose chains exist in disordered coil structure. Upon cooling, gelation occurs, with single chains transforming into an ordered structure, initially forming double helices through hydrogen bonding. As cooling progresses, these double helices aggregate [37]. Hence, a two-step gelation mechanism has been proposed for agarose. In the first step, randomly distributed coils associate via hydrogen bonding to create double helices. Subsequently, the double helices further aggregate to form a tight, three-dimensional network [37], [40].

These disordered agarose chains can adopt helical structures at certain temperatures, forming tetrahedral cavities occupied by water molecules [41]. X-ray diffraction and optical rotation studies have revealed that agarose exhibits a double helical supramolecular structure (Fig. 6). In this structure, each chain in the double helix forms a left-handed threefold helix with a pitch of 1.90 nm and is axially displaced by 0.95 nm relative to its parallel strand. This arrangement allows two chains, spaced apart by half a chain's pitch, to assemble into a sterically favourable, parallel double helix [42]. The double helix possesses a small inner cavity, 0.45 nm in diameter, with the C-H bonds directed towards the centre. The three equatorial hydrogen atoms on the 3,6-anhydrogalactose residues are involved in the gelation, as they force the molecule into the shape of a double helix by steric effects [43]. Additionally, the internal cavity is lined with hydroxyl groups, which may be involved in hydrogen bonding. More precisely, the interior

of the helix contains oxygen atoms, in particular O(2) of galactose and O(5) of 3,6-anhydrogalactose, which participate in intramolecular hydrogen bonding. Moreover, $^{1}$H-NMR relaxation investigations have revealed evidence of the presence of bound water inside the helix cavity [44].

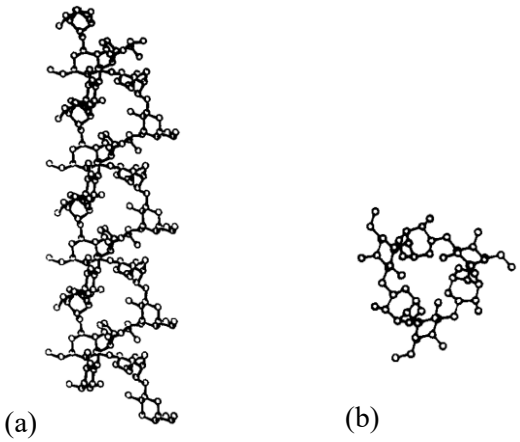


*Fig. 6. Agarose double helix: (a) side view of the helix axis and (b) top view of the helix axis* [42].

In addition, the hydrophobic interactions of the C-H bonds contribute to the formation of the hydrophobic cavity structure, which is crucial for stabilising the double helix and enabling higher-order hierarchical assemblies such as double and multi-helical structures. At the same time, the water molecule within the cavity contributes to its stabilisation by forming hydrogen bonds with the oxygen atoms lining the interior of the helix. Hence, the hydrophobic interactions are primarily responsible for shaping and forming the cavity structure, while hydrogen bonding ensure its stabilisation [45]. Indeed, it has been proposed that the water molecules, positioned without steric hindrance, are essential for double helix stabilisation by participating in hydrogen bonding interactions with the interior oxygen atoms [42], [46]. According to Arnott et al. (1974), the water molecule is precisely located from precisely located from the four oxygen atoms that line the cavity. These involve the O(2) of galactose and the O(5) of 3,6-anhydrogalactose from each chain of the double helix, arranged in an almost tetrahedral configuration [42], [46]. However, this reinforces the notion that water is essential for helix aggregation and junction zones formation in agarose gels [47]. Accordingly, the presence of sucrose or other low molecular weight co-solutes may disrupt helix formation and prevent aggregation [46].

Water molecules can form four hydrogen bonds in which the two hydrogen atoms interact with adjacent oxygen atoms, and the ion-electron pairs of the oxygen interact with two adjacent hydrogen atoms. This results in a tetrahedrally oriented hydrogen bond network, which plays a key role in gelation within an agarose solution. As hydrogen bonds develop between the polymer and water, as well as between water molecules, agarose molecules with intra- and intermolecular hydrogen bonds transform into an ice-like structure, causing gelation. This transformation occurs because the oxygen atoms of the 3,6-ring and the

OH-2 of the anhydrous-galactopyranose residues face each other (Fig. 7). As a result agarose molecules adopt double-, triple-, and multi-stranded conformations in parallel depending on the concentration [41]. The orientation of these active groups, combined with both inter- and intramolecular interactions, allows the agarose molecules to adopt these various conformations, which are crucial to the gelation process.

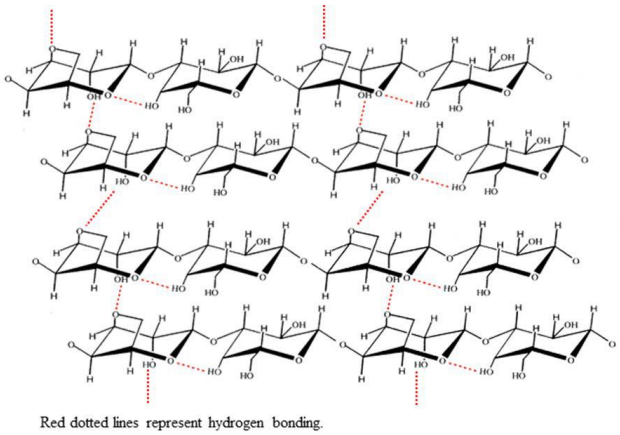


*Fig. 7. Multi-stranded hydrogen bonding between agarose molecules at high concentrations* [41]

Furthermore, Tako et al. studied the structure-function relationship of agarose, revealing a molecular-level mechanism involving water molecules. They reported double-stranded intermolecular hydrogen bond between OH-(2) and the 3,6- ring oxygen atoms of the anhydro-galactopyranose atoms (see Fig. 7), followed by a multi-stranded secondary association [39], [41]. The associated agarose molecules formed the centre of tetrahedral cavities, creating ice-like structures. This led to a thermodynamically cooperative effect caused by the cage and hydrophobic effect, leading to a decrease in entropy [41]. The study also found intramolecular hydrogen bonding between the hemiacetal oxygen atoms of anhydro-galactopyranose and the neighbouring D-galactopyranose residue, which stabilises the polymer at higher temperatures. In addition, further stabilisation occurs via intramolecular hydrogen bonding formed among the hemiacetal oxygen atom of the 1,4-linked 3,6-anhydro-galactopyranose and the OH-4 of the neighbouring 1,3-linked D-galactopyranose residue (see Fig. 7), which also comes into play already at higher temperatures (> 60 °C).

### 2.3.2 Applications

Agarose and agar hydrogels are highly advantageous in the food industry due to their exceptional properties. They form stable gels with high acid tolerance and thus are versatile ingredients for various applications. Their notable characteristics include the ability to form gels at concentrations as low as 0.2 wt%, a wide thermal hysteresis between gelling and melting temperatures, high heat resistance, and thermoreversibility. Importantly, gelation occurs without the need for counter ions. These properties enable liquid solutions to remain fluid at temperatures up to 40 °C, while gelled products resist melting up to 80 °C. Additionally, agarose and agar, provide consistent texture control, stability over a wide pH range, and compatibility with various food ingredients. This versatility supports a broad spectrum of applications in the food industry, ranging from confectionery and dairy products to meat analogues and functional foods [9].

## 2.4 Fluid gels

Due to the multiple aggregation of double helices and the dense three-dimensional network, agarose forms firm, highly elastic, brittle and cuttable gels, resulting in poor mouthfeel (see Fig. 8 (a)) [40]. This issue can be addressed by manipulating the processing conditions, such as applying different shear rates, altering concentrations, using biopolymers with varying inherent molecular properties, or adding co-solutes such as sucrose, which change the network properties at the molecular scale, thereby affecting texture and lubrication.

One effective approach involves creating fluid gels, which are particulate gel suspensions formed by applying a defined shear field to a biopolymer solution during gelation [48]. The focus of this work is the formation of fluid gels using a rheometer. This "in-situ" method allows precise control and monitoring of parameters such as shear rate, temperature rate, and viscosity, ensuring that gelation occurs under constant and controlled conditions. This precision enables a detailed study of the kinetic competition between crosslinking process and their breakup involved in fluid gel formation [5]. However, this process results in an alternative textural structure with irregularly shaped, elastic microparticles dispersed in a continuous aqueous phase [4], [49]. The unique structure of fluid gels imparts remarkable flow and textural properties, exhibiting shape-retaining behaviour like of solids at rest, but flowing like liquids when subjected to sufficient stress (see Fig. 8 (a-b)) [4].

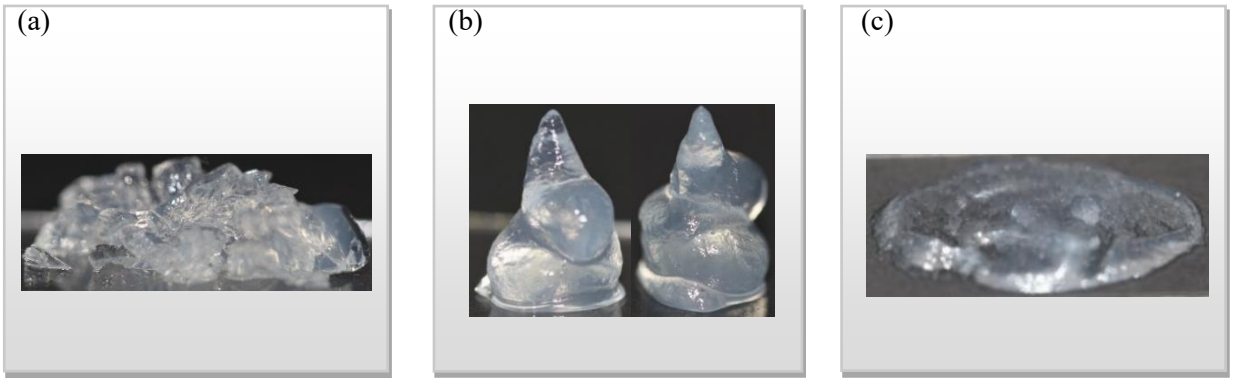


*Fig. 8. Images of 1 wt% agarose gel: (a) Gel formed under quiescent conditions, displaying rigid, brittle properties that allow it to be cut; (b) Fluid gels produced under shear during gelation, exhibiting a structure that maintains its shape and behaves like a solid at rest, (c) the same fluid gels exhibit fluid-like flow behaviour above a critical applied stress.*

The controllable particulate microstructure of fluid gels, obtained by precise formulation and processing, has substantially broadened their applications in a number of industries [50]. A major advantage of fluid gels lies in their versatility for texture manipulation. Unlike quiescently cooled gels, fluid gels enable the creation of a wide range of rheologically distinct structures from the same biopolymer by adjusting process conditions, particularly shear, during gel formation. This ability to fine-tune texture through process control, without altering the basic ingredients, represents a key benefit of fluid gel production and allows for greater customization. [51]. These adaptable structures have been developed using various food-grade gelling agents. Notable examples include gelatine [5], and especially hydrocolloids that undergo a thermally reversible transition, such as gellan gum [48], and agarose [4]. Detailed studies of their rheological, mechanical, and tribological behaviour – as conducted in this work – are required to fully understand and optimise fluid gels for various applications. supporting techniques such as atomic force microscopy are employed to investigate their underlying network structure.

However, under certain conditions of shear rate and biopolymer concentration, gelation takes place either through nucleation and growth or by undergoing a spinodal decomposition, leading to demixing into biopolymer-rich and biopolymer-poor domains [4], [52], [53]. Norton et al. suggested the first molecular model of fluid gel formation based on agarose sheared gels and outlined several principles. They posited that fluid gel particles form in a shear field when biopolymer gelation involves an aggregation step, with particles developing by nucleation and growth until reaching a size equilibrium determined by the applied shear forces. The process begins with the formation of gel nuclei, which are disrupted and separated by shear, preventing the complete arrangement of the gel matrix and leading to the formation of discrete gel particles. These authors proposed that shear does not affect the rate of molecular ordering, but significantly influences the particle size and number, which makes it a critical factor in controlling the fluid gel microstructure. These particles were described as ”hairy” due to the presence of disordered aggregated polymer chains on their surfaces before the completion of the structural ordering as proposed by the authors. They also proposed that the applied shear field disrupts the coil-to-helix transition, particularly at the surfaces of the forming particles. In this region near the

periphery of the particles, this disruption results in the formation of fewer helical domains and, consequently, fewer helical aggregates. As a result, the density of the gel network decreases towards the outer regions of the particle. Aggregation is impeded in these outer regions, resulting in delayed network cross-linking. This phenomenon results in particles with “hairy” surfaces, characterised by partially disordered polymer chains extending from the more densely cross-linked core of the particle [4].

The particle size and particle volume fraction are dependent on shear rate and polymer concentration, with the particle volume fraction dictating the fluid gel properties. Furthermore, fluid gels remain stable when stored below the melting temperature, avoiding de-aggregation and re-aggregation. Cox et al. (2009) developed a detailed schematic (Fig. 9) depicting the molecular mechanisms during fluid gel formation and their correlation with viscosity with decreasing temperature [54]. Furthermore, research by Frith et al. (2002) showed that fluid gel particles are highly deformable rather than rigid, as evidenced by the gradual increase in elastic modulus with increasing agar concentration [49]. They also observed that fluid gels tend to occupy the maximum volume fraction during formation, indicating a densely packed yet flexible particulate network.

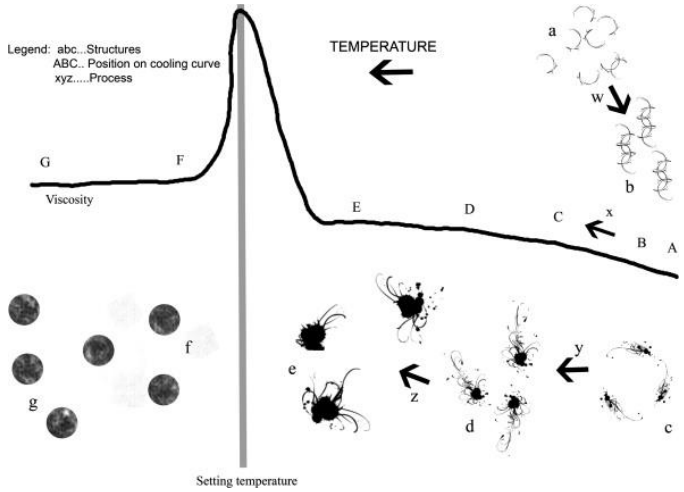


*Fig. 9. Schematic representation of molecular- and meso-scales events during fluid gel formation* [54].

Furthermore, the size of fluid gel particles, and hence their properties, is influenced not only by concentration but also by the dynamic balance between the shear rate and cooling rate during formation. The cooling rate primarily controls the growth of gel nuclei, while the shear rate governs particle coalescence or agglomeration and break-up [5], [53]. High cooling rates result in larger particles with different shapes due to the dominance of the gelation process over shear forces. Conversely, low cooling rates result in smaller particles and a narrower size distribution due to the dominance of the shear force. Therefore, at the same cooling rate, increasing the shear rate results in smaller particles and a narrow size distribution [6], [53], [54].

However, the gelation of biopolymers under shear conditions is a complex process involving competing mechanisms and multiple time scales. As proposed by De Carvalho et al., when biopolymers are subjected to shear during gelation, there is a competition between physical cross-linking and the breaking of these bonds by shear forces [5]. The resulting gel structure is influenced by the interplay between shear rates and the molecular dynamics of the agarose chains.

Additionally, the internal modes of polymer motion, as described by the Rouse-Zimm model, play a significant role in the formation of gel particles, especially as cluster size grows [55]. The cooling rate affects the gelation process in stages, first influencing the centre of mass of individual polymers, then the centre of mass of the cluster, and finally slowing down the cluster dynamics as they grow in size. Particle size and volume fraction in fluid gels are dependent on shear rate, temperature rate, and concentration, which in turn predict the properties of fluid gel [5]. This led to the assumption that the ordering rate of the biopolymers, and thus their cross-linking, is crucial for particle growth. The relationship between particle size (R) and various parameters can be approximated using Einstein's diffusion law at low Péclet numbers (Eq. 3). This equation relates particle size to the viscosity $\eta_s$ of the sol phase and the shear rate $\dot{\gamma}$.

$$R \simeq \left(\frac{k_B\, T}{6\pi\eta_s\, \dot{\gamma}}\right)^{1/3} \tag{3}$$

Earlier research suggests that sheared gel formation begins with initial nucleation and growth into spherical gel particles, either through an "enrichment" process from the surrounding non-gelled matrix or through the agglomeration of nucleating particles forced together by shear flow. These aggregated particles are then separated by shear forces, constraining molecular ordering and cross-linking within the particles [4]. However, this equation provides only a crude estimate of gelled particle size. The competition between the time scales imposed by the shear rate during gelation and the broad range of polymer time scales is significant. Before gelation begins, polymer chains diffuse to the lowest approximation according to the Rouse-Zimm model [55], with the centre of mass diffusion constant proportional to the square root of chain length. The longest relaxation time of the chains is determined by the same relationship. As cooling progresses, neighbouring chains form helices, introducing lower time scales. The diffusion of growing gel cluster slows down further, determined by their size and the number of agarose chains involved. Consequently, the particles develop irregular shapes with long extended "tails" growing from a spherical or ellipsoidal centre. This complex process highlights the dynamic balance of forces and time scales in biopolymer gelation under shear conditions, resulting in unique structural and dynamic properties of the formed gels.

## 2.5 The role of sugar

As mentioned before, the physico-chemical, rheological and lubricating properties of fluid gels are significantly influenced by low molecular weight co-solutes, demonstrating a strong correlation between atomic-scale interactions and macroscopic structural changes. This study investigates the impact of sucrose, chosen as a representative co-solute, on particle structure and rheological behaviour during fluid gel formation. It gives a comprehensive overview of how sugars, particularly sucrose, affect the gelling mechanism of agarose, focusing on chemical structure, solution properties, and the role of water as a solvent. Although the hydration behaviour of sucrose is not specifically examined, the study emphasises its interactions with water molecules and their effects on the water structure, which influences the viscoelastic and lubricating behaviour properties of agarose fluid gels.

Sugar hydration in water is governed by dipole nature of water and self-association. Disaccharides exhibit high solubility due to their equatorial hydroxyl groups. Vicinal hydroxyls, more effectively hydrated than axial ones, have an O-O spacing matching that of water molecules, enabling seamless integration into water's tetrahedral H-bond network with minimal disruption [56]. This integration enhances hydrogen bonding, increasing hydration shell size and hydration numbers, thereby stabilising water structure and influencing properties like solubility and gelation [57], [58].

As mentioned, the behaviour of water molecules around sugars in solution is primarily governed by polar interactions, especially those involving equatorial hydroxyl groups. Uedaira et al. (1985) found that sugars with a higher number of these groups, exert a stronger stabilising effect on the water structure [59]. While sucrose, interacts effectively with water molecules due to its high solubility, trehalose, which possesses only equatorial OH groups, forms even stronger hydrogen bonds, resulting in a higher water-holding capacity [57] Thus, the number of water molecules in the hydration shell is proportional to the number of hydroxyl groups, with the equatorial OH groups creating a stable, long-lasting hydration structure that integrates smoothly into the water lattice [59].

Water, as a highly effective solvating agent, forms hydrogen bonds not only with sugar molecules, but also between sugar molecules themselves. This leads to three main types of molecular interactions: water–water, water–sugar, and sugar–sugar. As sugar concentration increases, these interactions become more complex, often promoting sugar aggregation, conformational changes, and alterations in solvent polarity [60]. As a result, in the gel formation of biopolymer solutions, the hydration properties of sugars, which are determined by their stereochemical configuration, particularly the ratio of equatorial to axial hydroxyl groups, are of critical importance.

## 2.6 Sucrose–agarose interactions and their effect on gelation

Previous studies have shown that the addition of sugars significantly affects hydrocolloid systems by interacting with both the hydrocolloids and water molecules. Extensive research has been conducted to understand the hydration of sugars and their effects in these systems [14], [15], [61], [62]. Adding co-solutes causes physical changes on local length scales. Sucrose, with its strong binding affinity for water, reduces the availability of agarose to undergo gelation, which weakens gel formation at higher concentrations. The exact mechanism remains debated, but this interaction is thought to involve hydrogen bonding between sucrose and agarose, causing changes in helix formation and aggregation [62], [63]. Sucrose influences the mobility of agarose chains, affecting structure formation and elasticity, while changes in chain dynamics, such as those induced by shear rate and the water-binding properties of co-solutes, further modify the gel structure. As mentioned above, water stabilises agarose helices through hydrogen bonding, which is essential for gel network formation [41]. Thus, the addition of sucrose disrupts these bonds, destabilising helix formation and preventing aggregation, underscoring the critical role of water in agarose gelation [47], [64]. Consequently, introducing sucrose or other low molecular weight co-solutes into the hydrated agarose system can hinder helix formation and aggregation [46].

However, Nishinari et al. (1992) used DSC to investigate the agarose gel-sol transition. They noted a temperature shift with increasing sucrose concentration and a correlated increase in elastic modulus [17]. Watase et al. (1992) proposed an "Icing type zipper model", suggesting that sucrose enhances the formation of helical molecules, stabilises the junction zones, reduces their size, and increases their number through hydrogen bonding. This, in turn, results in a higher modulus [62]. Moreover, a stabilising effect of sucrose in polysaccharide systems has been described, leading to additional ordered linkages between the agarose chains due to increased hydrogen bonding [65], [66]. Excessive sucrose, however led to a decrease in modulus [17]. It has also been argued that the decreasing availability of water molecules at high sucrose concentrations (> 60 wt%) may induce crystallisation of the sugar molecules involved in network formation. In the case of sucrose, small crystals have been observed to precipitate from the agarose sol during gel preparation [13].

Furthermore, Shimizu et al. (2014) provided significant insights into how co-solvents enhance gelation in agarose systems, revealing that co-solvents influence the sol-gel transition through two mechanisms: restructuring of water around the biopolymers or (2) exclusion from the biopolymer surfaces. Their study concluded that co-solvent exclusion, which increases biopolymer compactness and promotes aggregation, is the primary driver of gelation [67]. This finding contradicts earlier theories that emphasized hydration changes due to competitive hydration between the biopolymer and co-solvent as the main driver of gel stabilisation [62], [63], [67]. This conclusion is particularly relevant for the fluid gels prepared in this study, where sucrose is dissolved in water before agarose. This suggests that co-

solvent exclusion, rather than direct changes in biopolymer hydration, plays a central role in gelation [67]. However, sugars may still indirectly influence the sol-gel equilibrium through preferential exclusion from the biopolymer surface, which alters the hydration dynamics due to competitive hydration between the biopolymer and co-solvent [62], [63], [67]. Moreover, regarding co-solvent induced changes in water structure and biopolymer hydration, Shimizu et al. summarised two perspectives: one proposes that highly hydrated sugars reduce the free water molecules available for biopolymer hydration, emphasizing the role of hydration number and high bound water content for optimal hydration. The other suggests that sol hydration becomes more ice-like, leading to entropic destabilisation of the sol. These findings further support the conclusion that co-solvent exclusion is a key driver of gelation in systems such as the one examined in this work [67].

In addition, the order of sugar addition when preparing biopolymer-based fluid gels affects their structural and mechanical properties, making it a critical factor in the formulation process. The impact of sugar addition before or after biopolymer dissolution has been thoroughly studied in quiescently cooled gels. Yang et al. (2015) found that when more than 40 wt% of sucrose was dissolved before agar addition, the resulting gel network became weaker and more inhomogeneous [68]. The order of addition was shown to significantly affect the fracture stress, strain, and the sucrose release ratio. As a result, other studies, albeit on agar fluid gels, have also opted to add sugar after dissolving the agar [12].

In this work, we deemed it essential to prepare the fluid gels, as in our previous studies, by first dissolving the agarose in water, to ensure the same initial state of the agarose-water system. This approach allowed us to accurately determine the effect of sucrose on this specific system.

## 2.7 Texture profile analysis

### 2.7.1 Basic principles

Texture Profile Analysis (TPA), one of the earliest methods of mechanical texture studies, is widely used to characterise the mechanical behaviour of semi-solid soft materials such as gels. It provides valuable information by measuring how a sample responds to applied controlled deformation, thereby reflecting the internal structural composition and surface interactions of the material [69], [70].

Food texture is understood as a combination of structural and mechanical properties that are perceived by both sensory and instrumental measurements. However, the way a food material responds to external deformation, which is derived from the structure of the food at the molecular, microstructural, and macroscopic levels, determines how its texture is perceived [71]. From a mechanical perspective, texture analysis can quantify properties such as hardness, cohesiveness, elasticity (or springiness), adhesiveness, and viscosity. While viscosity typically requires rheological tools such as oscillatory measurements, the

other parameters can be determined using texture profile analysis (TPA) [70]. In TPA, a sample – often prepared in a cylindrical form – is either compressed or penetrated by a plunger. The resulting force-displacement (time) curves offer insight into key mechanical features of texture. Fig. 10 presents a typical texture profile analysis (TPA) curve, depicting the force response of a gel sample subjected to a double compression cycle using a cylindrical plunger. The first peak $A_1$ corresponds to hardness, defined as the maximum force applied during the initial penetration of the sample. Cohesiveness is determined as the ratio of the area under the second penetration peak, $A_2$, to the first, $A_1$, which reflects the internal bonding strength and structural resistance of the material after deformation. Elasticity can be derived from the time interval $B$ between the start of the first and second compressions, i.e. penetration, indicating how quickly the material returns to its original shape after removal of the deformation force. Adhesiveness is represented by the negative force after the first compression/penetration, which quantifies the energy required to overcome the attractive forces between the sample and the probe surface [70].

However, while parameters such as hardness, cohesiveness, and elasticity are related to the internal forces between the biopolymers and the particles of the gel, adhesiveness is associated with the surface properties [70].

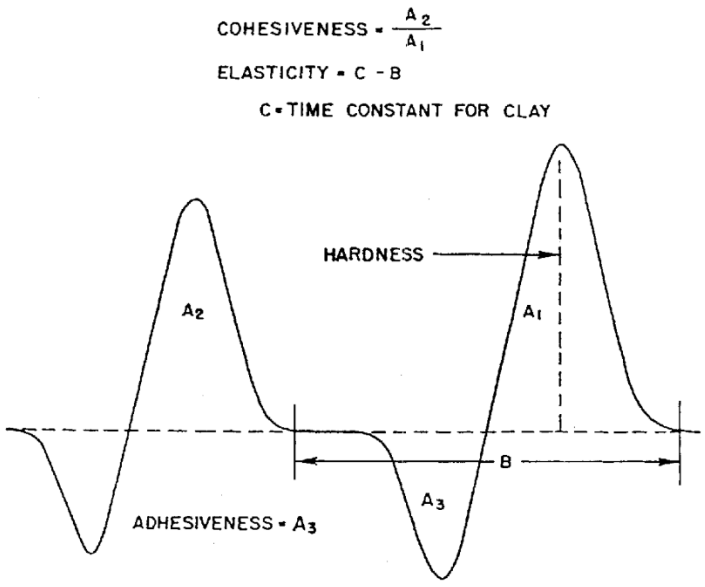


*Fig. 10. Typical force-time curve from a texture profile analysis test, read from right to left, with peak $A_1$ being the first chew and peak $A_2$ being the second chew. It shows the key mechanical parameters: hardness (first peak), cohesiveness (area ratio of second to first peak), elasticity (time between compressions/penetration) and adhesiveness (negative force when the plunger is pulled back) [70].*

### 2.7.2 Applications of texture analysis in fluid gels

Texture analysis is a valuable tool for characterising the mechanical properties of fluid gels. However, in general, the choice of the test method (compression or penetration) depends on the composition and preparation procedure of the sample [72]. When testing soft gels, such as fluid gels, penetration testing is particularly suitable because of the limited structural stability due to the heterogeneous structure of the particulate gel suspension. Depending on the gelling agent and processing conditions, fluid gels do not retain their shape to a certain extent when deformed, so penetration-based texture measurements are required to assess their structural properties. Indeed, as mentioned above, fluid gels exhibit a unique combination of solid-like elastic and liquid-like flow behaviour, with their structural response influenced by the cross-linking network within the gel particles and the attractive forces between the interconnected particles [73].

This interplay between the elastic cross-linked core and the frictional rearrangement of the particles by the surface structure makes this measurement useful for comparing the mechanical properties of differently formulated fluid gels and evaluating the effects of varying preparation parameters. In addition, texture analysis results can be linked to rheological data for a more comprehensive understanding of the mechanical behaviour of gels. The puncture test used in this work measures the resistance of the gel to local deformation, a critical property for understanding texture properties relevant to oral processing.

## 2.8 Rheology

### 2.8.1 Basic principles

Rheological measurements were performed to investigate the viscoelastic and flow properties of agarose fluid gels at different concentrations, as well as the effect of sucrose. The following section details the rheological principles and methods used to study the network of gel particles formed by cross-linked agarose polymers.

Rheology is the study of the flow and deformation behaviour of matter, providing insight into macroscopic properties that allow conclusions to be drawn about molecular structures. It is based on the resulting deformation of a sample when subjected to an external force. Fig. 11. illustrates the two-plate model used to represent the mechanical properties and rheological parameters that characterise a material. In this model, the sample is placed between two parallel plates separated by a distance $h$. A force $F$ applied to the upper plate area $A$ causes lateral movement, shearing the sample while the lower plate remains stationary. This produces a shear stress $\tau$ (Eq. 4), representing the energy required for

deformation. The deformation strain γ (Eq. 5) is derived from the displacement *x* relative to the sample height *h*, while the strain rate $\dot{\gamma}$ (in $s^{-1}$) (Eq. 6) represents the rate of the deformation. For accurate measurements, the sample must adhere firmly to both plates and deform uniformly in a laminar flow without slippage.

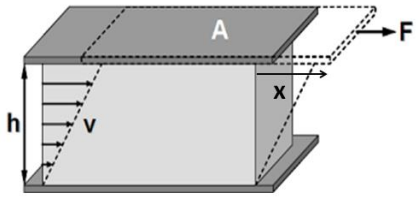


*Fig. 11. Parallel two-plate model for shear testing, illustrating the velocity distribution of flow in the shear gap* [26].

$$\tau = \frac{F}{A} \quad \text{where } [\tau] = \frac{N}{m^2} = Pa \tag{4}$$

$$\gamma = \frac{x}{h} \quad \text{where } [\gamma] = \frac{m}{m} = 1 \tag{5}$$

$$\dot{\gamma} = \frac{d\gamma}{dt} = \frac{v}{h} \text{ where } [\dot{\gamma}] = \frac{m/s}{m} = s^{-1} \tag{6}$$

Materials are generally classified as viscous, elastic, or viscoelastic, with their behaviour ranging from that of an ideally elastic solid (described by Hooke's law) to an ideally viscous fluid (described by Newton's law). In ideal viscous fluids, the shear stress (τ ) is proportional to strain rate ($\dot{\gamma}$), as described by Eq. 7:

$$\tau = \eta \cdot \dot{\gamma} \tag{7}$$

Here, the dynamic viscosity (η), defined as the ratio of shear stress to strain rate, represents the resistance of the material to flow. According to Newton's law, viscosity remains constant regardless of deformation or applied shear rate, with shear stress being directly proportional to shear rate, and η being the proportionality constant.

This study examines polysaccharides as non-Newtonian fluids, where viscosity varies with applied shear stress. Newtonian fluids, such as silicone oils or low-concentration dispersions, maintain a constant viscosity with a proportional shear stress-strain rate relationship. In contrast, non-Newtonian fluids, may exhibit shear thinning (pseudoplastic) behaviour, where viscosity decreases as shear rate increases, or shear-thickening (dilatant) behaviour, where viscosity increases with shear rate. Starch solutions, for

example, typically exhibit shear-thickening behaviour, while most polysaccharide dispersions exhibit shear-thinning behaviour, in some cases with an initial Newtonian range, depending on the material properties. These different flow behaviours are illustrated in Fig. 12 (a-b).

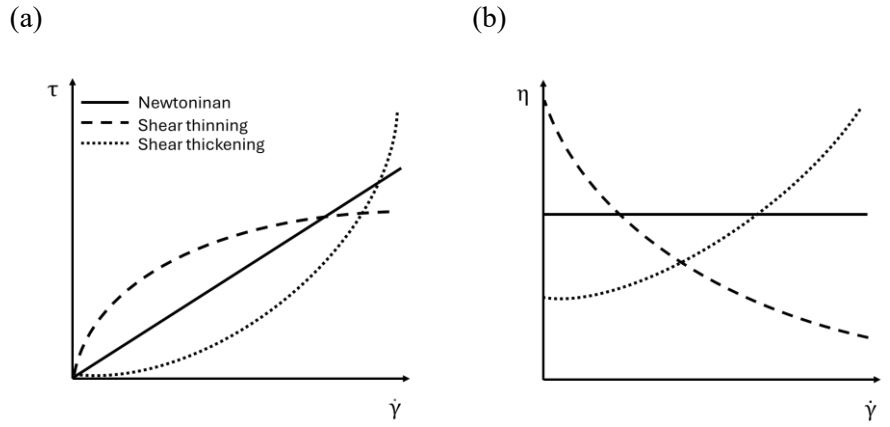


*Fig. 12. Shear rate $\dot{\gamma}$ versus a) shear stress $\tau$ and b) viscosity $\eta$ for different types of flow behaviour* [26].

For ideal elastic solids, deformation follows Hooke's law, which states that shear stress ($\tau$) is directly proportional to strain ($\gamma$) (Eq. 8), expressed as:

$$\tau = G \cdot \gamma \tag{8}$$

where *G* is the shear modulus, a constant that characterises the stiffness and resistance of a material. The modulus gives insights into the strength of intermolecular cohesive forces within the material and increases as these forces become stronger. This property is fundamental to understanding and predicting the mechanical behaviour of elastic materials under stress.

As mentioned earlier, soft materials such as polysaccharides exhibit both elastic and viscous behaviour, classifying them as viscoelastic. Depending on which component dominates, they display time-dependent flow and deformation under applied stress. The viscous component deforms immediately and irreversibly, while the elastic component responds with a delay and recovers slowly. Viscoelastic fluids retain a permanent deformation after shear stress, an irreversible effect due to the viscous component. Conversely, viscoelastic solids exhibit delayed elastic recovery once the stress is removed, although in some cases, this recovery may be partial (relaxation). This behaviour is especially common in cross-linked materials, such as gels.

### 2.8.2 Steady and dynamic rheological measurements

To evaluate the viscosity and flow properties of materials, rotational shear measurements can be performed using a shear rate sweep. This involves applying a defined range of shear rates ($\dot{\gamma}$) and measuring the corresponding viscosity ($\eta$) under steady-state conditions. The resulting data, plotted as viscosity versus shear rate, facilitates analysis of the flow behaviour and reveals distinct characteristic curves, as shown in Fig. 12.

Dynamic oscillatory measurements, on the other hand, are employed to determine the viscoelastic properties of materials. In this method, a sample is subjected to shear through the oscillation of the upper plate, which is driven by a rotating motor. Fig. 13 (a) illustrates the two-plate model used for the oscillation test. The upper plate reaches its maximum displacement to the right at 90° and the left at 270°. A complete oscillation cycle, corresponding to a full rotation of 360° angular displacement, describes the time-dependent functions $\gamma(t)$ and τ(t). The applied stress and resulting deformation are described using sinusoidal functions, as shown in Fig. 13 (b). These measurements provide valuable insight into the viscoelastic properties of materials, such as polysaccharides, by characterising their elastic and viscous components.

(a) (b)

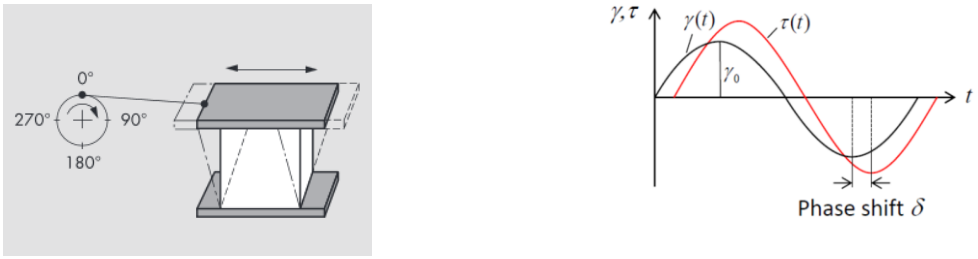


*Fig. 13. Deformation of a viscoelastic sample. (a) Two plate system for oscillation tests. (b): Sinusoidal deformation γ(t) and displaced shear stress τ(t), including phase shift δ, resulting from shear deformation* [26].

For sinusoidal deformation, the strain is expressed as follows:

$$\gamma(t) = \gamma_0 sin(\omega t) \tag{9}$$

with $\gamma_0$ as the deformation amplitude, $t$ as time, and ω as the angular frequency (in rad/s or $s^{-1}$), with

$$\omega = 2\pi \cdot f \tag{10}$$

where $f$ is the oscillation frequency. For viscoelastic behaviour, the shear stress curve is shifted by a phase angle δ relative to the deformation strain:

$$\tau(t) = \tau_0 sin(\omega t + \delta) \tag{11}$$

From the time derivate of (11), the strain rate is given by:

$$\dot{\gamma}(t) = \omega\gamma_0 cos(\omega t) \tag{12}$$

However, according to Hooke's law, strain and stress oscillate in phase for ideal elastic behaviour, whereas according to Newton's law, ideal viscous behaviour exhibits a phase shift of $\delta = 90°$. Viscoelastic materials show a phase shift $\delta$ ranging from 0 to 90° (Fig. 13).

The complex shear modulus $G^*$ for sinusoidal shear deformation is defined as:

$$G^* = \frac{\tau(t)}{\gamma(t)} \tag{13}$$

With $G^* = G' + i\,G''$, the terms can be obtained from the shear stress oscillating in and out of phase with the strain, thus quantifying the proportion of the elastic and viscous components of viscoelastic materials:

$$\tau = \tau'(t) + \tau''(t) = \tau'_0 sin(\omega t + \delta) + \tau''_0 cos(\omega t + \delta) \tag{14}$$

The in-phase component of the stress is the elastic (storage) modulus $G'$, while the out-of-phase component is the viscous (loss) $G''$.

$$G' = \frac{\tau_0 cos\delta}{\gamma_0} \tag{15}$$

$$G'' = \frac{\tau_0 sin\delta}{\gamma_0} \tag{16}$$

The storage modulus $G'$ represents the elastic part of the material and quantifies the deformation energy stored in it. In an ideal elastic solid, the energy absorbed during deformation is fully recovered when the stress is removed, allowing fully reversible deformation. Conversely, the loss modulus $G''$ characterises the viscous behaviour of a material. During shear, the energy required for deformation is dissipated as heat rather than stored, resulting in permanent deformation that cannot be recovered when the stress is removed [26].

The loss factor (tan δ), defined as the ratio of the loss modulus $G''$ to the storage modulus $G'$, is given by:

$$tan\delta = \frac{G''}{G'} \tag{17}$$

Ideal elastic behaviour occurs when $G'' \rightarrow 0$ and $\tan\delta \rightarrow 0$. Conversely, ideal viscous behaviour is observed when $G' \rightarrow 0$ and $\tan\delta \rightarrow \infty$. When the storage and loss moduli are equal ($G' = G''$), it follows that tanδ =1, indicating that the elastic and viscous properties of a material are equal. This condition is observed at the sol-gel transition point, where viscous behaviour dominates in the sol state and the elastic behaviour is dominant in the gel state [26].

## 2.9 Oral processing: Transition from rheology to tribology

Oral food processing is a complex dynamic process that involves a number of deformation processes and destruction mechanisms [71]. As food is chewed, it is continuously mixed with saliva and gradually transformed into a cohesive bolus ready to be swallowed [71], [74]. Subsequently, small amounts of food residue remain on the oral surfaces, thus contributing to the sensory experience, including physical and chemical sensations [75]. However, as chewing progresses, the particle sizes of food decrease, and the thickness of the food-saliva mixture between oral surfaces, such as the tongue and palate, is reduced. This change in length scale has significant implications for texture perception, shifting the dominant mechanism of texture perception from rheology to tribology [71].

Initially, rheological properties, such as hardness, elasticity, and viscosity dominate texture perception and determine how foods respond to deformation forces during biting and chewing [71]. In addition, texture profile analysis (TPA) measures parameters such as hardness, springiness, elasticity, plasticity, adhesiveness, and cohesiveness in the early stages of oral processing. These parameters correlate well with sensory perceptions like firmness, softness, chewiness, brittleness, and stickiness [71], [75]–[79]. However, as the food continues to break down and the film thickness decreases, rheology and texture analysis alone become insufficient to explain textural and mouthfeel properties. Instead, lubrication behaviour between oral surfaces becomes the primary mechanism influencing texture perception and mouthfeel. Hence, the sensory perception becomes less dependent on bulk rheological properties and more influenced by surface interactions and lubrication [71], [80].

In these later stages of oral processing, tribological effects governing friction and lubrication in the food-saliva mixture become increasingly important. These effects shape sensory attributes as the food transitions into a smoother, more fluid state. Friction and lubrication between oral surfaces, particularly as the tongue moves against the palate while the food is being sheared and squeezed, play a critical role in determining sensory attributes such as smoothness, slipperiness, creaminess, etc. In addition, after eating, the mouth still senses residues and after-effects of the food consumed, such as astringency and mouth coating, known as after-feel, as a mechanical sensation [71], [75]. The friction coefficient, a key parameter in tribology, becomes crucial in determining these sensory attributes, which will be discussed in more detail in the following chapter. Furthermore, the oral lubrication regime in the mouth can vary from hydrodynamic lubrication (where a thick fluid film separates the surfaces) to boundary lubrication (where surfaces are in close contact with minimal fluid film), and in between mixed lubrication (where a thin fluid separates the surfaces but are just about to touch), which will also be explained in detail [71] [71], [81].

Fig. 14 summarises the complex process of texture perception described above, involving multiple physical and sensory mechanisms. It highlights that texture properties linked to rheology and texture analysis are perceived relatively quickly, whereas those related to tribology are perceived more slowly

[71], [75]. Here, Stokes et al. presented six key stages during the oral processing of solid foods, emphasising the role of mechanics, rheology, and tribology. The six process stages (i) first bite, (ii) chewing, (iii) granulation, (iv) bolus formation, (v) swallow, and (vi) residue all overlap in situ but need to be studied separately to investigate the underlying physical properties. Characteristics of the early stages are initially perceived at first bite (i) and (ii) mastication by the teeth and tongue. Tribology is particularly important in stage (iii), where interactions between food particles and oral surfaces occur, whereas (iv, v and vi) are mainly due to interactions between oral surfaces. The study also showed how dominant sensations evolve over time [75].

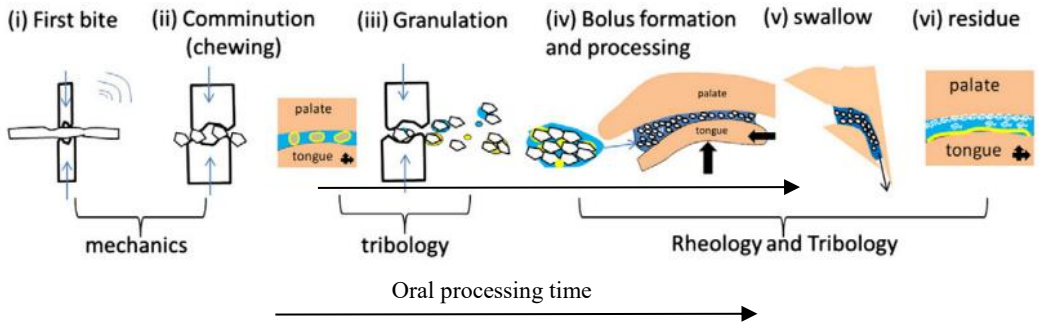


*Fig. 14. Illustration of the six stages during oral processing of solid food (adapted from Figure 3 from Stokes et al. (2013))* [75].

As noted above, transitions from bulk-dominated deformation and flow properties to surface-dominated characteristics during oral processing underscore the dynamic nature of texture perception. This complex process involves multiple physical and sensory mechanisms. As mentioned, a range of in vitro techniques are required to qualify and quantify these physical properties of foods. Fig. 15 illustrates the reduction in film thickness of liquid-like foods or beverages between oral surfaces as they are consumed, highlighting the shift from a rheology-dominated deformation process to a tribology-dominated mechanism (i.e., surface properties). In addition, the figure outlines examples of techniques suitable for studying multi-scale deformation and identifies the location of typical textural mouthfeel attributes [75].

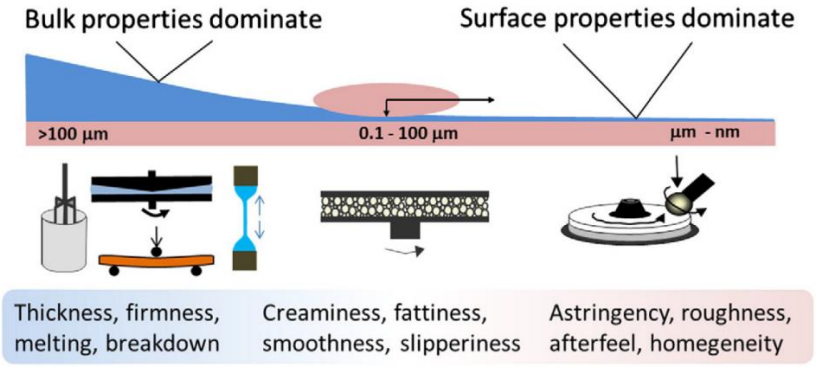


*Fig. 15. Transition in film thickness between oral surfaces during consumption, showing the shift from rheology- to tribology-dominated mechanisms. Highlights techniques for studying multi-scale deformation and the location of key textural mouthfeel attributes* [75].

Understanding this approach of multi-scale transition, supported by various techniques for texture studies, is crucial for food product design. The underlying phsico-chemical properties of texture perception, derived from the food structure at molecular, microstructure, and macroscopic levels, play an important role. By considering textural properties at different stages of oral processing, a comprehensive insight into texture perception can be gained, and products can be developed that provide a desirable sensory experience throughout the entire eating process, from the first bite to the final swallow [71], [75].

## 2.10 Tribology

### 2.10.1 Tribology in soft materials and food systems

Tribology, the study of friction, lubrication, and wear between interacting surfaces in relative motion, has traditionally been applied in mechanical engineering. For decades, it has been used to analyse lubrication and friction effects on rubbing, contacting, and moving surfaces prone to wear. Lubricants play a fundamental role in reducing friction, enhancing operating efficiency, and lengthening the lifespan of mechanical devices [82], [83].

One of the most prominent applications of food tribology is the study of smoothness, creaminess, and slipperiness, key textural attributes influenced by the presence of oil or fat, but also hydrocolloids (i.e., polysaccharides and proteins), which is closely related to food lubrication [84], [85]. A key methodology in this discipline is soft tribology, focusing on the effects of friction, lubrication, and wear on deformable surfaces [81]. Soft tribology provides quantitative insights into mouthfeel and the complex process of oral processing, which involves mechanical manipulation by oral surfaces, such as the tongue moving upwards towards the palate before swallowing. Attention must also be paid to the sensation that remains

after swallowing, such as after mouthfeel or astringency [86]. Predicting oral behaviour is a major key aspect of oral tribology and food lubrication in the field of functional food research. These fields aim to understand the mouthfeel of food products by studying friction and lubrication between food particles and oral surfaces. Lubrication is a critical factor in food oral processing, as it directly influences texture perception and sensory outcomes [74].

This chapter outlines the principles of tribology, the measurement systems used, and their application in studying fundamental physical question related to soft materials in model food systems, such as semi-solid foods. In this work, tribological measurements were conducted to investigate the lubrication and frictional properties of fluid gels, providing insight into their behaviour between interacting surfaces for a more in-depth evaluation of the microgel particles.

### 2.10.2 Basic principles of tribology

When two surfaces are in contact and subjected to a loading force perpendicular to the direction of motion, friction will oppose the relative motion of the surfaces. This frictional force is quantified by the friction coefficient $\mu$, which is simply the ratio of the frictional force $F_F$ to the loading force e.g. normal force $F_N$, (which acts perpendicular to the direction of friction) (Eq. 18) [71], [87].

$$\mu = \frac{F_F}{F_N} \tag{18}$$

The coefficient of friction (COF), a key tribological parameter, quantifies the frictional behaviour of distinct systems and allows the characterisation of the surface interaction. Under dry conditions, it remains constant and is dependent on the properties of the contacting surfaces, including surface roughness and the geometry of the surface asperities. However, the COF varies with applied load and fluid viscosity in the presence of a thin fluid layer between the surfaces. With lubrication, the coefficient of friction becomes a reliable indicator of lubrication efficiency and is no longer constant. Instead, it is determined by surface characteristics, applied load, speed of movement and lubrication properties such as viscosity [71], [83], [87].

Consequently, it should be noted that tribology is a system property rather than a material property, which involves the interaction of a measurement system, the surfaces, and the lubricant. The surface can be soft, hard, hydrophilic, hydrophobic, rough, or smooth, and the lubricant can be a complex fluid with particles, droplets, or surface active ingredients [83], [88].

Traditional “hard” tribology relies on stainless steel contacts. However, to mimic the softer oral surface (e.g., tongue and palate), soft tribology is used, involving soft, deformable surfaces. A preferred material at this point is polydimethylsiloxane (PDMS). PDMS is preferred due to its adjustable mechanical properties, simple fabrication, and the possibility to change its hydrophobic character [81], [89], [90].

Other materials, such as isolated whey protein hydrogels or pig tongue, have also been investigated to match better the roughness, viscoelastic properties, and wettability of the human tongue [91]–[94].

Such studies show how surface roughness, hydrophobicity, and modulus affect the magnitude of the friction coefficient, lubrication mechanisms, and transitions between lubrication regimes, emphasising the importance of selecting surfaces relevant to oral tribology. In addition, the wetting ability of the lubricant on the substrate significantly affects the coefficient of friction (COF). Therefore, careful consideration of tribopair surfaces is essential [91]–[95].

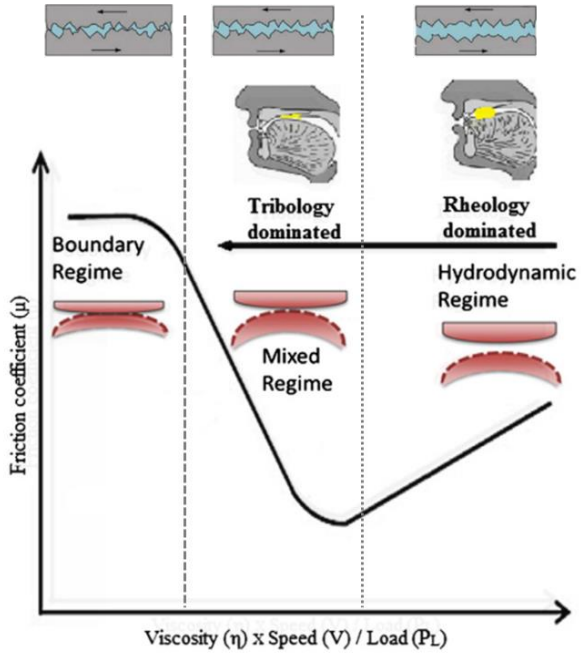


*Fig. 16. A typical Stribeck curve illustrating the relationship between the friction coefficient and the sliding or entrainment speed. It shows the three lubrication regimes: boundary (surface contact), mixed (partial separation), and hydrodynamic (full separation). Modified according to Corvera-Parades et al. (2022) and Prakash et al. (2013)* [74], [86].

The lubrication behaviour of samples is commonly analysed using the well-known Stribeck curve. Fig. 16 shows the friction coefficient as a function of sliding speed, illustrating the transition between the lubrication regimes: boundary, mixed, and hydrodynamic regimes.

The boundary regime takes place where the relative motion between the two surfaces is low and the lubricant viscosity is insufficient to generate full fluid film, indicating independence of the entrainment speed. In this regime, the surface separation is minimal, allowing asperities to come into direct contact. The increase in COF is, therefore, due to the fact that bulk lubricant is excluded from the contact as the surfaces are in full or close contact, and the applied normal load is fully supported by the contact between the two surfaces. The surface roughness correlates with the friction in the boundary regime. The higher the surface roughness, the more asperities are in contact. Consequently, the physico-chemical surface

properties and the chemical structure of the thin lubricating film covering the surfaces are two of the most critical factors determining the boundary regime.

The mixed lubrication regime occurs at moderately high sliding speeds, which is reflected in a decreasing coefficient of friction due to the entrainment of additional lubricant between the surfaces. As the speed increases, only the largest asperities remain in contact, resulting in this reduced friction. This trend continues with further increases in speed, as illustrated by the Stribeck curve (Fig. 16). During this regime, the normal load is supported partly by asperity contact and partly by hydrodynamic pressure. Hence, both the surface contact properties and the lubricant bulk properties are crucial. As the speed continues to increase, asperity contact diminishes until complete surface separation is achieved, at which point the coefficient of friction reaches its minimum value.

With further increase in sliding speed, the Stribeck curve enters the hydrodynamic lubrication regime, characterised by the rise in the coefficient of friction. This increase is attributed to the entrainment of sufficient lubricant of a continuous fluid film that separates the interacting surfaces and prevents direct contact. Hence, the friction coefficient and the separation distance between the surfaces increase with the lubricant entrainment speed and due to the hydrodynamic pressure of the fluid. In the hydrodynamic regime, the friction coefficient is primarily governed by the fluid dynamics, which are mainly determined by the bulk properties, i.e., the bulk rheological properties [71], [74], [83].

## 2.11 Light microscopy

Light microscopy is a basic imaging technique used to study the microstructural features of fluid gels – gelled microparticles dispersed in a continuous phase. The method magnifies samples using visible light and a lens system, which makes it an effective instrument for studying the size, shape, and aggregation behaviour of dispersed gel particles in semi-solid systems and providing direct visualisation of structural features that influence macroscopic properties [4], [96], [97].

Among the various light microscopy techniques, this work used bright-field microscopy to observe the microgel particles of the different fluid gels, providing critical insights into their microstructures. Conventional brightfield microscopy transmits light through samples, generating contrast by absorption or scattering [97]. Although limited for low refractive index systems, features such as particle shape and structure of agarose microgel particles can be visualised, for example, by staining with toluidine blue to enhance light absorption and contrast between the stained sample and illuminated background. These imaging techniques are essential for understanding how different conditions affect the gelling mechanism of fluid gel formation.

Typically, a standard compound light microscope consists of a light source (usually halogen or LED), a condenser lens that focuses the light onto the sample plane, objective lenses (20x to 100x magnification) that collect transmitted light, and an eyepiece. Light is transmitted through the specimen, and the image is obtained through the objective, which collects either transmitted or reflected light and further magnifies the image for direct observation through the ocular or digital recording (see Fig. 17) [97].

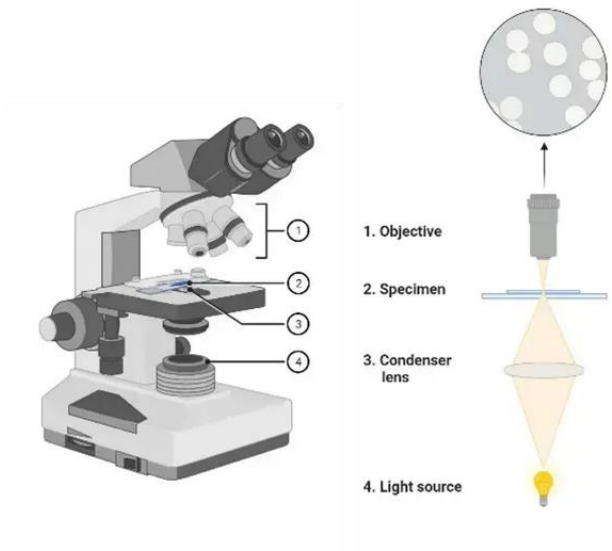


*Fig. 17. Principle and set-up of a Brightfield Microscope* [98].

However, the bright-field micrographs of the particulate fluid gel systems revealed insights such as unique features of morphology (size and shape), aggregate states, foremost, a denser network core structure, and aggregated chains protruding from the particle surfaces. These attributes are critical for understanding and predicting the textural, rheological, and tribological properties of the systems. In particular, they govern bulk rheological behaviour (e.g., yield stress, shear thinning, modulus) and flow dynamics during processing while directly influencing tribological interactions that determine oral texture perception and mouthfeel in food applications.

## 2.12 Particle size measurement

Particle size measurements were conducted using different agarose and co-solute concentrations to complement the microscopic examination and systematically characterise the different particle morphologies in fluid gels. In this work, the primary particle sizes and their aggregation play a key role in defining the microstructure and the mechanical strength of the final particulate gel network of fluid gels. Since the system is shear sensitive and the mechanical response under flow conditions is dictated

by the structural arrangement of the gel network, this relationship is crucial. These investigations are essential, as the rheological properties, textural attributes, and tribological performance of the material are significantly influenced by the particulate size distribution.

Laser diffraction based on static light scattering (SLS) was employed in this work to assess the particle size distribution. The light scattering technique estimates particle size by analysing the interaction between incident light and dispersed particles. When the light beam (e.g., laser) illuminates a particle suspension, the incident light undergoes scattering processes, including diffraction, absorption, refraction, and reflection. The spatial distribution and intensity of the scattered light are directly influenced by the particle size, shape, and refractive index contrast with the surrounding medium. However, the particle size is obtained from the angle dependent scattered intensities. The angular dependence of the scattered light intensity provides not only size information but also insight into particle interactions within the gel network. Hence, particle sizes can be detected from a few hundred nanometres up to several micrometres [99], [100].

Particles in fluid gels are three-dimensional objects that exhibit irregular morphologies/shapes rather than perfect spherical shapes. To quantify their size, the concept of equivalent spherical diameters is used, where irregular particles are represented by spheres with identical properties, such as weight, surface area, volume, etc. (Fig. 18). This allows the average particle size of the non-spherical shapes to be estimated based on the mean diameter [99].

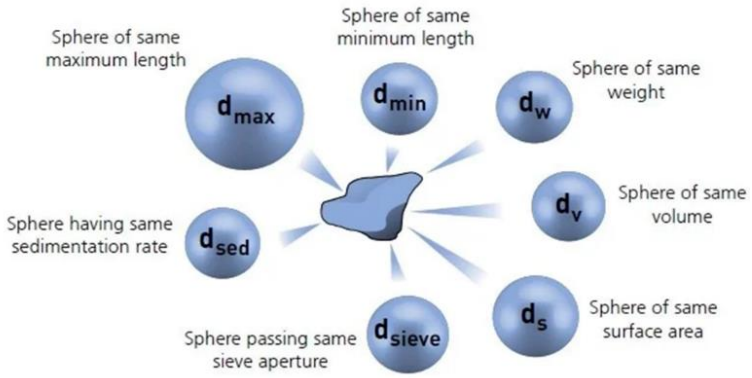


*Fig. 18. Concept of equivalent spheres* [101].

Additionally, this approach facilitates quantitative comparison of polydisperse systems using normalized frequency distributions ($q_x$) and cumulative distributions ($Q_x$). Depending on the analysis method, particle size distributions (PSDs) can be weighted by number, volume, or signal intensity, resulting in mean diameters such as the number-weighted D[1,0] and volume-weighted D[4,3], which offer distinct perspectives on particle population characteristics [102].

For fluid gels systems, the volume-weighted distribution (D[4,3]) is particularly relevant, as it correlates more effectively with the mechanical properties due to its emphasis on network forming gel particles. In Eq. 19, the volume-weighted mean diameter is calculated, where $n_i$ represents the number of particles in size class $i$, and $D_i$ is the mean diameter of that class [103]:

$$D[4,3] = \frac{\sum n_i D_i^4}{\sum n_i D_i^3} \tag{19}$$

Static light scattering (SLS) has proven valuable for the characterisation of fluid gel samples, operating on the principle of the Ryleigh, Mie, and Frauenhofer scattering theories. The fundamental relationship between scattering intensity ($I$) and particle properties, expressed as $I \propto D/\lambda$, with $D$ representing the particle diameter and λ the wavelength of incident light, determines the effectiveness of the technique.

However, Rayleigh scattering takes place when particles are smaller than the incident beam wavelength (D < 0.1 λ). In a Rayleigh scattering process, light is scattered equally in all directions, and therefore, no angular information can be obtained, information that is valuable in a laser diffraction test. Consequently, the Fraunhofer and Mie theories support most types of laser particle size analysers. Mie scattering applies when particles are similar in size to the light wavelength (0.1 λ<D< 10λ). Fraunhofer diffraction theory, on the other hand, is used for larger particles (D< 10λ), where the incident light is mainly diffracted at their outer edges. For very large particles, the scattering roughly resembles Mie scattering, with scattered intensities at narrow angles. For large particles, the scattering intensity is concentrated in the forward direction, usually at angles less than 10 degrees. Therefore, Fraunhofer diffraction is also referred as forward scattering[99], [100].

Polarisation Intensity Differential Scattering (PIDS) technology is utilized in the particle size analyser for this work. A schematic layout of the Laser Particle Size Analyser (LS 13320) is shown in Fig. 19, which illustrates the principle of dual detection systems that combine standard diffraction measurements with PIDS technology for comprehensive size analysis. PIDS provides primary size information for particles ranging from 0.017 to 0.4 μm. Diffraction patterns alone are not sufficient to distinguish between particles smaller than 0.4 μm in diameter [103].

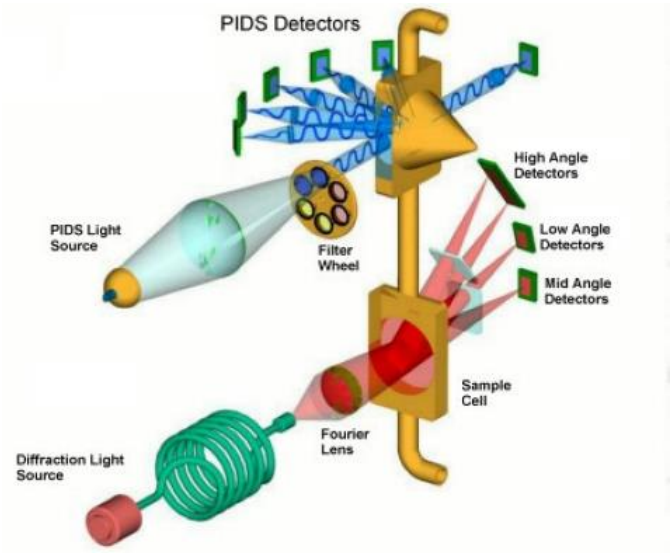


*Fig. 19: Optical system of the LS 13320* [103].

To ensure a homogeneous distribution of particles of varying sizes in the LS 13320 optical system, the sample suspension is continuously circulated through both sample cells. The standard setup includes an illumination source, a sample chamber where the particles interact with the illumination beam, a Fourier lens system to focus the scattered light, and photodetectors to capture the resulting light intensity patterns. A spatial filter and projection lens convert the laser radiation into a light beam before it enters the sample cell, where the suspended particles scatter the light in size-dependent patterns. The diffracted light is then focused onto three sets of detectors using Fourier optics: low-angle, mid-angle, and high-angle scattering. Additionally, the PIDS optical assembly incorporates a tungsten-halogen lamp along with three sets of vertically and horizontally polarized filters to produce polarized monochromatic light at three distinct wavelengths: 450 nm (blue), 600 nm (orange), and 900 nm (near-infrared, invisible) [103].

# 3 Limitation of post-gelation shear and the shift to controlled fluid gel formation

In the early stages of this work, preliminary experiments explored conventional methods for producing fluid gels, such as those used in gastronomic applications. One approach involves allowing a hydrocolloid like agarose to fully gel and solidify, followed by mechanical disruption – such as pureeing in a blender – to obtain a fluid gel.

The pureed gel concept is based on disrupting a pre-formed dense network to produce gel particles dispersed in a continuous liquid phase. While this approach is widely used in culinary contexts, it has significant scientific limitations for producing well-defined and reproducible fluid gels. Initial investigations have shown that such methods result in highly inconsistent microstructures and poorly characterised macroscopic properties.

Shear applied after gelation introduces a high degree of variability in key attributes (e.g., particle size and shape), depending on the specific equipment and processing conditions used for pureeing. Consequently, the viscoelastic and lubricating properties of the resulting fluid gels are inconsistent and difficult to interpret within a reproducible framework. This lack of control limits reproducibility and makes it difficult to establish clear structure-function relationships, particularly regarding the viscoelastic and lubricating properties of the resulting fluid gels. For instance, such inconsistencies are demonstrated by the representative microscopic image (Fig. 20) and the particle size distribution (Fig. 21). Fluid gels were prepared by applying shear after gelation using two different devices: the Ultra-Turrax Tube Drive (IKA -Werke GmbH & Co KG, Staufen, Germany), as shown in Fig. 20 (a-c) and Fig. 21 (a-c), and the Ultra-Turrax T25 Homogenizer, shown in Fig. 20 (d-f) and Fig. 21 (d-f).

These observations motivated a shift towards more controlled and scientific preparation methods. In response, gelation under shear, performed directly in a rheometer, was adopted. This method allows simultaneous control of gelation and mechanical disruption under defined and reproducible conditions, enabling precise tuning of microgel particle size, shape and network formation and the resulting sample properties.

As already mentioned, the advantage of this in-situ method for preparing fluid gels is that gelation occurs at a constant, continuously applied shear rate, ensuring controlled conditions, particularly for shear rate and, most critically, temperature. This approach provides control over critical process parameters such as shear rate, temperature rate, and gelation time, while also monitoring the viscosity change. As a result, it facilitates the systematic investigation of the relationships between formulation, processing conditions, and material functional properties.

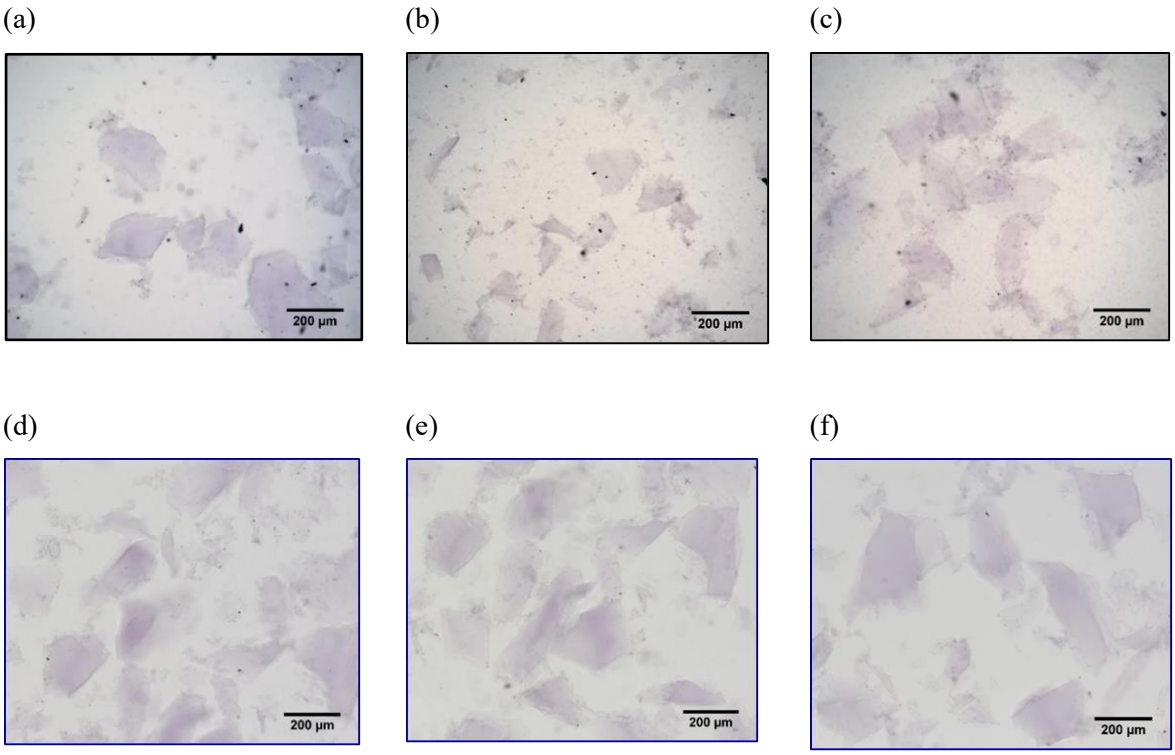


*Fig. 20. Microscope images of 1 wt% agarose fluid gels shared after gelation, prepared using different equipment: Ultra Turrax Tube Drive (a-c) and Ultra Turrax T25 Homogenizer (d-f).*

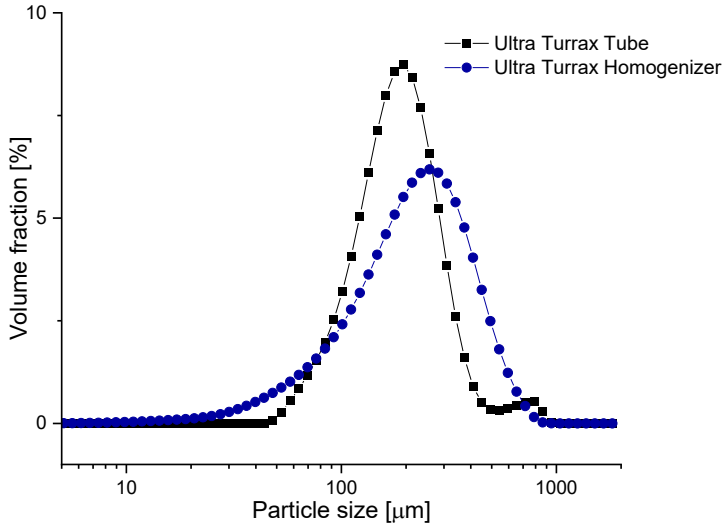


*Fig. 21. Particle size measurements of 1 wt% agarose fluid gels shared after gelation, prepared using different equipment: Ultra-Turrax Tube Drive and Ultra-Turrax T25 Homogenizer.*

Although the early experiments provided a useful reference and starting point, they also highlighted the scientific limitations of the shearing process after gelation. The decision to implement controlled gelation under shear in a rheometer laid the foundation for the experimental work presented in the subsequent publications. It advances understanding the underlying physical principles linking gelation dynamics, molecular interactions, particle morphology, and bulk behaviour.

# 4 Conclusion and outlook

This work provides comprehensive and fundamental insights into fluid gel formation, with a particular focus on how microstructure influences the viscoelastic, textural, and lubricating behaviour. By combining multiple characterisation methods – including microscopy, particle analyser, rheological and tribological measurements – a clear relationship was established between the microstructure of the gel particles, particularly their irregular, heterogenous morphology, and their macroscopic functional properties. These microstructural changes result from the dynamic competition between gelation and chain disruption during shear, directly impacting the rheological and tribological properties of the resulting fluid gels. This work has shown how particle size and shape change at different agarose concentrations, affecting bulk properties and frictional behaviour under thin-film conditions. Furthermore, a model was proposed a model that explain the underlying effect of microstructure on viscoelastic and flow behaviour.

In addition, atomic force microscopy was used to visualise, for the first time, the network structure of particulate agarose fluid gels. With increasing agarose concentration, the network becomes denser, exhibiting a clear structural gradient with decreasing in density towards the particle periphery. This change in network structure was found to be related to the viscoelastic properties. Based on these observations, a gelation mechanism under shear was proposed, highlighting how the agarose concentration governs the internal network structure of microgel particles. Not only the dense core, but also the peripheral region of the particles plays a crucial role in determining the interaction between the particles, which ultimately defines the length scale for their elastic response in the bulk. Moreover, the elasticity and friction properties were shown to depend on the ratio between the inner core and the peripheral regions. This is attributed to a broader mesh size distribution from the centre to the outer region, influenced by agarose concentration and competing time scales such as shear rate and molecular motion.

Further findings from this work show the critical role of sucrose as a co-solvent in modifying agarose gelation and, consequently, influencing fluid gel behaviour. Sucrose is proposed to affect the hydration dynamics within the systems by disturbing the water-agarose interactions and hindering helix formation. In the presence of sucrose, the hydration shells surrounding both sugar and agarose molecules are modified, ultimately altering the agarose-agarose association. This competition for hydration water affects network formation, leading to differences in particle morphology and aggregation behaviour that directly influence the viscoelastic and lubricating properties of the fluid gels. Varying the concentration of co-solvents significantly affects the size, shape, and interconnected network structure of microgel particles. Additionally, the gelation process is further influenced by the order of solvent addition. Whether sucrose or agarose is dissolved first reveals distinct molecular mechanisms underlying the structural formation of sucrose-modified agarose fluid gels. Studying the interplay between the agarose

polymer, water and sucrose provided further valuable insights into the physical and chemical process that govern the fluid gel formation. A deeper understanding of this interplay at the molecular level, as well as the competition for hydration water and hydrogen bonding between agarose and additives such as sugars, is therefore required to clarify and exploit the behaviour of fluid gel system.

Future investigations into molecular interactions in the presence of low molecular weight co-solvent could employ methods commonly used to study helix formation in polysaccharides. In addition, it would be interesting to investigate the effects of changing the solvent composition by introducing different sugars and examining their impact on the network formation, microparticle morphology, and the resulting viscoelastic and lubricating properties. In this work, agarose served as a model hydrocolloid for fluid gel preparation and for investigating gelation behaviour under shear. However, other gelling polysaccharides with similar characteristics may also be suitable. For instance, low-acyl gellan gum and κ-carrageen form firm, brittle gels in the presence of cations, a prerequisite behaviour for fluid gel formation.

These findings would significantly advance the understanding and optimisation of fluid gels for various applications, particularly in modifying the texture and flow behaviour of foods and beverages. The multifunctionality of fluid gels, ranging from pleasant mouthfeel in gastronomy to therapeutic applications in geriatric nutrition, demonstrates their important role in the advancement of food science, pharmaceutical technology and medical applications.

This adaptability, combined with their unique physicochemical characteristics, keeps sparking continuous research interest in investigating and designing of novel edible soft matter systems based on polysaccharides. Fluid gels are particularly promising for addressing challenges such as dysphagia, where precise control of texture, flow and lubrication behaviour is essential. Tailoring particle interactions not only enhances the functional properties of fluid gels but also paves the way for new applications requiring improved mechanical properties and specific targeted functionalities.

# 5 References


[1] A. Imeson, *Food stabilisers, thickeners and gelling agents*. John Wiley & Sons, 2011.

[2] P. Fischer and E. J. Windhab, "Rheology of food materials," *Current Opinion in Colloid and Interface Science*. 2011. doi: 10.1016/j.cocis.2010.07.003.

[3] D. Saha and S. Bhattacharya, "Hydrocolloids as thickening and gelling agents in food: A critical review," *J. Food Sci. Technol.*, vol. 47, no. 6, pp. 587–597, 2010, doi: 10.1007/s13197-010-0162-6.

[4] I. T. Norton, D. A. Jarvis, and T. J. Foster, "A molecular model for the formation and properties of fluid gels," *Int. J. Biol. Macromol.*, vol. 26, no. 4, pp. 255–261, 1999, doi: 10.1016/S0141-8130(99)00091-4.

[5] W. De Carvalho and M. Djabourov, "Physical gelation under shear for gelatin gels," *Rheol. Acta*, vol. 36, no. 6, pp. 591–609, 1997, doi: 10.1007/BF00367355.

[6] R. J. A. Moakes, A. Sullo, and I. T. Norton, "Preparation and characterisation of whey protein fluid gels: The effects of shear and thermal history," *Food Hydrocoll.*, vol. 45, pp. 227–235, 2015, doi: 10.1016/j.foodhyd.2014.11.024.

[7] I. Fernández Farrés, M. Douaire, and I. T. Norton, "Rheology and tribological properties of Ca-alginate fluid gels produced by diffusion-controlled method," *Food Hydrocoll.*, vol. 32, no. 1, pp. 115–122, 2013, doi: 10.1016/j.foodhyd.2012.12.009.

[8] M. H. Mahdi, B. R. Conway, and A. M. Smith, "Evaluation of gellan gum fluid gels as modified release oral liquids," *Int. J. Pharm.*, vol. 475, no. 1–2, pp. 335–343, 2014.

[9] A. Imeson, "3 Agar," *Food stabilisers, Thick. gelling agents*, p. 31, 2009.

[10] D. Nordqvist and T. A. Vilgis, "Rheological Study of the Gelation Process of Agarose-Based Solutions," *Food Biophys.*, vol. 6, no. 4, pp. 450–460, 2011, doi: 10.1007/s11483-011-9225-0.

[11] N. Russ, B. I. Zielbauer, K. Koynov, and T. A. Vilgis, "Influence of nongelling hydrocolloids on the gelation of agarose," *Biomacromolecules*, vol. 14, no. 11, pp. 4116–4124, 2013, doi: 10.1021/bm4012776.

[12] A. L. Ellis, T. B. Mills, and I. T. Norton, "Food Hydrocolloids The e ff ect of sugars on agar fl uid gels and the stabilisation of their foams," *Food Hydrocoll.*, vol. 87, no. August 2018, pp. 371–381, 2019, doi: 10.1016/j.foodhyd.2018.08.027.

[13] S. Maurer, A. Junghans, and T. A. Vilgis, "Impact of xanthan gum, sucrose and fructose on the viscoelastic properties of agarose hydrogels," *Food Hydrocoll.*, vol. 29, no. 2, pp. 298–307, 2012, doi: 10.1016/j.foodhyd.2012.03.002.

[14] N. Russ, B. I. Zielbauer, and T. A. Vilgis, "Impact of sucrose and trehalose on different agarose-hydrocolloid systems," *Food Hydrocoll.*, vol. 41, pp. 44–52, 2014, doi: 10.1016/j.foodhyd.2014.03.020.

[15] M. Deszczynski, S. Kasapis, W. Macnaughton, and J. R. Mitchell, "Effect of sugars on the mechanical and thermal properties of agarose gels," vol. 17, pp. 793–799, 2003, doi: 10.1016/S0268-005X(03)00100-0.

[16] M. Deszczynski, S. Kasapis, and J. R. Mitchell, "Rheological investigation of the structural properties and aging effects in the agarose/co-solute mixture," *Carbohydr. Polym.*, vol. 53, no. 1, pp. 85–93, 2003, doi: 10.1016/S0144-8617(02)00327-2.

[17] K. Nishinari *et al.*, "The effect of sucrose on the thermo-reversible gel-sol transition in agarose and gelatin," *Polym. J.*, vol. 24, no. 9, pp. 871–877, 1992.

[18] K. Nishinari, H. Zhang, and S. Ikeda, “Hydrocolloid gels of polysaccharides and proteins,” *Curr. Opin. Colloid Interface Sci.*, vol. 5, no. 3–4, pp. 195–201, 2000, doi: 10.1016/S1359-0294(00)00053-4.

[19] D. Saha and S. Bhattacharya, “Hydrocolloids as thickening and gelling agents in food: A critical review,” *Journal of Food Science and Technology*. 2010. doi: 10.1007/s13197-010-0162-6.

[20] J. M. Li and S. P. Nie, “The functional and nutritional aspects of hydrocolloids in foods,” *Food Hydrocoll.*, vol. 53, no. 2016, pp. 46–61, 2016, doi: 10.1016/j.foodhyd.2015.01.035.

[21] Alistair M. Stephen and Shirley C. Churms, “Introduction,” in *Food Polysaccharides and Their Applicatio*, Second., A. M. Stephen, G. O. Phillips, and P. A. Williams, Eds., Taylor & Francis Group, 2006.

[22] R. L. Whistler and J. N. BeMiller, *Industrial gums: Polysacchraides and Their Derivates*. Elsevier, 1993.

[23] M. Ghebremedhin, C. Schreiber, B. Zielbauer, N. Dietz, and T. A. Vilgis, “Interaction of xanthan gums with galacto- And glucomannans. Part II: Heat induced synergistic gelation mechanism and their interaction with salt,” *JPhys Mater.*, vol. 3, no. 3, 2020, doi: 10.1088/2515-7639/ab9ac9.

[24] C. Schreiber, M. Ghebremedhin, B. Zielbauer, N. Dietz, and T. A. Vilgis, “Interaction of xanthan gums with galacto- And glucomannans. part I: Molecular interactions and synergism in cold gelled systems,” *JPhys Mater.*, vol. 3, no. 3, 2020, doi: 10.1088/2515-7639/ab9ac8.

[25] P. Chinachoti, “Carbohydrates: functionality in foods.,” *Am. J. Clin. Nutr.*, vol. 61, no. 4, pp. 922S-929S, 1995.

[26] T. G. Mezger, *Das Rheologie Handbuch: Für Anwender von Rotations- und Oszillations-Rheometern*, 3. Auflage. Hannover: Vincentz Network GmbH & Co. KG, 2010.

[27] G. O. Phillips and P. a. Williams, *Handbook of hydrocolloids Second edition Edited by*. 2009. doi: 10.1533/9781845695873.

[28] D. Saha and S. Bhattacharya, “Hydrocolloids as thickening and gelling agents in food: A critical review,” *J. Food Sci. Technol.*, vol. 47, no. 6, pp. 587–597, 2010, doi: 10.1007/s13197-010-0162-6.

[29] E. R. Morris and D. a Rees, “Principles of biopolymer gelation: Possible models for mucus gel structure,” *Br. Med. Bull.*, vol. 34, no. 1, pp. 49–53, 1978, [Online]. Available: https://oup.silverchair-cdn.com/oup/backfile/Content_public/Journal/bmb/34/1/10.1093/oxfordjournals.bmb.a071457/2/34-1-49.pdf?Expires=1498217125&Signature=AES0EqT8QIeHyr9q5c8LrilltsbKH5MKXf021lWAlRiHKvHs~GHswVaHYIBMyRkSHE7moixaeQQH55iaq593W-Zr6gkg9VJyP3rV

[30] V. J. Morris, “Gels,” in *The chemical physics of food*, P. Belton, Ed., John Wiley & Sons, 2008, pp. 151–199.

[31] S. M. CLEGG, “Thickeners, gels and gelling,” in *Physico-Chemical Aspects of Food Processing*, 1995, pp. 117–140. doi: 10.1007/978-1-4613-1227-7.

[32] P.-G. De Gennes and P.-G. Gennes, *Scaling concepts in polymer physics*. Cornell university press, 1979.

[33] B. I. Zielbauer, N. Schönmehl, N. Chatti, and T. A. Vilgis, “Networks: From Rubbers to Food,” in *Designing of Elastomer Nanocomposites: From Theory to Applications*, Springer, 2016, pp. 187–233.

[34] P. Burey, B. R. Bhandari, T. Howes, and M. J. Gidley, “Hydrocolloid gel particles: Formation, characterization, and application,” *Crit. Rev. Food Sci. Nutr.*, vol. 48, no. 5, pp. 361–377, 2008,

doi: 10.1080/10408390701347801.

[35] M. Rinaudo, “Main properties and current applications of some polysaccharides as biomaterials,” *Polym. Int.*, vol. 57, no. 3, pp. 397–430, 2008, doi: 10.1002/pi.2378.

[36] D. A. Rees and E. J. Welsh, “Secondary and Tertiary Structure of Polysaccharides in Solutions and Gels,” *Angew. Chemie Int. Ed. English*, vol. 16, no. 4, pp. 214–224, 1977, doi: 10.1002/anie.197702141.

[37] N. Russ, B. I. Zielbauer, K. Koynov, and T. A. Vilgis, “Influence of nongelling hydrocolloids on the gelation of agarose,” *Biomacromolecules*, vol. 14, no. 11, pp. 4116–4124, 2013, doi: 10.1021/bm4012776.

[38] Z. H. Mohammed, M. W. N. Hember, R. K. Richardson, and E. R. Morris, “Carbohydrate Polymers Kinetic and equilibrium processes in the formation and melting of agarose gels,” *Cp*, vol. 36, pp. 15–26, 98AD.

[39] M. Tako and S. Nakamura, “Gelation mechanism of agarose,” *Carbohydr. Res.*, vol. 180, no. 2, pp. 277–284, 1988, doi: 10.1016/0008-6215(88)80084-3.

[40] D. Nordqvist and T. A. Vilgis, “Rheological Study of the Gelation Process of Agarose-Based Solutions,” *Food Biophys.*, vol. 6, no. 4, pp. 450–460, 2011, doi: 10.1007/s11483-011-9225-0.

[41] M. Tako, T. Teruya, Y. Tamaki, K. Uechi, and T. Konishi, “Molecular Origin for Strong Agarose Gels : Multi-Stranded Hydrogen Bonding Molecular Origin for Strong Agarose Gels : Multi-Stranded Hydrogen Bonding,” no. May, 2021, doi: 10.12691/jpbpc-9-1-2.

[42] S. Arnott, A. Fulmer, W. E. Scott, I. C. M. Dea, R. Moorhouse, and D. a Rees, “Agarose Double Helix and Its Function in Agarose-Gel Structure,” *J. Mol. Biol.*, vol. 90, no. 2, pp. 269–284, 1974, doi: 10.1016/0022-2836(74)90372-6.

[43] A. Nussinovitch, *Hydrocolloid applications: gum technology in the food and other industries*. Springer, 1997.

[44] S. Ablett, P. J. Lillford, S. M. A. Baghdadi, and W. Derbyshire, “Nuclear magnetic resonance investigations of polysaccharide films, sols, and gels. I. Agarose,” *J. Colloid Interface Sci.*, vol. 67, no. 2, pp. 355–377, 1978, doi: 10.1016/0021-9797(78)90020-6.

[45] G. Fittolani, P. H. Seeberger, and M. Delbianco, “Helical polysaccharides,” *Pept. Sci.*, vol. 112, no. 1, 2020, doi: 10.1002/pep2.24124.

[46] M. Deszczynski, S. Kasapis, and J. R. Mitchell, “Rheological investigation of the structural properties and aging effects in the agarose / co-solute mixture,” vol. 53, pp. 85–93, 2003.

[47] M. Watase, K. Nishinari, and T. Hatakeyama, “DSC study on properties of water in concentrated agarose gels,” *Food Hydrocoll.*, vol. 2, no. 6, pp. 427–438, 1988.

[48] G. Sworn, G. R. Sanderson, and W. Gibson, “Gellan gum fluid gels,” *Top. Catal.*, vol. 9, no. 4, pp. 265–271, 1995, doi: 10.1016/S0268-005X(09)80257-9.

[49] W. Frith, X. Garijo, T. Foster, and I. Norton, “Microstructural origins of the rheology of fluid gels. Special Publication.” Royal Society of Chemistry, 2002.

[50] I. F. Farrés, R. J. A. Moakes, and I. T. Norton, “Food Hydrocolloids Designing biopolymer fl uid gels : A microstructural approach,” *Food Hydrocoll.*, vol. 42, pp. 362–372, 2014, doi: 10.1016/j.foodhyd.2014.03.014.

[51] I. T. Norton, W. J. Frith, and S. Ablett, “Fluid gels, mixed fluid gels and satiety,” *Food Hydrocoll.*, vol. 20, no. 2-3 SPEC. ISS., pp. 229–239, 2006, doi: 10.1016/j.foodhyd.2004.03.011.

[52] A. Onuki, “Viscosity enhancement by domains in phase-separating fluids near the critical point: proposal of critical rheology,” *Phys. Rev. A*, vol. 35, no. 12, p. 5149, 1987.

[53] A. Gabriele, F. Spyropoulos, and I. T. Norton, “Kinetic study of fluid gel formation and viscoelastic response with kappa-carrageenan,” *Food Hydrocoll.*, vol. 23, no. 8, pp. 2054–2061, 2009, doi: 10.1016/j.foodhyd.2009.03.018.

[54] P. W. Cox, F. Spyropoulos, and I. T. Norton, “CHAPTER 6 - Effect of Processing on Biopolymer Interactions,” in *Modern Biopolymer Science*, S. Kasapis, I. T. Norton, and J. B. Ubbink, Eds., San Diego: Academic Press, 2009, pp. 199–224. doi: https://doi.org/10.1016/B978-0-12-374195-0.00006-9.

[55] M. Doi, S. F. Edwards, and S. F. Edwards, *The theory of polymer dynamics*, vol. 73. oxford university press, 1988.

[56] A. Gharsallaoui, B. Rogé, and M. Mathlouthi, “Water-disaccharides interactions in saturated solution and the crystallisation conditions,” *Food Chem.*, vol. 106, no. 4 SPEC. ISS., pp. 1329–1339, 2008, doi: 10.1016/j.foodchem.2006.12.068.

[57] C. Branca, S. Magazù, G. Maisano, F. Migliardo, P. Migliardo, and G. Romeo, “α,α-trehalose/water solutions. 5. Hydration and viscosity in dilute and semidilute disaccharide solutions,” *J. Phys. Chem. B*, vol. 105, no. 41, pp. 10140–10145, 2001, doi: 10.1021/jp010179f.

[58] D. Fioretto, L. Comez, S. Corezzi, and M. Paolantoni, “Solvent Sharing Models for Non-Interacting Solute Molecules : The Case of Glucose and Trehalose Water Solutions,” pp. 177–182, 2013, doi: 10.1007/s11483-013-9306-3.

[59] H. Uedaira and H. Uedaira, “Sugar-water interaction from diffusion measurements,” *J. Solution Chem.*, vol. 14, no. 1, pp. 27–34, 1985, doi: 10.1007/BF00646727.

[60] A. Gharsallaoui, B. Rogé, J. Génotelle, and M. Mathlouthi, “Relationships between hydration number, water activity and density of aqueous sugar solutions,” *Food Chem.*, vol. 106, no. 4 SPEC. ISS., pp. 1443–1453, 2008, doi: 10.1016/j.foodchem.2007.02.047.

[61] S. Maurer, A. Junghans, and T. A. Vilgis, “Impact of xanthan gum, sucrose and fructose on the viscoelastic properties of agarose hydrogels,” *Food Hydrocoll.*, vol. 29, no. 2, pp. 298–307, 2012, doi: 10.1016/j.foodhyd.2012.03.002.

[62] M. Watase, K. Kohyama, and I. L. Nishinari, “Effects of sugars and polyols on the gel-sol transition of agarose by differential scanning calorimetry,” vol. 206, pp. 163–173, 1992.

[63] M. Watase, K. Nishinari, P. A. Williams, and G. O. Phillips, “Agarose Gels : Effect of Sucrose , Glucose , Urea , and Guanidine Hydrochloride on the Rheological and Thermal Properties *,” pp. 1181–1187, 1990.

[64] T. A. Vilgis, “Gels: Model systems for soft matter food physics,” *Current Opinion in Food Science*. 2015. doi: 10.1016/j.cofs.2015.05.009.

[65] M. Deszczynski, S. Kasapis, W. MacNaughton, and J. R. Mitchell, “Effect of sugars on the mechanical and thermal properties of agarose gels,” *Food Hydrocoll.*, vol. 17, no. 6, pp. 793–799, 2003, doi: 10.1016/S0268-005X(03)00100-0.

[66] S. Kasapis, I. M. Al-Marhoobi, M. Deszczynski, J. R. Mitchell, and R. Abeysekera, “Gelatin vs polysaccharide in mixture with sugar,” *Biomacromolecules*, vol. 4, no. 5, pp. 1142–1149, 2003, doi: 10.1021/bm0201237.

[67] S. Shimizu and N. Matubayasi, “Gelation : The Role of Sugars and Polyols on Gelatin and Agarose,” 2014.

[68] K. Yang, Z. Wang, T. Brenner, H. Kikuzaki, Y. Fang, and K. Nishinari, “Food Hydrocolloids Sucrose release from agar gels : Effects of dissolution order and the network inhomogeneity,” vol. 43, pp. 100–106, 2015, doi: 10.1016/j.foodhyd.2014.05.005.

[69] A. S. SZCZESNIAK, “Classification of Textural Characteristics,” *J. Food Sci.*, vol. 28, no. 4, pp. 385–389, 1963, doi: 10.1111/j.1365-2621.1963.tb00215.x.

[70] M. PONS and S. M. FISZMAN, “Instrumental Texture Profile Analysis With Particular Reference To Gelled Systems,” *J. Texture Stud.*, vol. 27, no. 6, pp. 597–624, 1996, doi: 10.1111/j.1745-4603.1996.tb00996.x.

[71] J. Chen and J. R. Stokes, “Rheology and tribology: Two distinctive regimes of food texture sensation,” *Trends Food Sci. Technol.*, vol. 25, no. 1, pp. 4–12, 2012, doi: 10.1016/j.tifs.2011.11.006.

[72] K. T. Trinh and S. Glasgow, “On the texture profile analysis test,” *Proc. Chemeca*, no. September, pp. 23–26, 2012.

[73] M. Ghebremedhin, S. Seiffert, and T. A. Vilgis, “Physics of agarose fluid gels: Rheological properties and microstructure,” *Curr. Res. Food Sci.*, vol. 4, no. December 2020, pp. 436–448, 2021, doi: 10.1016/j.crfs.2021.06.003.

[74] S. Prakash, D. D. Y. Tan, and J. Chen, “Applications of tribology in studying food oral processing and texture perception,” *Food Res. Int.*, vol. 54, no. 2, pp. 1627–1635, 2013, doi: 10.1016/j.foodres.2013.10.010.

[75] J. R. Stokes, M. W. Boehm, and S. K. Baier, “Oral processing, texture and mouthfeel: From rheology to tribology and beyond,” *Curr. Opin. Colloid Interface Sci.*, vol. 18, no. 4, pp. 349–359, 2013, doi: 10.1016/j.cocis.2013.04.010.

[76] R. A. De Wijk and J. F. Prinz, “Mechanisms underlying the role of friction in oral texture,” *J. Texture Stud.*, vol. 37, no. 4, pp. 413–427, 2006.

[77] J. Chen, C. Karlsson, and M. Povey, “Acoustic envelope detector for crispness assessment of biscuits,” *J. Texture Stud.*, vol. 36, no. 2, pp. 139–156, 2005.

[78] M. Bourne, *Food texture and viscosity: concept and measurement*. Elsevier, 2002.

[79] J. Chen, M. Feng, Y. Gonzalez, and L. A. Pugnaloni, “Application of probe tensile method for quantitative characterisation of the stickiness of fluid foods,” *J. Food Eng.*, vol. 87, no. 2, pp. 281–290, 2008.

[80] J. R. Stokes, M. W. Boehm, and S. K. Baier, “Oral processing, texture and mouthfeel: From rheology to tribology and beyond,” *Curr. Opin. Colloid Interface Sci.*, vol. 18, no. 4, pp. 349–359, 2013, doi: 10.1016/j.cocis.2013.04.010.

[81] J. H. H. Bongaerts, K. Fourtouni, and J. R. Stokes, “Soft-tribology: Lubrication in a compliant PDMS-PDMS contact,” *Tribol. Int.*, vol. 40, no. 10-12 SPEC. ISS., pp. 1531–1542, 2007, doi: 10.1016/j.triboint.2007.01.007.

[82] H. Czichos and K.-H. Habig, *Tribologie-Handbuch*. 2010. doi: 10.1007/978-3-8348-9660-5.

[83] H. M. Shewan, C. Pradal, and J. R. Stokes, “Tribology and its growing use toward the study of food oral processing and sensory perception,” *J. Texture Stud.*, no. May, pp. 1–16, 2019, doi: 10.1111/jtxs.12452.

[84] J. Chen, Z. Liu, and S. Prakash, “Lubrication studies of fluid food using a simple experimental set up,” *Food Hydrocoll.*, vol. 42, pp. 100–105, 2014, doi: 10.1016/j.foodhyd.2014.01.003.

[85] M. E. Malone, I. A. M. Appelqvist, and I. T. Norton, “Oral behaviour of food hydrocolloids and emulsions. Part 1. Lubrication and deposition considerations,” *Food Hydrocoll.*, vol. 17, no. 6, pp. 763–773, 2003, doi: 10.1016/S0268-005X(03)00097-3.

[86] B. Corvera-Paredes, A. I. Sánchez-Reséndiz, D. I. Medina, R. S. Espiricueta-Candelaria, S. Serna-Saldívar, and C. Chuck-Hernández, “Soft Tribology and Its Relationship With the Sensory Perception in Dairy Products: A Review,” *Front. Nutr.*, vol. 9, no. May, 2022, doi: 10.3389/fnut.2022.874763.

[87] R. E. Rudge, E. Scholten, and J. A. Dijksman, “Advances and challenges in soft tribology with

applications to foods," *Curr. Opin. Food Sci.*, vol. 27, pp. 90–97, 2019, doi: 10.1016/j.cofs.2019.06.011.

[88] C. Pradal and J. R. Stokes, "Oral tribology: Bridging the gap between physical measurements and sensory experience," *Curr. Opin. Food Sci.*, vol. 9, pp. 34–41, 2016, doi: 10.1016/j.cofs.2016.04.008.

[89] G. E. Yakubov, T. E. Branfield, J. H. H. Bongaerts, and J. R. Stokes, "Tribology of particle suspensions in rolling-sliding soft contacts," *Biotribology*, vol. 3, pp. 1–10, 2015, doi: 10.1016/j.biotri.2015.09.003.

[90] L. MacAkova, G. E. Yakubov, M. A. Plunkett, and J. R. Stokes, "Influence of ionic strength on the tribological properties of pre-adsorbed salivary films," *Tribol. Int.*, vol. 44, no. 9, pp. 956–962, 2011, doi: 10.1016/j.triboint.2010.12.006.

[91] F. Di Cicco, F. Oosterlinck, H. Tromp, and A. Sein, "Comparative study of whey protein isolate gel and polydimethylsiloxane as tribological surfaces to differentiate friction properties of commercial yogurts," *Food Hydrocoll.*, vol. 97, no. September 2017, p. 105204, 2019, doi: 10.1016/j.foodhyd.2019.105204.

[92] H. S. Joyner, C. W. Pernell, and C. R. Daubert, "Beyond surface selection: The impact of different methodologies on tribological measurements," *J. Food Eng.*, vol. 134, pp. 45–58, 2014.

[93] H. S. Joyner, C. W. Pernell, and C. R. Daubert, "Impact of parameter settings on normal force and gap height during tribological measurements," *J. Food Eng.*, vol. 137, pp. 51–63, 2014.

[94] D. M. Dresselhuis, E. H. A. de Hoog, M. A. Cohen Stuart, and G. A. van Aken, "Application of oral tissue in tribological measurements in an emulsion perception context," *Food Hydrocoll.*, vol. 22, no. 2, pp. 323–335, 2008, doi: 10.1016/j.foodhyd.2006.12.008.

[95] R. E. D. Rudge, J. P. M. Van De Sande, J. A. Dijksman, and E. Scholten, "Uncovering friction dynamics using hydrogel particles as soft ball bearings," *Soft Matter*, vol. 16, no. 15, pp. 3821–3831, 2020, doi: 10.1039/d0sm00080a.

[96] J. M. Aguilera and D. W. Stanley, *Microstructural principles of food processing and engineering*. Springer Science & Business Media, 1999.

[97] D. B. Murphy and M. W. Davidson, *Fundamentals of Light Microscopy and Electronic Imaging*, Second Edi. Hoboken, New Jersey: John Wiley & Sons, 2012. doi: 10.1002/9781118382905.

[98] S. Panurav, "Bright Field Microscope: Definition, Parts, Working Principle, Application.," Microbiologynote. Accessed: Mar. 25, 2025. [Online]. Available: https://microbiologynote.com/bright-field-microscope-definition-parts-working-principle-application/

[99] P. A. Webb, "A primer on particle sizing by static laser light scattering," in *Technical Workshop Series: Introduction to the Latest ANSI/ISO Standard for Laser Particle Size Analysis*, 2000.

[100] A. Rawle, "Basic of principles of particle-size analysis," *Surf. coatings Int. Part A, Coatings J.*, vol. 86, no. 2, pp. 58–65, 2003.

[101] Malvern Panalytical, "Overview of Particles and Particle Properties," Azo Materials. Accessed: Mar. 28, 2025. [Online]. Available: https://www.azom.com/article.aspx?ArticleID=9936

[102] H. G. Merkus, *Particle size measurements: fundamentals, practice, quality*, vol. 17. Springer Science & Business Media, 2009.

[103] I. Beckman Coulter, "LS 13 320 Particle Size Analyzer Manual," *Instr. Use*, no. October, p. 246, 2011.

# 6 Publication list

**This thesis is based on the following publications:**

M. Ghebremedhin, [redacted]
*Physics of agarose fluid gels: Rheological properties and microstructure*, Current Research in Food Science, 4, 436-448, 2021

M. Ghebremedhin, [redacted]
*Molecular behavior of fluid gels – the crucial role of edges and particle surface in macroscopic properties*, Food & Function, 13, 6902-6922, 2022

M. Ghebremedhin, [redacted]
Effect of sugar molecules on the rheological and tribological properties and on the microstructure of agarose-based fluid gels, Frontiers in Soft Matter, 4, 2024

**Further publications:**

M. Ghebremedhin, [redacted]
*Meat-, vegetarian-, and vegan sausages: Comparison of mechanics, friction, and structure Meat-, vegetarian-, and vegan sausages: Comparison of mechanics, friction, and structure,* Physics of Fluids, 34, 2022

M. Ghebremedhin, [redacted]
*Interaction of xanthan gums with galacto- and glucomannans. Part II: Heat induced synergistic gelation mechanism and their interaction with salt,* Journal of Physics: Materials, 3, 2020

[redacted] M. Ghebremedhin, [redacted]
*Interaction of xanthan gums with galacto- and glucomannans. part I: molecular interactions and synergism in cold gelled system,* Journal of Physics: Materials, 3, 2020

[redacted] M. Ghebremedhin, [redacted]
*Soft gels from bovine colostrum*, International Journal of Gastronomy and Food Science, 23, 2021

# 7 Publications

## 7.1 Physics of agarose fluid gels: Rheological properties and microstructure

Marta Ghebremedhin[1], [redacted]

[1]Max Planck Institute for Polymer Research, Ackermannweg 10, 55128 Mainz

[redacted]

Published in *Current Research in Food Science*, 4, 436-448, 2021

The published version is available at: DOI: 10.1016/j.crfs.2021.06.003

Authors contributions:

M.G. carried out the conceptualisation, methodology, and the planning and execution of all experiments, including rheology, tribology, texture analysis, microscopy, and particle size analysis, as well as data analysis, visualisation, and manuscript drafting.

Current Research in Food Science 4 (2021) 436–448

Contents lists available at ScienceDirect

Current Research in Food Science

journal homepage: www.editorialmanager.com/crfs/

# Physics of agarose fluid gels: Rheological properties and microstructure

Marta Ghebremedhin [a,*], Sebastian Seiffert [b], Thomas A. Vilgis [a]

[a] Max Planck Institute for Polymer Research, Department of Polymer Theory, Food Science and Statistical Physics of Soft Matter, Ackermannweg 10, 55128, Mainz, Germany

[b] Department of Chemistry, Johannes Gutenberg University Mainz, Duesbergweg 10-14, 55128, Mainz, Germany

ARTICLE INFO

*Keywords:*
Agarose
Fluid/sheared gels
Microgel particles
Physical gelation
Rheology
Friction coefficient

ABSTRACT

Agarose, a strongly gelling polysaccharide, is a common ingredient used to optimize the viscoelastic properties of a multitude of food products. Through aggregation of double helices via hydrogen bonds while cooling under quiescent conditions it forms firm and brittle gels. However, this behavior can be altered by manipulating the processing conditions *viz* shear. For example, gelation under shear leads to microgel particles with large surface area, which in turn leads to completely different rheological properties and texture. Such fluid gels are shown to play an important role in texture modification of foods and beverages for dysphagia patients. In this study, different concentration of agarose fluid gel (0.5 % wt, 1 % wt and 2 % wt) were considered. Rheological measurements of the microgel particles showed an increase of storage and loss modulus with increasing concentration. However, 1 % wt fluid gel exhibited the lowest viscosity in the low shear range and the shortest LVE range. Furthermore, the effect on the microstructure and size of gel particles were also investigated by using light microscopy and particle size analysis. It was observed that as the concentration of agarose increased the particle size and unordered chains present at the particle surface decreases. Based on our results, we propose specific models suggesting the impact of the particle size, the concentration and the "hairy" projections on the rheological and tribological properties that could help in understanding the differences in characteristics of fluid gels.

## 1. Introduction

Hydrocolloids have a wide range of applications in the food, cosmetics and pharmaceutical industries due to their versatile functional properties (Nishinari, Zhang and Ikeda, 2000). To improve the quality and texture of the product, they are mainly used as emulsifiers, stabilizers, thickeners and gelling agents (Saha and Bhattacharya, 2010). Hydrocolloids are in most cases natural biopolymers such as polysaccharides that have a thickening and gelling effect when hydrated in water above a critical concentration and subjected to physico-chemical process. The interest of using polysaccharides in food applications is due to their ability to modify and improve the rheological and textural properties, which results in better mouth feeling by precisely controlling the texture and viscoelastic properties (Li and Nie, 2016; Nishinari et al., 2000).

In the present work, the underlying physico-chemical properties of fluid gels prepared using polysaccharides such as agarose are investigated to study their impacts on rheological, mechanical as well as tribological behavior. At this point, we emphasize that this study here is not motivated by food engineering properties, but rather on the fundamental physical question of soft material in model food systems such as fluid gels in this case. Fluid gels are particulate gel suspension and are formed by applying a shear field to a biopolymer solution while it gels (Farrés et al., 2014; Frith et al., 2002; Gabriele et al., 2010; Norton et al., 1999). Many elastic gel particles become immersed in a water phase and as a result, fluid gels exhibit novel rheological properties. They exhibit structures that remain textured and behave like a solid at rest, but exhibit fluid-like flow behavior above a critical value of applied stress (Norton et al., 1999). This change in formulation and the creation of food materials based on biopolymer gel materials with controlled microstructure enabled an even much broader range of applications in the food industry for potential use as a fat replacer in low energy food products but also for pharmaceutical applications for controlled drug release (Farrés et al., 2014; Mahdi et al., 2014). Furthermore, the fact that different texture properties can be produced from identical biopolymers simply by controlling the process conditions, such as shear, is a major advantage (Norton et al., 2006).

Agarose used in this study is the main gelling agent of agar-agar extracted from red algae (Rhodophyceae) and its linear polymer is composed of (1–3)-linked agarobiose units of β-D-galactopyranose (1–4)-

* Corresponding author.
*E-mail addresses:* ghebre@mpip-mainz.mpg.de (M. Ghebremedhin), vilgis@mpip-mainz.mpg.de (T.A. Vilgis).

https://doi.org/10.1016/j.crfs.2021.06.003
Received 31 December 2020; Received in revised form 13 June 2021; Accepted 15 June 2021

linked to 3,6-anhydro-α-L-galactopyranose (Imeson, 2009). Agarose solution undergoes very quickly a sol-gel transition upon cooling and form a three-dimensional network, due to its molecular structure and physico-chemical properties. During gelation under cooling, the single chains first associate via hydrogen bonds to form double helices. Further cooling leads to aggregation of these double helices (Russ et al., 2013). A two-step gelation mechanism for agarose was proposed: first, the connection of the randomly distributed coils by hydrogen bonds to form a double-helical association, followed by the aggregation of the double helices to form a tight three-dimensional network (Nordqvist and Vilgis, 2011; Russ et al., 2013). Furthermore, the coil to helix transition which takes place while cooling can be described by a mean field Zimm-Bragg approach (Nowak and Vilgis, 2004; Vilgis, 2015; Zimm and Bragg, 1959). Agarose gels are known for their tendency to release water and are susceptible to syneresis, which increases with decreasing of agarose concentration meaning that the water holding capacity increases with increasing agarose concentration. Syneresis in physical aqueous gels has been studied and discussed in detailed by Ako (2017) and Nishinari & Fang (Nishinari & Fang, 2016, 2017) and other workers cited therein. Water was noted to exude out at the surface of the gels and even though it resulted in an increase in concentration due to syneresis, a decrease in elastic modulus was reported due to network loosening and volume contraction (Nishinari & Fang, 2016, 2017). Such tendency of water release can be taken as an indication for the storage stability and is, additional to the texture properties, also of high importance for the mouthfeel (Fiszman and Durán, 1992; Nordqvist and Vilgis, 2011). Due to the dense three-dimensional network and the fast kinetics of the gelling process, agarose forms hard, highly elastic gels that result in poor mouthfeel (Nordqvist and Vilgis, 2011). A way to improve the mouthfeel can be therefore by manipulating the processing condition.

It has been proposed that when biopolymers are subjected to shear during their gelation, a competing mechanism occurs between gelation by physical crosslinking via hydrogen bonds and their breakup by the shear forces (De Carvalho and Djabourov, 1997). Furthermore, the gel structure formed by gelation under shear results from the competition between at least two time scales: shear rates and the molecular dynamics of the agarose chains. Moreover, the entire cascade of the internal modes of the polymer motion as expressed for the Rouse-Zimm model play a role under growing cluster size inside the forming gel particles (Doi and Edwards, 1986). Furthermore, cooling rate: influence first the center of mass of individual polymers, then the center of mass of the cluster, then the growing size slows the cluster dynamics further to smaller time scales and shorter spatial displacements. In addition, it was suggested that particle size and particle volume fraction are shear rate, temperature rate and concentration dependent and predict the properties of the fluid gel (De Carvalho and Djabourov, 1997; Norton et al., 1999). In turn, this led to the assumption that the order rate of the biopolymer is the crucial factor for particle growth. The particle size ($R$) dependence on these parameters can be described to lowest order using Einstein diffusion law at low Péclet number. This equation defines a relationship between particle size and viscosity $\eta_s$ of the sol phase, which is also determined by the shear rate $\dot{\gamma}$

$$R \simeq \left(\frac{k_B\, T}{6\pi\eta_s\dot{\gamma}}\right)^{1/3} \tag{1}$$

and $k_BT$ is the thermal energy. Furthermore, previous work proposed that the mechanism for the formation of the sheared gel is based on the initial nucleation and growth into spherical gel particles due to either the 'enrichment' process from the surrounding non-gelled matrix or due to the agglomeration of the nucleating particles that are forced together in the shear flow. These are then separated by shear forces, which constrain molecular ordering within the discrete particles (Norton et al., 1999). However, eq. (1) can only be viewed as a crude scaling estimate of the size of the gelled particles. The gelling process of agarose gels is a highly non-equilibrium process, as can be seen by the pronounced hysteresis under cooling and heating (refer Vilgis 2015 for a recent review) (Vilgis, 2015). Even at low cooling rates an equilibrium state gel will be reached. Therefore the competition between the time scales imposed by the shear rate during gelation and the broad range of polymer time scales will matter. Before the gelling starts the chains diffuse to lowest approximation according to a Rouse-Zimm model (Doi et al., 1988), suggesting that the center-of-mass diffusion constant $D_{CM}$ of the polymer chains in good solvent behaves as

$$D_{CM} \propto \frac{k_B T}{N^{1/2}} \tag{2}$$

where $N$ is the average dimensionless chain length of the polymer. Consequently the longest relaxation time $\tau$ of the chains is determined by $\tau \propto N^{1/2}$. Under cooling, the time scales change accordingly until the two neighboring chains are close enough to form helices, which introduce much lower time scales. The diffusion of the growing gel clusters slows down further and is again determined by its size, and thus the number of agarose chains involved. In consequence the shape of the particles become irregular, and long, extended excess parts, "tails", growing from a spherical or ellipsoid center.

Moreover, a detailed study of the lubrication behavior of agarose fluid gels with different concentration was investigated and showed that fluid gel particles with different elasticity influence their rheological and tribological behavior (Gabriele et al., 2010). Additionally, a strong effect of particle shape of blends of different biopolymers on viscosity properties was reported by Wolf et al. (Wolf et al., 2001).

In a recent paper by Holland et al. the formation of the "hairy" agar fluid gel particles was reported by comparing two different agars and concentration prepared by different processes, which resulted in different particle size and shape besides the presence or absence of "tails". From this study, it was concluded that the "tails" give the particles a much larger hydrodynamic volume than if only the core were present, and thus the effective volume of the "tails" present has an effect on the thermal and rheological behavior. They also conclude a distinct correlation between the dependence of particle size, shape and rheological properties on the type of agar that is used, the preparation method and the concentration (Holland et al., 2018).

Despite many previous studies, a precise gelling mechanism under shear and the resulting physical behavior of fluid gels is not yet fully understood, especially the resulting shapes.

Therefore, our study focuses on finding the detailed gelling mechanism of agarose as a function of concentration and its effect on fluid gel particle size and shape. The agarose fluid gels were prepared in a rheometer using a vane tool geometry for investigating their rheological and tribological properties. Rheological characterization such as: amplitude sweep, frequency sweep and flow sweep was carried out in order to understand in detail effect of concentration on gel network formation. Furthermore, texture analysis of fluid gel was evaluated and compared their results with the lubrication properties at the boundary regime for better assessment of the micro gel particle. Moreover, in order to understand the different behavior, gel particles were examined by microscopy and further reconfirmed by particle size determination. Additionally, scanning electron microscopy was conducted to provide further structural information of the bulk properties. Thus, with aforementioned analysis, we proposed a schematic model which describes the effect of agarose concentration on rheological and tribological properties of fluid gel.

## 2. Materials and methods

### 2.1. Materials

Agarose [CAS: 9012-36-6] (Fisher Scientific GmbH Schwerte, Germany) is used in the current study to understand the fluid gel mechanism. According to the manufacturer, the agarose powder has a gelling

temperature ($T_{gel}$) between 34 and 45 °C and reaches a gel strength of >100 g/cm$^2$.

### 2.2. Preparation of agarose fluid gels using a rheometer

For the respective concentration of 0.5 % wt, 1 % wt and 2 % wt, agarose was slowly added to Milli-Q water while stirring on a magnetic stirrer (500 rpm). As agarose is only soluble in hot water, the suspension was heated to 85 °C for about 20 min to ensure complete hydration of agarose while stirring in a sealed beaker.

The fluid gels were prepared using the Discovery HR-3 Rheometer (TA Instruments) with a cup (diameter = 30.37 mm) and vane (diameter = 28 mm and length = 42 mm) tool geometry of a concentric cylinder Peltier Jacket which can be electrically heated. The hot agarose solution (30 g) was poured into the cup preheated to 85 °C and then allowed to equilibrate for 5 min before measurements were started. To minimize evaporation during the measurement a two-piece cover was used.

Gelation was performed at a constant shear rate (400 $s^{-1}$) while cooling to 25 °C at a temperature rate of 1 °C/min and subsequently sheared for another 15 min at 25 °C at the shear rate of 400 $s^{-1}$. A pourable smooth gel was produced, showing structures that retain their textures at rest and behave like a solid, but exhibit liquid-like flow behavior when subjected to sufficient stress. The samples were then removed from the rheometer and stored at 4 °C for 24 h prior to the further characterization tests.

### 2.3. Rheological measurements

Dynamic viscoelastic and viscosity measurements of the different concentrations of the agarose fluid gels were performed by a Discovery HR-3 Rheometer (TA Instruments) using a 40 mm diameter parallel plate with a pre-set distance of 500 μm and a solvent trap to prevent evaporation. To avoid disrupting the fluid gel structure, the samples were placed on the geometry with a spoon and overflowing sample material was carefully removed with a spatula. All rheological measurements were performed in triplicate.

Amplitude sweep test was performed to examine the viscoelastic properties of the fluid gels. Using this method, storage ($G'$) and loss ($G''$) moduli were measured to describe the deformation behavior of the samples in the non-destructive range defined as the linear-viscoelastic (LVE) range. The limits of the LVE range and the characterization of the behavior after exceeding this range, which is defined as non-linear viscoelastic range, was also evaluated.

The oscillation deformation was applied at constant frequency $f = 1$ Hz and the storage ($G'$) and loss ($G''$) moduli were measured as a function of the strain $\gamma$ ranging between 0.001% and 1000% and at a temperature of 25 °C.

Frequency sweeps were performed in the range of 0.1–100 rad/s (0.0159–15.9 Hz) at a constant strain of 0.05%, hence within the LVE range of the amplitude sweep.

For the flow sweep test, rotational steady shear was performed to measure the flow behavior of the fluid gels and the viscosity as a function of the shear rate, increasing from 0.001 to 1000 $s^{-1}$ before decreasing the shear rate from 1000 to 0.001 $s^{-1}$. The two-step flow was carried out to examine the extent to which the hysteresis between the two stages, which indicate a change in viscosity, alters. In the present study, only the first step was considered for the viscosity investigation.

### 2.4. Light microscopy

The microstructure of the gel particles was studied by light microscopy using a Carl Zeiss Axio Scope.A1 microscope (Carl Zeiss AG, Oberkochen, Germany). Images were captured by using transmission bright field microscopy with the objective lenses magnifying 10×, 20×, and 40× and thus total magnifications of 100×, 200 x, 400 x. ImageJ software was used to insert the scale bar. The fluid gel samples have been diluted with Milli-Q water (1:5) after it was carefully transferred on a microscope slide. The diluted sample was stained with toluidine blue solution (0.1 % wt) to enhance contrast.

### 2.5. Particle size determination

To determine the particle size distributions, static light scattering experiments have been performed with the LS 13320 laser diffraction particle analyzer by Beckmann Coulter, enabling particle size detections in the range of 0.040–2000 μm.

The particle size was analyzed based on the theory of the Fraunhofer model, which is provided by the supplier's software. For this calculation, no additional data such as refractive index or absorption coefficient were needed. In order to avoid multiple scattering, samples were diluted by the particle size analyzer. The sample was pipetted into the measuring cell filled with distilled water until a certain obscuration was reached. Triplicate measurements were performed to determine the average distribution.

### 2.6. Texture analysis

For the texture analysis, the samples were stored and tested in transparent round boxes (d = 16.5 mm; h = 12 mm; Licefa GmbH & Co. KG, Germany) with airtight sealed lids. The gel strength measurements of the different concentration of the fluid gels were carried out at room temperature (22 °C) in triplicate measurements, using the Z005 All-roundLine texture analyzer by Zwick Roell attached with a 50 N cell.

The texture analyzer set-up was chosen as a cylindrical shaped stainless steel stamp (d = 1 mm), which penetrates the sample at a constant speed of 10 mm/min, with 15 cycles and a strain increase of 5% at the point of load application of each cycle. The plunger first punctured the sample for a strain of 5% of the initial height, returned to its starting position, and moved downwards to puncture the sample again to a strain increased by 5%. The processes were repeated until the sample was finally punctured to 75% strain of the initial height. In addition, deformation cycles were performed with no resting time in between. A trigger force of 0.002 N was set to determine a reproducible zero point.

### 2.7. Tribology

The friction of the different concentrations of produced fluid gels was measured using a Tribo-Rheometry Accessory available for Discovery HR-3 Rheometers (TA Instruments). The measurements were performed at 25 °C.

In the set-up for the tribology test, a three balls on a plate geometry was used, which for the upper part consisted of three spheres arranged on a circular plate with a radius of 15 mm and a lower plate attached with a silicon substrate. The contact surface of the tribopairs consisted of a stainless steel ball and a silicon rubber with a diameter of 40 mm and a thickness of 0.5 mm. The stainless steel balls provided by the manufacturer of the DHR-3 Rheometer are hemispheres with a diameter of 7.9375 mm (5/16″), which maintain point contact with the silicon surface. The hemispheres can be screwed onto the plate, which is attached to a helical-spring-like aluminum beam coupling suitable for load forces <20 N. This self-aligned design ensures uniform solid-solid contact and axial force distribution between the surfaces. This allows axial compliance to provide uniform axial force control for good alignment between the two surfaces and even distribution of normal force during rotation (specified by *Trios manual* 2019). For stable temperature control, the lower plate geometry is attached to the Peltier plate of the DHR-3 Rheometer. The tribology measurements were performed at 25 °C and fluid gel samples were carefully placed onto the silicon surface using a spatula. Normal forces of 3 N were used which resembles the normal forces applied during oral processing (He et al., 2018; Laiho et al., 2017; Nguyen et al., 2017), and the sliding speed was conducted from 100 to 1000000 μm/s by rotating the upper three ball geometry while the lower

plate geometry is stationary. The tribology tests were carried out in triplicate. Using the trios software the friction force $F_F$ and friction coefficient $\mu$ were calculated for the three balls on plate geometry, with the torque $M$ as an independent variable (see Table 1). Thus, the friction coefficient was calculated as the ratio of the measured friction force to the normal force $F_N$ and is given as a function of the sliding speed (μm/s) for each testing.

### 2.8. SEM

Scanning electron microscopy was implemented by using a Hitachi SU 8000 (Hitachi, Krefeld; Germany) with an acceleration voltage of 0.750 kV between 0.487 and 0.750 kV to examine the structure of the network of different concentration of the fluid gels. The fluid gels were cooled rapidly with liquid nitrogen before placing in a freeze dryer (Christ Alpha 1–2 LD plus). After drying overnight, the completely freeze-dried samples were then carefully placed on the SEM sample stubs and transferred to the microscope.

## 3. Results and discussion

### 3.1. Formulation and characterization of agarose fluid gels

Agarose fluid gels were prepared by using a rheometer having a cup and a vane geometry in a Peltier concentric cylinder system. The advantage of this "*in-situ*" method for preparing fluid gels is that gelation takes place at a constant, permanently imposed shear rate, thus ensuring the preparation of fluid gels under controlled conditions such as shear rate and especially temperature rate (De Carvalho and Djabourov, 1997). As agarose is only soluble in hot water it was heated up at 85 °C for 20 min with stirring to ensure complete hydration of agarose. Subsequently, the hot agarose solution was poured into the Peltier cup of the rheometer before measuring.

Fig. 1 exhibits the changes in viscosity for the different fluid gel concentrations of 0.5 % wt, 1 % wt and 2 % wt as the function of the time and the temperature. The sample was cooled from 85 °C to 25 °C at 1 °C/min rate and subsequently held for 15 min with a constant shear rate of 400 $s^{-1}$. The red line that shows a linear profile represents the temperature ramp and indicates the decreasing temperature between 85 °C and 25 °C, which was then kept at 25 °C. It can be seen for all agarose concentrations that there is an increase in viscosity with decreasing temperature. All three samples show a similar trend on change in viscosity: initially a gradual increase in viscosity as the temperature decreases; followed by a sharp increase in viscosity (indicated by the ellipse), which is later succeeded by a plateau region. Despite the higher viscosity within the whole measurement of the 2 % wt concentration sample, it also exhibits an earlier sharp increase of the viscosity (at about 33 °C) followed by the 1 % wt (at about 31 °C) and finally the 0.5 % wt (at about 27 °C) agarose sample concentration. The point where sharp increase in viscosity was detected is referred as 'inflection point' of the viscosity curve. This point is the one with the largest slope and thus indicates the largest change in viscosity value at a particular temperature. In this process, under imposed flow, a competing mechanism takes place between the gelation by physical cross-linking (via hydrogen bonds) and its breakup by the shear forces (De Carvalho and Djabourov, 1997).

The region where the viscosity shows a sharp rise and exhibits an

**Table 1**
The quantities used are $F_N$: normal force (N); $F_F$; friction force (N); M torque (Nm); d: arm length at 0.015 m.

| | |
|---|---|
| Friction coefficient $\mu$ | $\mu = \frac{F_F}{F_N}$ |
| Friction force $F_F$ | $F_F = \frac{M}{d}$ |
| Friction coefficient $\mu$ | $\mu = \frac{M}{dF_N}$ |

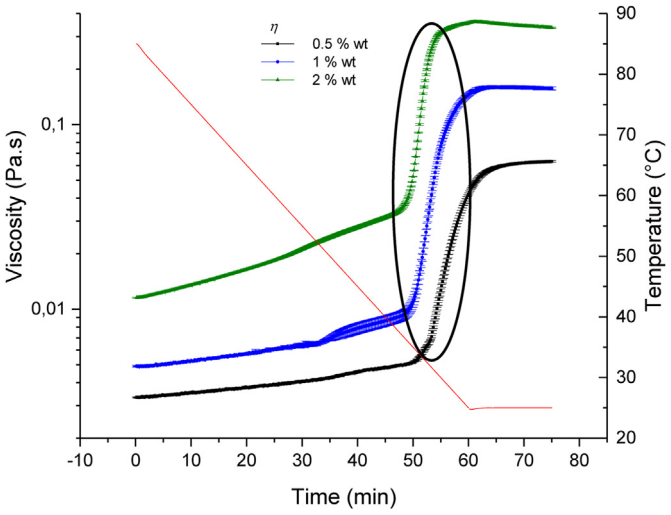


**Fig. 1.** Gelation under shear. Viscosity profile during agarose fluid gel production for the three concentrations: 0.5 % wt (black), 1 % wt (blue) and 2 % wt (green). The samples are subjected to a constant applied shear rate of 400 $s^{-1}$ and were cooled from 85 °C to 25 °C at 1 °C/min and then held for 15 min at 25 °C. The thin red line represents the change of temperature with respect to the time. (For interpretation of the references to colour in this figure legend, the reader is referred to the Web version of this article.)

inflection point is the temperature at which the polysaccharide molecules undergo a sol-gel transition under shear conditions and begin to gel (De Carvalho and Djabourov, 1997). The gradual increase of the viscosity between 85 °C (0 min) and approximately 55 °C (30 min) corresponds to an Arrhenius behavior, whereas the slight steeper slope between 55 °C and 45 °C (40 min) indicated the beginning of the gelation. Agarose molecules begin to aggregate, forming helices and join to small (nano and micro) networks throughout the sample. This is in agreement with previous publications, the increase in viscosity was attributed to the initial association of individual biopolymer chains and their beginning of ordering to form double helices that begin to aggregate, and subsequently the formation of small gel nuclei which starts around the gelation temperature of the biopolymer (Norton et al., 1999). Further detailed studies on agarose gels with different concentrations and their modification has been done, suggesting a two-step gelation mechanism, by formation of double helices via hydrogen bonds and their aggregation into a three-dimensional network (Nordqvist and Vilgis, 2011). In addition, confocal laser scanning microscopy (CLSM) was used to show for the first time the network structure of different agarose concentrations, densifying with increasing concentration (Russ et al., 2013). In fact, the observation that the gelling temperature increases with increasing agarose concentration is a consequence of faster gelation due to a higher number of particles. Thus, a higher agarose concentration is associated with a higher volume fraction and thus a higher viscosity (Norton et al., 1999).

For the agarose used in this study, the gelling temperature would be between 34 and 35 °C, as stated by the manufacturer. With further decreasing temperature, the starting gel nuclei further grow until an equilibrium particle size is reached, which is controlled by the shear regime. The temperature range in which the rapid viscosity increase occurs, indicated by the ellipse in Fig. 1, represents as mentioned above the aggregation of the multiple helices of the agarose chain polymers, into micro gel cluster.

In addition, fluid gel production with the rheometer was also performed with different shear rates, temperature rates, and other geometries such as parallel-plate and cone-plate geometry (refer the supporting information). It was observed that all these parameters have an effect on viscosity and modulus. As the shear rate decreased (800 $s^{-1}$, 400 $s^{-1}$, 200 $s^{-1}$), the viscosity increased as well as the modulus (shown in the

supporting information, Figure S1 (a-b)). This is in agreement with previously reported studies (Farrés et al., 2014; Gabriele et al., 2009; Norton et al., 1999). However, at shear rate of 800 $s^{-1}$, increasing the temperature cooling rate from 1 °C/min to 3 °C/min showed a shift in the sharp increase in viscosity to lower temperatures (by about 4 °C), but no change in viscosity and modulus at 25 °C. As already mentioned, due to the faster cooling rate, gel formation dominates and the average particle size becomes larger compared to the particle size for a slow cooling rate. Similarly, these previous studies emphasized that at high cooling rates, the shear forces are dominated by the gelation, resulting in the formation of larger gel particles.

At low cooling rates, applied shear dominates, resulting in the formation of smaller particles and a narrower size distribution (Gabriele et al., 2010; Moakes et al., 2015). However, in the case of the 3 °C/min cooling rate, even though the gelation was observed at a lower temperature, there was no effect on storage ($G'$) and loss ($G''$) moduli observed in the amplitude sweep. This can be explained by the fact that the shear rate of 800 $s^{-1}$ is fast enough so that the breakup of the gel clusters dominates their formation. Thus, the faster temperature rate has no effect on the formation of the gel particles. This would be different for the slower shear rates, leading to higher storage ($G'$) and loss ($G''$) moduli. In previous works, a strong dependence on the temperature rate has been observed in terms of particle size reduction as a function of the applied shear rate (Farrés et al., 2014; Gabriele et al., 2009; Moakes et al., 2015; Norton et al., 1999). Moreover, the size of fluid gel particles was shown to be determined by the dynamic equilibrium between two competing factors with respect to the formation process: the shear rate vs. the cooling rate, which determines the molecular dynamics. At the beginning the chain dynamics matters and the center of mass of polymer chains scales with the inverse square root of the chain length, ($D_{CM} \propto k_B T / N^{-1/2}$). When gel clusters are formed, the most important time scale is given by the cluster diffusion, i.e., $D_{Cluster} \propto k_B T / R_{Cluster}$. While the growth of the gel nuclei is primarily controlled by the cooling rate, the breakup of the particles are controlled mainly by the shear rate (De Carvalho and Djabourov, 1997).

In addition, fluid gel preparation was also conducted within the rheometer using a parallel-plate geometry with a diameter of 40 mm and a cone-plate geometry with a diameter of 40 mm, a cone angle of 2°, and a truncation of 56 μm (shown in the supporting information, Fig. S2 (a)). The measurements were performed at different shear rates and the effect of the different geometries on the formation of agarose fluid gels was considered. These gels were collected for optical microscopy examination or remained in the rheometer for further amplitude sweep tests (shown in the supporting information, Fig. S2 (b) and S3 (a-b)). The purpose of this procedure was to investigate the extent to which the different geometries affect particle formation. Microscopic studies of agarose fluid gels using both geometries revealed microstructures of gel particles with similar shape and unordered chains present on the surface, but a larger particle size distribution when using the parallel-plate geometry. The viscosity profiles and amplitude sweep tests with the cone-plate geometry resulted in lower viscosity and storage ($G'$) and loss ($G''$) moduli at 25 °C compared to the parallel-plate geometry as shown in the supporting information, Figure S2 (a-b). This is due to the uniform shear conditions in the entire cone gap during the measurements, resulting in smaller aggregates. The values of the moduli $G'$ and $G''$ showed the same trend, that is, an increase of the modulus value when applying a lower shear rate and using the parallel plate geometry. However, in this work, for further characterization of agarose fluid gels, a vane geometry was applied for the preparation of larger quantities of agarose fluid gels using a DHR-3 Rheometer.

### 3.2. Characterization and particle size distribution of agarose fluid gels

To investigate the microstructure of the agarose fluid gels, light microscopy was used initially in order to support the results of particle size and rheology measurements. Fig. 2 shows the microstructure of the gel particles of the different agarose concentration 0.5 % wt, 1 % wt, 2 % wt, prepared with the rheometer using the vane cup geometry. The samples were diluted with Milli-Q water and stained with toluidine blue solution (0.1 % wt) for better contrast. In all sample concentrations, agarose fluid gels appeared as spherical like structure with dense core and unordered chains present on the surface. Fluid gels prepared under controlled shear and temperature conditions using a rheometer were first described as “hairy” (irregularly shaped) particles by Norton et al. (1999). The microscope image for the 0.5 % wt sample reveals approximately 200 μm large particles with hairy parts. On the other hand, the microstructure of the particles of the 1 % wt fluid gels exhibit slightly smaller size than the 0.5 % wt samples and a less hairy structure on the surface. Fluid gel samples with 2 % wt agarose show much smaller size at about 50 μm with even less hairy parts. The results of these microscopic observations suggest that with increasing concentration the particle size reduces and the numbers of unordered chains on the surface (hairy parts) decrease.

In order to understand the differences in particle size and shape of fluid gel through microscopic investigations, the particle size distribution was examined. As particle size plays an important role in understanding rheological measurements and properties. Fig. 3 shows the particle size determination, which indicates variations in particle size distribution at different concentrations of agarose fluid gels. A slight decrease in mean particle size is observed with increasing concentration from 0.5 % wt to 1 % wt for fluid gels. However, a greater decrease in particle size is observed for the 2 % wt sample with significantly broader particle size distribution. Thus, this result of particle size determination is in accordance with the microscopic observations.

The observation that the particle size decreases with increasing concentration can be described to lowest order using Einstein diffusion laws at low Péclet number of a particle (see equation (1)). This equation defines a relationship between particle size and viscosity of the sol phase, which is also determined by the shear rate (De Carvalho and Djabourov, 1997). That is, increasing concentration results in a broader size distribution and a smaller mean diameter. These experimental observations are consistent with findings from the literature and previous studies that reported a trend of decreasing particle size with increasing concentration

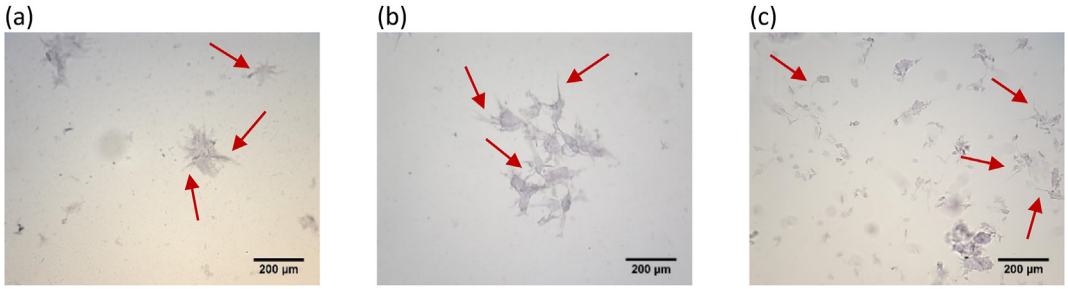


**Fig. 2.** Optical microscopy picture of (a) 0.5 % wt, (b) 1 % wt and (c) 2 % wt agarose fluid gel particles stained with toluidine blue. The red arrows indicate the chains i.e. the “hairs” on the microparticle surface. (For interpretation of the references to colour in this figure legend, the reader is referred to the Web version of this article.)

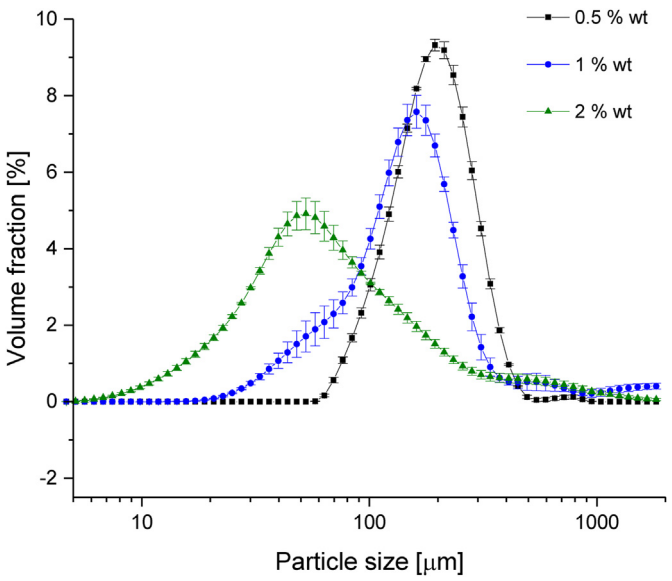


**Fig. 3.** Particle size distribution of fluid gel particle with different agarose concentration.

of various biopolymers such as agar, alginate, whey protein and carrageenan (Farrés et al., 2014; Garrec and Norton, 2012; Norton et al., 1999).

### 3.3. Rheological properties

In order to understand the viscoelastic and flow properties of the different concentrations of agarose fluid gels, these systems were characterized with various rheological methods. Moreover, it was of interest to investigate how the size and shape of the gel particles influence this mechanical behavior.

Fig. 4 shows the result of the amplitude sweep of the different concentrations of the agarose fluid gels. In Fig. 4, the mean value and the standard deviations of the elastic and viscous moduli as a function of the strain for the different fluid gel concentrations is plotted. For all samples, storage ($G'$) and loss ($G''$) moduli exhibit a constant plateau value of $G'$ and $G''$ followed by a decrease in moduli as the applied strain increases. As expected, storage ($G'$) and loss ($G''$) moduli increase with increasing concentration of agarose. The 2 % wt fluid gel sample measurement displays approximately 920 Pa as the highest storage modulus, whereas the storage modulus of the 1 % wt sample is lower with a value of about 370 Pa and the storage modulus for the 0.5 % wt exhibits the lowest value of about 130 Pa. Thus, all samples exhibit unsurprisingly an elastic dominated behavior (gel-like or solid structure) at the linear viscoelastic (LVE) range.

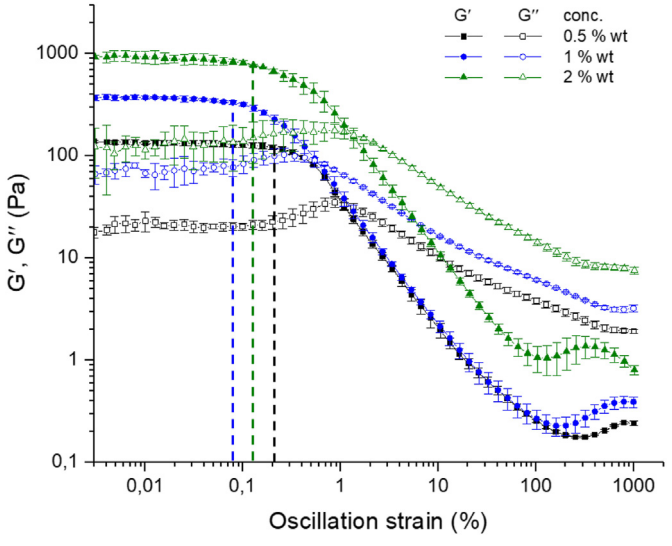


**Fig. 4.** Amplitude sweep profile of agarose fluid gels with 0.5 % wt (black), 1 % wt (blue) and 2 % wt (green) concentration. Dependence of G′ (filled symbols) and G″ (empty symbols) on strain at constant frequency ($f$ = 1 Hz) and temperature (T = 25 °C). The vertical dashed lines indicate the limit of the LVE range $\gamma_L$ (also called yield point). (For interpretation of the references to colour in this figure legend, the reader is referred to the Web version of this article.)

Furthermore, each concentration of the fluid gels exhibits a slight increase and a maximum of the loss modulus $G''$ at larger deformation (between approximately 0.2% and 2% oscillation strain) before the final decrease; more pronounced for the 0.5 % wt and 1 % wt, although a bump for the sample with 0.5 % wt is more distinct. This observation of the $G''$ peak with increasing deformation suggests an interconnected network of gel particles formed by cross-linked polymers. The rise of $G''$ is an indication of an increase in the deformation energy transferred to the environment before parts of the inner structure are deformed and finally the interparticle connectivity is disturbed. The occurrence of the $G''$ bump could be explained by the relative motion of molecules of free dangling chain ends, such as the disordered chains as mentioned earlier, which are found at the surface of the "hairy" particles. Besides, long network bridges which are not permanently embedded in the network could be responsible for this observation (Hyun et al., 2002; Hyun et al., 2011; Mezger, 2010). In addition, the $G'$ bump at high deformation larger than 100–1000% strain can be attributed to the jamming of the gel particles, leading to an earlier occurrence of the 2 % wt fluid gel due to the dense packing and higher concentration, which in turn yield stiffer and less deformable particles, followed by the 1 % wt and 0.5 % wt agarose fluid gels.

When comparing the LVE range within the different concentrations, a nonlinear correlation with the concentration is revealed in contrast to the linearity of the moduli with the concentration. The plateau where structures remain intact is known as the linear viscoelastic (LVE) range. In Fig. 4, the vertical dashed lines indicate the limit of the LVE range (also called yield point), i.e. the range until which the tests are performed without destroying the samples or initiating flow through the required applied strain. The LVE limit $\gamma_L$ was calculated as the strain required to decrease the storage modulus ($G'$) by 10% from the LVE range. This reveals that the 1 % wt sample having the shortest LVE range with $\gamma_L = 0.08$ ($\pm 0.03$) %, followed by the 2 % wt sample with $\gamma_L = 0.15$ ($\pm 0.07$) % and finally the 0.5 % wt sample displaying the highest limit of LVE value with $\gamma_L = 0.21$ ($\pm 0.03$) %. Earlier studies on fluid gels conclude that an increase in hydrocolloid concentration results in an increase in storage modulus, but also an increase in the limit of the LVE range, due to enhanced particle interaction (Ellis et al., 2017).

For better understanding and further interpretation of the obtained findings, based on all experimental results mentioned earlier, such as microscopy examinations, particle size determination and amplitude sweep tests, a schematic model is shown in Fig. 5.

As can be seen in Fig. 5 (a), the particles of the 0.5 % wt fluid gel sample are largest with a very high proportion of disordered chains projecting at the surface. The 1 % wt gel particles (Fig. 5 (b)), illustrated here with slightly smaller size, exhibit fewer chains on the particle surface. Finally, the 2 % wt fluid gel samples show the smallest particle sizes with considerably fewer chains (hairy parts) on the particle surface. As mentioned before, the increase of the storage modulus with increasing agarose concentration can be explained by increased particle interaction, especially the higher percolation between the smaller particles, which is caused by the higher volume fraction. This is clearly indicated for the 2 % wt sample compared for the 1 % wt and more distinctly for the 0.5 % wt fluid gel.

However, when looking back at the LVE range (Fig. 4), the observed nonlinearity with respect to the concentration can be visualized with the

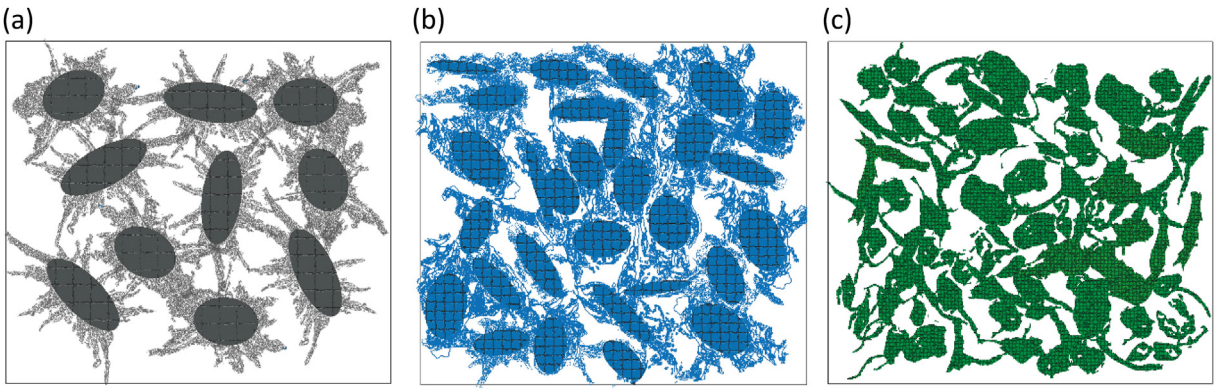


**Fig. 5.** Schematic model of fluid gel particle size and shape with varying agarose concentration (a) 0.5 % wt, (b) 1 % wt and (c) 2 % wt. The fluid gel of 0.5 % wt agarose is drawn with slightly larger particle size compared to 1 % wt and higher proportion of unordered chains on the surface. Whereas the 2 % wt sample shows the smallest particle size and the least proportion of unordered chains on the surface.

illustration in Fig. 5. The LVE limit of the 2 % wt sample, which is between that of the 0.5 % wt and 1 % wt sample, can obviously be explained by the higher uniform density due to the volume fraction and smaller particles that require some deformation until the particles slide against each other and finally the whole superstructure breaks down. In contrast, when comparing the LVE range of the 0.5 % wt with the 1 % wt sample, the latter exhibits a shorter LVE range. This is not consistent with the previous explanations and understanding. Since, as mentioned above, the particles of the 1 % wt sample are slightly smaller but have a larger volume fraction than those of the 0.5 % wt sample. However, this observation can be explained by the larger proportion of the hairy parts of the particles of the 0.5 % wt sample, which begin to interpenetrating one another and entangled with increasing deformation, resulting in an extended LVE range.

To investigate the flow behavior of the same fluid gel samples and to support the results of the previous amplitudes sweep, Fig. 6 shows the shear rate dependent viscosity profiles obtained by performing the flow sweep test.

The viscosities were measured initially for increasing and subsequently decreasing shear rate. As expected, the viscosity of all tested fluid gels decreases with increasing shear rate and thus shows a shear-thinning behavior. Moreover, an increase in viscosity with increasing agarose concentration is observed, especially noticeable at higher rates above 100 $s^{-1}$. At these high shear conditions, the particles move along each other and are strongly deformed under the exposed stress. Since fluid gels produced with higher agarose concentrations yield stiffer and less deformable particles, the result is an increase in shear viscosity at high shear conditions.

This trend is in agreement with previous studies of viscosity measurements in relation to hydrocolloid concentrations, which show this typical tendency of linearity between the increasing shear viscosity with increasing concentration of hydrocolloids (Ellis et al., 2017; Garrec et al., 2013; Moakes et al., 2015).

However, considering low shear rates, a discrepancy can be observed, as shown in Fig. 6 (b). While the concentration of the 2 % wt fluid gel still has the highest viscosity, when comparing the 0.5 % wt with the 1 % wt sample, it can be seen that the former has a higher viscosity despite a lower concentration. Again, this cannot be explained by considering particle sizes (approximately the same size) or volume fraction only and seemingly contradicts according to the current explanations and understanding. Referring to the schemes in Fig. 5, it is likely that the higher proportion of the projecting tails play a significant role. At rest, the chains of the aggregate helices become entangled with each other, which leads to higher friction and thus an increase in viscosity at this very low shear rate. This nonlinear trend and observation applies to both the upward and downward curves of the flow sweep test.

Further, Fig. 7 (a) shows the result of the frequency sweep of the respective fluid gels, with storage ($G'$) and loss ($G''$) moduli in dependence of frequency at constant strain ($\gamma = 0.05\%$). This was carried out to describe the time-dependent behavior of the fluid gels and to understand the mechanical reaction at small oscillation strains in the range of non-destructive deformations, i.e. in the LVE range. Also here it can be visualized, how the moduli increase as expected with increasing concentration. Moreover, it can be seen that the moduli of the respective

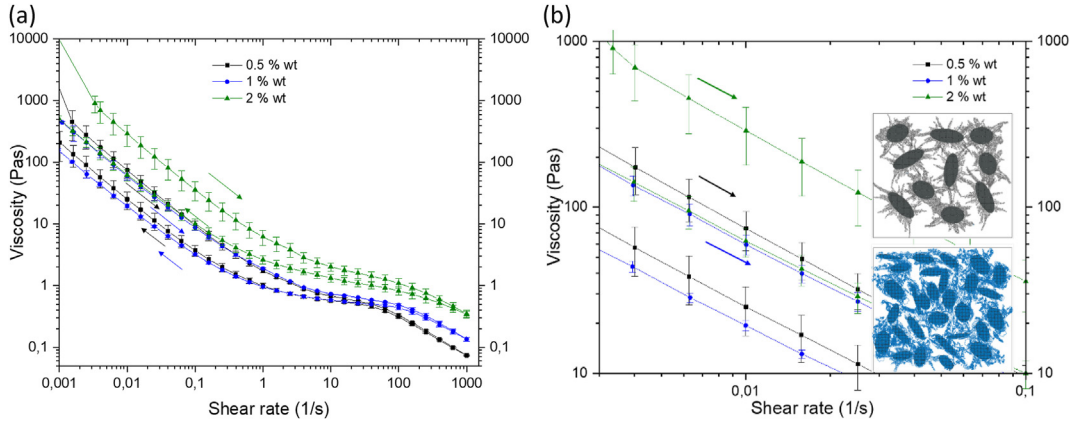


**Fig. 6.** (a) Flow behavior of the agarose fluid gel with different concentration: 0.5 % wt (black), 1 % wt (blue) and 2 % wt (green). (b) Viscosity of the different fluid gel concentrations at low shear rate, with the 0.5 % wt concentration having a higher viscosity value than the 1 % wt concentration due to entanglement of the chain on the particle surface. (For interpretation of the references to colour in this figure legend, the reader is referred to the Web version of this article.)

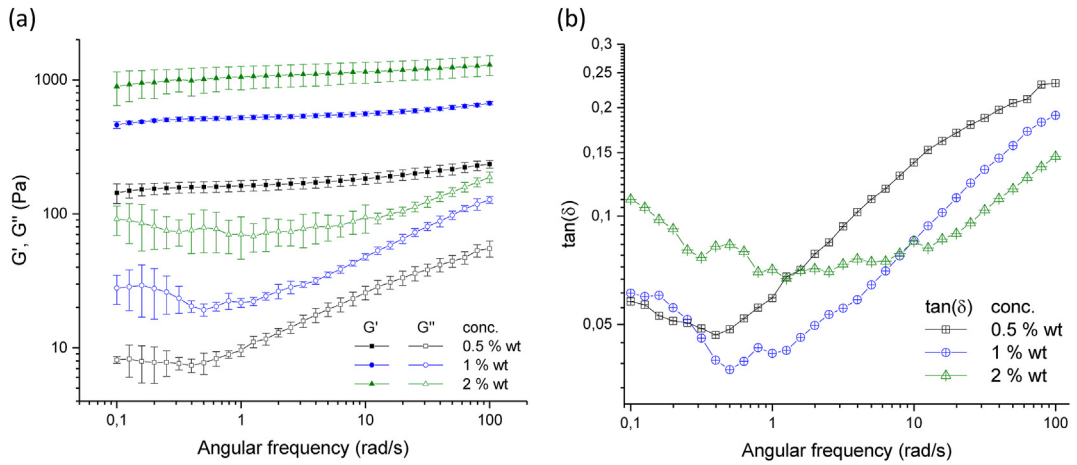


**Fig. 7.** (a) Frequency dependence of storage and loss moduli G′ (filled symbols), G″ (empty symbols) and (b) Frequency dependence of tan (δ) at constant strain ($\gamma$ = 0.05%) and temperature (T = 25 °C) for agarose fluid gels with different concentrations 0.5 % wt (black), 1 % wt (blue) and 2 % wt (green). (For interpretation of the references to colour in this figure legend, the reader is referred to the Web version of this article.)

fluid gels increase slightly with increasing frequency. This can be explained as follows: The fluid gel particles moving at a certain frequency experience only a negligible change at low frequency. They are surrounded by other particles which, when sheared slowly, all followed simultaneously. As the frequency increases, the particle's movement becomes faster. The dangling chains on the particle surfaces, which are quite flexible, also move and show an earlier motion as the frequency increases, while the centers move more sluggishly. With increasing frequency, the particles are pushed together and interfere with each other, as do these dangling chains. Since the agarose gel particles are in a good solvent, this causes the hydrophilic chains to protrude from the surface of the particles into the continuous phase due to the surrounding water. Thus, the higher the frequency, the more the chains can interfere with each other. When these chains move faster and follow with the frequency, the excluded volume becomes smaller. This in turn implies that the chains interfere even more with each other. This description is consistent when considering the loss moduli as a function of frequency for all three fluid gels in Fig. 7 (a). While the 0.5 % wt fluid gel sample shows an increase in loss modulus ($G''$) at a frequency below 1 rad/s, the 1 % wt sample displays a $G''$ increase above 1 rad/s, whereas the 2 % wt sample reveals a relatively constant $G''$ curve over the entire frequency range. As already explained, the chains on the surface swing with increasing frequency and collide against the neighboring chains causing a higher resistance. As a result, the loss modulus i.e. the viscous part increases with the frequency. In other words, the loss modulus can be attributed to the movement of the dangling chains on the surfaces. Since the "hairy" parts decrease with increasing concentration, this effect is most pronounced for the 0.5 % wt sample, followed by the 1 % wt and finally barely for the 2 % wt agarose fluid gel sample. As mentioned previously, it is known that agarose releases water and that syneresis is higher with decreasing concentration (Nishinari & Fang, 2016, 2017). The microgel particles consist of a center with a dense three-dimensional network that retards syneresis and has a higher water-binding capacity than the dangling chains, which have a lower water-binding capacity compared to the bulk systems. This is in accordance with previous studies on water properties in concentrated agarose gels by Watase, M., Nishinari, K., and Hatakeyama, T. (Watase et al., 1988). Based on differential scanning calorimetry measurements, these authors proposed a higher water binding capacity of the junction zones i.e. in the denser network region. In this study, however, this is more likely to be the case with samples containing 2 % wt fluid gels with a denser network core and less "hairy" parts. Whereas the 0.5 % wt samples have a less dense network core, but much more "hairy" parts on the microparticle surface. At this point it can be noted that more syneresis would be expected with the 0.5 % wt and 1 % wt fluid gel samples than with the 2 % wt sample. However, the exuded water on the surface of the microgel particles might have an impact on the frequency-dependent properties of the fluid gels, as it could interact with the dangling chains of the particulate gel suspension. Thus, this released water is held by the dangling chains through hydrogen bonding. In addition, at the same time, the released water also acts as a solvent on the surface of the microgel particles and is therefore responsible for the unique smooth texture and plasticity of the agarose fluid gel. The water released is very fast in its dynamics and the diffusion of the water molecules to the surface depends on their mobility and speed. Additionally, the water has a much faster time scales than the polymer chains. It is not clarified to what extent these water molecule dynamics contribute significantly to the frequency dependence of the storage and loss moduli compared to the "hairy" parts. Nevertheless, the contribution of the dangling chains to the frequency dependence can be supported by other results in this study and thus play a crucial role in the mechanical behavior. On the other hand, it has been reported that the "hairy" particles have a larger hydrodynamic volume, which in turn affects the rheological properties and causes an increase in moduli (Holland et al., 2018). This in turn could be attributed to the increase in storage $(G')$ modulus for all three samples within these frequency ranges.

To obtain further information, tan ($\delta$) was plotted against frequency for the frequency sweep test as shown in Fig. 7 (b). According to the tan ($\delta$) profile, which is dimensionless and describes the ratio of the two parts of the viscoelastic behavior $G''/G'$, the value hardly differs with increasing frequency for 2 % wt agarose. This suggests that the 2 % wt sample is relatively constant over the entire frequency range and less frequency dependent compared to the other samples. On the other hand, for the fluid gel samples of 0.5 % wt and 1 % wt, a lower tan ($\delta$) is observed at very low frequency or at rest. With increasing frequency, however, there is a sharp increase in tan ($\delta$) and thus an increase in the viscous part, respectively a higher proportion of the loss modulus. The lower frequency dependence of the 2 % wt sample can be explained by the fact that the gel particles are densely packed and have a higher percolation. Therefore, the particles experience only a negligible change with frequency.

Conversely, the particles are less densely packed for the 0.5 % wt and the 1 % wt samples and therefore show an increase in loss modulus and viscous ratio at higher frequencies. Therefore, an easier flow behavior at higher frequency is obtained. When comparing the 0.5 % wt with the 1 % wt sample, this can perhaps be explained by the presence of the hairy part in addition to the previous explanation by the higher dependence on frequency due to packing. The tails on the surface of the particle, entangled at a very low frequency, have a higher elasticity, which

corresponds to a low tan ($\delta$). The sharp increase in the tan ($\delta$) could possibly be caused by the fact that the entangled hairy part becomes disentangled under shear or frequency causing the particles to slide against each other and the sample to flow.

For the 0.5 % wt sample, this rise occurs earlier and ends at a higher tan ($\delta$) value due to the higher proportion of the hairy parts that has disentangled. Additionally, it is obvious that 0.5 % wt has a lower concentration and thus a lower network structure, i.e. a lower elastic proportion.

### 3.4. Texture analysis

In previous publications on fluid gels, texture analysis was carried out on quiescently cooled agarose gels and the behavior obtained was assumed to be that of the individual particles of fluid gels of the same concentration. This was based on the findings that textural properties of the individual particles in a fluid gel system are the same as that of a quiescently cooled gel of the same hydrocolloid concentration (Gabriele et al., 2010).

To examine the textural properties of each of the fluid gel samples, the samples were penetrated by a stainless steel plunger. Textural properties of each of the fluid gel samples are shown in Fig. 8. Therefore, all the samples are punctured for a certain distance in strain and the responsive force was measured, which can be used to examine the gel strength and elasticity of the particles. This was carried out by performing a multi cycle deformation test in which the strain was gradually increased by 5% at each deformation cycle until the final strain set at 75%. The plotted force-strain (force-displacement) curves in Fig. 8 represent the resistance of the sample to deformation and indicate the elastic properties resulting from the slope at initial strain and hence the initial force response, respectively, the linear range of the initial force-strain curves. With each cycle and increasing strain, the responsive force also increased. This trend is observed for all fluid gels under investigation. As expected, the measured force of the respective deformation cycles increases with increasing concentration.

Nevertheless, the increase in measured force increases less and less with each successive cycle. As the concentration of fluid gels decreases, the maxima of the measured force increase to a lesser extent and the curves become flatter, i.e., softer. This softening becomes more pronounced with decreasing concentration and reflects the plasticity behavior of the sample. With respect to the maximum force obtained for each cycle, the values of the 2 % wt fluid gel are larger than those of the 1 % wt and the 0.5 % wt samples. The increase in the force implies that the dense cross-linking network in the particles lead to higher elasticity. Thus, it is suggested that the higher agarose concentration leads to a higher number of forming helices to aggregation, which in turn results in gel particles with more junction zones. This reflects the well-known correlation between the mesh size and the modulus, i.e. elasticity for cross-linked gels (De Gennes, 1979), which suggests the proportionality of the shear modulus with the cube of the invers mesh size of the gel. Furthermore, this could be verified by Russ et al. by confocal light scanning microscopy (CLSM) of agarose gels with different concentration. For this purpose, agarose molecules were stained with a fluorescence dye, which enable the visualization of the decreasing mesh size with increasing concentration (Russ et al., 2013). The increasing concentration of agarose polymers leads not only to denser cross-linked particles, but also to their higher connectivity, which causes a stronger percolation effect of the particles in the fluid gel and enables the formation of a resistant fluid gel network to a certain extent of deformation. These two facts lead to the observed increase of the measured force with increasing strain and are therefore also consistent with the considerations that the modulus of the individual particles of the fluid gels corresponds to the modulus of the same concentrations of the quiescent cooled gels (Gabriele et al., 2009). The 0.5 % wt sample shows an earlier and faster flattening with increasing cycle as compared to the 1 % wt sample, followed by the 2 % wt fluid gel sample. With each further puncturing of the stamp, the particles are subjected to increasing deformations. Due to the higher elasticity of the single particles of the 2 % wt sample, a less distinct flattening of the force with increasing strain can be observed. This results indicate, how the different length, thickness and shape of the tails contribute to the beginning elastic regime between 0% and roughly 10% strains. The samples with 0.5 % wt and 1 % wt show almost a linear elastic increase for the stress above 20% strain, which shows an interplay between network elastic form the cross-linked core and spatial rearrangement of the particles via frictional forces by the tails. On the contrary, the sample with 2 % wt agarose shows at higher strains (~ 50%) a slight increase of the force. This slight strain hardening corresponds to the elastic response of the densely packed gel particles with larger modulus. An additional note is that when the stamp is pulled up, the force becomes more negative as the concentration increases and with each increasing cycle.

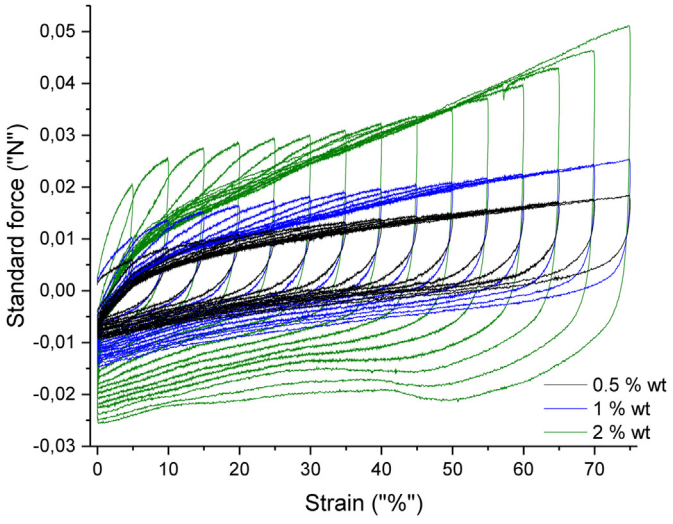


**Fig. 8.** Multiple force-strain curves for 0.5 % wt (black), 1 % wt (blue) and 2 % wt (green) of agarose fluid gels. (For interpretation of the references to colour in this figure legend, the reader is referred to the Web version of this article.)

The force generated when the plunger is pulled up from the sample, which is visible as a negative force area is the adhesiveness and is linked to the separation force from the puncture test. It defines the work required to overcome the attractive forces between the interconnected particles as well as the surface of the sample and the surface of the materials with which the sample is in contact. Moreover, it provides information about the attractive forces between particles within the fluid gels (Chen et al., 2008; Chen and Stokes, 2012; Kilcast & Roberts, 1998). From this experiments, it can be concluded that the higher particle connectivity of the higher agarose concentration is in agreement with the observed increased adhesiveness.

In addition, a three-cycle test was performed for each sample, by puncturing the sample to a maximum strain of 75%, then pulling back to its starting position and moving down to puncture the sample again to 75% strain (data not shown). When cycling until maximum strain of 75% and then back to minimum strain of the starting position, the responsive force hardly decreased after the second cycle. Since with a deformation of 75% strain during the first cycle, the samples had already been exposed to considerable deformation. Furthermore, when comparing this three-cycle test with the multi-cycle test, it was observed that the tips of the gradually increasing maximum forces of the individual curve of the multi-cycle test overlapped with the first curve of the three-cycle test. This in turn shows that the fluid gels, despite their liquid-like flow behavior, do exhibit elastic behavior due to the particles formed by cross-linked polymers.

### 3.5. Tribology of agarose fluid gels

Tribology measurements were carried out in order to examine the coefficient of friction of the agarose fluid gels in dependence of the concentration. The study of lubrication between two interacting surfaces and the behavior of fluid gels in a thin layer allows the results obtained from the tribology test to support the previous findings on bulk examinations. For the measurements, a normal load of 3 N was applied which represents the normal force applied during oral processing. Fig. 9 shows the Stribeck curve displaying the friction coefficient as a function of the increasing sliding speed conducted from 100 to 1000000 μm/s. For all systems, there is initially a slight increase in the coefficient of friction in the boundary regime, followed by sharp decrease as the sliding speed increases above 238 μm/s.

In former studies on the lubrication of agarose fluid gels, the increase in the coefficient of friction at low speeds has been interpreted due to the exclusion of particles from the gap between the two surfaces, resulting from a smaller lubrication thickness compared to the larger particle size (Gabriele et al., 2010). The sharp decrease in sliding speed between 250 μm/s and 600000 μm/s can be related to a dominated mixed regime that provides a maximum lubrication effect, where the surface of the stainless steel ball and the silicon substrate are separated by a thin layer of fluid gel particles, due to bulk entrainment and therefore barely touch each other (Chen and Stokes, 2012). A further increase of the sliding speed of more than 1000000 μm/s close to the hydrodynamic regime results in an increase of the friction for all three samples. It has been explained and observed in general measurements that the coefficient of friction and the separation distance between the two surfaces increases with the lubricant entrainment speed and thus due to the hydrodynamic pressure of the fluid gel flow (Shewan et al., 2019). Not surprisingly, as can be seen in Fig. 9, an increase in friction is observed with increasing concentration. Since the film thickness and friction induced at this high speed depends on the viscosity of the sample (Prakash et al., 2013). Moreover, the entrainment of the thin layer agarose particles was proposed by the mechanism based on micro-elastohydrodynamic lubrication (EHL), suggesting that the fluid dynamics is depended on the particle elasticity and thus affects the coefficient of friction (Meeker et al., 2004).

In contrast to the previously assumed lubricating properties with increasing concentration of hydrocolloids observed for bulk deformation and bulk flow, in Fig. 9 the coefficient of friction at low sliding speed (boundary regime) displays a somewhat unusual behavior. At this low sliding speed a non-linearity can be seen, revealing a higher friction coefficient for the 1 % wt fluid gel concentration followed by the 0.5 % wt and 2 % wt concentration. The lowest friction coefficient of the 2 % wt can be explained by the expectation that less deformable particles will provide lower friction results due to less surface contact, since stiffer particles have a larger modulus, greater elasticity and thus greater resistance to compressive forces (Farrés et al., 2014). Furthermore, the boundary friction decreases with particle volume fractions (Garrec and Norton, 2013). This suggestion regarding the friction in the boundary regime is in agreement with the findings in this study. However, these predictions are contradicted when comparing the coefficient of friction of the 0.5 % wt sample with that of the 1 % wt sample. However, they can be explained by the larger proportion of aggregated chains protruding from the particle surface. As shown in Fig. 10, the entanglements of the aggregated chains of the lower concentration samples lead to a lower frictional force in the boundary regime despite their lower elasticity. These observations are therefore consistent with the models shown in Fig. 5 and the findings of the viscosity measurements as well as the amplitude sweep (LVE-range) and the frequency sweep.

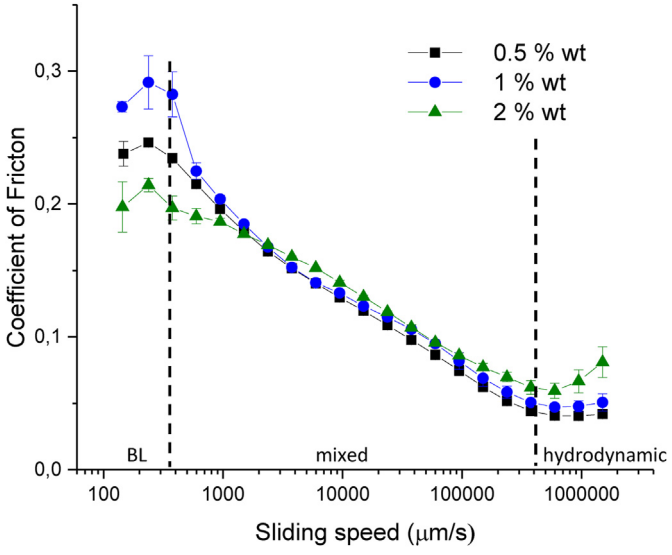


**Fig. 9.** Stribeck curves with applied normal load of 3 N of fluid gels with different agarose concentration 0.5 % wt (black), 1 % wt (blue) and 2 % wt (green). Effect of the particle shape in the boundary regime (BL). The vertical dashed lines indicate the different lubrication regimes: boundary lubrication (BL), mixed lubrication and hydrodynamic lubrication. (For interpretation of the references to colour in this figure legend, the reader is referred to the Web version of this article.)

Furthermore, it can be concluded that it is not only the higher volume fraction, but also the structure of the particles matters, especially their shape, the number of tails, their stiffness, and the core cross-link density. In case for the 0.5 % wt sample, the particles are still elastic at the beginning, although softer compared to the other samples, but the tails are much longer. The numerous tails can be pushed into each other at low sliding speeds, they become entangled and the friction increases. For the 1 % wt sample, there is an in-between, there are still enough tails, although less than for the 0.5 % wt sample, but they are much stiffer because of the higher cross-linking. At the same time, their center is denser cross-linked, thus harder compared to those of the 0.5 % wt. At low sliding speeds, therefore, the tails need to be deformed first, but then collide with the centers, which are also highly cross-linked. Furthermore, the particles of the 2 % wt sample are stiffer, but having smaller size. Also, they are smoother on the surface and with hardly any “hair”, thus nothing gets entangled. With the 2 % wt samples, more particles can pass through the gap between the two surfaces. They are therefore easier to orient at low sliding speeds, thus friction is lower, compared to the 0.5 % wt sample, not least due to the small size and smoother surface. However, at high sliding speeds, due to the dense packing, they jam just in front of the stainless steel ball before their entrainment and are squeezed and deformed until they fit between the gap respectively the ball slides over it, resulting in higher friction at high sliding speeds than for the others samples.

The syneresis and the water exuding from the surface of the particles could also have an influence on the tribological properties. The fact that the water on the surface acts as a lubricant between the particles and thus affects friction suggests that the effect of water release might influence tribological behavior. To explain this, as the higher water release is expected with decreasing concentration, more lubrication is provided and thus the subsequent effect on friction. However, the results of the coefficients of friction to be taken at low sliding speeds (boundary regime) cannot simply be attributed to the water: 1) Because the water obeys much faster time scales compared to the sliding speed; even though the water is still held via hydrogen bonding 2) the trend of friction in the boundary regime would have been linear with the syneresis instead of the current trend. Therefore, the structure of the gel particles, their shape, the core cross-link density and number of dangling chains is a decisive factor in this respect. Nevertheless, at higher sliding speeds from 10,000 μm/s, the effect of syneresis could be presumed, as the friction coefficient of the 0.5 % wt sample appears to be lowest, followed by the 1 % wt and finally the 2 % wt samples. The sliding speed is sufficiently fast so that the structural effects become less relevant. Therefore the influence of water as a lubricant can be more pronounced. Thus, the following

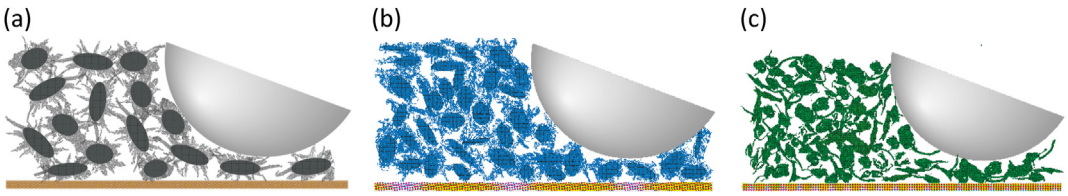


**Fig. 10.** Schematic illustration of the proposed behavior of the gel particles of the fluid gel with varying agarose concentration (a) 0.5 % wt, (b) 1 % wt and (c) 2 % wt, between the two surfaces (stainless steel ball on silicon substrate) in the boundary regime. Not drawn to scale. (For interpretation of the references to colour in this figure legend, the reader is referred to the Web version of this article.)

assumptions could be made: The 2 % wt sample with the least water on the surface shows the highest friction, followed by the 1 % wt sample, while the 0.5 % wt sample, which releases the most water on the surface and therefore having more lubricant, exhibits the lowest friction.

### *3.6. Network structure analysis with scanning electron microscopy (SEM)*

Fig. 11 shows SEM images of the different fluid gel concentrations. To provide supplemental structural information in addition to the results of the texture studies and the rheological as well as the lubrication properties, SEM was performed on all fluid gels prepared with the different concentrations. The results are shown in Fig. 11(a–c) and show fibril-like microstructure formed by interconnected pores surrounding the fibers with a wide size distribution up to several micrometers. Furthermore, it can be seen that, as expected, a denser network forms with increasing concentration. Thus, a densification of the network takes place. In particular, by comparing the images of 0.5 % wt and 2 % wt, the most significant difference can be noticed as the structure of the lowest concentration is observed as a less tightly packed structure compared to the higher concentrations and displays a far lower degree of network. In fact, the densification of the network taking place with increasing fluid gel concentration agrees very well with the dense packing and percolation illustrated in Fig. 5. From the findings of the micrographs, rheological and mechanical properties can be deduced, since the gel strength of the sample varies with the density of the structural patterns.

## 4. Conclusion

In this work, we have investigated the underlying physical characteristics of agarose fluid gels and their structural influence on rheological, mechanical as well as tribological behavior. We have shown how their particle size and shape with varying agarose concentration affect the bulk properties and friction behavior under thin film conditions and have proposed a model that explains the underlying effect of microstructure on viscoelastic and flow behavior.

Continuous and oscillatory measurements including flow sweep, amplitude sweep and frequency sweep were performed to obtain the viscosity and viscoelastic properties of the microgel particles, affected by the microstructure of the gel particles as the result of varying agarose concentration (0.5 % wt, 1 % wt and 2 % wt). It is shown that the storage and loss modulus increases with increasing concentration as expected, however, a discrepancy appears when considering the LVE limit and the viscosity at low shear rate. The 1 % wt fluid gel exhibited the shortest LVE range and the lowest viscosity at low shear rate. Furthermore, investigation of the microstructure by microscopy and particle size determination concluded that the presence of disordered helically aggregated polymer chains on the particle surfaces plays an important role in this nonlinearity with respect to the rheological properties. It was observed that with increasing concentration of agarose, the particle size and disordered chains present on the particle surface decreased.

However, the LVE limit of the 2 % wt sample, which lies between that of the 0.5 % wt and 1 % wt samples, can be explained by the enhanced percolation between the particles due to its volume fraction and smaller particle size. In contrast, the larger LVE range of the 0.5 % wt sample compared to the 1 % wt fluid gel sample and also its higher viscosity at low shear rate can be explained by the entanglement of the agglomerated helical polymer chains leading to increased particle interaction.

Moreover, tribology measurements provided supportive results and showed a higher coefficient of friction for the 1 % wt fluid gel concentration at low sliding velocity (boundary regime), followed by the 0.5 %

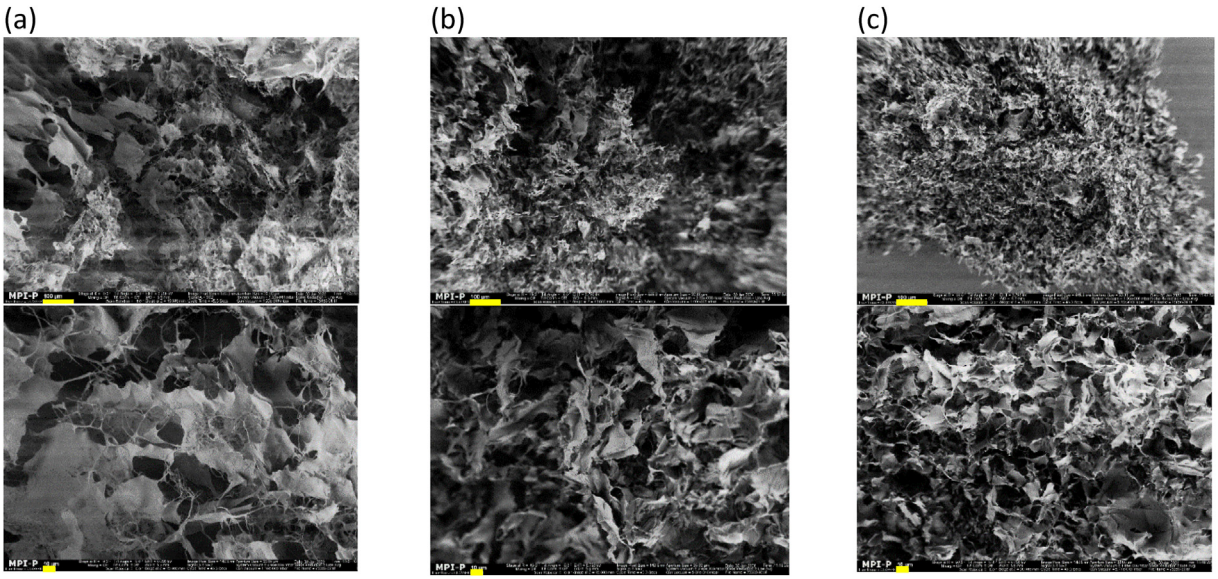


**Fig. 11.** SEM images of freeze dried fluid gels with (a) 0.5 % wt, (b) 1 % wt and (c) 2 % wt agarose concentration. Scale bars are, 100 μm for (a–c) top images and 10 μm for (a–c) bottom images.

wt and 2 % wt concentrations. In addition, the texture analysis provides a correlation between the bulk rheology and the thin film rheology. In the case of the 2 % wt sample, the increase in force is an indication that the dense cross-linking network in the particles leads to higher elasticity. This is consistent with the increasing coefficient of friction in the hydrodynamic regime, but also with the lower coefficient of friction in the boundary regime due to the lower surface contact resulting from the stiffer particles and higher elasticity.

It is further clear, how the shape of the particles matter. The length of the tails, their elasticity compared to the elasticity of the denser center and the shape dependent bending energy of the tails are definitely the most important physical quantities, which determine the rheological behavior, as well as the friction of the fluid gels. These depend on the macroscopic process parameters, here just the mixing speed, and the concentration of the hydrocolloids. These pure physical insights provide methods of a special design of fluid gels for use in dysphagia.

Future studies on network structure are required to provide additional correlation between the network meshes of the gel particles and their experimental properties shown in this work and predictive models. Overall, the results have shown the importance of combining different methods for fundamental understanding in the formation of fluid gels, as they serve as a simple physical model system to better understand the behavior of water-rich and structured foods.

## CRediT authorship contribution statement

**Marta Ghebremedhin:** Conceptualization, Writing- original draft, Methodology, Investigation, Validation, Visualization. **Sebastian Seiffert:** Supervision, Conceptualization. **Thomas A. Vilgis:** Supervision, Conceptualization, Writing – review & editing, Visualization.

## Declaration of competing interest

The authors declare that they have no known competing financial interests or personal relationships that could have appeared to influence the work reported in this paper.

## Acknowledgment

The authors would like to thank Dr. Kaloian Koynov and especially Andreas Hanewald for the technical support during rheology, tribology and texture analysis experiments. Furthermore we thank the members of the MPIP soft matter food science group for fruitful discussion and proofreading the manuscript.

## Appendix A. Supplementary data

Supplementary data to this article can be found online at https://doi.org/10.1016/j.crfs.2021.06.003.

## References

Ako, K., 2017. Yield study with the release property of polysaccharide-based physical hydrogels. Int. J. Biol. Macromol. 101, 660–667.
Chen, J., Feng, M., Gonzalez, Y., Pugnaloni, L.A., 2008. Application of probe tensile method for quantitative characterisation of the stickiness of fluid foods. J. Food Eng. 87 (2), 281–290.
Chen, J., Stokes, J.R., 2012. Rheology and tribology: two distinctive regimes of food texture sensation. Trends Food Sci. Technol. 25 (1), 4–12. https://doi.org/10.1016/j.tifs.2011.11.006.
De Carvalho, W., Djabourov, M., 1997. Physical gelation under shear for gelatin gels. Rheol. Acta 36 (6), 591–609. https://doi.org/10.1007/BF00367355.
De Gennes, P.-G., 1979. Scaling Concepts in Polymer Physics. Cornell university press.
Doi, M., Edwards, S.F., 1986. The Theory of Polymer Dynamics. Oxford University Press (Clarendon, London New York.
Doi, M., Edwards, S.F., Edwards, S.F., 1988. The Theory of Polymer Dynamics, vol. 73. oxford university press.
Ellis, A.L., Norton, A.B., Mills, T.B., Norton, I.T., 2017. Stabilisation of foams by agar gel particles. Food Hydrocolloids 73, 222–228. https://doi.org/10.1016/j.foodhyd.2017.06.038.
Farrés, I.F., Moakes, R.J.A., Norton, I.T., 2014. Food Hydrocolloids Designing biopolymer fl uid gels : a microstructural approach. Food Hydrocolloids 42, 362–372. https://doi.org/10.1016/j.foodhyd.2014.03.014.
Fiszman, S.M., Durán, L., 1992. Effects of fruit pulp and sucrose on the compression response of different polysaccharides gel systems. Carbohydr. Polym. 17 (1), 11–17. https://doi.org/10.1016/0144-8617(92)90018-L.
Frith, W., Garijo, X., Foster, T., Norton, I., 2002. Microstructural Origins of the Rheology of Fluid Gels. Special Publication. Royal Society of Chemistry.
Gabriele, A., Spyropoulos, F., Norton, I.T., 2009. Kinetic study of fluid gel formation and viscoelastic response with kappa-carrageenan. Food Hydrocolloids 23 (8), 2054–2061. https://doi.org/10.1016/j.foodhyd.2009.03.018.
Gabriele, A., Spyropoulos, F., Norton, I.T., 2010. A conceptual model for fluid gel lubrication. Soft Matter 6 (17), 4205–4213. https://doi.org/10.1039/c001907k.
Garrec, D.A., Guthrie, B., Norton, I.T., 2013. Kappa carrageenan fluid gel material properties. Part 1: Rheology. Food Hydrocolloids 33 (1), 151–159. https://doi.org/10.1016/j.foodhyd.2013.02.014.
Garrec, D.A., Norton, I.T., 2012. Understanding fluid gel formation and properties. J. Food Eng. 112 (3), 175–182. https://doi.org/10.1016/j.jfoodeng.2012.04.001.
Garrec, D.A., Norton, I.T., 2013. Kappa carrageenan fluid gel material properties. Part 2: Tribology. Food Hydrocolloids 33 (1), 160–167. https://doi.org/10.1016/j.foodhyd.2013.01.019.
He, Q., Bramante, F., Davies, A., Elleman, C., Fourtouni, K., Wolf, B., 2018. Material properties of ex vivo milk chocolate boluses examined in relation to texture perception. Food and Function 9 (6), 3532–3546. https://doi.org/10.1039/c8fo00548f.
Holland, S., Tuck, C., Foster, T., 2018. Fluid gels: a new feedstock for high viscosity jetting. Food Biophys. 13 (2), 175–185. https://doi.org/10.1007/s11483-018-9523-x.
Hyun, K., Kim, S.H., Ahn, K.H., Lee, S.J., 2002. Large amplitude oscillatory shear as a way to classify the complex fluids. J. Non-Newtonian Fluid Mech. 107 (1–3), 51–65.
Hyun, Kyu, Wilhelm, M., Klein, C.O., Cho, K.S., Nam, J.G., Ahn, K.H., McKinley, G.H., 2011. A review of nonlinear oscillatory shear tests: analysis and application of large amplitude oscillatory shear (Laos). Prog. Polym. Sci. 36 (12), 1697–1753. https://doi.org/10.1016/j.progpolymsci.2011.02.002.
Imeson, A., 2009. 3 agar. Food Stabilisers, Thickeners and Gelling Agents 31.
Kilcast, D., Roberts, C., 1998. Perception and measurement of stickiness in sugar-rich foods. J. Texture Stud. 29 (1), 81–100.
Laiho, S., Williams, R.P.W., Poelman, A., Appelqvist, I., Logan, A., 2017. Effect of whey protein phase volume on the tribology, rheology and sensory properties of fat-free stirred yoghurts. Food Hydrocolloids 67, 166–177. https://doi.org/10.1016/j.foodhyd.2017.01.017.
Li, J.M., Nie, S.P., 2016. The functional and nutritional aspects of hydrocolloids in foods. Food Hydrocolloids 53, 46–61. https://doi.org/10.1016/j.foodhyd.2015.01.035, 2016.
Mahdi, M.H., Conway, B.R., Smith, A.M., 2014. Evaluation of gellan gum fluid gels as modified release oral liquids. Int. J. Pharm. 475 (1–2), 335–343.
Meeker, S.P., Bonnecaze, R.T., Cloitre, M., 2004. Slip and flow in pastes of soft particles: direct observation and rheology. J. Rheol. 48 (6), 1295–1320. https://doi.org/10.1122/1.1795171.
Mezger, T.G., 2010. *Das Rheologie Handbuch: Für Anwender von Rotations- und Oszillations-Rheometern* (3. Auflage). Vincentz Network GmbH & Co. KG, Hannover.
Moakes, R.J.A., Sullo, A., Norton, I.T., 2015. Preparation and characterisation of whey protein fluid gels: the effects of shear and thermal history. Food Hydrocolloids 45, 227–235. https://doi.org/10.1016/j.foodhyd.2014.11.024.
Nguyen, P.T.M., Kravchuk, O., Bhandari, B., Prakash, S., 2017. Effect of different hydrocolloids on texture, rheology, tribology and sensory perception of texture and mouthfeel of low-fat pot-set yoghurt. Food Hydrocolloids 72, 90–104. https://doi.org/10.1016/j.foodhyd.2017.05.035.
Nishinari, K., Zhang, H., Ikeda, S., 2000. Hydrocolloid gels of polysaccharides and proteins. Curr. Opin. Colloid Interface Sci. 5 (3–4), 195–201. https://doi.org/10.1016/S1359-0294(00)00053-4.
Nishinari, K., Fang, Y., 2016. Sucrose release from polysaccharide gels. Food and Function 7 (5), 2130–2146. https://doi.org/10.1039/c5fo01400j.
Nishinari, K., Fang, Y., 2017. Relation between structure and rheological/thermal properties of agar. A mini-review on the effect of alkali treatment and the role of agaropectin. Food Struct. 13 (September), 24–34. https://doi.org/10.1016/j.foostr.2016.10.003.
Nordqvist, D., Vilgis, T.A., 2011. Rheological study of the gelation process of agarose-based solutions. Food Biophys. 6 (4), 450–460. https://doi.org/10.1007/s11483-011-9225-0.
Norton, I.T., Frith, W.J., Ablett, S., 2006. Fluid gels, mixed fluid gels and satiety. Food Hydrocolloids 20 (2–3), 229–239. https://doi.org/10.1016/j.foodhyd.2004.03.011.
Norton, I.T., Jarvis, D.A., Foster, T.J., 1999. A molecular model for the formation and properties of fluid gels. Int. J. Biol. Macromol. 26 (4), 255–261. https://doi.org/10.1016/S0141-8130(99)00091-4.
Nowak, C., Vilgis, T.A., 2004. Rod-coil multiblock copolymers: structure and stability. EPL (Europhysics Letters) 68 (1), 44.
Prakash, S., Tan, D.D.Y., Chen, J., 2013. Applications of tribology in studying food oral processing and texture perception. Food Res. Int. 54 (2), 1627–1635. https://doi.org/10.1016/j.foodres.2013.10.010.
Russ, N., Zielbauer, B.I., Koynov, K., Vilgis, T.A., 2013. Influence of nongelling hydrocolloids on the gelation of agarose. Biomacromolecules 14 (11), 4116–4124. https://doi.org/10.1021/bm4012776.
Saha, D., Bhattacharya, S., 2010. Hydrocolloids as thickening and gelling agents in food: a critical review. J. Food Sci. Technol. https://doi.org/10.1007/s13197-010-0162-6.

Shewan, H.M., Pradal, C., Stokes, J.R., 2019. Tribology and its growing use toward the study of food oral processing and sensory perception. J. Texture Stud. (May), 1–16. https://doi.org/10.1111/jtxs.12452.

Vilgis, T.A., 2015. Gels: model systems for soft matter food physics. Current Opinion in Food Science. https://doi.org/10.1016/j.cofs.2015.05.009.

Watase, M., Nishinari, K., Hatakeyama, T., 1988. DSC study on properties of water in concentrated agarose gels. Food Hydrocolloids 2 (6), 427–438.

Wolf, B., Frith, W.J., Singleton, S., Tassieri, M., Norton, I.T., 2001. Shear behaviour of biopolymer suspensions with spheroidal and cylindrical particles. Rheol. Acta 40 (3), 238–247. https://doi.org/10.1007/s003970000133.

Zimm, B.H., Bragg, J.K., 1959. Theory of the phase transition between helix and random coil in polypeptide chains. J. Chem. Phys. 31 (2), 526–535.

# Physics of agarose fluid gels: Rheological properties and microstructure

## Supplementary Information

Marta Ghebremedhin[1], Sebastian Seiffert[2], Thomas Vilgis[1]

[1]Max Planck Institute for Polymer Research, Department of Polymer Theory, Food Science and Statistical Physics of Soft Matter, Ackermannweg 10, 55128 Mainz,

[2]Department of Chemistry, Johannes Gutenberg University Mainz, Duesbergweg 10-14, 55128 Mainz, Germany

E-mail: ghebre@mpip-mainz.mpg.de (M. Ghebremedhin), vilgis@mpip-mainz.mpg.de (T.A. Vilgis)

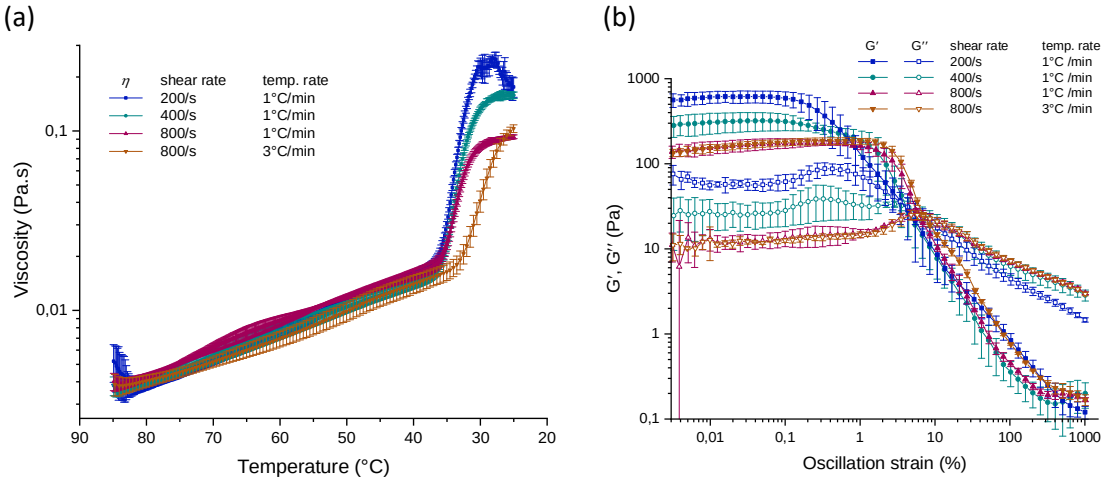


*Figure S1. (a) Gelation under shear in a parallel-plate geometry. Viscosity profile during agarose fluid gel production of 1 % wt for the different applied shear rate and temperature rate: 200 $s^{-1}$ and 1 °C/min (blue), 400 $s^{-1}$ and 1 °C/min (green), 800 $s^{-1}$ and 1 °C/min (red), 800 $s^{-1}$ and 3 °C/min (brown). The samples are subjected to a constant applied shear rate and were cooled from 85 °C to 25 °C at a constant temperature rate and then held for 15 min at 25 °C. (b) Amplitude sweep profile of the respective agarose fluid gels, which remained in the parallel-plate geometry after formation. Dependence of G′(filled symbols) and G″(empty symbols) on strain at constant frequency ($f$ = 1 Hz) and temperature (T = 25 °C). Figure S1 (a) and (b) show an increase in viscosity and modulus as the shear rate decreases. However, at shear rate 800 $s^{-1}$ increase in cooling rate from 1 °C/min to 3 °C/min results in a shift of the sharp viscosity increase to lower temperature, but no increase in viscosity and moduli at 25 °C.*

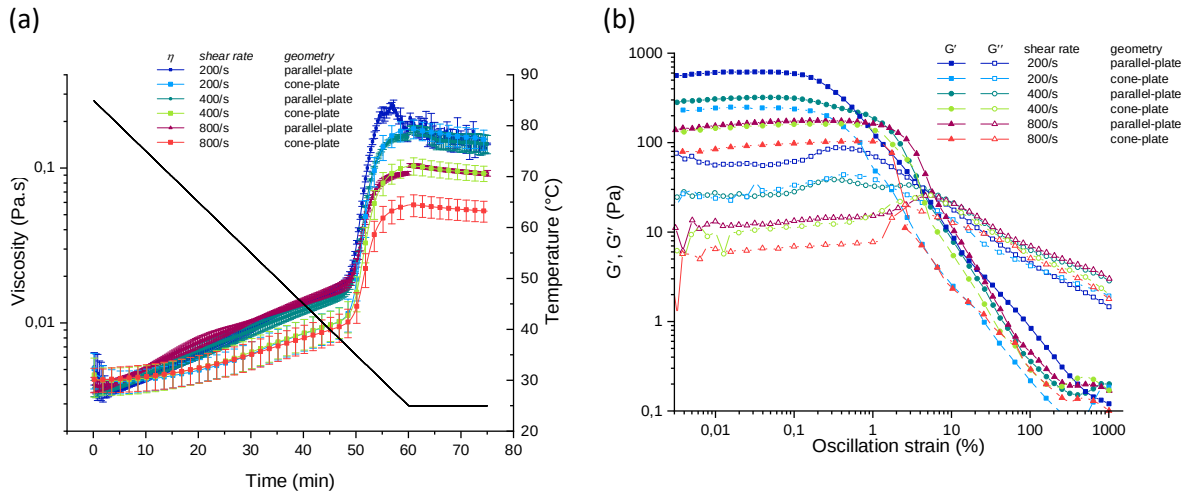


*Figure S2. (a) Gelation under shear in a parallel-plate (pp) vs. a cone-plate (cp) geometry. Viscosity profile during agarose fluid gel production of 1 % wt for the different applied shear rate and geometry: 200 $s^{-1}$with pp (dark blue) and cp (light blue), 200 $s^{-1}$ with pp (dark blue) and cp (light blue), 400 $s^{-1}$ with pp (dark green) and cp (light green), 800 $s^{-1}$ with pp (dark red) and cp (light red). The samples are subjected to a constant applied shear rate and were cooled from 85 °C to 25 °C at 1 °C/min and then held for 15 min at 25 °C. The thin black line represents the change of temperature with respect to the time. It shows a higher viscosity at 25 °C for fluid gel production in a parallel-plate compared to cone-plate as well as resulting in an increase in viscosity with lower shear rate. (b) Amplitude sweep profile of the respective agarose fluid gels, which remained in the parallel-plate or cone plate geometry after formation. Dependence of G´(filled symbols) and G˝(empty symbols) on strain at constant frequency (ƒ = 1 Hz) and temperature (T = 25 °C). Showing an increase in storage (G') and loss (G'') moduli at 25 °C when applying a lower shear rate during gel production and using parallel-plate compare to cone-plate geometry.*

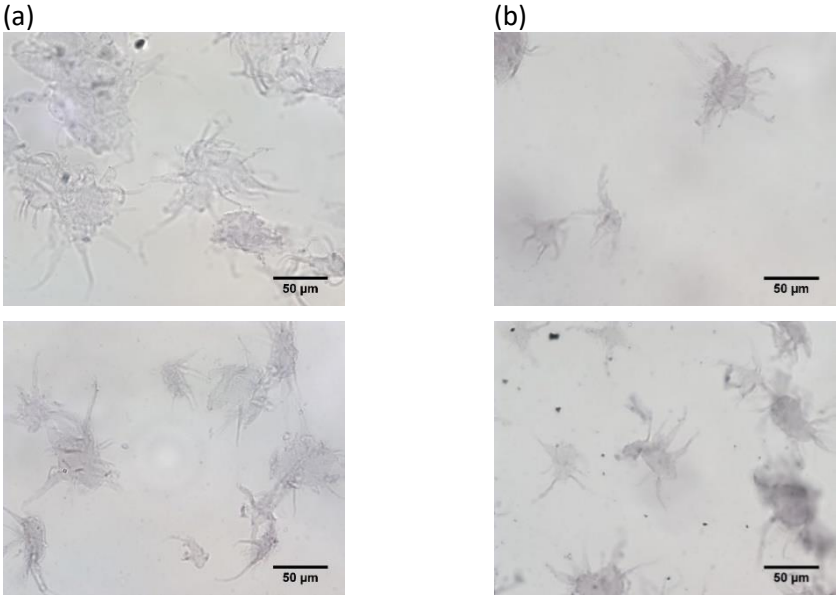


*Figure S3.Optical microscopy picture of 0.5 % wt agarose fluid gel particles stained with toluidine blue. Prepared in (a) a parallel-plate geometry and (b) a cone-plate geometry. Produced at a constant shear rate of 400 $s^{-1}$, cooled at 1 °C/min from 85 °C to 25 °C and then held at 25 °C for 15 min*

## 7.2 Molecular behavior of fluid gels – the crucial role of edges and particle surface in macroscopic properties

Marta Ghebremedhin[1], [redacted]

[1]Max Planck Institute for Polymer Research, Ackermannweg 10, 55128 Mainz

[redacted]

Published in *Food & Function*, 13, 6902-6922, 2022

The published version is available at: DOI: 10.1039/d2fo00102k

Authors contributions:

M.G. carried out the conceptualisation, methodology, and the planning and execution of all experiments, as well as data analysis, visualisation, and manuscript drafting.

Volume 13
Number 13
7 July 2022
Pages 6845-7394

# Food & Function

Linking the chemistry and physics of food with health and nutrition

rsc.li/food-function

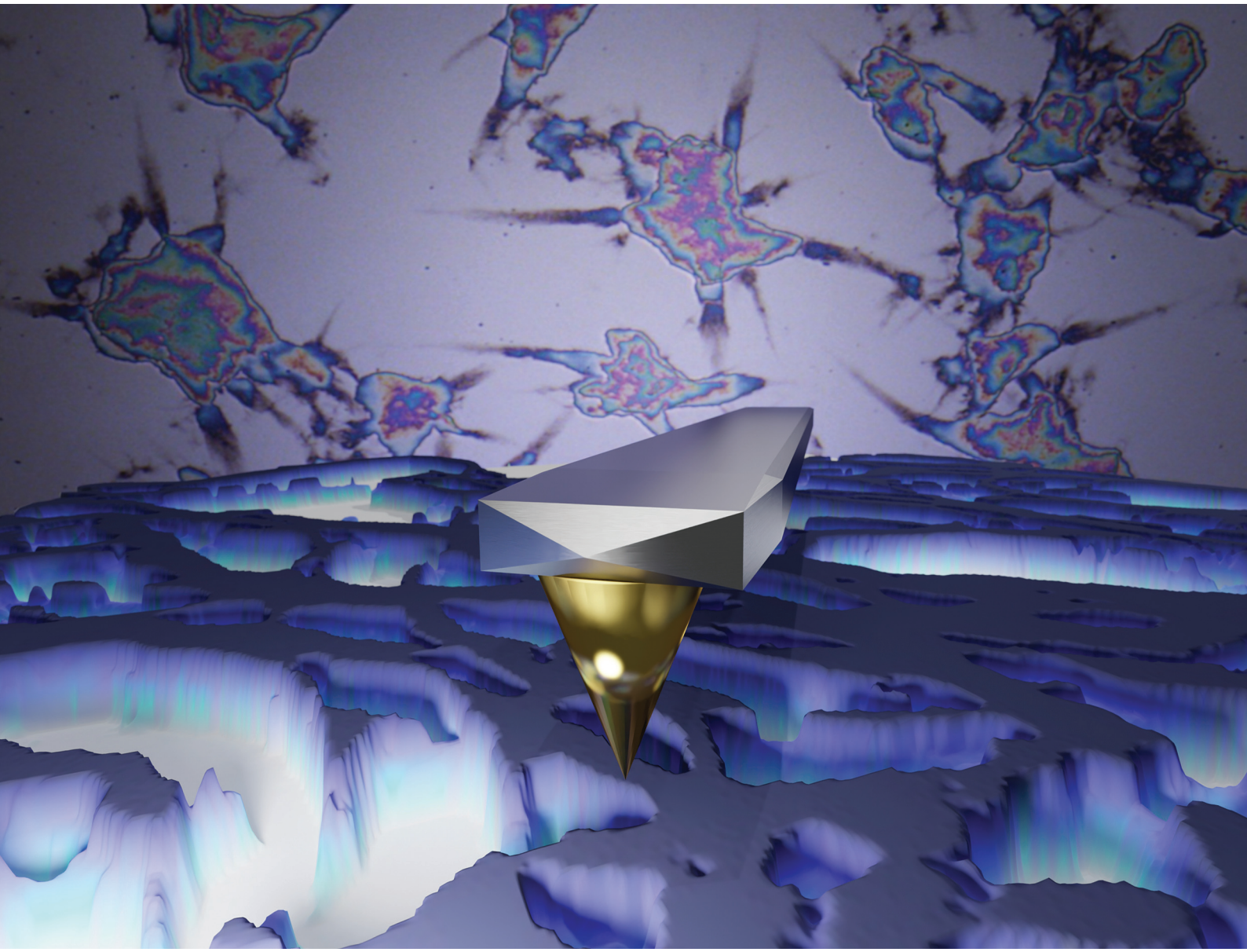

ISSN 2042-650X

ROYAL SOCIETY OF CHEMISTRY

**PAPER**

Marta Ghebremedhin, Thomas A. Vilgis *et al.*
Molecular behavior of fluid gels – the crucial role of edges and particle surface in macroscopic properties

Food & Function

ROYAL SOCIETY OF CHEMISTRY

PAPER



Cite this: *Food Funct.*, 2022, **13**, 6902

# Molecular behavior of fluid gels – the crucial role of edges and particle surface in macroscopic properties†

Marta Ghebremedhin, *[a] Sebastian Seiffert [b] and Thomas A. Vilgis *[a]

Fluid gels exhibit unique properties during oral processing and thus are well known in gastronomy as well as for use in dysphagia patients. Agarose fluid gels, which are produced by gelation under shear, in particular, show elastic solid-like behavior at rest but a fluid-like behavior once critical stress is exceeded. In a previous study this special behavior is addressed to the "hairy" structure of the microgel particles – dangling gel parts and chains on the particle surface – which plays a crucial role in the rheological, mechanical and tribological properties of the gels. In this paper, atomic force microscopy (AFM) was used to investigate the underlying microscopic structures and develop a consistent physical model, which relates the irregular particle structures and their heterogonous shape to the experimental observation of the previous studies. One crucial point is the inner structure of the gel particles, which show a dense area in the center, whereas towards the periphery the network and thus the elastic properties change. Agarose gels by forming helices and meshes, which defines the basic length scale for their elastic response in bulk. These properties in turn depend on the concentration and preparation conditions. The present study is meant to address the still prevalent lack of understanding regarding a direct structure–property relationship of these novel fluid gels. Controlling the properties of such fluid gels may play a crucial role in the texture modification of foods and beverages for dysphagia.

Received 10th January 2022,
Accepted 16th May 2022

DOI: 10.1039/d2fo00102k

rsc.li/food-function

## 1 Introduction

Biopolymers, such as thickening and gelling agents, are often used in various foods and personal care products to optimize and control their texture, oral processing properties, and flavor release. Some of these biopolymers can be used to produce fluid gels, which are particulate gel suspensions. These gels are produced by applying a shear field to a biopolymer solution during gelation.[1–3] The irregularly shaped, elastic gel particles are immersed in the continuous water phase and exhibit novel flow properties, which result in unusual textural properties and an improved mouthfeel. Fluid gels show the properties of a shape-retaining elastic material, but exhibit liquid-like flow behavior when subjected to sufficient stress.[3] Modifying the formulation of biopolymer-based products and creating a controlled microstructure enables a broader range of applications in food systems.[1] In addition, fluid gels have also been extensively investigated in the pharmaceutical field for various pharmaceutical applications such as controlled drug delivery and drug release.[4,5] The different shapes and sizes of the gel particles show distinct elasticity and lubrication properties, and thus impact the mouthfeel during consumption: during oral processing and swallowing, they are easily squeezed between the tongue and the palate, forcing the gel particles to mechanically interact with each other as well as with the oral surfaces.[6] Furthermore, there is growing interest in fluid gels made from polysaccharides with unique physico–chemical properties such as agarose, which is spurring research into such novel edible soft matter systems to understand their basic properties and functions. Detailed knowledge of the rheological, mechanical and tribological behavior of such materials is necessary for understanding the process development and product formulation, especially in view of developing dysphagia food systems.[7] To support these findings and investigate the underlying network structure, atomic force microscopy measurements were carried out in this study.

Agarose, the main gelling agent of agar-agar extracted from red algae (Rhodophyceae), is a linear polymer composed of a (1–3)-linked agarobiose unit of β-D-galactopyranose (1–4)-linked to 3,6-anhydro-α-L-galactopyranose.[8] Agarose solution undergoes a sol–gel transition very quickly on cooling due to

[a]*Max Planck Institute for Polymer Research, Ackermannweg 10, 55128 Mainz, Germany. E-mail: ghebre@mpip-mainz.mpg.de, vilgis@mpip-mainz.mpg.de*
[b]*Department of Chemistry, Johannes Gutenberg University Mainz, Duesbergweg 10–14, 55128 Mainz, Germany*

† Electronic supplementary information (ESI) available. See DOI: https://doi.org/10.1039/d2fo00102k

its fast gelation kinetics, and forms a three-dimensional network due to its molecular structure and physicochemical properties.[9] Beyond that, the transition from the coil to the helix of agarose polymer chains that occurs during cooling can be described by a mean field Zimm–Bragg approach.[10–12] Furthermore, agarose gels tend to release water and are prone to syneresis. This effect increases with a decrease in concentration and has been studied and discussed in detail on quiescently cooled physical aqueous gels.[13,14] This tendency to release water affects the texture properties and thus has an influence on the mouthfeel.[9,15] Finally, due to the aggregation of double helices, agarose forms firm and slightly brittle gels when cooled under quiescent conditions, resulting in a poor mouthfeel. This behavior can be altered by manipulating the processing conditions, *e.g.* by applying different shear rates, concentration changes, or the use of biopolymers with different inherent molecular properties.

During gelation, as biopolymers are subjected to shear, a competing mechanism takes place between gelation by means of physical cross-linking *via* hydrogen bonds and their breaking by the induced shear force.[16] Moreover, during gelation under shear, the resulting disordered network structure of the gel particles is subjected to the competition of two time scales: the shear rates on the one hand and the molecular dynamics of the polymer chains as expressed by the Rouse–Zimm model on the other hand both play a role in the growing cluster size inside of the forming gel particle.[17] Since the cooling rate first affects the center of mass of the individual polymers and then that of the cluster, the dynamics of the cluster slows down with an increase in size, which also changes its shape.[7] Thus, the order rate of the polymer is crucial for particle growth. In fact, the key requirement for a fundamental understanding of such fluid gels is the knowledge of particle growth of the network structure underlying the gelation mechanism of biopolymers under shear.

In one of the earliest studies on agarose fluid gels, confocal microscopy was used to reveal that fluid gels consist of highly concentrated, irregularly shaped gel particles suspended in a continuous water phase.[3] These findings were supported by phase contrast micrographs, showing "hairy" particle structures.[18,19] However, there are no publications yet on systematic investigations of the network structure at the molecular level of such fluid gels.

Moreover, particle size and particle volume fraction were found to depend on shear rate, temperature and concentration and determine the properties of the fluid gel.[3,16] In earlier studies on agarose fluid gels, texture analysis was conducted on gels prepared under quiescent conditions and the obtained behavior was assumed to be that of individual gel particles of the fluid gels of the same concentration.[6] In addition, the rheological properties of quiescently cooled agar gels have been compared with those of agar gels prepared under shear.[2]

Despite numerous studies on fluid gels, the exact gelation mechanism that occurs under shear and the resulting viscoelastic, textural and lubrication behavior is not yet understood on a molecular basis. Therefore, this study focuses on the characterization of fluid gels by establishing systematic fundamental relationships between the microstructure and bulk properties, in order to support the mechanical, tribological and textural properties based on the AFM findings. These investigations were motivated by gaining a deeper understanding of the concentration-dependent characteristics of agarose fluid gels, which in our previous work were found to be influenced by the size and shape of the gel particles.[7] In addition, these findings were assisted by comparing the viscoelastic properties of gels prepared under quiescent conditions with those of fluid gels using rheology.

# 2 Materials and methods

## 2.1 Materials

The agarose [CAS: 9012-36-6] used in this work was purchased as a white powder with a number-average molar mass $M_n$ of ≈74 557.8 g mol$^{-1}$, weight-average molar mass $M_w$ of ≈213 949 g mol$^{-1}$ and polydispersity index of 2.87 (Fig. S4†) from Fisher Scientific GmbH (Schwerte, Germany). According to the manufacturer, the gelling temperature is specified between 34 and 45 °C and the substance reaches a gel strength of >100 g cm$^{-2}$. Furthermore, a sulfate content of 0.15% max was given.

## 2.2 Sample preparation

**2.2.1 Preparation of fluid gels using a rheometer.** For the preparation of fluid gels, a Discovery HR-3 Rheometer (TA Instruments, New Castle, Delaware, USA) with a cup (diameter = 30.37 mm) and vane (diameter = 28 mm and length = 42 mm) tool geometry was used together with a concentric cylinder Peltier Jacket that can be electrically heated. Agarose was slowly added to Milli-Q water for the respective concentrations of 0.5 wt%, 1 wt% and 2 wt%, stirred with a magnetic stirrer (500 rpm), and heated to 85 °C for about 20 minutes in a sealed beaker to ensure complete hydration. The hot agarose solution (30 g) was then poured into the cup, which had been preheated to 85 °C, and allowed to equilibrate for five minutes before starting the measurements; a two-piece cover was used to minimize evaporation during measurements. Gelation under shear was conducted at a constant shear rate of 400 s$^{-1}$ while cooling from 85 °C to 25 °C was conducted at a temperature rate of 1 K min$^{-1}$, followed by an additional 15 min of shearing at 25 °C. Therefore, pourable and spoonable smooth gels were obtained which showed properties of a shape-retaining elastic material but exhibited liquid-like flow behavior when subjected to sufficient stress. The fluid gel samples were then taken from the rheometer and stored at 4 °C for 24 h prior to further characterization experiments.

**2.2.2 Preparation of quiescently cooled gels.** For the preparation of agarose gels under quiescent conditions hot agarose solutions were prepared for the respective concentrations (0.5 wt%, 1 wt% and 2 wt%) as described above. Agarose solution in its heated sol-state was pipetted on a preheated (85 °C) Peltier-plate using a 40 mm diameter parallel plate of a

Discovery HR-3 Rheometer with a pre-set gap of 500 μm, corresponding to a sample volume of approx. 650 μl and a solvent trap to prevent evaporation. In order to ensure an equilibrium of the agarose sol-state system of the sample before starting the measurements, an equilibrium time of 300 s at 85 °C was achieved. The hot agarose solution was cooled down from 85 °C to 25 °C at a rate of 1 K $min^{-1}$, constant strain $\gamma$ = 0.001% and frequency $f$ = 1 Hz, followed by a time sweep at 25 °C for 15 min before finally conducting an amplitude sweep test.

### 2.3 Rheological measurements

Dynamic viscoelastic measurements of different concentrations of the agarose fluid gels as well as the quiescent gels were performed on a Discovery HR-3 Rheometer (TA Instruments), by amplitude and temperature-dependent oscillatory measurements using a 40 mm diameter parallel plate with a pre-set distance of 500 μm and a solvent trap. All rheological measurements were performed in triplicate. The amplitude sweep test was performed to investigate and compare the viscoelastic properties of the gels prepared under shear with those of the gels prepared under quiescent conditions. Using this method, oscillatory deformation was applied and storage ($G'$) and loss ($G''$) moduli were measured to describe the deformation behavior of the gel samples in the non-destructive range, which is defined as the linear-viscoelastic (LVE) range. All amplitude sweeps were carried out at a constant frequency $f$ = 1 Hz, and storage ($G'$) and loss ($G''$) moduli were measured as a function of strain $\gamma$ ranging from 0.001% to 1000% and at a temperature of 25 °C.

### 2.4 Atomic force microscopy (AFM)

Atomic force microscopy measurements were conducted to examine the agarose polymer network structure at the periphery and the dangling chains formed by the aggregation of double-helical agarose molecules at the particle surface. This was done to gain insight into the effect of the microstructure of the gel particles on their texture and lubricating properties. The imaging was performed in tapping mode in air at ambient temperature using a Bruker Dimension Icon AFM with ScanAsyst. Standard tapping mode cantilevers VTESPA from Bruker with a resonance frequency of $f$ = 300 Hz, a spring constant of 42 N $m^{-1}$ and a back side coating of reflective aluminum were used. All images were scanned at a resolution of 512 × 512 pixels and a scan rate of 0.698 Hz. For the topographical imaging, agarose fluid samples were diluted in Milli-Q water to a concentration of 1 : 100 and pipetted onto a silicon wafer (1 cm × 1 cm) treated and cleaned with argon plasma for 10 minutes at a pressure of approximately 2 × $10^1$ mbar (Harrick Plasma Cleaner/Sterilizer PDC-002, 200W, Harrick Scientific Corp., USA). We used silicon wafers instead of freshly cleaved mica because reflected light microscopy was performed on the same sample before AFM measurement, and silicon wafers proved to be suitable for using the same substrate for both reflected light microscopy for the preliminary investigation and subsequent AFM measurements, as suggested by Bertula *et al.*[20] also. After carefully dropping about 3 μL of the samples onto the silicon wafer, they were allowed to dry under ambient temperature before scanning. Gwyddion,[21] an open-source data analysis software for scanning probe microscopy (SPM), was used for flattening the images and for further image analysis.

### 2.5 Scanning electron microscopy (SEM)

Scanning electron microscopy was implemented using a Leo Gemini 1530 microscope (Zeiss, Germany) with an acceleration voltage of 0.750 kV to examine the network structure of the gels cooled under quiescent conditions and of fluid gels, each at different concentrations. Gels which were stored at 4 °C for 24 h were cooled rapidly with liquid nitrogen before placing in a freeze dryer (Christ Alpha 1–2 LD plus). After drying overnight, the completely freeze-dried samples were stored at room temperature. For SEM measurements, the dried samples were not coated and were carefully placed on standard aluminum stubs (Plano GmbH, Wetzlar, Germany) attached with double sided adhesive carbon tapes (Plano) and transferred to a microscope.

### 2.6 Statistical analysis

The experiments were performed in triplicate and reported as average values ± standard deviation (SD). The rheological data were statistically analyzed using the OriginPro 9.65 software (OriginLab Corporation, Northampton, MA, USA). One-way analysis of variance (ANOVA) was applied to determine the significant difference between gels in terms of rheological parameters and to compare the means with a significance level of $p < 0.05$.

## 3 Results and discussion

### 3.1 AFM images of agarose fluid gels

AFM scanning was performed to investigate the network structure of aggregated double-helical agarose polymer chains formed during cooling under shear. Fig. 1 illustrates a schematic experimental AFM setup in which different areas of the

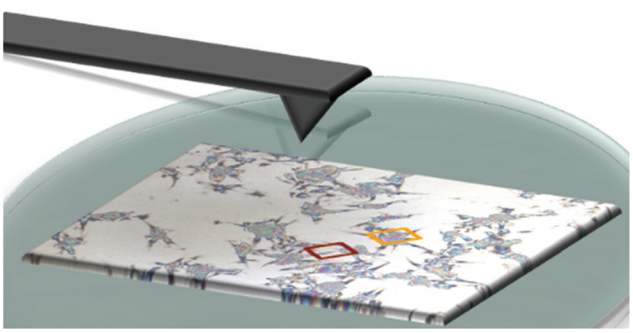

Fig. 1 A schematic illustration of the AFM experimental setup displaying the two different regions being investigated. Images were scanned from both the periphery (red), *i.e.* the chains on the particle surface, and the denser region (orange).

samples are scanned, both at the periphery and in the denser region at the center of a gel particle. As scanning was performed in tapping mode in air, the diluted fluid gels were dried beforehand on the silicon wafers as previously mentioned. This leads to the consideration that due to the adhesion of the agarose polymers on the silicon surface, the resulting network structures on the wafer seen in the AFM images are flattened from a 3D to a rather 2D + $h$ surface after drying (where $h$ is given by the layers of agarose bundles folded on top of each other). However, this in turn may cause the polymer molecules to become overstretched when adhering to the silicon wafer surface. Nevertheless, the typical characteristic structure formation, *i.e.* the association of single chains into double helices and their further aggregation, is preserved and provides a first insight into the structure of agarose molecules in fluid gels. On the other hand, it is also reported that the measurement of the height would be a more precise method to estimate the biopolymer diameters. This is because the measurement of width is considerably oversized not only due to the adhesion of the samples to the surface, leading to its overstretching but also due to the effect of probe broadening.[22,23] Nevertheless, in order to correlate the microscopic and macroscopic properties, such a method allows for comparing the different three-dimensional scaffold network structures of the varied concentrations to different significant rheological, tribological and textural properties.

Fig. 2 shows the AFM images of the particle gels of all three concentrations (0.5 wt%, 1 wt% and 2 wt%) taken at the center of the gel particles. At first glance, no distinct difference may be observed between the different concentrations. As mentioned in our previous publication,[7] the micro-gel particles consist of a very dense region, the inner core with a dense cross-linked three-dimensional network of aggregated double helices of agarose polymer chains. This assertion can be illustrated by the height AFM images in Fig. 2(a–c). All three concentrations show very dense network structures, which are characterized by a blurred, not clearly distinguishable network due to the much higher concentration in the center, so that no aggregated conformation of the double helices can be identified and thus can only be assigned by considering the height bars. Accordingly, the maximum height is 27.5 nm for the 0.5 wt% sample, up to 32.5 nm for the 1 wt% sample, and a maximum height of 36 nm for the 2 wt% sample. On this basis, and taking into account that the width of an agarose double helix is between 1 and 2 nm,[24,25] these images imply a multilayered cross-linked, stacked network of ordered agarose assemblies. Hence, the pictures show a three-dimensional network, although it turns out to be much flatter due to the drying process during sample preparation and consequently the adhesion to the silicon surface.

Fig. 2(d–f) shows the corresponding AFM phase micrographs, which give a better visual impression of the very

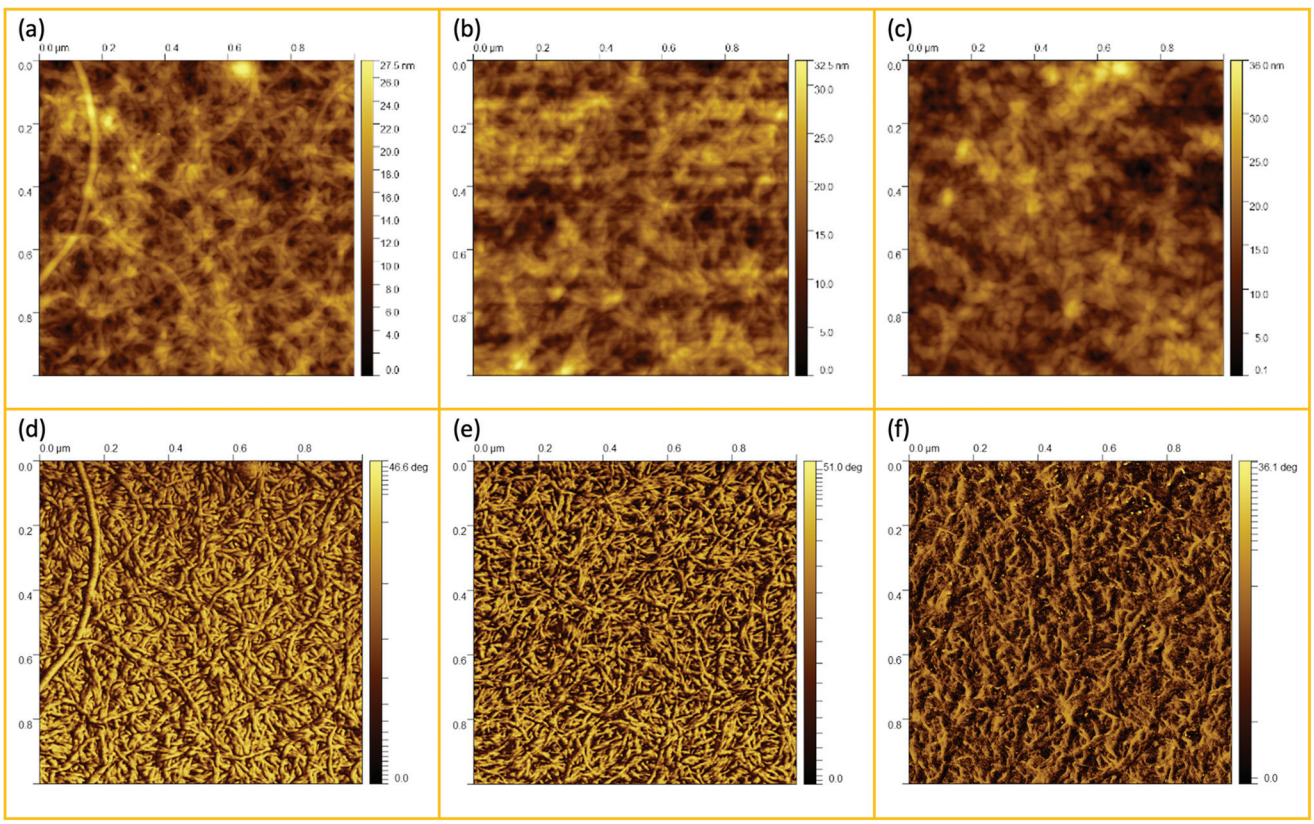


**Fig. 2** AFM height (a–c) and phase (d–f) images taken from the center of the gel particles: (a and d) 0.5 wt%, (b and e) 1 wt%, and (c and f) 2 wt%.

densely packed agarose gel network structure. The phase mode allows the detection of single chains of multiple aggregated double helices of agarose molecules. While it is not possible to distinguish between the different concentrations of the samples using the height mode, the AFM phase images for the 0.5 wt% samples show a less densely packed network than for the 1 wt% sample. From the AFM phase image of the 0.5 wt% sample, more distinct and longer agarose strands can be seen than for the 1 wt% sample. The fact that the strands appear shorter and narrower on average in the image of the 1 wt% sample could be because the strands are so densely packed due to the higher concentration that too many strands are overlapped and thus appear shorter and narrower. Thus, for the 1 wt% sample, the length of the strands seen in total without being overlapped by other strands is shorter than for the 0.5 wt% sample, indicating that in three dimensions, before the gel dries, the mesh size is also smaller. The phase images of the network structure for the 2 wt% sample appear different and less clear, yet aggregated polymer chains can still be identified. An almost flat surface is seen here and yet it can be observed that the strands are much shorter until they are overlapped by another aggregated chain. This loss of quality in the case of Fig. 2(f) may be due to the artifacts caused by contamination of the cantilever tip with the gel samples, which in turn is due to the densely packed, highly concentrated core.

These phase micrographs of the densely cross-linked network in the particles are in agreement with the findings of not only the rheological (viscoelastic) and tribological (friction and lubrication) properties but also the textural (elasticity and plasticity) properties from previous work. It has been reported that an increase in agarose concentration leads not only to higher elasticity, as measured by texture analysis, and higher storage ($G'$) and loss ($G''$) moduli, but also to a lower coefficient of friction in the boundary regime and to higher friction in the hydrodynamic regime of a Stribeck curve.[7] This is explained by a denser cross-linked network in the particles, as a higher agarose concentration leads to a higher number of aggregated double helices, which in turn results in gel particles with more junction zones. This is substantiated by the well-known correlation between the mesh size $\xi$ and the elastic modulus for permanently cross-linked gels, indicating the proportionality of the shear modulus $G$ with the cube of the inverse mesh size of the gel (see eqn (1)).

$$G \simeq \frac{k_B T}{\xi^3} \quad (1)$$

According to this scaling estimate eqn (1), the modulus of the gels is determined by the thermal energy $k_B T$ and the mean mesh size $\xi$ of the network.[26] Consequently, the modulus is determined by the mean distance between two adjacent cross-links (see Fig. 3).

Despite the cross-links being formed by spatially extended double helices, a simple scaling relation can be applied to bulk agarose gels, too.[28] The mesh size $\xi$ depends strongly on the concentration and can be roughly estimated by $\xi \sim c^{-1/3}$. It is expected that these ideas lead also to a better understanding of the elasticity and dynamics of the fluid gel particles and will be proven in the next sections on experimental grounds.

Fluid gel particles consist of cross-linked cores and looser surfaces. The cross-link density of the core is expected to resemble the quiescent gel and shows a smaller mesh size $\xi$, whereas the outer arms and hairy parts are anticipated to show larger mesh sizes for the outer parts. These will be depending on the local concentration and, more importantly, on the competing timescales, defined by the shear rate and the molecular chain motions. Therefore the mesh size in the arms increases from the center to the periphery. It is also expected that the width of this transition region decreases with

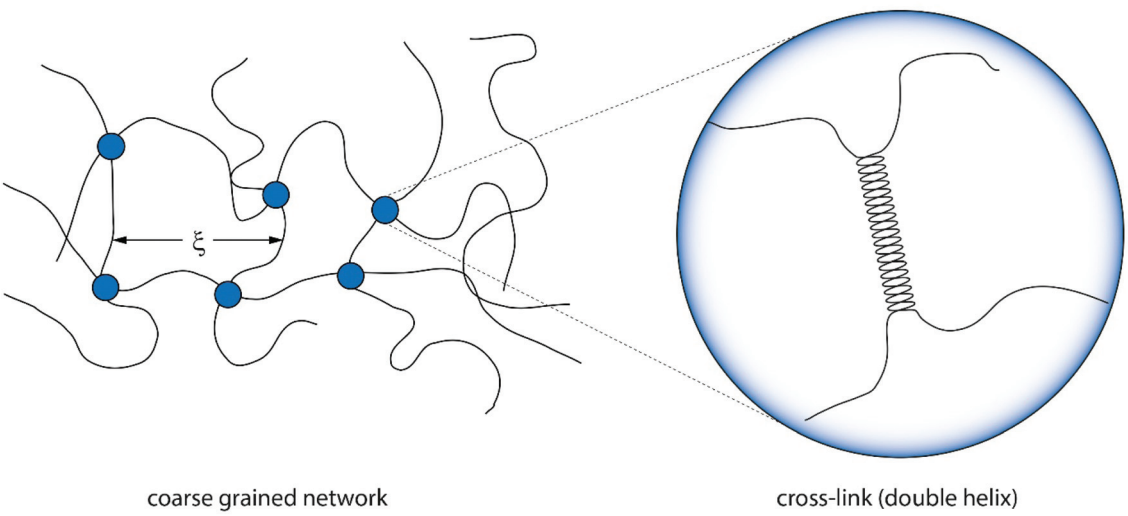


Fig. 3 Illustration of a coarse grained version of an agarose gel connected by cross-links of polymers. The mean mesh size $\xi$ is determined by the number of cross-links and thus the concentration.[27] The cross-links themselves are formed by double helices.

the increasing chain concentration: the higher the agarose concentration, the smaller the transition scale, and the "smoother" the surfaces, as has already been suggested by light microscopy earlier.[7]

The AFM images of all three samples in Fig. 4 were taken in the region of interest at the periphery of the gel particle structure. All three fluid gel concentrations exhibit a network structure that becomes progressively less dense from the interior of the core to the exterior region of the core all the way to the periphery of the gel particle. Although it appears challenging to determine the exact mesh size, the AFM images do provide a substantial indication for the proposed specific model of the fluid gel particles and their aggregated agarose chains, referred to as the hairy structures at the periphery, along with their impact on the rheological, tribological and textural properties. When comparing the images of the different concentrations of 0.5 wt% (a), 1 wt% (d) and 2 wt% (g), it is interesting to note that the gradient of network density between the inner core and the periphery of the probed sample decreases with an increase in concentration.

Fig. 4(a) shows a loose network structure extending over a large area for the 0.5 wt% fluid gel. On the other hand, the network structure for 1 wt% shows a denser network towards the periphery in comparison to the 0.5 wt%, with a shorter distance and range until this network becomes compact towards the center. Images of the 2 wt% fluid gel sample reveal an even more densely packed network at the periphery, as already expected. When considering the physical gelation of biopolymer solution under shear, it here becomes apparent that the formation of gel particles is restricted by a competition between two processes: the aggregation of the agarose chains into increasing clusters on the one hand, and increasing hydrodynamic forces and shear forces, which increase with an increase in viscosity, on the other hand.[16] Therefore, not only the shear rate but also the shear force exerted on the gelation of the polymer chains during shearing is directly related to

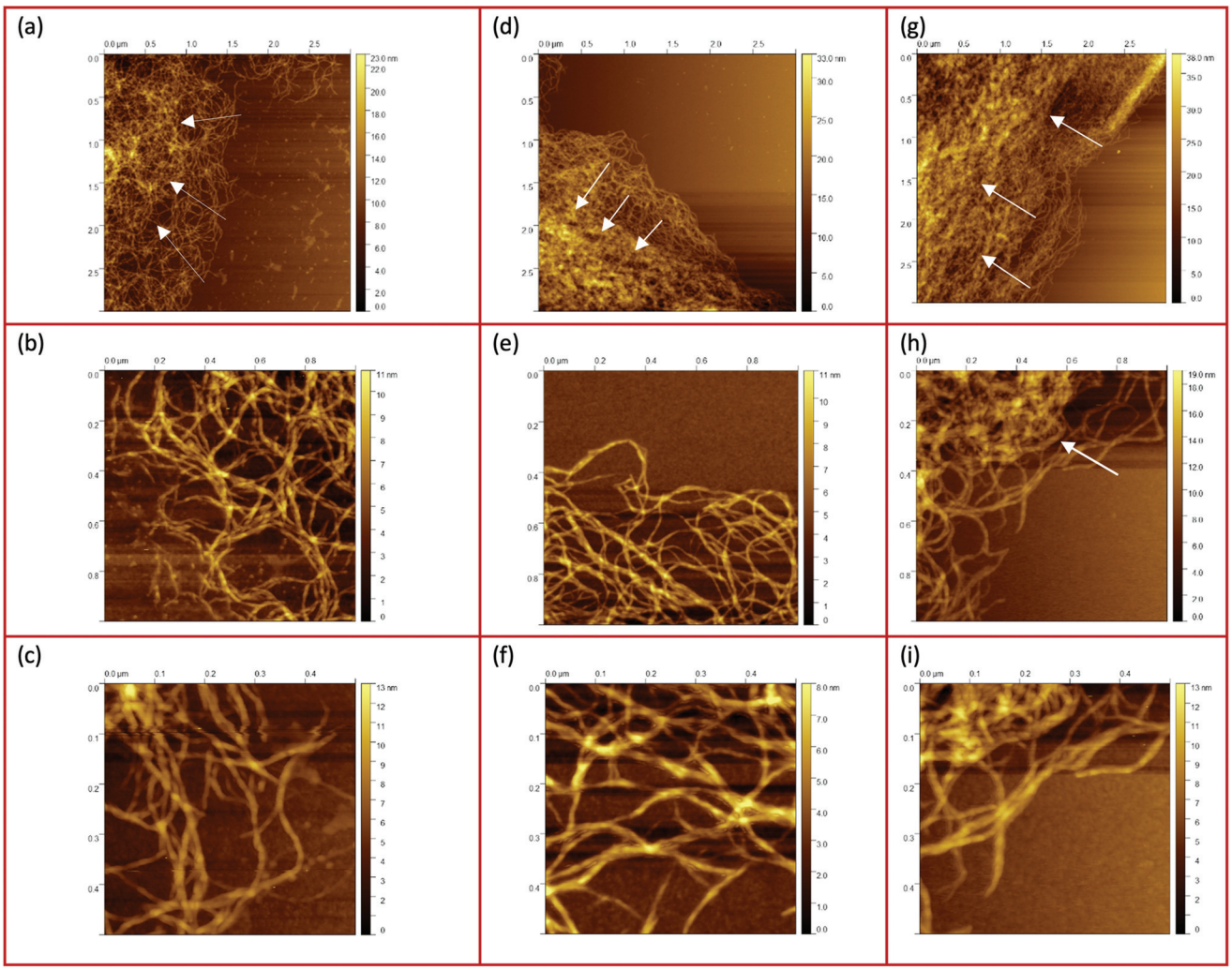


**Fig. 4** AFM images taken from the peripheries and edges of the gel particles : (a–c) 0.5 wt%, (d–f) 1 wt%, and (g–i) 2 wt%. The white arrows indicate the increase of the network density towards the center.

their assembly and particle size. This leads to the fact that at a high concentration of 2 wt% in Fig. 4(g), at the edge a continuous network is no longer visible, but instead part of the network appears to be disrupted.

Furthermore, the figures with a higher magnification (b, e and h) show the trend more clearly. Again it can be seen that the network structure of the 0.5 wt% sample becomes looser towards the edge upon increasing the mesh size, while the structure of the 1 wt% sample shows a larger area with a dense three-dimensional network. Here, only a smaller area at the edge is visible where the network becomes looser but seems to be still denser than for the lower concentration. In Fig. 4(h), on the other hand, the 2 wt% sample again reveals an unevenly distributed, very dense network structure (indicated by a white arrow) surrounded by an even smaller area with a loosely formed network. Finally, the AFM images of the corresponding fluid gels in Fig. 4(c, f and i) at the highest magnification indicate that the gel particles of the different concentrations consist of single strands of presumably aggregated double helices of agarose polymers that associate to form further multiple aggregated helices upon further cooling.

For some exemplary cases, the AFM images shown in Fig. 4 are evaluated in more detail in the following section.

Fig. 5(a) shows a representative example of an AFM image for the 0.5 wt% sample, which is also shown in the overview AFM images in Fig. 4(a). In order to gain more insight into the structure of the gel particles, representative lines were drawn parallel and perpendicular to the surface in Fig. 5(a) and the profiles were evaluated (Fig. 5(b–d)). Furthermore, the inner core is indicated by the dashed semicircle whereas the outer

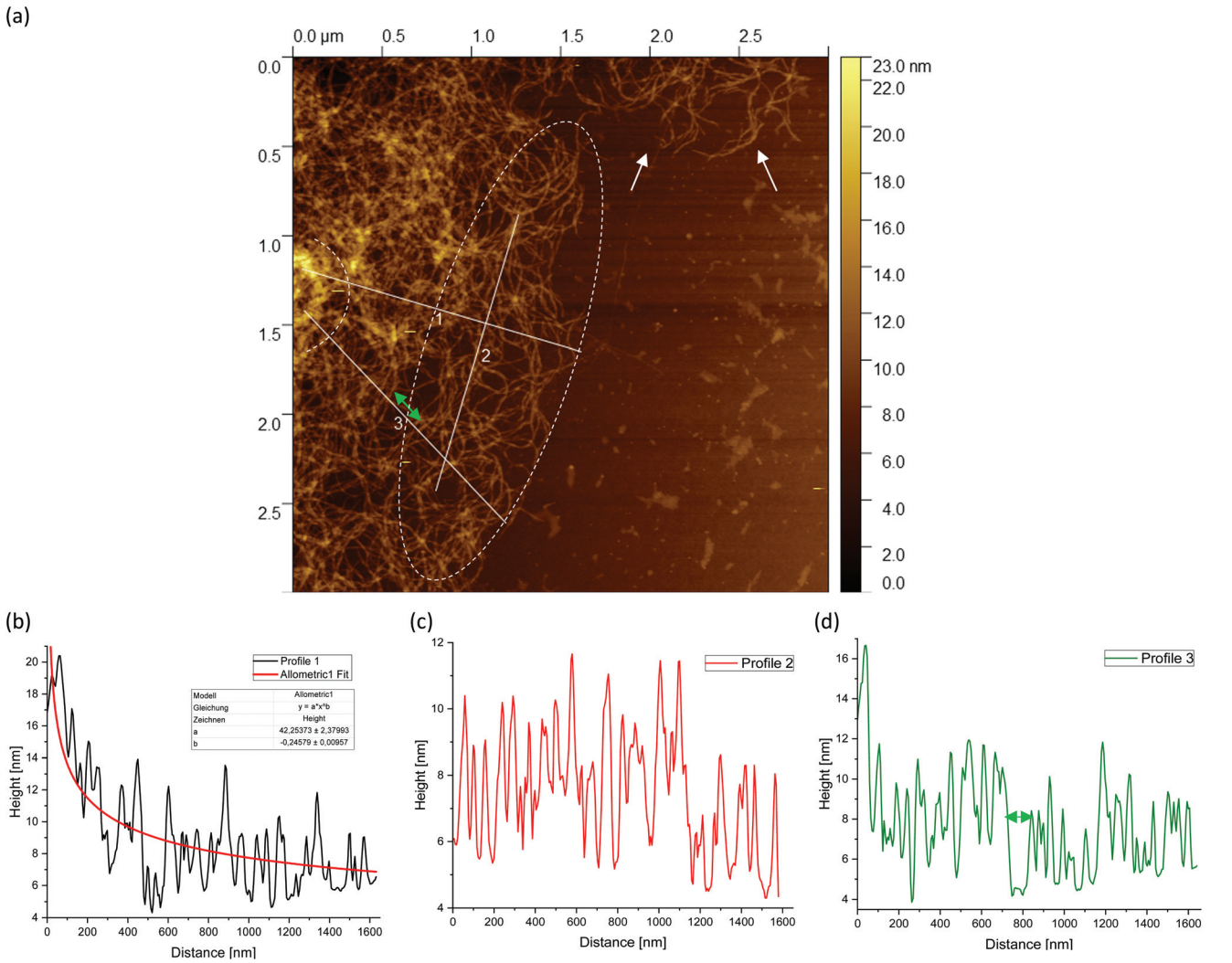


**Fig. 5** AFM image taken from the periphery of a (a) 0.5 wt% agarose fluid gel network with white lines showing the location of the corresponding height profiles (b–d) of the network structure. The green double arrow in (a) and (d) indicates a loose mesh with a distance of approx. 100 nm. Loose dangling chain ends are indicated by white arrows. Profile 1 (b) shows a fit based on an overestimated scaling for a mesh size of a fluid gel resulting from gelation during shear $\xi(r) \sim r^{-1/3}$, where $r$ is the radial distance of the cross-links from the core to the periphery. The inner core is indicated by the dashed semicircle and the outer core *i.e.* periphery is indicated by the dashed ellipse. The periphery shows a larger number of dangling chains *i.e.* hairy structures (image size = 3 × 3 µm).

core, *i.e.* periphery containing the dangling chains, is indicated by a dashed ellipse. In profile 1 (Fig. 5(b)), from the center to the periphery, it can be seen that the peaks representing aggregated double helices exhibit a characteristic trend. At a distance of about 60 nm, the highest peak can be taken at about 20 nm, followed by a continuous decrease in peak heights towards the outer periphery, until finally, the peaks towards the edge become smaller and more clearly distinguishable with an increase in distance, as the network becomes less dense. Furthermore, profile 1 (b) shows a fit based on a scaling estimate for a mesh size variation during gelation under shear from the core to the periphery, $\xi(r) \sim r^{-1/3}$, where $r$ is the radial distance along line profile 1. The progression of the graph is to be expected when examining the corresponding AFM image in Fig. 5(a).

The higher value of the peaks in the interior of the gel particle can be explained by the fact that this area is denser and contains more material and an extended three-dimensional network. Furthermore, the peaks in the inner region show a larger width and become narrower towards the exterior, which can be attributed to a lower number of (aggregated) double helices. Thus, the decrease in peak heights and widths toward the outer region can eventually be attributed to a decrease in average density. The peak height in profile 2 (Fig. 5(c)) suggests an almost constant mesh size. The heights and widths of the peaks do not differ much from each other and are distributed evenly. This is due to the fact that the network is very loose due to the lower local concentrations in the outer regions of the gel particle. Profile 3 (Fig. 5(d)) shows a similar tendency to profile 1, although considerably less pronounced, with the highest peak of about 16 nm in the inner area at a distance of about 40 nm, which then declines directly. Again, the height and width of the peaks in the outer region are smaller and narrower and more clearly detectable. A typical example of a loose mesh can be seen in profile 3, which has a spacing of about 100 nm and is marked with a green double arrow both on the profile and in the AFM image in Fig. 5(a). In the radius of this region, however, more loose meshes can be seen, which also turn out to be larger. Comparing the number of peaks, it can be noted that the profile parallel to the edge has fewer peaks than the profiles perpendicular to it, which run from the inside of the core to the outside. This anisotropy results from the fact that the distances between the peaks are wider apart in the peripheral region, showing a lower density. The average distance between the peaks is about 57 nm and 59 nm for profiles 1 and 3, respectively, and 66 nm for profile 2. This suggests that the meshes are looser around the edges. The reason lies in the preparation process. As the gel particles are subjected to continuous shear during gelation, fewer agarose polymers aggregate outwards and the network becomes less dense towards the edge, resulting in wider meshes, as will be explained below. The network structure in Fig. 5(a) indicates a correlation between the core region in the AFM image and the junction zone *i.e.*, the denser network region described in Ghebremedhin, Seiffert, and Vilgis.[7] Indeed, it seems that the core region corresponds to the junction zones with its abundant bound water due to its higher water binding capacity and thus is consistent with the previous publication. Moreover, since the AFM image in Fig. 5(a) displays that the network density varies between the inner core and the periphery, it can be assumed that the mobility of the agarose chains and of the water molecules also varies. This seems to be in accordance with earlier studies on water properties in concentrated agarose gels by Watase, Nishinari, and Hatakeyama.[29] In this work, these authors propose higher water binding capacity of the junction zones and that water molecules are less mobile in the junction zones, *i.e.* in the core region.

Fig. 6(a) shows an AFM image for the 1 wt% fluid gel samples shown previously in Fig. 4(d). Also in this AFM image, three white lines can be seen corresponding to the height profiles in Fig. 6(b–d). Line 2 runs parallel to the edge of the gel particle network and both lines 1 and 3 run perpendicular to it from the inner core of the network of gel particles outward to the periphery. Once again, the inner core is indicated by the dashed semicircle and the periphery regime by the dashed ellipse. For the 1 wt% sample, line 1 (Fig. 6(b)) shows a profile with a systematic decrease of the total height of the peaks. The highest peak lies at about 30 nm at a distance of about 55 nm and is higher than the highest peak value of the 0.5 wt% fluid gels in Fig. 5(b) due to the higher concentration. In addition, the trend of the peak heights shows a decreasing density distribution from the center to the outer periphery similar to profile 1 in Fig. 5(b). Similarly, the meshes and the average distance between the peaks increase outward. For line 2 (Fig. 6(c)), on the other hand, no continuous decrease in the peak height and density is observed over the entire drawn line. Looking at Fig. 6(a) and taking into account that it is a three-dimensional network structure, a thinning of the network and thus a decrease in density between the three lines and especially parallel to line 2 can be seen. By comparing the height profile of line 2 with that of line 3 (Fig. 6(d)) in the less dense network region, the latter (indicated by green double arrows) lies below that of line 2, but increases again in peak height and thus in density towards the edge. Such micro cracks are caused by the shear that takes place during gelation.

Fig. 7(a) shows the AFM images of the 2 wt% sample (as already shown in Fig. 4(g)). Again, line 2 is parallel to the edge of the gel particle network while both lines 1 and 3 are perpendicular to it starting from the inner core of the network of gel particles outwards to the periphery. Furthermore, the corresponding profiles of the diagrams are shown in Fig. 7(b–d). Profile 1 again shows a continuous decrease in peak height from the inner core of the gel network towards the periphery, with a highest peak of about 38 nm at a distance of around 68 nm, which is higher than the highest peak of the 0.5 wt% (Fig. 5(b)) and 1 wt% (Fig. 6(b)) fluid gel samples due to the higher concentration. In the area where line 3 runs, indicated by green double arrows in Fig. 7(a and d), a thinning of the three-dimensional network structure can be seen, similar to that already observed for the 1 wt% sample and interpreted as a microcrack. While the surface is smooth in the upper region at the edge, a ruptured network structure can be seen further

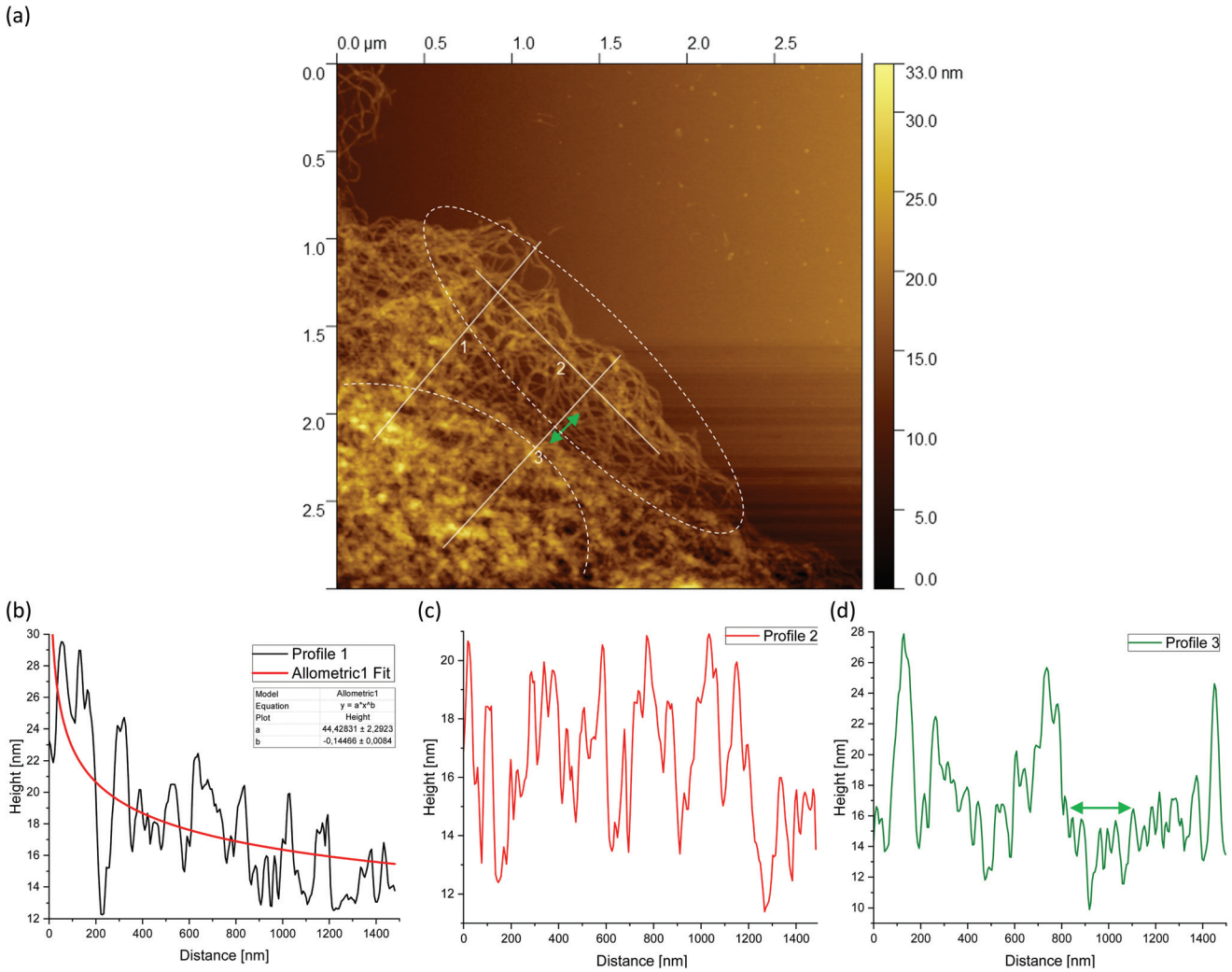


**Fig. 6** AFM image taken from the periphery of a (a) 1 wt% agarose fluid gel network with white lines showing the location of the corresponding height profiles (b–d) of the network structure. The green double arrow in (a) and (d) indicates the thinning of the network structure as a result of the microcracks formed during shear (image size = 3 × 3 µm).

down in Fig. 7(a), which runs parallel to the edge and is indicated by a blue double arrow. This network disruption can be explained by the fact that the gel particles tend to detach along the edge due to the high crosslinking of the 2 wt% sample under shear. It can be seen that a crack has formed and parts of the network have almost detached, although some connections to the core are still present. This area of loose network structure is similar to the network structure of the 0.5 wt% sample in Fig. 5(a).

The observed structures of the gel particles can be easily motivated by physical arguments: gel particles form when the temperature decreases below the concentration dependent critical value.[7] The gelling temperature depends on the concentration. A crude two body interaction based argument suggests $T_{gel} - T_0 \sim N(c - c_0)$, where $T_{gel}$ is the actual gelling temperature, $T_0$ is the bulk gelling temperature, $N$ is the degree of polymerization as before, $c$ is the concentration, and $c_0$ is the lowest concentration at which gelation occurs, which is obviously close to the overlap concentration, well known from the physics of polymer solution.[26] Highly concentrated solutions can gel already at higher temperatures, meaning higher thermal and kinetic energy, than lower concentrated solutions. This aspect, which is trivial for gels cooled under quiscent conditions, becomes relevant for gelation under shear.

When small gel particles are formed under cooling and shear, growth can only take place at the surface. The surface shows a large number of dangling agarose chains, which can form helices with still freely dissolved chains when they come close to each other. Since the fluid is rotating with a constant shear rate $\dot{\gamma}$, a time scale of $\tau = 1/\dot{\gamma}$ is obtained, which competes with the time scales for gelling. Firstly, this leads to the finite particle size of the gel particles, estimated to be $R \simeq (k_B T/6\pi\eta_s\dot{\gamma})^{1/3}$,[16] secondly to a growing mesh size towards the periphery of the particles. Since the particles are rotating in a tumbling motion at different radii inside the rheometer tool,

 

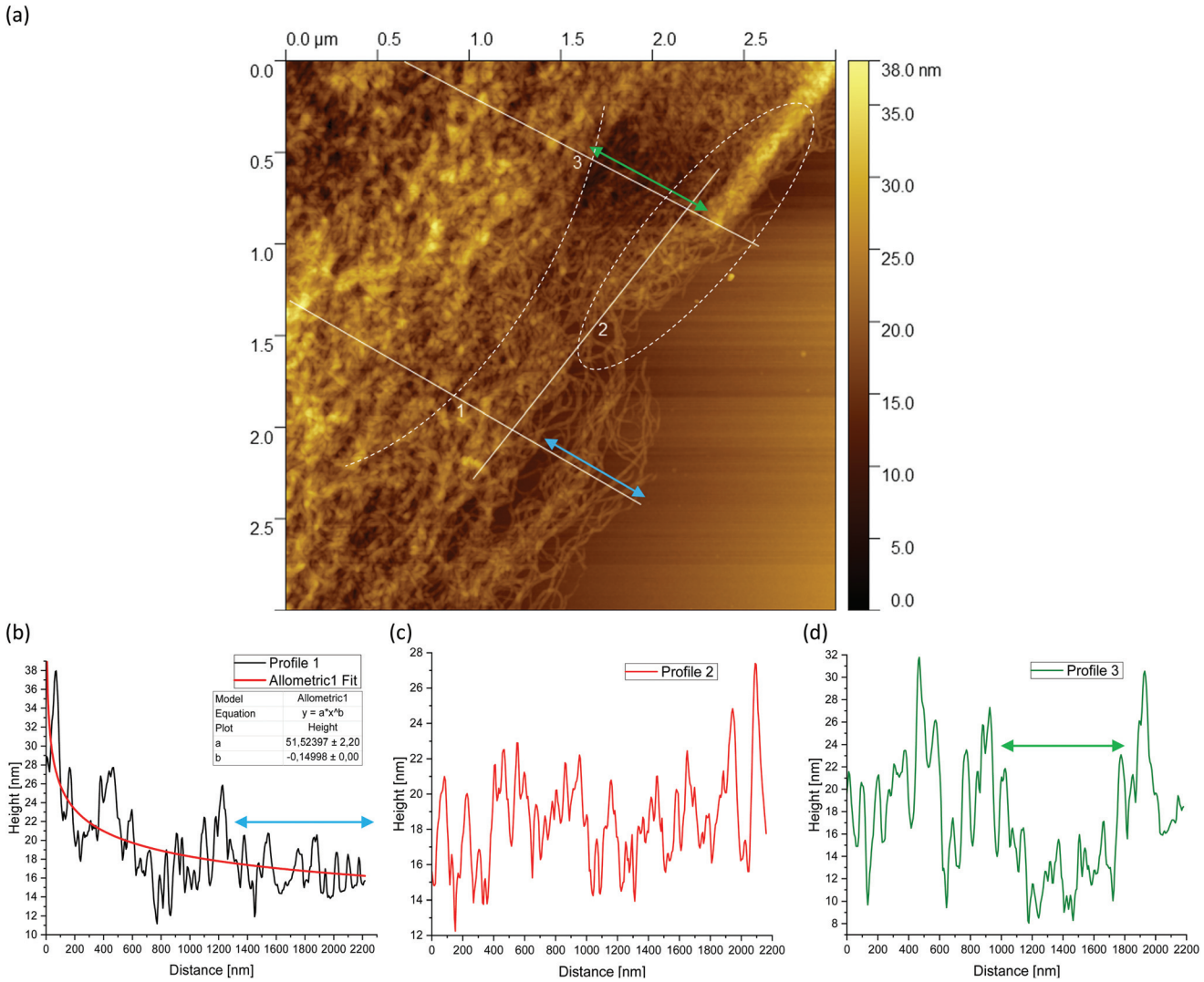


**Fig. 7** AFM image taken from the periphery of a (a) 2 wt% agarose fluid gel network with white lines showing the location of the corresponding height profiles (b–d) of the network structure. The green double arrow in (a) and (d) indicates thinning of the network structure, and the blue double arrow (a and b) indicates a partially ruptured network structure, both as a result of shear stresses during gelation (image size = 3 × 3 µm).

the local speed at the perimeter changes according to the shear rate $\dot{\gamma}$. The maximum local velocity $v$ at the perimeter of a particle of size $r$ is therefore $v(r) \sim \dot{\gamma} r$, which needs to be compared with the free chain (center of mass) diffusion following a Fick's law, yielding an (overestimated) scaling for the mesh size $\xi(r) \sim r^{-1/3}$, where $r$ is the radial distance from the quiescent gel type cross-linked particle core to the periphery. Apparently, the mesh size parallel to the periphery, apart from statistical variations, does not change as observed in the AFM experiments.

As a result, shear has a more pronounced effect on the edge of the forming gel particle. This in turn means that gelation at the surface is hindered at this point and consequently there is an apparently lower concentration and thus a looser network structure in this area of the edge of the 2 wt% sample than in the interior of the gel particle. This loose network structure in Fig. 7(a) has a length of about 500–600 nm. Comparing this with the network structure of the 0.5 wt% sample in Fig. 5(a), this corresponds to a length of about 1500 nm and thus an extension of the loose network structure by a factor of 3.

This observation can be understood by considering again the competing time scales and molecular motions for concentrations larger than the overlap concentration. Thus, depending on the chain length, the molecules in these highly viscous solutions become increasingly entangled with higher concentrations. Consequently, the chain dynamics becomes slower.[17] When chains move faster than the shear imposed time $1/\dot{\gamma}$, they are able to form gels, comparable to the quiescent case. In concentrated polymer solutions the self-diffusion constant $D_s$ of the polymer chains follows a reptation like motion, $D_s \sim k_B T/(\zeta N^2)$, where $\zeta$ is the monomer friction coefficient and $N$ is the degree of polymerisation. The longest relaxation time scale is $\tau_R \sim N^3$ and is much larger compared to $1/\dot{\gamma}$. In conclusion the core is densely cross-linked and reaches closer to the per-

iphery of the particles for high agarose concentrations, but the particles remain smaller. They appear also much smoother compared to the surface particles generated at lower concentrations.

The fitting results deserve some attention. As mentioned already before, the power law $(r) \sim r^{-b}$, where $b = 1/3$ overestimates the decay of the cross-link density towards the periphery of the particles. The AFM results show clearly concentration dependent power laws, as shown in Table 1.

These results suggest that the exponent $b$ saturates with an increase in concentration, in other words with a higher overlap between the chains during the gelation process. Following the arguments of de Gennes[26] the exponent $b = 1/8$, which is closer to the results for concentrations far below the overlap conditions. This assumes, however, that all pairs of the neighboring chains within a distance of $\xi$ form cross-linking helices, which is questionable for gelation under steady state shear conditions.

Upon further comparison of the AFM images obtained for different concentrations, Fig. 5(a) shows loose dangling bundles or chain ends in the upper region marked with white arrows. This results from the fact that at the shear rate, due to the low concentration of 0.5 wt%, the chains cannot completely gel into a coherent network compared to the higher concentrations. These dangling ends do not appear to the same extent at the other concentrations. At the higher concentrations of 1 wt% (Fig. 6(a)) and 2 wt% (Fig. 7(a)) in the upper region parallel to the extended line 2, it can be seen that the agarose chains recede towards the core due to the high concentration and cross-linking at the periphery. It can be assumed that in the already disrupted network structure of the 2 wt% sample the agarose chains do not have much chance to cross-link further, because they do not find a second chain to form helices at appropriate time scales compared to $1/\dot{\gamma}$.

In Fig. 8, for concentrations of 0.5 wt% ((a), *cf.* Fig. 4(b)), 1 wt% ((b), *cf.* Fig. 4(e)), and 2 wt% ((c), *cf.* Fig. 4(h)) representative AFM images with higher magnifications are used to determine the mesh size. The mesh sizes of the different fluid gel concentrations were measured manually by evaluating the area using ImageJ. Here an attempt was made to choose closed meshes, as these mainly contribute to the elasticity. To determine the mesh size, the diameter was calculated from the area and assumed to be the distance length of the mesh.

The average mesh sizes for the respective fluid gel concentrations are given in Table 2, and it was found that the mesh sizes increase with a decrease in concentration as expected. However, as suggested in Fig. 8 the mesh sizes vary significantly and become larger towards the outer region of the fluid gel particles. The large variety of mesh sizes is therefore reflected in a large standard deviation. As mentioned in eqn (1), the modulus is mainly determined by the mesh size. By inserting the estimated mesh sizes into this equation, a theoretical modulus can be obtained in a highly simplified approximation, which is shown in Table 2. For comparison, the measured storage moduli at a strain of $\gamma = 0.01\%$ (LVE range) are given in Table 2. Comparing both the measured and estimated elastic moduli, it can be seen that the order of magnitude within the concentration is close. Indeed, the 2 wt%/1 wt% ratio for the elastic modulus is about 4.03 for the theor-

**Table 1** Estimated values for the concentration dependence for exponent $b$

| $c$ (wt%) | 0.5 | 1 | 2 |
|---|---|---|---|
| $b$ | 0.25 | 0.14 | 0.15 |

**Table 2** Average mesh sizes ($\xi_{c\ (FG)}$) estimated from the AFM images in Fig. 8 using ImageJ, and the corresponding calculated moduli $G_{c\ (FG)}$ [Pa] according to eqn (1) compared to the measured storage moduli $G'_{m\ (FG)}$ [Pa] from amplitude sweep (see Fig. 13 and Table 3) for the different agarose fluid gel concentrations

| | $\xi_{c\ (FG)}$ [nm] | $G_{c\ (FG)}$ [Pa] | $G'_{m\ (FG)}$ [Pa] |
|---|---|---|---|
| 0.5 wt% | 83 ± 101 | 7.2 ± 26.4 | 132.5 ± 4.3 |
| 1 wt% | 59 ± 85 | 20.3 ± 88.6 | 369.6 ± 14.3 |
| 2 wt% | 37 ± 61 | 81.9 ± 406.7 | 920.2 ± 133.0 |

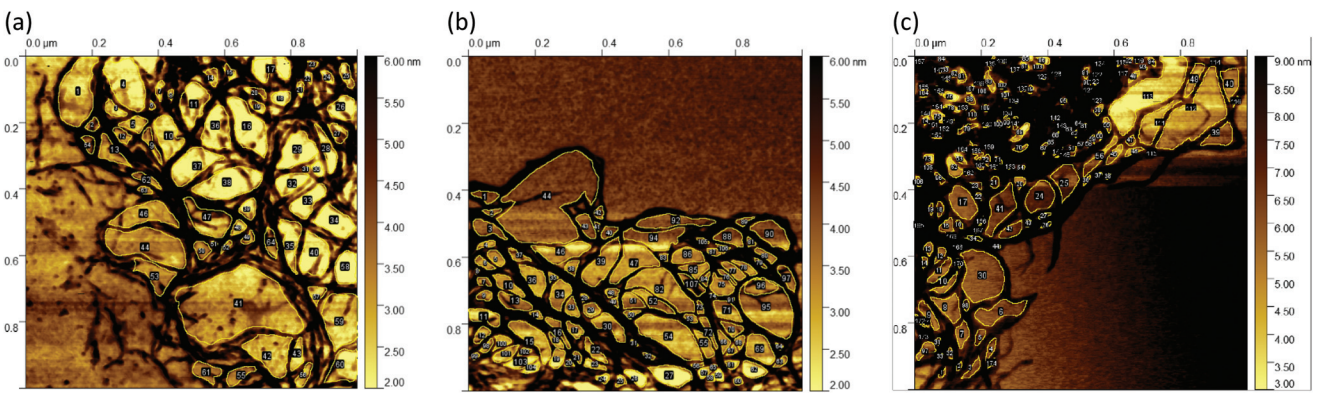


**Fig. 8** Mesh size determination for the (a) 0.5 wt%, (b) 1 wt% and (c) 2 wt% agarose fluid gel networks. Mesh sizes were analyzed manually by evaluating the area using ImageJ after changing the contrast of the AFM images for better visualization (image size = 1 × 1 μm).

etically estimated value and 2.49 for the measured value, whereas the 1 wt%/0.5 wt% ratio is 2.82 for the theoretically estimated value and 2.79 for the measured value. This consistency supports the idea of using detailed information from AFM to gain a deeper fundamental understanding of fluid gels. Moreover, it supports and confirms the ideas proposed in the previous paper.[7]

A further comparison of the mesh distribution in Fig. 8(a–c) shows that the loose meshes of the 0.5 wt% and 1 wt% samples extend over a wider area, while the 2 wt% sample shows only a small area of loose structures and a large part is dominated by the dense core.

Finally, Fig. 9(a), 10(a) and 11(a) (*cf.* Fig. 4(c, f and i)) show the AFM images for different agarose concentrations at the highest magnification. Again, the three lines indicate the paths for the height profiles in the corresponding Fig. 9, 10 and 11(b–d). It can be clearly seen here, once again, that the meshes increase on average with a decrease in concentration, whereas in the case of the 2 wt% sample, large meshes but also thick strands can be observed due to edge effects. The enlarged regions shown in the figures are of interest because the height profiles at this magnification allow clearer visualization and distinction of the peaks and thus the individual strands. It can be recognised that the different concentrations of agarose fluid gels have the same origin and are formed by single agarose chains associated with double helices, with the consequent aggregation of the double helices into multiple helices (indicated by white arrows). The profile height for the concentrations 0.5 wt% (Fig. 9(b–d)) and 1 wt% (Fig. 10(b–d)) showed an approximated measured value between 4 nm and 8 nm and a width range between 10 and 30 nm. If we assume that the width of a double helix is about 2 nm, we can assume about 10–30 agarose chains or 5–15 double helixes within such a broader peak. For the 2 wt% sample (Fig. 11(b–d)), the

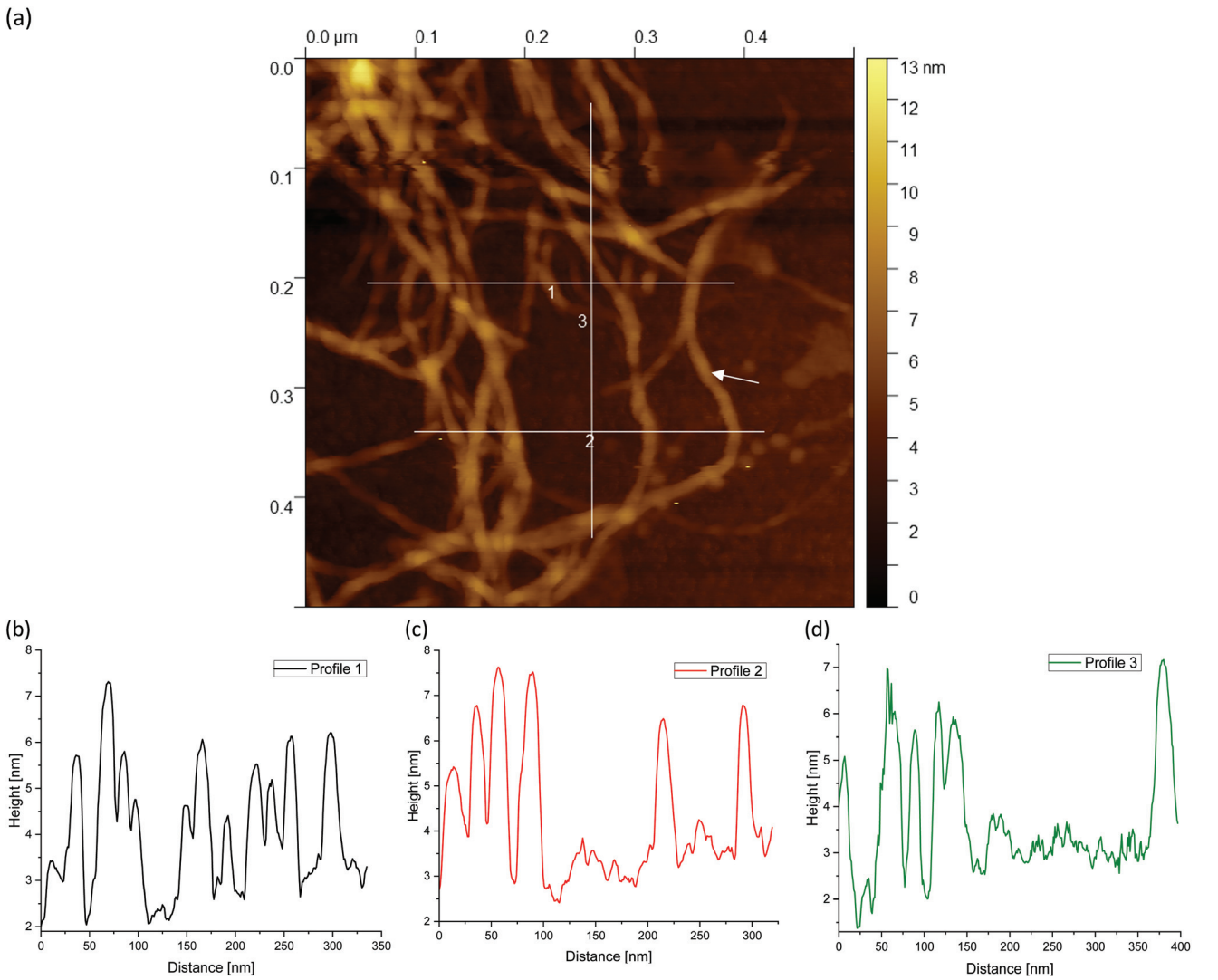


**Fig. 9** AFM image taken from the periphery of a (a) 0.5 wt% agarose fluid gel network with white lines showing the location of the corresponding height profiles (b–d) of the network structure. Number 2 is related to the horizontal line (image size = 0.5 × 0.5 µm).

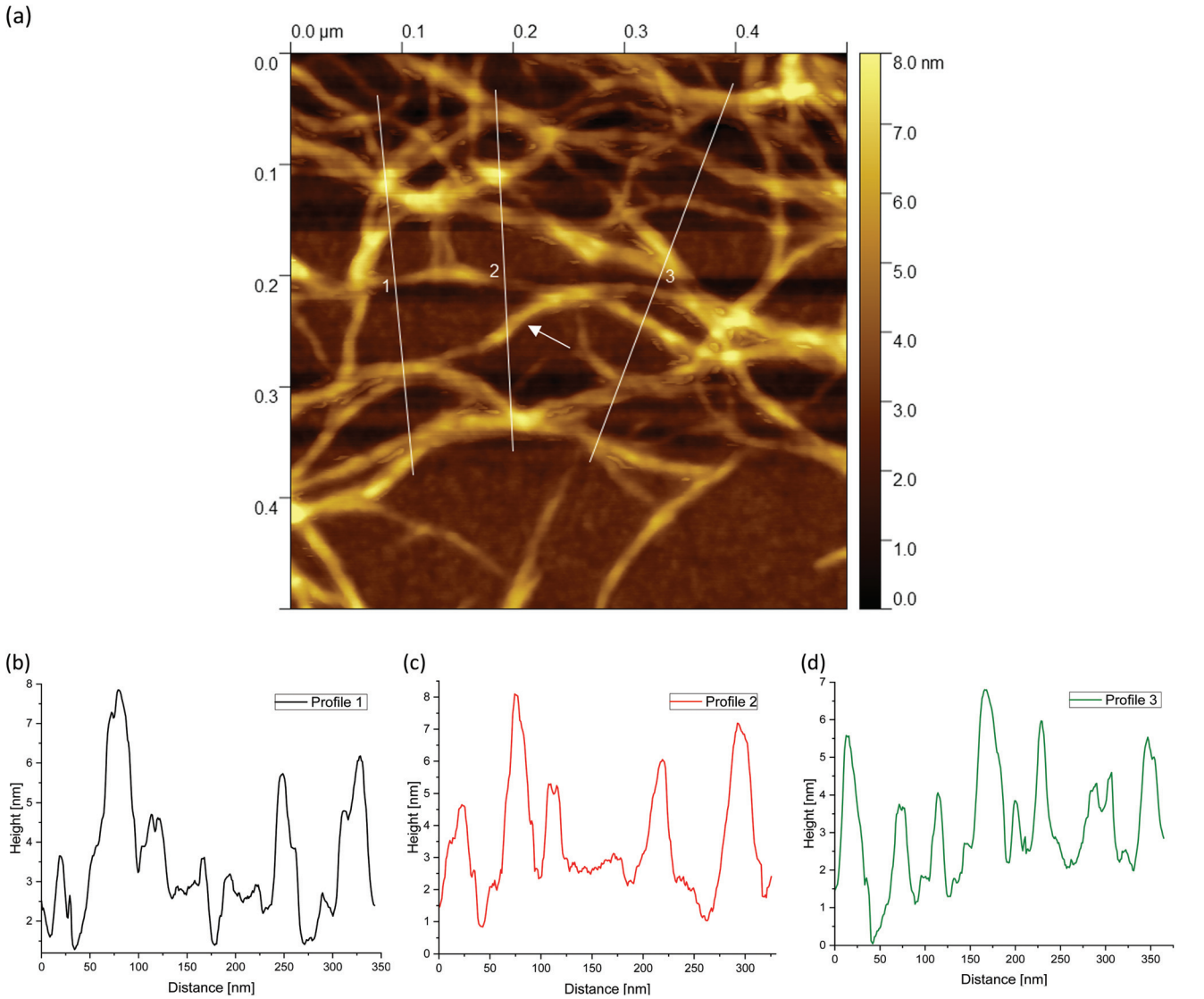


**Fig. 10** AFM image taken from the periphery of a (a) 1 wt% agarose fluid gel network with white lines showing the location of the corresponding height profiles (b–d) of the network structure (image size = 0.5 × 0.5 μm).

heights of the aggregated polymer chains are measured up to 12 nm, and the widths range up to a size of 40 and even 60 nm, whereby multiple aggregated helical strands are distinctly seen to form larger strands again.

The observations in Fig. 11 are consistent with the findings from the previous AFM images. At the periphery, several strands are present (indicated by a blue arrow) that actually intend to crosslink with the core. Due to the high concentration degree of crosslinking, multiple helical structures already aggregate at the periphery, but are prevented from further crosslinking with the core due to the imposed shear. With a shear rate of 400 $s^{-1}$, the time during gelation is not enough for the molecules to assemble sufficiently, so only a few molecules are able to associate to form such a network structure. With respect to the location indicated by the blue arrow, with a width of about 40 nm, it is estimated that approx. 40 agarose polymer chains link to form assembled double helices.

The faster crosslinking time with respect to the inverse of the shear rate leads to these large aggregated agarose polymer chains at the periphery. As mentioned in the introduction, these aggregated chains diffuse much slower, which becomes even slower with further crosslinking of such chains *i.e.* the dynamics of the cluster slows down. As a result, the linkage to the gel core is no longer possible. As a result agarose chains and bundles remain unlinked with the cores of the gel particles.

The AFM micrographs offer additionally distinct structural elements, which contribute differently to the dynamics, *i.e.*, elastic and loss moduli. Fig. 5(a), 8(a), and 9(a) of the 0.5 wt% samples (*cf.* Fig. 4(a, b and c)) show loose dangling chains at the periphery; these are no longer present for the 2 wt%

 

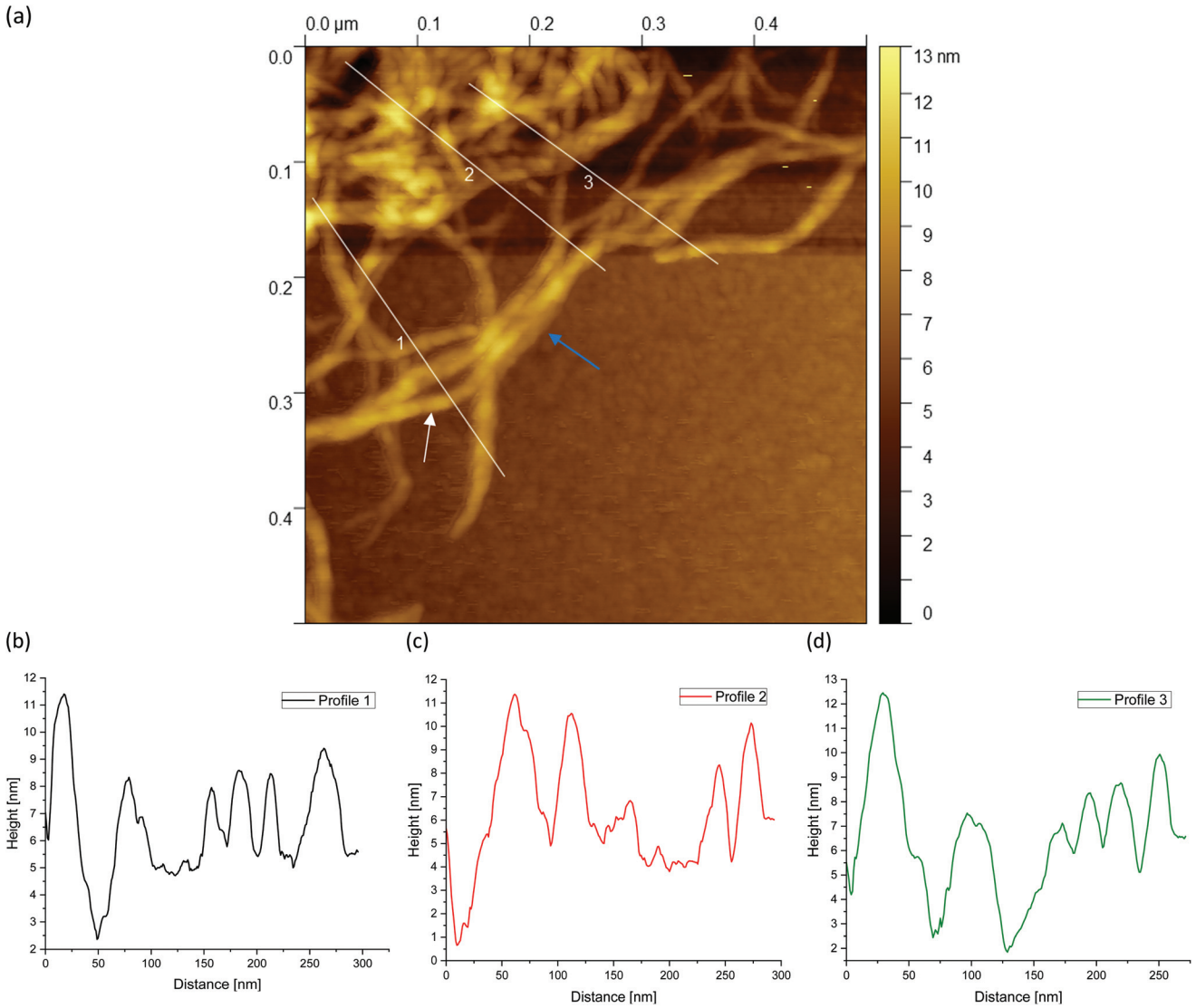


**Fig. 11** AFM image taken from the periphery of a (a) 2 wt% agarose fluid gel network with white lines showing the location of the corresponding height profiles (b–d) of the network structure (image size = 0.5 × 0.5 µm).

sample in Fig. 7(a), 8(c), and 11(a) (*cf.* Fig. 4(g, h and i)). These detailed structural elements at the particle surfaces must be discussed together with the previous results of the rheology, especially with the frequency sweeps (see Fig. 12).[7] For the 0.5 wt% sample, an increase in loss modulus ($G''$) with an increase in frequency was observed which was due to the dangling chains but also their less dense volume fraction and mesh size. For the 2 wt% sample, the loss modulus remains constant up to 10 rad $s^{-1}$ (see Fig. 12), which was attributed not only to the smooth and less irregularly "hairy" structure on the surface but also to the high volume fraction and dense packing. Moreover, the dense meshes contribute to the restriction and thus frequency-independent behavior of this sample.

The comparison of the measured height and width of the associated agarose strands of the different samples, which do not significantly differ from each other, further emphasizes how not only different textures but also rheological and tribological properties can arise from identical biopolymers simply by controlling the concentration and the process conditions, such as shear.[7] Moreover, the processing conditions combined with the concentration of the biopolymers in use influence the formulated molecular network structure of the particulate gel suspension at the microscopic level. This in turn determines the macroscopic response of the material to external forces, leading to a unique change in biomaterial gel-based food products. In fact, shear rate-dependent gelation leads to specific network structures of gel particles which have a defined ratio between the network density of the inner core and the outer core as well as the size of the chains at the surface of the particles.

The very loose particle surface structure at low concentrations of 0.5 wt% requires a separate discussion. The corres-

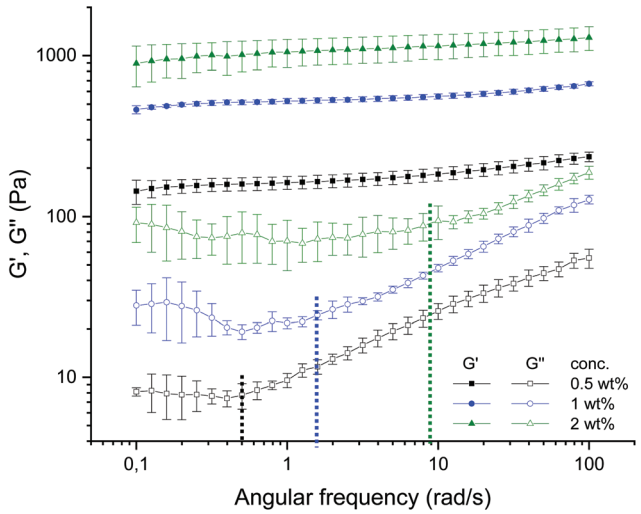


**Fig. 12** Frequency dependence of storage and loss moduli $G'$ (filled symbols), $G''$ (empty symbols) at a constant strain ($\gamma$ = 0.05%) and temperature ($T$ = 25 °C) for agarose fluid gels with different concentrations 0.5 wt% (black), 1 wt% (blue) and 2 wt% (green). The dashed lines indicate the angular frequency ($\omega_c$) where $G''$ starts to increase for the respective concentrations (reproduced from Ghebremedhin, Seiffert, and Vilgis[7]).

ponding time scales do not follow the predictions in the high concentration regimes, but can be estimated using a Rouse–Zimm model.[17]

The polymer chains diffuse to the nearest approximation before gelation begins, implying that the centre-of-mass diffusion constant DCM of the polymer chains in a good solvent behaves (apart from constant factors) as:

$$D_{CM} \propto \frac{k_B T}{N^{1/2}} \quad (2)$$

where $N$ is the degree of polymerization. Accordingly, the longest relaxation time follows $\tau \propto N^{1/2}$. In accordance with this, the time scales change during cooling with the time at which two neighboring chains become close enough to form helices, which in turn results in much smaller time scales. As a consequence, the diffusion of the growing gel cluster slows down further, which in turn depends on the size and thus the number of agarose chains involved. Thus, the shape of the particle grows irregularly at low agarose concentrations, resulting in extended dangling of excess parts.[7]

All these assumptions are in agreement with the findings of the AFM measurements in this work. Moreover, these results are additionally supported by the findings of the previous publication. It was proposed that the dangling chains, which were most pronounced in the 0.5 wt% samples, were responsible for a distinct increase in moduli during the frequency sweep.[7] Fig. 12 shows the frequency sweep of the resulting time-dependent behavior of the corresponding fluid gels at small oscillation strain. The observation is in agreement with the findings of the AFM images in this paper. It was suggested that the increase in $G'$ with an increase in frequency was due to the particle movement becoming faster, being pushed together and interfering with each other. The increase in $G''$, on the other hand, was attributed to the flexible dangling chains on the particle surfaces, which show faster motion and were more pronounced for the 0.5 wt% sample compared to the 1 wt% and 2 wt% fluid gel samples. This is explained by the fact that with a decrease in concentration the aggregated chains present at the particle surface and the particle size increase, whereas the volume fraction and thus the percolation decrease. However, an extended LVE range during amplitude sweep was also attributed to these hairy structures on the particle surface. Furthermore, not only an increased coefficient of friction during tribological measurements, but also an increased viscosity during flow sweep measurements at small shear rates were attributed to the aggregated helical chains.[7] Indeed, all these observations ascribed to the dangling ends and the higher proportion of the hairy structures could now be verified by AFM measurements.

More detailed knowledge of the loose surface structure allows the observations already made in Ghebremedhin, Seiffert, and Vilgis[7] to be interpreted more accurately. As shown in Fig. 12, the frequency at which $G''$ increases systematically depends on the concentration. Higher frequencies mean smaller time scales. However, this is precisely what suggests different surface structures. Assuming that the free ends behave in a first approximation according to the Rouse–Zimm model, relaxation times can be estimated with $\tau \sim N^{3/2}$.[17] The dangling parts are significantly longer at low agarose concentrations, so the time scales are longer. At high concentrations they are shorter. Consequently, the frequency at which the free ends of the external heavy movements can no longer follow the imposed oscillations increases. At these points, $G''$ increases practically linearly with a slope, and their values are indicated in Fig. 12 by dashed lines for the frequency ($\omega_c$) for the respective concentrations. While the 0.5 wt% fluid gel sample shows an increase in loss modulus $G''$ starting at a frequency of 0.5 rad $s^{-1}$ with a slope of 0.387 ± 0.004, the 1 wt% sample exhibits an increase in $G''$ starting at about 1.6 rad $s^{-1}$ with a slope of 0.419 ± 0.007, whereas the 2 wt% sample displays an increase in $G''$ starting at 9 rad $s^{-1}$ with a slope of 0.347 ± 0.007.

The physical interpretation is quite striking. For low frequencies $G''$ is not sensitive to frequency changes. The overdamped chain motion follows the imposed oscillatory shear from the rheometer. At higher frequencies the networks respond to their cross-link density accordingly. Assuming that the chain dynamics between two consecutive cross-links behaves close to a Rouse–Zimm-type motion, the frequency $\omega_c$, where $G''$ starts to increase, is given by $(\omega_c \tau_R) \approx 1$. However, the relaxation time $\tau_R$ depends on the molecular weight of the mesh size roughly as $\xi^3$ between two consecutive cross-links. Therefore $\omega_c$ scales as $1/\xi^3$. This simple argument shows that $\omega_c$ is shifted to larger values by decreasing the mesh size, and increasing the cross-link density. This trend can be seen by inserting the ratios of the mesh size at different concentrations (see Table 2) and calculating the shift factor of $\omega_c$ as a function

 

of the concentration. Hence, a determined $\omega_c$ of 1.39 rad $s^{-1}$ for the 1 wt% fluid gel sample and 6.5 rad $s^{-1}$ for the 2 wt% fluid gel sample is obtained. Even considering the large standard deviations of the mesh size distribution, an agreement can be found with $\omega_c$ given in Fig. 12. The slope of $G''$ seems to vary only marginally in the measured frequency range, which indicates its origin from the peripheral chains as well. The frequency range where $G''$ seems to increase linearly with the frequency may indicate the motion of the less restricted, loose and dangling network parts at the particle surfaces.

### 3.2 Comparison of the particle core with quiescent set gels

Another important question is whether the cross-link density of the gel core corresponds to the cross-link density of the quiescent set gels of the same concentration. In the previous sections it was assumed that the core gelation of the particles at time scales less than $1/\dot{\gamma}$ is compared directly to the quiescent gels. Consequently, the core shear modulus should be similar to the shear modulus of the bulk gel. This assumption can be attempted to be verified experimentally, as will be shown in the following paragraphs.

An amplitude sweep was performed to investigate and compare the viscoelastic properties of the hydrogels prepared under shear with those of the gels prepared under quiescent conditions.

This was done to gain a deeper understanding of the concentration-dependent characteristics of agarose fluid gels, which in our previous work were found to be influenced by the size and shape of the gel particles.[7] Furthermore, in the course of these rheological measurements, together with the findings of atomic force microscopy, the aim is to achieve a better physical insight into the interaction between the gel particles.

The approach of directly comparing the properties of agar hydrogels prepared under shear with those prepared under quiescent conditions has also been carried out in previous work on rheological measurements.[2] Furthermore, in other work on agarose fluid gels, texture analysis was performed on quiescently cooled agarose gels by assuming that the stress-deformation behavior exhibited corresponds to the behavior of individual particles.[6] Thus, assuming that the number of crosslinks in the core of a fluid gel particle is the same as that of the corresponding unsheared gel, it seems apparent that this approach will be useful in understanding the network formation of the particles.

Fig. 13 displays the results of the amplitude sweep for different concentrations of the agarose fluid gels and the agarose gels prepared under quiescent conditions. The mean value and standard deviations of the elastic and viscous moduli are shown as a function of the strain. For all samples, storage ($G'$) and loss ($G''$) moduli were specified within the linear-viscoelastic (LVE) range, thus describing the deformation behavior in the non-destructive range.

The limits of the LVE range and the characterization of the behavior after exceeding this range, which is called the non-linear viscoelastic range, have not been evaluated here. This has already been discussed in detail in the recent publication on fluid gels, where it was found that it is not the concentration and size of the particles but the structure that plays an important role in the mechanical properties, and is not relevant when comparing the fluid gels with the gels prepared under quiescent conditions.[7]

As expected, storage moduli ($G'$) (Fig. 13(a)) and loss moduli ($G''$) (Fig. 13(b)) increase with an increase in agarose concentration, and it is also not surprising that both the

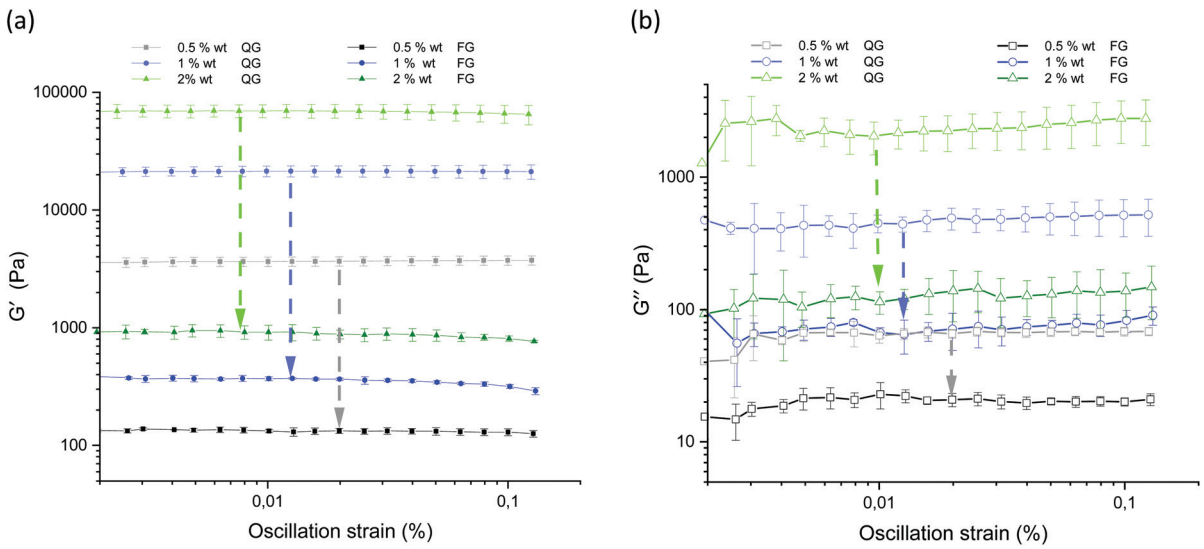


**Fig. 13** Amplitude sweep for the gels prepared under shear and non-sheared gels for the different agarose concentrations. (a) Storage ($G'$) moduli for the 0.5 wt% QG (gray) and FG (black), 1 wt% QG (light blue) and FG (dark blue) and 2 wt% QG (light green) and FG (dark green). (b) Loss ($G''$) moduli for the 0.5 wt% QG (gray) and FG (black), 1 wt% QG (light blue) and FG (dark blue) and 2 wt% QG (light green) and FG (dark green). As a function of applied oscillatory strain at a constant frequency (f = 1 Hz) and temperature ($T$ = 25 °C). The arrows indicate the strong decrease of the moduli of the differently prepared gels of the respective agarose concentration (QG = quiescently cooled gel, FG = fluid gel).

moduli of the quiescently cooled gels increase by multiple orders of magnitude compared to those of the fluid gels. Such a strong decrease of the moduli for the differently prepared gels is indicated by arrows for the respective agarose concentrations. For easier comparison, Fig. 14 shows the mean and their standard deviations of the respective storage and loss moduli depending on the concentration at a strain of $\gamma$ = 0.01%. When comparing the storage and loss moduli between different concentrations, the values are significantly different ($p < 0.05$) for both the fluid gels and quiescently cooled gels. For all gels, the corresponding mean values and their standard deviation are given in Table 3.

As can be seen from Table 3, the 2 wt% fluid gels exhibit a storage modulus of 920 (± 133) Pa and a loss modulus of about 114 (± 21.9) Pa, while the quiescently cooled gel of the same concentration exhibits a much higher storage modulus by a factor of about 76, and a loss modulus higher by a factor of about 18. For the agarose concentration of 1 wt%, the fluid gels show a $G'$-value of about 369.6 (± 14.3) Pa and a $G''$-value of 66.9 (± 5.9) Pa, whereas the corresponding quiescently cooled gel exhibits an increase in storage modulus by a factor of ~58 and an increase in $G''$ by a factor of ~7. Finally, the 0.5 wt% fluid gel reveals a $G'$ of 132.5 (± 4.3) Pa and a $G''$-value of 22.9 (± 5.2) Pa, where the corresponding quiescently cooled gel displays an increase in $G'$ by a factor of ~28 and an increase in $G''$ by a factor of ~3.

These very high moduli of the gels cooled under quiescent conditions arise from the already mentioned fact that as a strong gelling polysaccharide, agarose forms firm and brittle gels. The agarose polymer chains, which form double helices *via* hydrogen bonding, aggregate into thick bundles of junction zones that lead to the formation of these strong gels.[9] Consequently, according to the correlation between the mesh size and the elastic modulus for permanently cross-linked gels, an increase in the modulus with increasing agarose concentration is observed (see eqn (1)). Furthermore, for the fluid gels, storage and loss moduli increase with an increase in agarose concentration and the samples show an elastic dominated behavior *i.e.* a gel-like behavior, indicating an interconnected network of gel particles formed by a highly cross-linked agarose polymer.

By considering the decrease of the storage moduli of the fluid gels to those of the non-sheared gels and comparing them within the different concentrations, it can be observed that the increase from 0.5 wt% to 1 wt% gels is greater than the increase of the storage modulus from 1 wt% to 2 wt% samples. These observations no longer hold for the loss modulus (see Table 4). Thus, this observed trend is consistent with the assumption that the textural behavior of quiescently cooled gels is the same as that of the individual particles of the fluid gels of the same concentration.[6] Furthermore it was assumed in earlier work that the moduli of the sheared agar gel would scale with the moduli of microgel particles, which correspond to the moduli of a quiescently cooled agar gel.[2]

To compare the cross-link density of the gel core of the fluid gel particle corresponding to the cross-link density of the quiescently cooled gels of the same concentration, we consider the calculated mesh size estimated by the measured storage modulus of the quiescently cooled gel with the mesh size of the core of the fluid gel particle estimated by the AFM phase image in Fig. 2. According to eqn (1) and since $k_BT$ is given, $\xi^3$ was computed by inserting the measured $G'$-value of the quiescently cooled gel (see Table 3).

Based on the AFM phase images in Fig. 2, one approach to estimating the mesh size would be to determine the distance of an agarose strand at the top level until it is overlapped by a next strand, either by entanglement or by cross-links. This means that this length corresponds to a distance between two

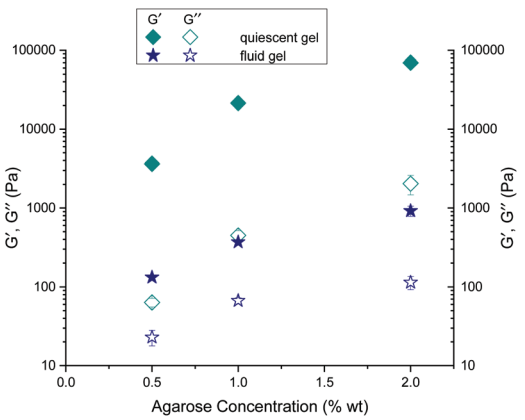


**Fig. 14** Comparison of the mean values of the storage ($G'$) and loss ($G''$) moduli for the gels prepared under shear and non-sheared gels for different agarose concentrations at a strain of $\gamma$ = 0.01%.

**Table 3** Averages of amplitude sweep of storage ($G'$) and loss ($G''$) moduli for the agarose gels prepared under shear and non-sheared gels for different concentrations at a constant strain of $\gamma$ = 0.01% (QG = quiescently cooled gel, FG = fluid gel). Data are presented as means ± SD of triplicate and the values in the table are significantly different ($p < 0.05$) as obtained by analysis of variance (one-way ANOVA)

| Gels | $G'$ [Pa] | $G''$ [Pa] |
|---|---|---|
| 2 wt% QG | 69 888.3 ± 8819.7 | 2041.4 ± 566.2 |
| 2 wt% FG | 920.2 ± 133.0 | 114.3 ± 21.9 |
| 1 wt% QG | 21 442.1 ± 2261.7 | 447.9 ± 68.9 |
| 1 wt% FG | 369.6 ± 14.3 | 66.9 ± 5.9 |
| 0.5 wt% QG | 3643.0 ± 333.6 | 63.6 ± 7.9 |
| 0.5 wt% FG | 132.5 ± 4.3 | 22.9 ± 5.2 |

**Table 4** Comparison of the ratios of the moduli of the agarose gels prepared under shear (FG) and non-sheared gels (QG) within the different concentrations

| Gels | $G'_{QG}$ | $G''_{QG}$ | $G'_{FG}$ | $G''_{FG}$ |
|---|---|---|---|---|
| 2 wt%/1 wt% | 3.3 (± 3.9) | 4.6 (± 8.2) | 2.5 (± 9.3) | 1.7 ± (3.7) |
| 1 wt%/0.5wt% | 5.9 (± 6.8) | 7.1 ± (8.7) | 2.8 (± 3.3) | 2.9 ± (1.1) |

cross-links *i.e.* junction zones, as already shown in Fig. 3. That is, if the length of the distinctly visible strands on the surface in Fig. 2 is shortened, it would imply a smaller mesh size. In fact, the distance between these cross-links would be the mesh size that determines the modulus. However, it should be noted that the distance $\xi$ only applies in a good solvent. This is because the estimated mesh size in Fig. 2 corresponds to a gel that has been squeezed and shrunk into two dimensions by drying. Therefore, the distance in question should be multiplied by a factor of the water volume, which is thus the third root of the volume of the water fraction of the corresponding agarose gel concentration. The calculated mesh sizes from the storage moduli of the quiescently cooled gels measured by amplitude sweep (see Fig. 13 and Table 3) are given in Table 5.

By comparing the calculated mesh sizes of about 48 nm for the 0.5 wt% sample, 27 nm for the 1 wt% sample, and 18 nm for the 2 wt% sample of the quiescently cooled gels with the AFM phase images of the fluid gels in Fig. 2 and tracing these calculated values over such an undisturbed strand, it can be seen that the distances calculated here are somewhat shorter than those seen in the AFM phase images. Nevertheless, the magnitudes of the calculated $\xi$ values agree with the lengths of the strands.

This is an indication of the fact that in the core of a fluid gel particle, the time scales of gel formation are faster than that of the imposed shear rate and therefore comparable gelling occurs as in a quiescently cooled gel. Indeed, this conclusion is consistent with the aforementioned assumption that when the chains move faster than the time $1/\dot{\gamma}$ imposed by the shear, they are able to form gels comparable to the quiescent conditions.

Fig. 15 shows the AFM phase images from Fig. 2 with the indicated lengths of the previously determined mesh size. This is to illustrate the extent to which the mesh size determined from the storage modulus approximates the lengths of the strands in the core of the AFM phase images. A total of 20 points were measured per concentration with an average of 56.1 ± 10.3 nm for 0.5 wt%, 29.7 ± 4.7 nm for 1 wt% and 22.2 ± 2.6 nm for 2 wt% fluid gel samples.

In previous work on fluid gels made of agar, the dependence on the concentration and method of preparation of sheared gels was compared with spherical microgel suspensions and also with gels prepared under quiescent conditions, all from the same material.[2] They also found a dependence of the moduli on the concentration and more on the internal structure and particle shape.[2]

These results are in agreement with the findings of the AFM images shown here and with the assumption that the bulk rheology of the fluid gels is influenced by the particle shape, size and also elasticity. This in turn is governed by the elasticity of the higher network density in the inner core of the particles, which becomes less dense in the outer region. In addition, the chains on the particle surface play a role, which also depends on the agarose concentration.

**Table 5** Average calculated mesh size $\xi_{c\ (QG)}$ [nm] from the measured storage moduli $G'_{m\ (QG)}$ [Pa] obtained from amplitude sweep and the respective calculated mesh size considering the factor of the water volume fraction (($\xi_{c\ (QG)}$ [nm]) × factor)

| Gels | $G'_{m\ (QG)}$ [Pa] | $\xi_{c\ (QG)}$ [nm] | ($\xi_{c\ (QG)}$ [nm]) × factor |
|---|---|---|---|
| 2 wt% QG | 69 888.3 ± 8819.7 | 3.9 ± 0.1 | 17.9 ± 0.7 |
| 1 wt% QG | 21 442.1 ± 2261.7 | 5.8 ± 0.2 | 26.7 ± 0.9 |
| 0.5 wt% QG | 3643.0 ± 333.6 | 10.4 ± 0.3 | 48.2 ± 1.5 |

### 3.3 Scanning electron microscopy (SEM)

Fig. 16 shows the SEM micrographs of the different concentrations of the fluid gels and the corresponding gels prepared under quiescent conditions. To provide supplemental structural information in addition to the results of the rheological properties, SEM was performed on all fluid gels prepared with the different concentrations and the corresponding quiescently cooled gels. The images for the fluid gels (a–c) show fibril-like microstructures formed by interconnected pores surrounding the fibers with a wide size distribution of up to several micrometers. Furthermore, it can be seen that as

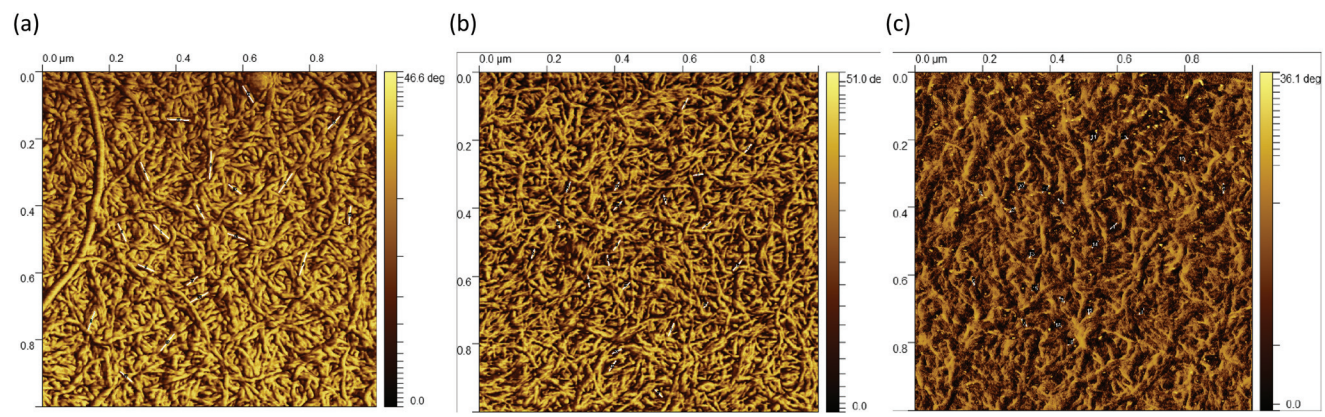


**Fig. 15** AFM phase images taken from the center (a) 0.5 wt%, (b) 1 wt% and (c) 2wt%. The indicated length was approximated to 48 nm for the 0.5 wt%, 27 nm for the 1 wt% and 18 nm for the 2 wt% fluid gel samples.

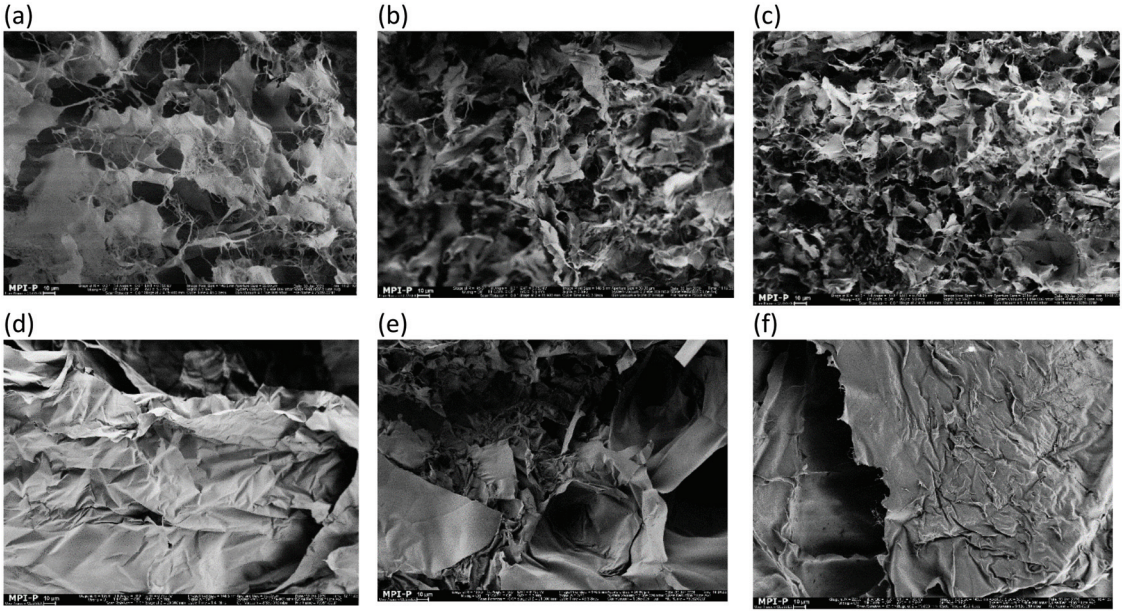


**Fig. 16** SEM images of the freeze dried fluid gels with (a) 0.5 wt%, (b) 1 wt%, and (c) 2 wt% agarose concentrations and gels cooled under quiescent conditions with (d) 0.5 wt%, (e) 1 wt% and (f) 2 wt% agarose concentrations. Scale bars are 10 μm. (a, b and c are reproduced from Ghebremedhin, Seiffert, and Vilgis[7]).

expected, a denser network forms with an increase in concentration. Thus, a densification of the network takes place.[7] On the other hand the images of the gels prepared under quiescent conditions (d–f) display a completely different structure, namely a leaflet type structure. From the findings of the micrographs, the rheological and mechanical properties can be deduced, since the gel strength of the sample varies with the density of the network of structural patterns. Furthermore, the comparison of the SEM images of the different gels produced depicts how different properties can arise from identical biopolymers.

## 4 Conclusion

In this work we have investigated the underlying physical and microscopic characteristics of fluid gels linked with their macroscopic properties. Agarose based fluid gels were prepared during gelation under shear, resulting in gel particles with various network structures that influence the macroscopic behavior. We used AFM measurements to investigate the network structure of the fluid gels. Representative examples of the AFM images of the network structures of the different agarose gel concentrations were analyzed. The height profiles and mesh sizes were determined to characterize and evaluate the AFM images. The focus of this work, however, was to determine the mesh size as this determines the structure and the elasticity as well as the dynamics that are reflected in $G'$ and $G''$. In fact, these AFM images were intended to support the assumptions of the findings of our recent paper.

It was found that the dense region of the network structure changed towards the periphery of the gel particles. Moreover, this network structure and its elasticity also changed with the concentration (0.5 wt%, 1 wt%, 2 wt%). In addition, the correlation that cracks at the edge of the network is more likely to occur at higher concentrations, as observed at concentrations of 1 wt% and 2 wt%, can be explained by the mechanism that takes place during the preparation of fluid gels. It was assumed that with a higher concentration, the probability of rapid gelation of agarose chains is higher because more chains are present that can associate to form double helices and subsequently aggregate. When this aggregated network forms, but at the same time, the gelation in the rheometer is subjected to shear, these cracks occur at the edge, and they are more pronounced the faster the gelation takes place since the probability of gelation is much higher. Furthermore, the peripheral region plays a crucial role in the interaction between the gel particles and contributes to defining the length scale for their elastic response in bulk. In fact, it can be deduced that near the surface of the gel particles, the elasticity and friction properties change as the ratio between the inner core and the outer core *i.e.* peripheral region changes. This is due to the fact that the mesh size shows a broader distribution from the center towards the periphery, depending on the concentration and competing time scales such as shear rate and molecular motion. Using oscillatory measurement the viscoelastic properties of the fluid gels were compared with gels prepared under quiescent conditions. With these measurements we could support the assumption that the textural behavior of quiescently cooled gels corresponds to that of the individual particles of the fluid gels of the same concentration. In

 

addition, the assumption that the mesh size of the densely cross-linked core of the fluid gel particle is approximately the same as that in the quiescently cooled gel was confirmed. Accordingly, during gelation under shear, the molecules move faster on the time scale, than the shear imposed time due to concentration and temperature and associate into double helices and aggregate into larger clusters, resembling the quiescently cooled gels.

Finally, from the scanning electron microscopy (SEM) results, the result of rheological measurements could be deduced, showing that the viscoelastic properties of the gels vary with the density of the network of structural patterns.

Overall, this study illustrates the importance of understanding the interplay between the length and time scales of biopolymers during gelation under shear for the preparation of fluid gels in order to design fluid gels for tailored applications with specific viscoelastic, textural, and lubricating properties.

## Author contributions

Marta Ghebremedhin: conceptualization, writing – original draft, methodology, investigation, validation, visualization, and data interpretation. Sebastian Seiffert: supervision and conceptualization. Thomas A. Vilgis: supervision, conceptualization, writing – review and editing, visualization, and interpretation.

## Conflicts of interest

The authors declare no conflicts of interest.

## Acknowledgements

The authors would like to thank Dr Rüdiger Berger and especially Helma Burg for the technical support with the atomic force microscopy measurements. Many thanks also to Gunnar Glaßer for recording the SEM images and Christine Rosenauer for the SEC measurements. Furthermore, we thank the members of the MPIP soft matter food science group for fruitful discussion and proofreading of the manuscript. Open Access funding was provided by the Max Planck Society.

## References

1 I. F. Farrés, R. J. A. Moakes and I. T. Norton, Food Hydrocolloids Designing biopolymer fluid gels: A microstructural approach, *Food Hydrocolloids*, 2014, **42**, 362–372, DOI: **10.1016/j.foodhyd.2014.03.014**.

2 W. Frith, X. Garijo, T. Foster and I. Norton, *Microstructural origins of the rheology of fluid gels*, Special Publication, 2002.

3 I. T. Norton, D. A. Jarvis and T. J. Foster, A molecular model for the formation and properties of fluid gels, *Int. J. Biol. Macromol.*, 1999, **26**(4), 255–261, DOI: **10.1016/S0141-8130(99)00091-4**.

4 M. H. Mahdi, B. R. Conway, T. Mills and A. M. Smith, Gellan gum fluid gels for topical administration of diclofenac, *Int. J. Pharm.*, 2016, **515**(1–2), 535–542.

5 M. H. Mahdi, B. R. Conway and A. M. Smith, Evaluation of gellan gum fluid gels as modified release oral liquids, *Int. J. Pharm.*, 2014, **475**(1–2), 335–343.

6 A. Gabriele, F. Spyropoulos and I. T. Norton, A conceptual model for fluid gel lubrication, *Soft Matter*, 2010, **6**(17), 4205–4213, DOI: **10.1039/c001907k**.

7 M. Ghebremedhin, S. Seiffert and T. A. Vilgis, Physics of agarose fluid gels: Rheological properties and microstructure, *Curr. Res. Food Sci.*, 2021, **4**(December 2020), 436–448, DOI: **10.1016/j.crfs.2021.06.003**.

8 A. Imeson, *3 Agar, Food stabilisers, Thick gelling agents*, 2009, p. 31.

9 D. Nordqvist and T. A. Vilgis, Rheological Study of the Gelation Process of Agarose-Based Solutions, *Food Biophys.*, 2011, **6**(4), 450–460, DOI: **10.1007/s11483-011-9225-0**.

10 C. Nowak and T. A. Vilgis, Rod-coil multiblock copolymers: Structure and stability, *EPL (Europhys. Lett.)*, 2004, **68**(1), 44.

11 T. A. Vilgis, Gels: Model systems for soft matter food physics, *Curr. Opin. Food Sci.*, 2015, **3**, 71–84, DOI: **10.1016/j.cofs.2015.05.009**.

12 B. H. Zimm and J. K. Bragg, Theory of the phase transition between helix and random coil in polypeptide chains, *J. Chem. Phys.*, 1959, **31**(2), 526–535.

13 K. Nishinari and Y. Fang, Sucrose release from polysaccharide gels, *Food Funct.*, 2016, **7**(5), 2130–2146, DOI: **10.1039/c5fo01400j**.

14 K. Nishinari and Y. Fang, Relation between structure and rheological/thermal properties of agar. A mini-review on the effect of alkali treatment and the role of agaropectin, *Food Struct.*, 2017, **13**(September), 24–34, DOI: **10.1016/j.foostr.2016.10.003**.

15 S. M. Fiszman and L. Duran, Effects of fruit pulp and sucrose on the compression response of different polysaccharides gel systems, *Carbohydr. Polym.*, 1992, **17**(1), 11–17.

16 W D. Carvalho and M. Djabourov, Physical gelation under shear for gelatin gels, *Rheol. Acta*, 1997, **36**(6), 591–609, DOI: **10.1007/BF00367355**.

17 M. Doi and S. F. Edwards, *The theory of polymer dynamics*, Oxford University Press, (Clarendon) London, New York, 1986.

18 S. Holland, C. Tuck and T. Foster, Fluid Gels: a New Feedstock for High Viscosity Jetting, *Food Biophys.*, 2018, **13**(2), 175–185, DOI: **10.1007/s11483-018-9523-x**.

19 A. L. Ellis, A. B. Norton, T. B. Mills and I. T. Norton, Stabilisation of foams by agar gel particles, *Food Hydrocolloids*, 2017, **73**, 222–228, DOI: **10.1016/j.foodhyd.2017.06.038**.

20 K. Bertula, L. Martikainen, P. Munne, *et al.*, Strain-Stiffening of Agarose Gels, *ACS Macro Lett.*, 2019, **8**(6), 670–675, DOI: **10.1021/acsmacrolett.9b00258**.

21 D. Nečas and P. Klapetek, *Gwyddion*, 2021, **https://gwyddion.net/** (Accessed: 30th November 2021).
22 A. P. Gunning, A. R. Kirby, V. J. Morris, B. Wells and B. E. Brooker, Imaging bacterial polysaccharides by AFM, *Polym. Bull.*, 1995, **34**(5), 615–619.
23 V. J. Morris, A. R. Kirby and P. A. Gunning, *Atomic Force Microscopy for Biologists*, World Scientific, 2009.
24 M. Martínez-Sanz, A. Ström, P. Lopez-Sanchez, *et al.*, Advanced structural characterisation of agar-based hydrogels: Rheological and small angle scattering studies, *Carbohydr. Polym.*, 2020, **236**(September 2019), DOI: **10.1016/j.carbpol.2019.115655**.
25 S. A. Foord and E. D. Y. Atkins, New x–ray diffraction results from agarose: Extended single helix structures and implications for gelation mechanism, *Biopolymers*, 1989, **28**(8), 1345–1365, DOI: **10.1002/bip.360280802**.
26 P.-G. De Gennes, *Scaling Concepts in Polymer Physics*, Cornell University Press, 1979.
27 B. I. Zielbauer, N. Schönmehl, N. Chatti and T. A. Vilgis, Networks: From Rubbers to Food, in *Designing of Elastomer Nanocomposites: From Theory to Applications*, Springer, 2016, pp. 87–233.
28 N. Russ, B. I. Zielbauer, K. Koynov and T. A. Vilgis, Influence of nongelling hydrocolloids on the gelation of agarose, *Biomacromolecules*, 2013, **14**(11), 4116–4124, DOI: **10.1021/bm4012776**.
29 M. Watase, K. Nishinari and T. Hatakeyama, DSC study on properties of water in concentrated agarose gels, *Food Hydrocolloids*, 1988, **2**(6), 427–438.

**Electronic Supplementary Information**

# Molecular behavior of fluid gels – the crucial role of edges and particle surface for macroscopic properties

Marta Ghebremedhin[1], Sebastian Seiffert[2], Thomas A. Vilgis[1]

[1]Max Planck Institute for Polymer Research, Ackermannweg 10, 55128 Mainz, Germany

[2]Department of Chemistry, Johannes Gutenberg University Mainz, Duesbergweg 10-14, 55128 Mainz, Germany

E-mail: ghebre@mpip-mainz.mpg.de (M. Ghebremedhin), vilgis@mpip-mainz.mpg.de (T.A. Vilgis)

## S1 Materials and methods

### S1.1 Preparation of quiescently cooled gels (*Ex situ*)

To verify the amplitude test of the quiescently cooled gels prepared *in situ* directly in the rheometer (as described in section 2.2.2 Preparation of quiescently cooled gels), they were compared with gels prepared outside the rheometer (*ex situ*) using amplitude sweep measurements (see Figure S2). Therefore, disposable aluminum plates with a diameter of 25 mm and a height of 3 mm, and Teflon molds with an inner diameter of 25 mm and a height of 6 mm that were slipped over the aluminum plates were used. To produce the gels with defined height and diameter, the still hot agarose solution was pipetted into the Teflon mold and evenly distributed with a razor blade. The set gels were then cooled to room temperature and cured overnight in the refrigerator at 4 °C. To minimize water evaporation, the molds were covered with disposable weighing dishes that were greased around the edges to seal them airtight. The next day, the molds were carefully removed and the samples were adjusted to room temperature before measurements.

### S1.2 Rheological measurements of the quiescently cooled gels (*Ex situ*)

For the quiescently cooled gels prepared *ex situ*, amplitude oscillatory measurements were performed on a Discovery HR-3 Rheometer (TA Instruments) using a 25 mm diameter plate at a constant temperature of 25 °C and a soak time of 120 s. The amplitude sweeps were carried out at a constant frequency $f$ = 1 Hz, and storage ($G'$) and loss ($G''$) moduli were measured as a function of strain $\gamma$ ranging from 0.001 % to 1000 %. To avoid slippage effect of the samples, sandpaper with a grit size of P80 was used and glued on both plates with double sided adhesive tapes.

Since the height of the gels differed from the intended 3 mm during cooling, the gap size between the two plates needed to be varied to ensure sufficient adhesion and to prevent the sample from slipping

during measurements. Therefore, sufficient pressure had to be applied on the sample between the plates. However, squeezing the sample should be avoid. Hence, an axial force of about 0.15 N for the 0.5 wt% gels, 0.5 N for the 1 wt%, and 1 N for the 2 wt% gels, was applied in order to obtain appropriate contact for the amplitude sweep. This indicates that the gels were not completely flat and that more normal force had to be applied the stiffer the samples were to achieve better contact between the upper plate and the sample.

### S1.2 Size exclusion chromatography (SEC)

Size exclusion chromatography measurements were performed on a PSS SECcurity$^2$ system (PSS, Polymer Standards Service Mainz, Germany) equipped with a refractive index detector and a UV detector (280 nm). Chromatographic separation was performed by using a SUPREMA Linear XL column (10µm, 8 x 300 mm) (PSS). All experiments were performed in 0.1M NaNO3 at a flow rate of 1 ml/min and 60°C. The sample with a concentration of 1 mg/ml was first heated at 90°C for 3 h, then cooled to 60°C and finally filtered through a 0.45 syringe filter prior to measurement. An injection volume of 50 µl was used. Calibration was carried out with pullulane stadards (molar masses between 180 g/mol and 800000 g/mol ) provided by PSS. All data were recorded and evaluated by using PSS WinGPC UniChrom.

## S2 Results

### S2.1 The significance of the trend of tan($\delta$) of fluid gels compared to quiescently cooled gels

In order to obtain further information from the amplitude sweeps (Figure 13), tan($\delta$) was plotted against the deformation strain as shown in Figure S1. These values of tan($\delta$) are higher for the fluid gels than for the gels cooled under quiescent condition. This is explained by the fact that the elastic behavior of the unsheared gels is extremely dominant over the viscous behavior, which is due to the aforementioned three-dimensional continuous network of aggregated double helices in thick bundles of junction zones that lead to strong gels. The fluid gels and the corresponding gels prepared under quiescent conditions were turned upside down to demonstrate the solid-like properties (see Figure S1 (a and b)). Furthermore, taking into account the smaller error bars for the fluid gels, a slight increase in tan($\delta$) can be seen with increasing strain. This indicates an increase in $G''$, and thus an increase in the deformation energy transferred to the environment before deforming parts of the inner structure to a certain extent, and finally disrupting the connection between the particles. The values of tan($\delta$) at a strain $\gamma$ = 0.01 of the different fluid gel concentrations are significantly different ($p < 0.05$, one-way ANOVA). However, if considering the small deformation strains below $\gamma$ = 0.01 %, it can be observed that the smallest tan ($\delta$) value are resulting for the 2 wt% fluid gels followed by the 0.5 wt% gels, which show a higher value, and finally the highest tan($\delta$) for the 1 wt% fluid gels. These observations are consistent with the results on tribology, textural analysis and rheology measurements such as amplitude sweep, frequency sweep and flow sweep. They are attributed to the high volume fraction and percolation of the densely packed gel particles of the 2 wt% sample on the one hand, and to the loose surface structure and less densely packed gel particles of the 0.5 wt% and 1 wt% samples on the other hand.[1] In addition, the reason why the 1 wt% fluid gel samples show a higher tan($\delta$) than the

0.5 wt% fluid gel can be explained by the presence of a higher proportion of hairy structures on the particle surfaces of the lower concentrated fluid gel, which was already observed in Ghebremedhin, Seiffert, and Vilgis.[1] The aggregated chains on the particle surface become entangled at low strain (within the LVE range), resulting in higher elasticity and thus lower tan ($\delta$) for the 0.5 wt% than for the 1 wt% fluid gels sample. Moreover, the differences of tan ($\delta$) at a strain $\gamma$ = 0.01 of the gels cooled at quiescent conditions are not significant with respect to the concentration ($p < 0.05$). On the other hand, there is an increase not only in the error bars but also in the tan($\delta$). As mentioned earlier, this is due the fact that as the deformation increases, the gels break up and thus the viscous part increases. Although a trend of increasing storage and loss moduli with increasing concentration is obvious from the results shown in Figure 13 and Table 3, a one-way ANOVA revealed no statistically significant difference in tan($\delta$) at strain $\gamma$ = 0.01 of the gels cooled under quiescent conditions. Note in Figure S1 that, in contrast to the fluid gels, the tan($\delta$) of the quiescently cooled gels increases with increasing concentration. However, this observation is not consistent with previously published results in which the authors reported that tan($\delta$) of agarose gels decreases with increasing concentration and requires further investigation.[2] Therefore, supplementary amplitude sweep measurements were performed with gels previously gelled outside the rheometer (*ex situ*) under quiescent conditions. This examination will be discussed in detail below.

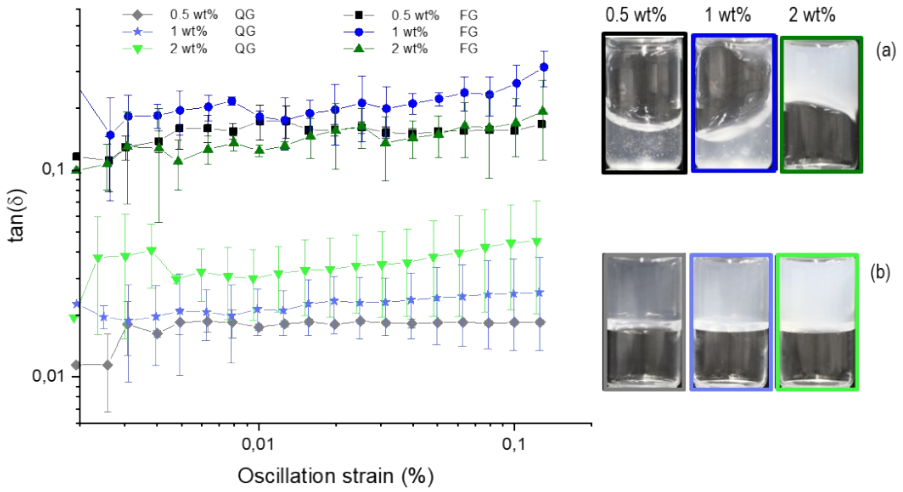


*Figure S1. Amplitude sweep for the gels prepared under shear and non-sheared gels for the different agarose concentrations. Dependence of tan ($\delta$) on strain at constant frequency ($f$ = 1 Hz) and temperature (T = 25 °C). Fluid gels (a) and corresponding gels prepared under quiescent conditions (b) were turned upside down to demonstrate the solid-like properties.*

Figure S2 show the comparison of the amplitude sweeps of the different prepared quiescently cooled gels: the gels prepared directly in the rheometer (*in situ*) and the gels prepared under quiescent conditions outside the rheometer in molds of defined diameter and height (*ex situ*). As expected, it can be seen that the storage and loss moduli increase with increasing concentration for both the *in situ* and the *ex situ* quiescently cooled gels. However, compared to the gels prepared *ex situ*, the gels prepared *in situ* show a higher value for the storage moduli for all concentrations (see Figure S2 (a)). For the loss moduli, on the other hand, the differences between the various prepared gels are smaller (see Figure S2 (b)).

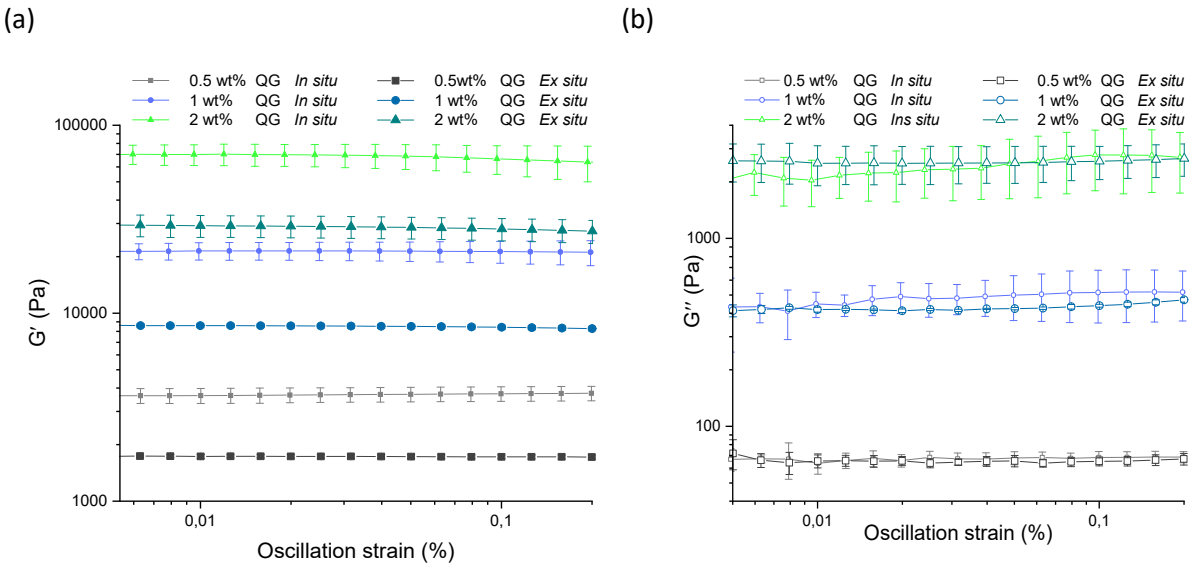


*Figure S2. (a) Storage (G') and loss (G'') moduli of the amplitude sweep of the different prepared quiescently cooled gels. Gels prepared directly in the rheometer (in situ) and outside the rheometer (ex situ).*

However, when comparing the tan ($\delta$) in Figure S3 of the differently prepared quiescently cooled gels for both the same trend of an increase of tan($\delta$) with increasing concentration can be observe. As mentioned earlier, this is not in agreement with some previously published results. Nevertheless, on the other hand a similar trend was observed in studies on agar microgel suspensions.[3] However, the tendency observed in this work here can be explained by the fact that, in contrast to an ideal network in which each chain is continuously cross-linked, the gels produced here are not. According to the size exclusion chromatography (SEC) results in Figure S4, the molecular weight of the agarose used in this work exhibits a broad distribution. This indicates that shorter chain ends remain uncrosslinked and therefore move, leading to an increase in deformation energy and thus an increase in viscous dissipation. The relative movement of the free chain ends, which are not permanently embedded in the network, could explain this inconsistency of increasing tan ($\delta$) with increasing concentration. Moreover, since not all agarose chains can be cross-linked, more uncross-linked chains dangle freely between the meshes at higher concentrations.

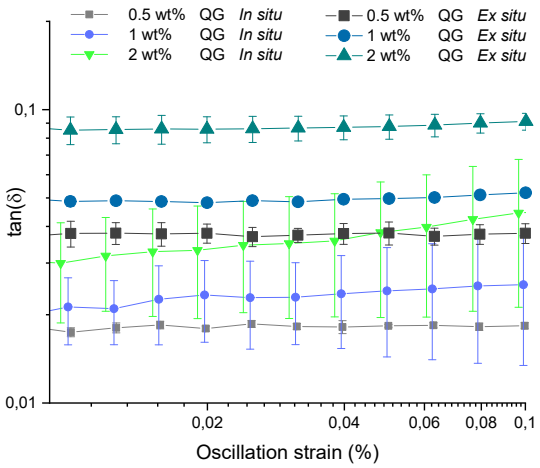


*Figure S3. Tan(δ) of the amplitude sweep of the different prepared quiescently cooled gels. Gels prepared directly in the rheometer (in situ) and outside the rheometer (ex situ).*

## S2.2 Size exclusion chromatography (SEC)

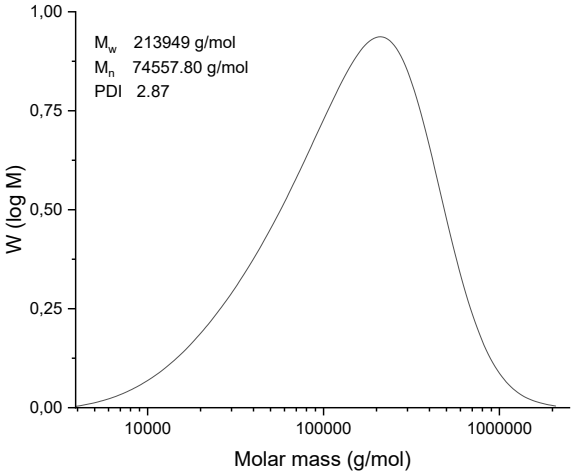


*Figure S4. Molecular weight distributions of agarose estimated by SEC. Number average molar mass ($M_n$), weight-average molar mass ($M_w$) and polydispersity index (PDI) are also shown.*

# References


1. M. Ghebremedhin, S. Seiffert and T. A. Vilgis, Physics of agarose fluid gels: Rheological properties and microstructure, *Current Research in Food Science*, 2021, **4**, 436-448.
2. K. Nishinari, M. Watase, K. Kohyama, N. Nishinari, D. Oakenfull, S. Koide, K. Ogino, P. A. Williams and G. O. Phillips, The effect of sucrose on the thermo-reversible gel-sol transition in agarose and gelatin, *Polymer Journal*, 1992, **24**, 871-877.
3. S. Adams, W. J. Frith and J. R. Stokes, Influence of particle modulus on the rheological properties of agar microgel suspensions, *Journal of Rheology*, 2004, **48**, 1195-1213.

## 7.3 Effect of sugar molecules on the rheological and tribological properties and on the microstructure of agarose-based fluid gels

Marta Ghebremedhin[1], [redacted]

[1]Max Planck Institute for Polymer Research, Ackermannweg 10, 55128 Mainz

[redacted]

Published in *Frontiers in Soft Matter*, 4, 2024,

The published version is available at: DOI: 10.3389/frsfm.2024.1363898

Authors contributions:

M.G. carried out the conceptualisation, methodology, and the planning and execution of all experiments, including rheology, tribology, texture analysis, microscopy, and particle size analysis, as well as data analysis, visualisation, and manuscript drafting.

frontiers | Frontiers in Soft Matter

TYPE Original Research
PUBLISHED 26 April 2024
DOI 10.3389/frsfm.2024.1363898



OPEN ACCESS

EDITED BY
Lester Geonzon,
The University of Tokyo, Japan

REVIEWED BY
Luben Arnaudov,
Unilever's Foods Innovation Centre, Netherlands
Raffaele Mezzenga,
ETH Zürich, Switzerland

*CORRESPONDENCE
Marta Ghebremedhin,
ghebre@mpip-mainz.mpg.de
Thomas A. Vilgis,
vilgis@mpip-mainz.mpg.de

RECEIVED 31 December 2023
ACCEPTED 08 April 2024
PUBLISHED 26 April 2024

CITATION
Ghebremedhin M, Seiffert S and Vilgis TA (2024), Effects of sugar molecules on the rheological and tribological properties and on the microstructure of agarose-based fluid gels. *Front. Soft Matter* 4:1363898. doi: 10.3389/frsfm.2024.1363898



# Effects of sugar molecules on the rheological and tribological properties and on the microstructure of agarose-based fluid gels

Marta Ghebremedhin[1]*, Sebastian Seiffert[2] and Thomas A. Vilgis[1]*

[1]Max Planck Institute for Polymer Research, Mainz, Germany, [2]Department of Chemistry, Johannes Gutenberg University Mainz, Mainz, Germany

**Introduction:** Fluid gels exhibit a unique flow behaviour. Their pronounced viscoelastic behaviour arises from irregular microgel particles, leading to plasticity and yielding, as well as a characteristic transition from a solid to a fluid-like state. This is defined by both the core and the surface structures of the particles. Adding co-solutes such as sucrose alters the network properties at the molecular scale, affecting texture and lubrication. This study investigates how the microscopic changes due to sucrose addition correlate with macroscopic changes.

**Material and methods:** Agarose fluid gels with varying sucrose concentrations were prepared and studied using the rheometer. Temperature dependent viscosity behaviour during gelation under shear was investigated *in situ*. Light microscopy and particle size measurements were examined, and complemented by amplitude, frequency and flow sweeps as well as tribological studies. These tests allow us to understand the influence of sucrose on the particle network formation.

**Results and discussion:** Sucrose concentration influenced the sizes, shapes, and interconnected network structure of the microgel particles. These microstructural changes are closely related to the dynamic competition between gelation and disruption of the agarose chains during shear, which directly influences the rheological and tribological properties of the resulting fluid gels. Additionally, the association of the agarose chains and their gelation process is also influenced depending on whether the sucrose or agarose was first dissolved in water. The experimental observations suggest specific molecular mechanisms, explaining the role of sucrose in structure formation of agarose-based fluid gels. These results have the potential to expand the applications of fluid gels, which play a crucial role in modifying the texture and flow behaviour of foods and beverages, particularly in addressing challenges such as dysphagia.

KEYWORDS

**agarose, fluid gels, microgel particles, physical gelation, rheology, tribology, sucrose, microstructure**

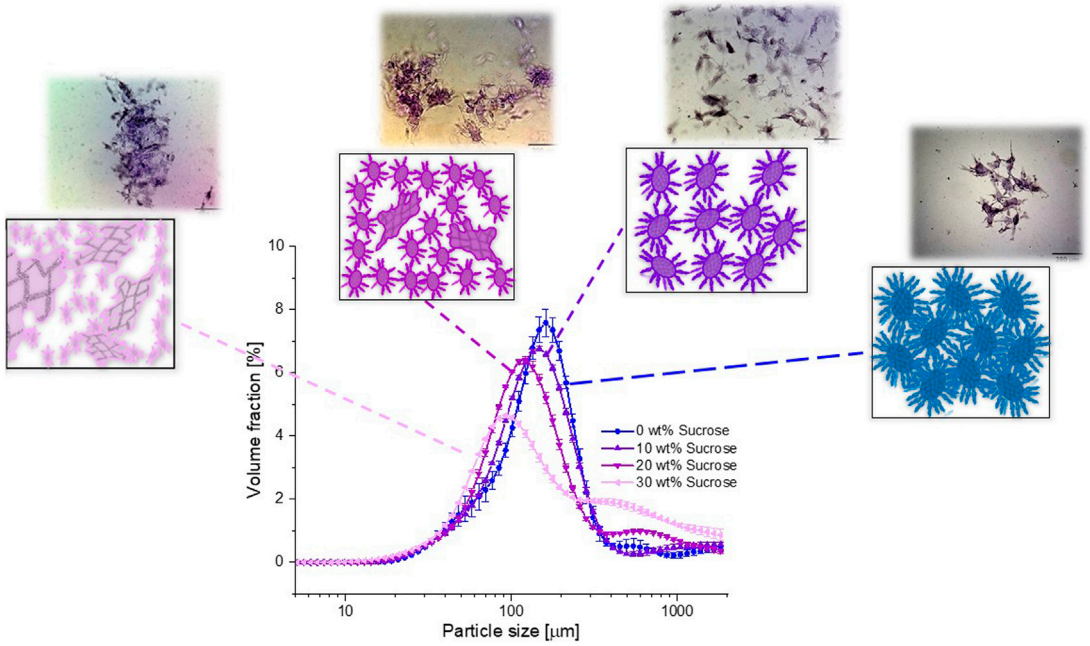


GRAPHICAL ABSTRACT

## 1 Introduction

Fluid gels are based on gelling polysaccharides such as agarose, where gelling occurs at defined shear rates, resulting in systems with controlled microstructures consisting of particulate gel suspensions (Frith et al., 2002; Gabriele et al., 2010; Farrés et al., 2014; Norton et al., 1999). The particles have an elastic core, are irregularly shaped and immersed in a continuous water phase. Due to this, fluid gels provide unique flow and textural properties, which makes them of considerable interest in various applications, including food, cosmetics, and pharmaceuticals. They offer a pleasant mouthfeel for gastronomic applications. Their cohesion is important for geriatric applications and medically induced swallowing disorders. Fluid gels exhibit the properties of shape-retaining elastic materials but have a fluid-like flow behaviour under sufficiently high stress.

This combination contributes to the special mouthfeel during oral processing. However, the texture and lubrication felt in the oral cavity, can be strongly influenced by the presence of low molecular weight co-solutes, indicating a strong effect of local (atomistic) scales with macroscopic structural changes. For a systematic illustration sucrose has been chosen as an example. As shown earlier, the addition of sugars significantly affects the properties of hydrocolloids systems by interacting with each other and with the water molecules (Nishinari et al., 1992; Watase, Kohyama, and Nishinari, 1992; Deszczynski et al., 2003a; Maurer, Junghans, and Vilgis, 2012; Russ, Zielbauer, and Vilgis, 2014). The main objective here is the investigation of the underlying physicochemical effects, the molecular interaction during gelation under shear, and the resulting fluid gel properties. In particular, this study focuses on the influences of sucrose on the resulting particle structure and the rheological and tribological behaviour of the fluid gel formation.

Adding co-solutes causes physical changes on local length scales. Sucrose has a strong binding affinity for water, causing the "bound" water to become no longer available to the agarose for unobstructed gel formation. Sufficiently higher concentrations of sucrose weaken the ability of agarose to form a gel. The mechanism promoting gel formation is not entirely clear, but is suggested to involve hydrogen bonding between sugar and agarose, leading to helix formation and aggregation (Watase et al., 1990; Watase, Kohyama, and Nishinari, 1992). However, this remains a topic of ongoing debate. Higher sucrose concentrations strongly influence the mobility of agarose chains, affecting both structure formation and changes in elasticity. The altered chain dynamics effects the structure formation, for example, via the shear rate, and the water binding of the co-solute modifies the elasticity of the resulting gel particles.

Agarose, isolated from red algae (Rhodophyceae), is a linear polar, water soluble polymer composed of units of (1–3)-linked agarobiose, which in turn consists of β-D-galactopyranose (1–4)-linked to 3,6-anhydro-α-L-galactopyranose (Imeson, 2009). The gelation mechanism involves a "two-step" mechanism during cooling (Valéry Normand et al., 2000), starting with the association of polymer chains into double helices, which then further aggregate to form a continuously denser meshed three-dimensional network and immobilize the water as investigated experimentally and emphasised earlier (Nordqvist and Vilgis, 2011; Russ et al., 2013; Russ et al., 2014). It should be emphasised that this sol-gel transition appears to be much more complex, involving different transition states. Within these two steps, described by *Nordqvist et al.* as major steps, the agarose chains undergo a coil-helix transition that exist in a variety of hierarchical structures.

Different chain associations for agarose by forming helical structures at the molecular level have been suggested to influence mechanical properties, as reported by Matinez-Sanza et al. (2020). These authors proposed that agarose chains in some of the samples do not only exist in a coil structure at a temperature of 75°C, but also in some form of molecular association, indicating a variety of hierarchical structures (Martínez-Sanz et al., 2020). Thus, some agarose did not show true solution behaviour (at 75°C) but rather the behaviour typical of a transient (entangled) network. They reported that although it is known that agarose chains associate by forming ordered helical structures, this observation does not necessarily mean that these helixes are already formed, but it does imply the existence of some kind of molecular association (Martínez-Sanz et al., 2020).

Recent studies using methods such as AFM and computer simulations have demonstrated that charged polysaccharides undergoing coil-helix transitions exist in a multitude of hierarchical structures (Schefer, Adamcik, and Mezzenga, 2014; Schefer et al., 2015a; Schefer, Usov, and Mezzenga, 2015b; Diener et al., 2019; 2020; Tavagnacco et al., 2023). By studying negatively charged carrageenan as a model polysaccharide for ion-mediated gelation, the authors demonstrated the presence of several structural levels determined by statistical analysis of AFM images. These works refined the understanding of ion-induced structural hierarchies, revealing coil, single helix, coiled-coiled helices, and double and multiple supercoiled helices, corresponding to primary, secondary, tertiary, and quaternary structures, respectively (Diener et al., 2019; 2020). However, these findings on ion-induced structural changes and gelation mechanism cannot be readily applied to agarose. Controlled ion-mediated gelation, which enables a targeted modification and observation of chain association, may be challenging due the lack of charge of agarose and its strong gelling properties without the addition of ions.

Thus, the investigation of intramolecular conformational changes at the secondary structure level and their influence on structural properties, particularly in response to the addition of counterions and charge screening, remains unexplored for agarose.

In contrast, Agarose, is an uncharged polysaccharide and was therefore specifically chosen by us due to its special model system for polar systems. These short ranged polar interactions make them ideal for studying the nature of biopolymer gelation (Xiong et al., 2005).

Under certain temperatures, disordered agarose chains form helical structures with tetrahedral cavities occupied by water molecules (Tako et al., 2021). The left-handed threefold helix structure of agarose, featuring a specific axial displacement and pitch of 1.90 nm, allows for the formation of a sterically acceptable parallel double helix. This structure contains a small inner cavity with inward-directed C-H bonds, lined with hydroxyl groups that promote hydrogen bonding, involving specific oxygen atoms (Ablett et al., 1978; Nussinovitch, 1997). Hydrophobic C-H bonds contribute to the cavity stability and enable higher hierarchical structures, such as multi-helical assemblies (Tako et al., 2021). The precise positioning of the water molecules within the tetrahedral cavity, determined by their specific interaction with certain oxygen atoms reinforces the double helix structure (Arnott et al., 1974; Deszczynski, Kasapis, and Mitchell, 2003b; Tako et al., 2021). Thus, hydrophobic interactions contribute to the formation of the cavity structure, while hydrogen bonds contribute to its stabilization (Fittolani, Seeberger, and Delbianco, 2020). However, this underlines the understanding that agarose gels rely solely on water as the solvent to promote helix aggregation and the formation of junction zones (Mineo Watase, Nishinari, and Hatakeyama, 1988; Vilgis, 2015). Therefore, adding sucrose to the hydrated agarose system induces strongly competing dipolar interactions and hydrogen bonding, which destabilize the helix formations and hinder their aggregation (Deszczynski, Kasapis, and Mitchell, 2003b).

Russ et al. (2014) attributed a decrease in elastic modulus with increasing sucrose concentration to the limited mobility and diffusion of the agarose polymer chains, resulting in fewer associations into double helices and their aggregation during cooling. This restriction results in a weaker three-dimensional network with larger meshes, reducing elasticity and stability (Russ, Zielbauer, and Vilgis, 2014; Vilgis, 2015). At sucrose concentrations above 40 wt%, competition for water prevents stable hydrogen bonds with agarose molecules, disrupting thermodynamically stable helix formation and depriving agarose chains of the hydration layer necessary for network formation (Deszczynski et al., 2003a; Kasapis et al., 2003; Maurer, Junghans, and Vilgis, 2012). Therefore, when a lower sucrose concentration is added, an increase in elastic modulus is explained by a reduction in free water and an increase in apparent local concentration (Deszczynski et al., 2003a; Kasapis et al., 2003).

Shimazu et al. (2014) further investigated co-solvent enhanced gelation of agarose. The authors suggested that co-solvents control the sol-gel transition by either restructuring water around the biopolymer or excluding co-solvents from the biopolymer surface. The driving force for gelation is attributed to co-solvent exclusion, followed by biopolymer aggregation due to increased compactness. This finding is relevant to the fluid gels in this study, where sucrose is dissolved in water before agarose, and supports the conclusion that co-solvent exclusion, rather than biopolymer hydration, i.e., the change in water structure around the biopolymer, drives gelation, as discussed below (Shimizu and Matubayasi, 2014). Another hypothesis suggests co-induced hydration changes, where sugar indirectly affects the sol-gel equilibrium through a change in biopolymer hydration that is influenced by competitive hydration between biopolymer and co-solvent (Watase et al., 1990; Williams et al., 1991; Watase, Kohyama, and Nishinari, 1992; Shimizu and Matubayasi, 2014). However, this concept is relevant to fluid gels, which in the current work were mainly prepared by dissolving agarose in heated water before adding sucrose. Sucrose addition to hydrocolloids, alters water structure through hydration shells (Vilgis, 2015). The dissolution of sucrose changes water structure, affecting its tendency to bind agarose polymers via hydrogen bonds. This challenges the notion of water as an inert solvent, leading to changes in gelling properties when sucrose is added (Vilgis, 2015).

Sugar significantly affects hydration water dynamics, by forming more stable hydrogen bonds with water than those between water molecules (Lee, Debenedetti, and Errington, 2005). This cumulative impact extends to the surrounding water (Zhao, Ma, and Yang, 2015) and hinders agarose polymer helix formation by removing water molecules from the helix cavity. Sucrose reduce the flexibility of agarose at high temperatures by hydrogen bonding with the hydration water of agarose molecules, causing a decrease in conformational entropy (Hédoux et al., 2006; Adrien Lerbret et al., 2007). Furthermore, a decrease in the hydration number, linked to increased sugar concentration, was observed due to overlapping of

distance outer layers within the dynamic hydration shells of sugar molecules (Gharsallaoui et al., 2008). This correlation affects agarose hydration and indirect interact with sucrose.

Studies on the effect of the sugar addition before or after agar dissolution, found that gels were weaker and more inhomogeneous when more than 40 wt% of sucrose was dissolved before agar addition (Yang et al., 2015). The order of addition affected fracture stress, strain and sucrose release ratio. Other studies have also opted to add sugar after agar dissolution (Ellis, Mills, and Norton, 2019). However, for the present paper, we considered it essential to prepare the samples by first dissolving agarose in water, as we did in previous studies, in order to obtain the same initial state of the agarose-water system and thus determine the effect of sucrose on this specific system (Ghebremedhin, Seiffert, and Vilgis, 2021).

However, despite previous studies on the effect of sucrose on biopolymer fluid gels and the resulting mechanical properties, the exact mechanism and interaction during gelation under shear at the molecular level are not yet understood. Therefore, the present study investigates the effect of sucrose on the gelling mechanism of agarose during the preparation of fluid gels. The paper is organized as follow: First, we investigated the behaviour of the temperature dependent shear viscosity of the prepared fluid gels in the rheometer using the *in situ* method. This "*in situ*" method for producing fluid gels has been utilized in our previous work as well (Ghebremedhin, Seiffert, and Vilgis, 2021; 2022). It offers the advantage inducing gelation at an imposed steady shear with controlled shear and temperature rates (De Carvalho and Djabourov, 1997; Ghebremedhin, Seiffert, and Vilgis, 2021). Supported by light microscopy and particle size measurements, we examined the resulting particle sizes and shapes to understand their impact on the textural and lubricating properties in relation to sucrose concentration. Rheological studies, including amplitude sweep, frequency sweep and flow sweep were performed to gain insight into the influence of sucrose on the particulate network formation. Finally, we employed tribology to support the previous assessment results of the microgel particles by evaluating the frictional behaviour of the different fluid gels. Consequently, based on the aforementioned characterization and our earlier studies, we have proposed a schematic model that describes the mechanism involving the interplay between sucrose, agarose and water during gelation under shear, along with its effects on the rheological and tribological properties of agarose gels with added co-solutes.

# 2 Materials and methods

## 2.1 Materials

The agarose [CAS: 9012–36-6] used in this study was purchased from Fisher Scientific GmbH (Schwerte, Germany) having a number-average molar mass Mn ≈ 74,557.8 g/mol, a weight-average molar mass Mw ≈ 213,949 g/mol, and a polydispersity index of 2.87 (Ghebremedhin, Seiffert, and Vilgis, 2022). The substance reaches a gel strength of >100 g/cm$^2$, and the manufacturer specifies a gelation temperature range of 34°C–45°C. A maximum sulphate content of 0.15% was also specified. Sucrose [CAS: 57–50-1] was purchased from Sigma Aldrich (St. Louis, MO, United States of America).

## 2.2 Sample preparation

In order to investigate the influence of disaccharides such as sucrose on the mechanical, viscoelastic, and tribological properties of agarose fluid gels, it is first interesting to understand their effect on the formation of the fluid gels during gelation under shear. For this purpose, agarose fluid gels with different sucrose concentrations were prepared.

### 2.2.1 Preparation of fluid gels using the rheometer

Fluid gels were prepared using the Discovery HR-3 Rheometer (TA Instruments New Castle, Delaware United States of America) with a cup (diameter = 30.37 mm) and vane (diameter = 28 mm, length = 42 mm) tool geometry used together with an electrically heatable concentric cylinder Peltier Jacket. For preparation of the 1 wt% agarose fluid gels with the respective sucrose concentration (0 wt%, 10 wt%, 20 wt%, 30 wt%), agarose was slowly added to Milli-Q water while stirring (500 rpm) and heated to 85 °C for about 20 min in the sealed beaker to ensure complete dissolution. The required sucrose concentration was then added with stirring. Subsequently, the hot agarose respectively agarose-sucrose solution was poured into the cup preheated to 85 °C and allowed to equilibrate for 5 minutes more before starting the measurements. While cooling from 85°C to 25°C at a temperature rate of 1 K/min, gelation under shear was carried out at a constant shear rate of 400 s$^{-1}$. This was followed by an additional 15 min of shearing at 25°C. As a result, pourable but set, spoonable smooth gels were produced with the characteristics of an elastic material that could hold its shape but also flow like liquid under sufficient stress. These fluid gel samples were then stored at 4°C for 24 h before being subjected to further characterization investigations.

It should be noted that for the fluid gel preparation mainly used in this study, the agarose concentration was kept constant at 1 wt%, while the sucrose content ranged from 0 wt% to 30 wt% and was added after dissolving agarose. Additionally, an alternative preparation method was employed for comparison purposes, where 20 wt% sucrose was initially dissolved in Milli-Q water, followed by the addition of agarose to the sucrose solution. This approach aimed to investigate and discuss the effect of the order of sucrose and agarose addition. The results and comparisons are provided in the Supplementary Material.

## 2.3 Rheological measurements

Dynamic viscoelastic measurements of the produced fluid gels were carried out on a Discovery HR- Rheometer (TA Instruments) with a 40 mm diameter parallel plate with a pre-set distance of 500 µm and a solvent trap. All rheological measurements were conducted in triplicate.

Amplitude sweep measurement was performed to investigate the viscoelastic properties of the different fluid gels. Using this method, oscillatory deformation was applied and storage $G'$ and loss $G''$ moduli were measured to describe the deformation behaviour of the gel samples in the non-destructive range, which is defined as the linear-viscoelastic (LVE) range. In addition, the characterization of the behaviour in the non-linear viscoelastic regime was of interest. All amplitude sweeps were carried out at a constant frequency $f$ =

1 Hz, and storage ($G'$) and loss ($G''$) moduli were measured as a function of strain $\gamma$, ranging from 0.001% to 1,000% at a constant temperature of 25°C. For comparison with the gels prepared under quiescent conditions, the preparation method and results are given in the Supplementary Figure S8.

The frequency sweeps of the fluid gels were carried out in a range of 0.1–100 rad/s (0.0159–15.9 Hz) at a constant strain of 0.05%, i.e., within the LVE range of their amplitude sweep measurements.

To investigate the flow behaviour of the fluid gels and the viscosity as a function of the shear rate, rotating steady shear was performed for the flow sweep test. The shear rate was increased from 0.001 to 1,000 $s^{-1}$ and then decreased from 1,000 to 0.001 $s^{-1}$. The two-step flow was conducted to determine how much the hysteresis varies between the two steps, indicating a change in viscosity.

## 2.4 Light microscopy

Microstructure examinations of the gel particles were performed by light microscopy using a Carl Zeiss Axio Scope.A1 microscope (Carl Zeiss AG, Oberkochen, Germany). Transmission bright field microscopy was used to capture the images, giving total magnifications of ×100 at objective magnifications of ×10. The scale bar was inserted using ImageJ software (National Institutes of Health (NIH), Maryland United States of America). Fluid gel samples were carefully transferred onto a microscope slide and then diluted with Milli-Q water (1:5). To enhance contrast, the diluted sample was stained with toluidine blue (0.1 wt%).

## 2.5 Particle size determination

Static light scattering experiments were performed to determine the particle size distributions using the Beckmann Coulter LS 13320 laser diffraction particle size analyser (Beckmann Coulter, CA United States of America), which can determine particle sizes between 0.040–2,000 µm. The diffraction data were analysed using the Fraunhofer model provided by the supplier's software. No additional data such as refractive index or absorption coefficient were required for this calculation. To avoid multiple scattering effects, samples were diluted by pipette into a measuring cell (universal liquid module) filled with distilled water until an obscuration of about 10% was attained, following the recommendation of Beckman Coulter. Size distribution measurements were conducted in triplicate.

## 2.6 Tribology

The lubricating properties of the fluid gels with the different sucrose concentrations were determined using a tribo-rheometry accessory obtainable for the Discovery HR-3 (TA Instruments New Castle, Delaware United States of America). A three balls on a plate set up was used, consisting of an upper part with three hemispheres (diameter of 7.9375 mm or 5/16″) screwed to a plate (diameter of 30 mm) and a lower plate attached with a silicone rubber (diameter of 40 mm and thickness of 1 mm). Hence, the contact surface of the tribopairs consisted of a stainless-steel ball and a silicone surface maintaining a point contact. To ensure a uniform solid-solid contact and axial force distribution, e.g., an even distribution of the normal force between the surfaces during rotation, a helical-spring-like aluminium beam coupling was used (specified by *Trios manual* 2019). The lower plate geometry is attached to the Peltier plate of the DHR-3 Rheometer for stable temperature control, and measurements were performed at 25°C. A normal force of 3 N was applied, which is considered to be similar to the normal forces acting during oral processing (Laiho et al., 2017; Nguyen et al., 2017; He et al., 2018). The sliding speed was varied from 100 to 1,000,000 µm/s by rotating the upper three-ball geometry, while the lower plate geometry was held stationary. The friction force $F_F$ and friction coefficient $\mu$ were calculated for the three balls on plate set up using the trios software, with the torque $M$ as an independent variable. As a result, the friction coefficient $\mu$ was determined as the ratio between the measured frictional force $F_F$ and the normal force $F_N$ and is displayed as a function of sliding speed µm/s for each test. The tribology tests were performed in triplicate.

# 3 Results and discussion

## 3.1 Effect of sucrose on the formation of agarose fluid gels and their characterization

Figure 1 illustrates the change in viscosity for the 1 wt% agarose fluid gels with the different sucrose concentrations (0 wt%, 10 wt%, 20 wt% and 30 wt%) as a function of time and temperature. All fluid gel samples exhibit a gelation controlled viscosity increase with decreasing temperature, with similar trends: (i) first, a gradually increasing viscosity (see Table 1) as temperature decreases (85°C–40°C) involving the onset of gelation and the Arrhenius behaviour (between 85°C and 55°C), (ii) followed by a rapid viscosity increase (40°C–25°C), (iii) and finally a plateau region (at 25°C) (Ghebremedhin, Seiffert, and Vilgis, 2021). A small step is observed within the gradual increase in (i) (indicated by arrows), shifting to higher temperatures with higher sucrose concentrations. However, no clear difference can be observed for the fluid gels with 0 wt% and 10 wt% sucrose concentration. Comparing the sharp increase in viscosity in (ii), a barely perceptible earlier increase can be observed for the fluid gel with the highest concentration of 30 wt%. All other samples show a similar steep viscosity increase around 31°C (Ghebremedhin, Seiffert, and Vilgis, 2021). This temperature, the gelation temperature of the agarose used, can be assigned to the aggregation of the associated double helices of the agarose chains into microgel cluster (Norton, Jarvis, and Foster, 1999).

This viscosity range indicates a sol-gel transition of agarose under shear, illustrating a dynamic interplay between gelation through physical cross-linking and shear force-induced limitation of gel growth (De Carvalho and Djabourov, 1997). This process, including of agarose concentration dependence and local microstructure, was comprehensively explored in our previous work (Ghebremedhin, Seiffert, and Vilgis, 2021).

However, a change is expected in the preparation of fluid gels as sugar affects the water of hydration by forming stable hydrogen

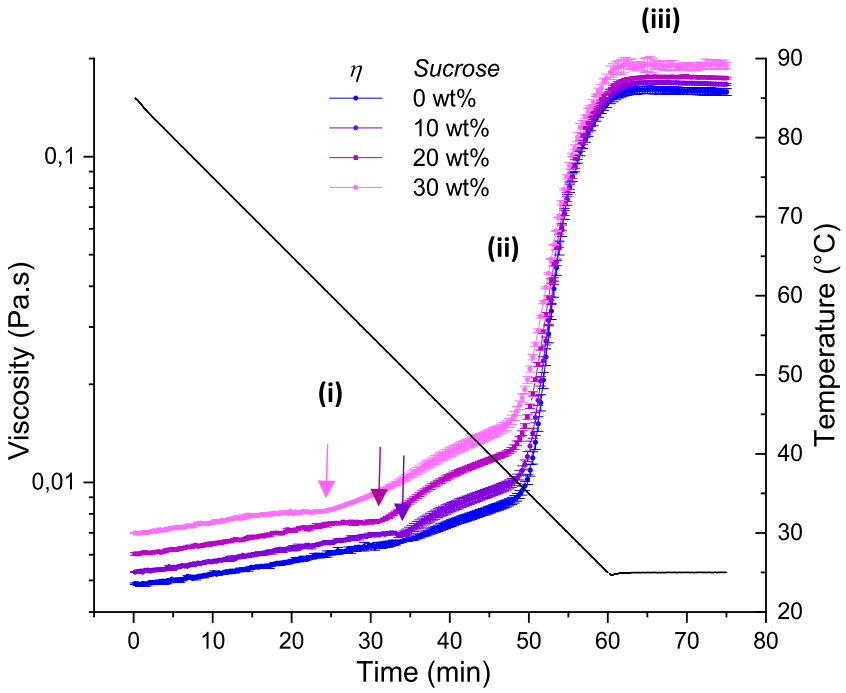


FIGURE 1
Viscosity profile during the production of 1 wt% agarose fluid gels with varying sucrose concentrations (0 wt%, 10 wt%, 20 wt%, 30 wt%). Samples were subjected to a constant applied shear rate of 400 $s^{-1}$, cooled from 85°C to 25°C at 1°C/min and then held at 25°C for 15 min. The arrows indicate the step-like increase in viscosity behaviour, which shifts to lower temperature with decreasing sucrose concentration. This shift is attributed to the onset of agarose double helix aggregation, influenced by sucrose interaction with water molecules through hydrogen bonding during the fluid gel formation process.

TABLE 1 Slope of the gradual increase in viscosity in region (i) with time (refer Figure 1) for 1 wt% agarose with varying sucrose content.

| Sucrose conc | (i) |
|---|---|
| 0 wt% | 0,00553 ± 1,04118E-4 |
| 10 wt% | 0,00487 ± 1,59367E-4 |
| 20 wt% | 0,00614 ± 3,56073E-4 |
| 30 wt% | 0,00879 ± 2,88253E-4 |

bonds with water and inhibits helix formation in agarose polymers by removing water molecules from helix cavity (Lee, Debenedetti, and Errington, 2005; Zhao, Ma, and Yang, 2015).

The hydration number of sucrose decreases with increasing sugar concentration and temperature (Gharsallaoui et al., 2008), which in turn affects the hydration of agarose polymers. Due to this indirect interaction, we propose, that when sucrose is added to heated agarose solutions, it competes with fully hydrated agarose polymers for H-bonds with water. This competition decreases with temperature, allowing more non-hydrated sucrose molecules to interact with agarose polymers, restricting their helix formation and reducing water activity. As the temperature decreases, the surrounding sucrose impedes the ordered conformation of the agarose into double helices and their further association. In Figure 1, the transition between the range of expected Arrhenius behaviour and the onset of initial gelation (between 60°C and 50°C) systematically shifts towards higher temperatures with rising sucrose concentration. This step-like increase in shear viscosity (indicated by arrows in Figure 1), which occurs with increasing concentration at higher temperatures, might be attributed to the initiation of the aggregation of agarose double helices. However, this change in viscosity indicates that the strong hydrogen bonding between sucrose and water molecules may influences the process of fluid gel formation. The viscosity increase caused by the addition of co-solutes impedes agarose polymer mobility and diffusion (Maurer, Junghans, and Vilgis, 2012; Russ, Zielbauer, and Vilgis, 2014), which alters the relation between the time scales given by shear rate and molecular relaxation times. A number of studies on the interaction between sucrose and water, using a variety of methods, support the above conclusions (Lee, Debenedetti, and Errington, 2005; Lerbret et al., 2011; Zhao, Ma, and Yang, 2015; Olsson and Swenson, 2020; Tas et al., 2022). The competitive formation of hydrogen bonds with water molecules and agarose chains seems to lead to earlier gel formation at a higher temperature with higher sucrose concentration.

Consequently, the addition of sucrose disturbs the sol-gel transition strongly. Gelation does not proceed properly and as mentioned above, the hydrophobic C-H interactions contribute to the formation of the cavity, allowing higher hierarchical structures, while hydrogen bonds contribute to the stabilization of the cavity. This is likely to result in a more random ordering and double helix formation between the agarose chains and spontaneous multi-helical assemblies, as

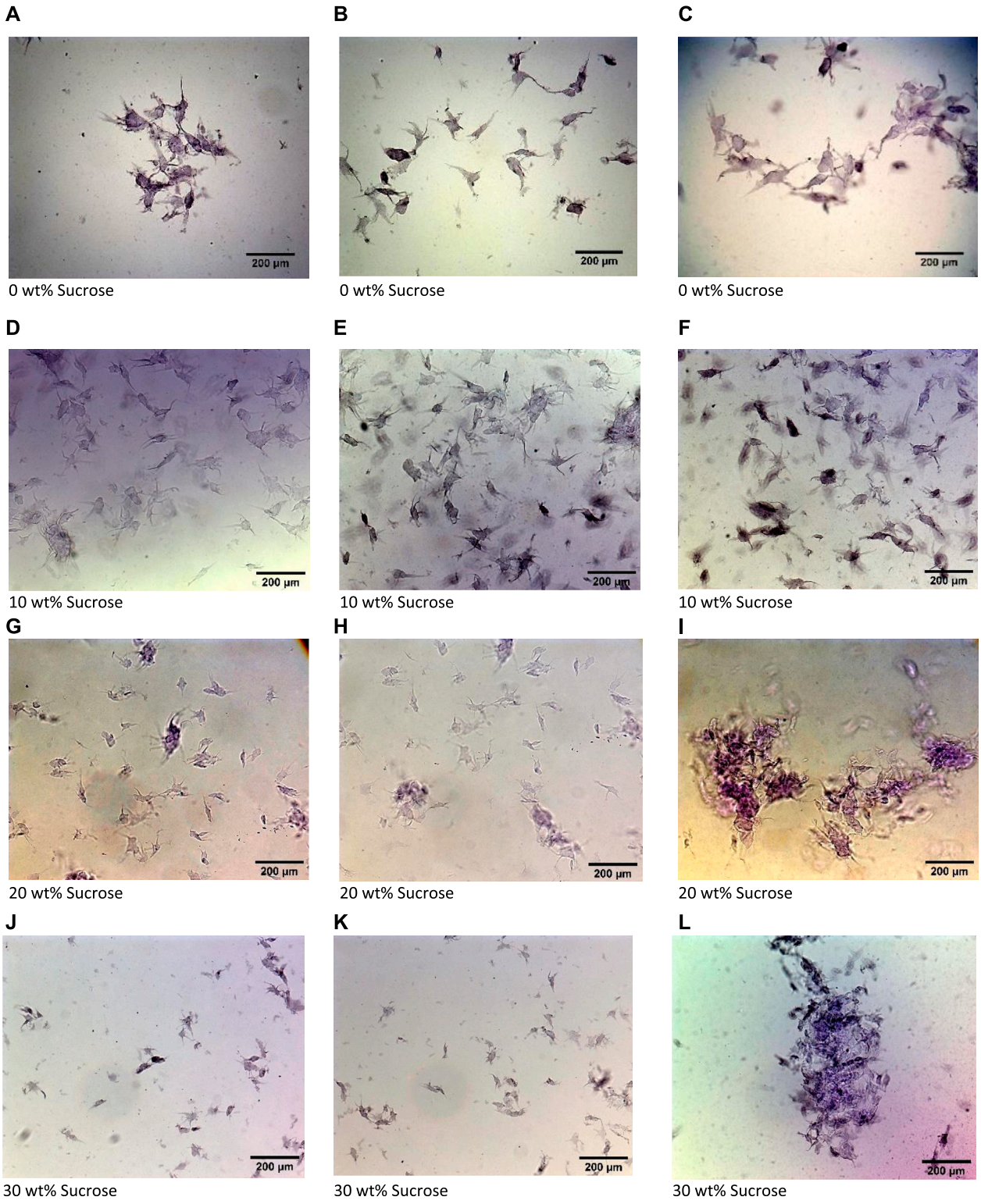


FIGURE 2
Optical microscopy images of 1 wt% agarose fluid gel particles with **(A–C)** 0 wt% sucrose, **(D–F)** 10 wt% sucrose, **(G–I)** 20 wt% sucrose and **(J–L)** 30 wt% sucrose.

indicated by the earlier increase in viscosity with increasing sucrose concentration at higher temperatures. This reduced hydration may alter the coil-helix transition, resulting in larger, softer, and weaker particles due to the dominance of randomly arranged cross-links over the shear rates (Fernández Farrés and Norton, 2015).

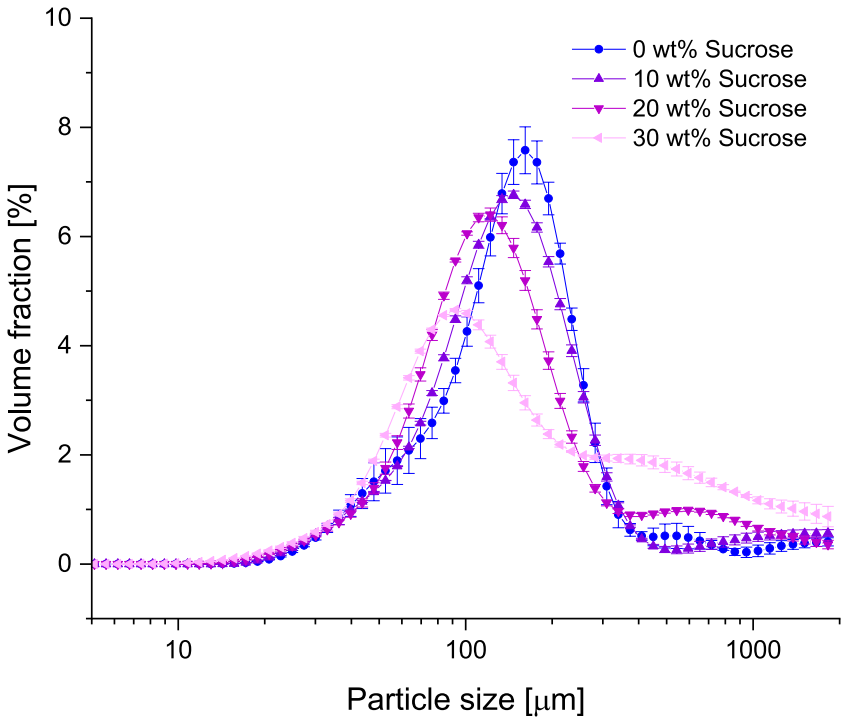


FIGURE 3
Particle size distribution of 1 wt% agarose fluid gels with different sucrose concentrations.

## 3.2 Effect of sucrose on the characteristic microstructure and particle size distribution of agarose fluid gels

As shown in previous work (Ghebremedhin, Seiffert, and Vilgis, 2021), the size and structure of the gel particles determines the flow properties of fluid gels and demonstrate the importance of taking this into account. Figure 2 displays microscopic images of the microgel particles of 1 wt% agarose fluid gels with varying sucrose concentrations (0 wt%, 10 wt%, 20 wt% and 30 wt%), revealing irregular microstructures with denser cores and disordered part towards the periphery. It can also be seen that as the sucrose concentration increases, the particle size decreases, whereas the disordered surfaces become less irregular. Observations of the microscope images in our previous studies have already demonstrated that an increase in agarose concentration, accompanied by an increase in the viscosity of the solution, results in a decrease in both particle size and the number of disordered trunks on the surface, referred to as "hairy" parts (Ghebremedhin, Seiffert, and Vilgis, 2021). Therefore, higher viscosity solutions due to sucrose provide more resistance, resulting in reduced shear and the formation of particles with a less hairy structure on the particle surface. Indeed, the trend in particle size and the reduction of disordered parts on the surface with increasing agarose concentration and, consequently, viscosity in sucrose-free systems were discussed in detail using Atomic Force Microscopy, AFM (Ghebremedhin, Seiffert, and Vilgis, 2022).

Figure 3 shows the concentration dependent particle size distribution at different sucrose concentrations. With increasing concentration, a slight decrease in the median particle size is observed, starting at about 150 μm for the sample without sucrose, and shifting to the smallest size of 100 μm for 30 wt% sucrose. This is in consistent with the observation of the microscope images. However, higher sucrose concentrations result in a broader particle size distribution and the appearance of additional larger particle aggregates. The larger aggregates are most pronounced in the sample with the highest sucrose concentration, clarifying the impact of sucrose on particle formation in fluid gels.

Additionally, the appearance of a shoulder at larger particle sizes is most likely caused by larger aggregates being caught between the blades of the vane geometry during gelation (Moakes, Sullo, and Norton, 2015).

The mechanism of fluid gel formation involves initial nucleation and growth into microgel particles due to agglomeration of the nucleating particles as they are pushed together during shear flow. The shear forces counteract particle growth, restrict the molecular cross-linking of agarose double helices and prevent further aggregation within the particles (Norton, Jarvis, and Foster, 1999).

However, these findings complement our previous studies on concentration dependence of fluid gel properties. Increased viscosity alters the competition between the imposed shear rate and the molecular diffusion of agarose chains, a competing time scale during the gelation under shear discussed earlier for agarose fluid gels (Ghebremedhin, Seiffert, and Vilgis, 2021). Due to the highly non-equilibrium gelation process of agarose, the competition between the shear

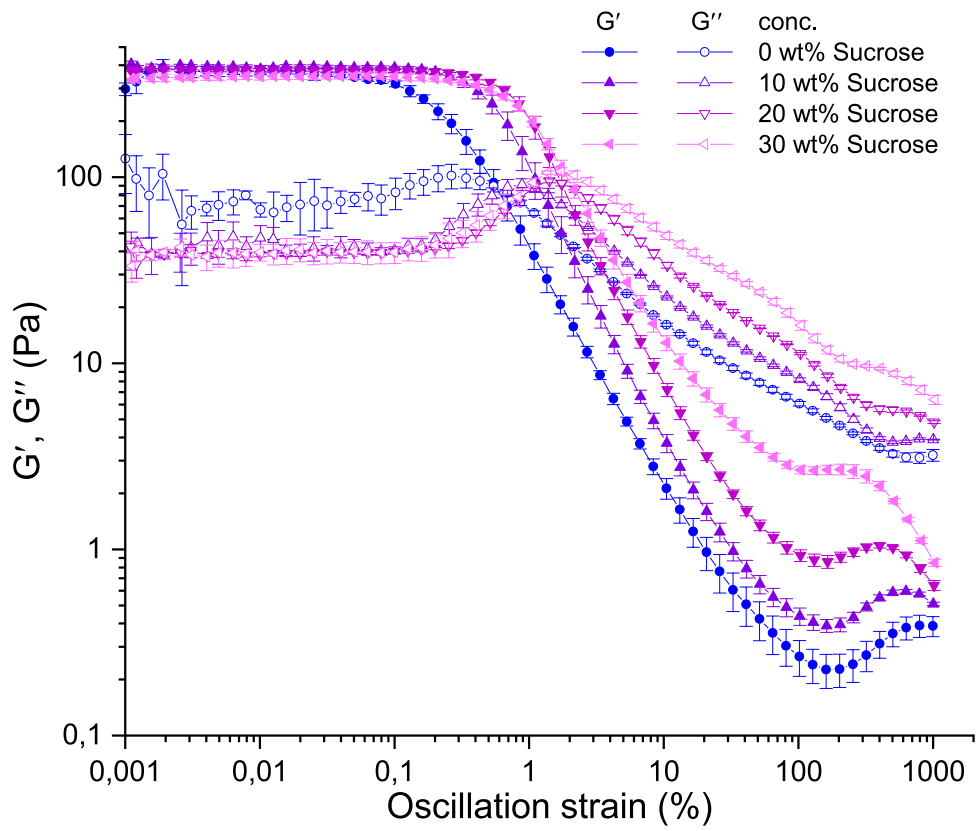


FIGURE 4
Amplitude sweep measurement of 1 wt% agarose fluid gels with different sucrose concentrations. Dependence of G′ (filled symbols) and G″ (empty symbols) on strain at constant frequency ($f$ = 1 Hz) and temperature (T = 25°C).

rate time scales and the broad spectrum of polymer time scales becomes crucial. The chains diffuse to the lowest approximation according to the Rouse-Zimm model before gelation onset, with the longest relaxation time determined by the center-of-mass diffusion constant $D_{CM}$ in good solvent. $D_{CM}$ and rotational relaxation time are influenced by the molecular weight, which, in turn, is related to the average chain lengths, but also to the viscosity of the solvent (Doi and Edwards, 1988). Therefore, changes in viscosity and diffusion due to co-solvents affect particle size and shape, as evidenced by the variation in particle size with sucrose concentration (see Figure 2).

Additionally, the increase in shoulder and decrease in particle size with increasing sucrose concentration can be further attributed to the reduction in available water required to hydrate the agarose chains and stabilize their tetrahedral arrangement. Consequently, the interplay between hydrogen bond formation involving water, agarose polymers and sucrose molecules, plays a pivotal role in influencing the diversity of particle size, shape, and gel formation. Higher sucrose concentration increases solution viscosity, reducing agarose chain mobility (Valery Normand et al., 2003; Ellis, Mills, and Norton, 2019). This hinders helix nucleation and limits the growth process into bundles, thereby slowing down the gelation kinetics. This viscosity driven effect explains the trends in Figures 2, 3: smaller particle size with wider distribution, and the appearance of a shoulder with increasing sucrose concentration.

## 3.3 Rheological properties

The impact of sucrose on the viscoelastic and flow characteristics of agarose fluid gels was investigated using rheological techniques. In Figure 4 amplitude sweep measurements show the storage ($G'$) and loss ($G''$) moduli plotted as a function of strain, representing the linear viscoelastic range followed by a nonlinear range.

The different samples appear to have similar $G'$ values within the LVE range. Although not clearly evident in Figure 4, a slight decrease in the storage moduli can be observed with increasing sucrose concentration of the fluid gels. Nevertheless, all samples show elastic and solid-like behaviour in the linear viscoelastic range, with the storage moduli significantly higher than the loss moduli.

The decrease in modulus can be attributed to the competition between agarose and sucrose for H-bond formation with water, reducing local water availability for agarose during cooling, which is crucial for helix formation. At the same time hydrated sucrose may form H-bonds with agarose, i.e., its hydration water, which also limits double helix formation. Therefore, if agarose is dissolved first and sucrose is added, the competitive reaction displaces water as sucrose interacts with agarose during cooling. This inhibits proper subsequent agarose association and aggregation, supported by faster binding of sucrose molecules. Ultimately, entropy plays a crucial role. The gelation process decreases the agarose coils transition into helices, thereby reducing helix aggregation. All these combined

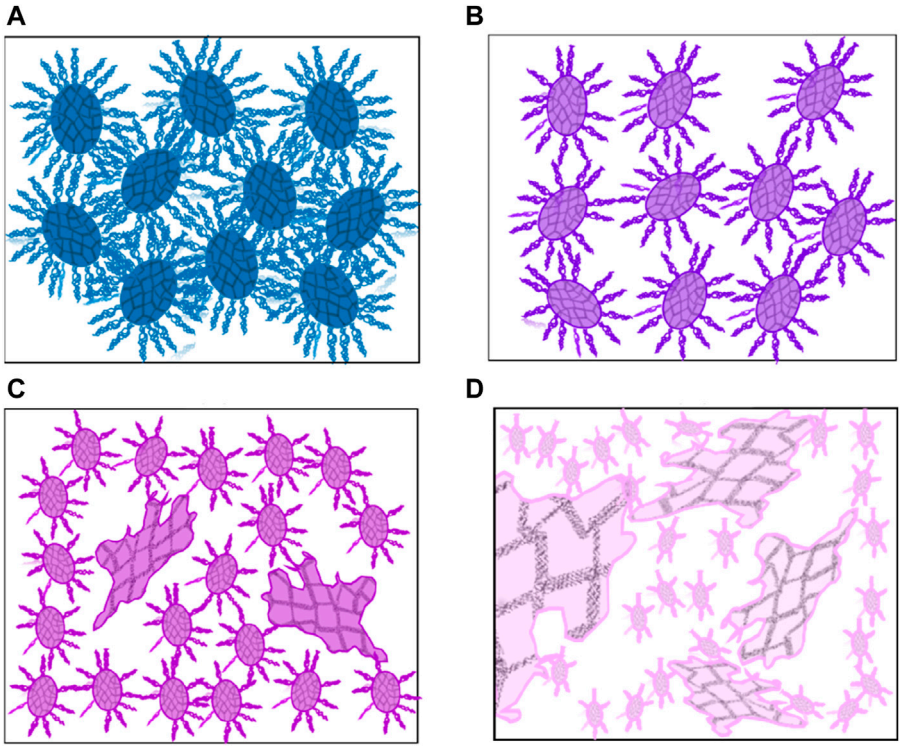


FIGURE 5
As sucrose concentration increases the 1 wt% agarose fluid gels, discrete particle sizes show an increase from 0 wt% sucrose **(A)**, 10 wt% sucrose **(B)**, 20 wt% sucrose **(C)** and 30 wt% sucrose **(D)**. Larger aggregates, forming a weaker network, increase in size from 20 wt% sucrose and 30 wt% sucrose.

effects result in fewer and weaker cross-links, leading to a decrease in $G'$ moduli. Consequently, sucrose increases viscosity and prevents agarose from forming double helices and aggregation into a dense network. The result is larger aggregates with weaker networks rather than particles with a discrete and narrow size distribution.

To illustrate the forthcoming interpretation, a schematic model of the different fluid gel particles is shown in Figure 5. As examined from the above findings, with increasing sucrose concentration, the particles become smaller with additional aggregate clusters containing fewer and weaker networks, which can be seen in Figures 5A–D.

In Figure 4, all samples show a local maximum in loss modulus $G''$ at larger deformation (approximately 0.2%–2% oscillation strain). This overshoot of the loss modulus is typical for soft materials that exhibit yielding behaviour with the characteristic ability to change from solid to liquid-like behaviour at sufficiently high deformation (Donley et al., 2020). The sucrose-free fluid gel displays this local maximum at lower strain compared to those with sucrose, which is addressed to the size of the particles. Higher sucrose concentrations result in softer and larger clusters (see Figure 2L and Figure 3), shifting the overshoot to higher strains required to deform and shear the largest particles. This implies an increased deformation dissipation before segments of the internal structure are deformed and the connectivity between particles is finally disturbed. In addition, the relative motion of regions with free dangling hairy-like structured parts and chain ends, explains the appearance of the $G''$ overshoot (see Ghebremedhin, Seiffert, and Vilgis, 2021; 2022 for more details). These observations are in agreement with other publications, for example, on soft hydrogel particles, which state that the overshoot results from viscous dissipation due to microstructure destruction and cluster rearrangement (Parthasarathy and Klingenberg, 1999; Sim, Ahn, and Lee, 2003; Wyss et al., 2007).

These ideas are consistent with the different LVE range. The sucrose-free fluid gel exhibits the lowest LVE range, followed by samples with increasing sucrose concentration, aligned with yield points and $G''$ maxima. Larger aggregate clusters at higher sucrose concentration account for the LVE limits and $G''$ overshoots at higher strain rates in sucrose-added fluid gels. This is because larger deformations are required to deform and slide the clusters against each other, before they reform, align, and finally break. As the oscillatory strain increases, steric interparticle interactions experience greater deformation and subsequent separation. Simultaneously, the rearrangement of percolation connectivity of the gel particles decreases, disturbing the equilibrium between both processes and causing a decline in interparticle bridges of densely packed gel particles. This indicates a critical region where the particle-particle interactions can no longer reform, causing irreversible damage to the interconnected network of the fluid gel particles.

The nonlinear behaviour of the fluid gels offers further structural insight. At sufficiently large strain amplitudes ($\gamma > 10\%$), where fluid-like flow properties are exhibited ($G'' > G'$), the influence of sucrose concentration on the storage modulus $G'$ becomes

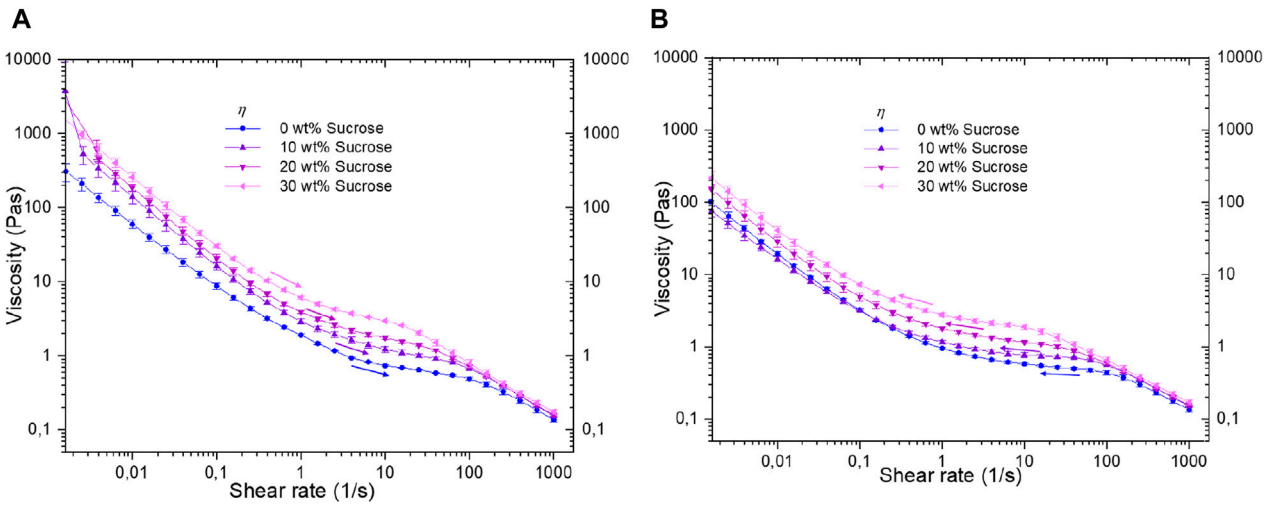


FIGURE 6
Flow behaviour (Viscosity profile) of 1 wt% agarose fluid gels with different sucrose concentrations, showing **(A)** ramp up and **(B)** rump down.

prominent. The crossover (flow) points of $G'$ and $G''$ shift to higher strains as the sucrose content increases, with the lowest flow point occurring for the sucrose-free fluid gel. This trend is consistent with the previously mentioned LVE limit and $G''$ overshoot observations. Increasing sucrose concentration induces a rise in $G'$ between 100% and 1,000% strain. The $G'$ hump at high deformation can be attributed to the jamming of aggregated gel particles when they are pushed together, which occurs earlier and tends to plateau in fluid gels with higher sucrose concentrations due to larger aggregate clusters. However, the different height and shape of the curves are related to the particle structure. The sucrose-free sample shows cross-linked gel particles with an irregular "hairy" surface, where deformation begins with the softer hairs before the stiffer cores. According to Figure 2, the length scales of the centre of the core and the hairs are of the same order. The hairs have graded moduli (Ghebrebmedhin, Seiffert and Vilgis, 2021) and are easily deformed (Ghebremedhin, Seiffert, and Vilgis, 2022). At about $\gamma$ ~100%, the particles need to be deformed and moved about their own size, when they are close to each other. This requires a slight deformation of the hairy parts before the cores, which have a much higher elastic response, are pushed together. Thus, $G'$ continues to decrease for sucrose-free samples before rising sharply between deformations $\gamma$ ~100–1,000% in the jamming regime. The higher the sucrose concentration, the lesser the influence of the "hairs". The minimum is systematically less pronounced with increasing sucrose concentration. The larger but softer aggregates present at 20 wt% sucrose and most at 30 wt% are softer, break apart, and lubricate the flow together with the smaller, "hairless" gel particles. Thus, the minimum shifts to lower deformations due to earlier jamming, but the difference between minima and maxima in the $G'$ curves become smaller until it vanishes for 30 wt% sucrose solutions.

The shear rate dependent viscosity profiles are shown in Figure 6 and confirm the results and ideas of the previous amplitude sweeps and temperature dependent viscosity measurements.

Rotational steady shear experiments cover a wide shear rate range, from high to low rates. Results primarily reflect viscosity properties with prominent shear thinning attributed to particle structure, encompassing the dense core, hairy component, and viscosity of the sugar solution between gel particles. This correlation enhances understanding of the structural response to shear, offering deeper insights as elaborated below.

Furthermore, the extent of hysteresis is assessed using a two-step flow sweep to measure changes in viscosity or its decrease between the two sequences. A rotational flow run with increasing (Figure 6A) and decreasing (Figure 6B) shear rates is conducted, covering shear rates from 0.001 $s^{-1}$ to 1,000 $s^{-1}$. The results indicate a shear thinning behaviour in all fluid gel samples. While at first glance, Figure 6A shows no significant differences in the curve profile at low shear rates for sucrose-containing fluid gels, Figure 6B shows an even greater similarity among all samples.

The viscosity curves initially decline gradually at lower shear rates for all samples, due to the increasing alignment of the gel particles. However, once the elastic gel particles align in the shear direction, further orientation is hindered, resulting in a plateau-like curve between 5 $s^{-1}$–50 $s^{-1}$. This behaviour is attributed to the prevention of additional particle orientation due to shear-induced alignment (Wolf et al., 2001). Previous studies have investigated the rheological behaviour of particulate gel suspensions based on particle properties such as shape and aggregate state (Tsenoglou, 1990; Zhou, Uhlherr, and Luo, 1995; Wolf et al., 2001). At higher shear rates, the viscosity curves of the various samples remain comparable and exhibit minor deviations. However, a distinct difference can be seen between the shear rates of 1 $s^{-1}$ and 100 $s^{-1}$. This plateau-like region, where viscosity changes minimally within the profile, displays an increase in viscosity with rising sucrose content, for both flow steps: rump-up (Figure 6A) and rump-down (Figure 6B). This rise in viscosity due to increased sucrose concentration is noticeable at even lower shear rates, but only during the ramp-up phase (see Figure 6A).

The difference in viscosity between ramp-up and ramp-down at low shear rates is attributed to the increase in larger aggregates with higher sucrose concentration and the impact of a more viscous solution, with the latter being particularly relevant during ramp-up. This effect of the viscous solution is no longer relevant during the

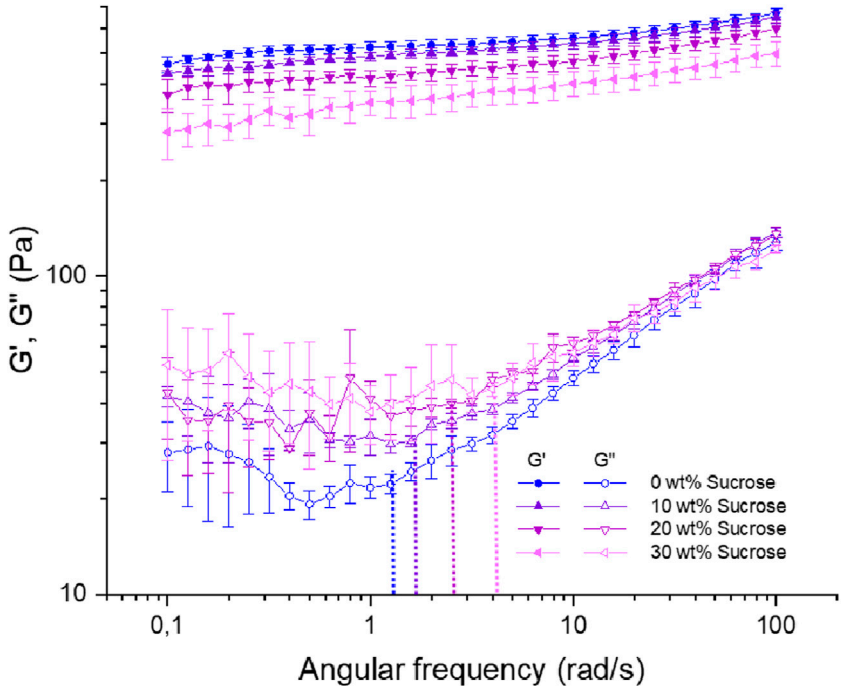


FIGURE 7
Frequency dependence of storage moduli G′ (filled symbols) and loss moduli G″ (empty symbols) at a constant strain (γ = 0.05%) and temperature ($T$ = 25°C) for 1 wt% agarose fluid gels with different sucrose concentrations. Dashed lines indicate the angular frequency ($\omega_c$) where G″ starts to increase for the respective concentrations.

ramp-down, as the structural changes that the aggregate particles have undergone due to the previous high shear rates prevail over the influence of the viscous solution. The viscosity trend at low shear rate during ramp-down (Figure 6B) is explained by considering the particle structure and size distribution shown in Figures 2, 3. Hence, the 30 wt% sucrose fluid gel exhibits the highest viscosity, followed by the 20 wt% sucrose fluid gels, consistent with the ramp-up phase and explained by the larger aggregates. In addition, the highly viscous solution of the continuous phase may impede the diffusion of the aggregates, thus preventing the disruption they have previously experienced at high shear rates. In contrast, the higher viscosity of the sucrose-free fluid gel compared to the 10 wt% sucrose fluid gel is ascribed to the larger particle size and higher proportion of protruding tails on the particle surface in the sucrose-free fluid gels. The entanglement and penetration of the tails of the hairy parts leads to increased friction and higher viscosity at very low shear rates (Ghebremedhin, Seiffert, and Vilgis, 2021). For the 0 wt% and 10 wt% sucrose fluid gels, only the effect of the discrete particles with the hairy structures is relevant, as these samples do not contain any larger aggregates. It is also striking that during the first flow step, the 10 wt% and 20 wt% sucrose fluid gel samples run alike viscosity profiles, whereas during the second flow step, the viscosity profiles of the 0 wt% and 10 wt% fluid gel samples run more similarly. This similarity for the downward curves can again be attributed to the absence of larger aggregates and the fact that the gel particles in the 0 wt% and 10 wt% fluid gel samples have gel cores with comparable elasticities.

However, at elevated shear rates, the particle clusters undergo significant deformation as they move past each other, most pronounced at higher steer rates. This is particularly true for the agarose gels prepared with higher sucrose concentrations, which, as the particle size measurements in Figure 3 show, yield larger particle clusters and thus an increase in shear viscosity. Despite variations in aggregate cluster formation, the identical viscosity values of all fluid gel samples at the highest shear rate can be explained by the breakdown of superstructures into their primary microgel particle aggregates. This is expected since the agarose concentration is the same for all samples.

The viscosity curve in Figure 6 remains flattened over a wider shear rate range for the sucrose-free fluid gels, suggesting discrete particles with a narrow size distribution and less aggregation. In Figure 6B, the flatter viscosity curves compared to Figure 6A result from the prior exposure to high shear rates during the initial ramp-up, causing persistent alignment of aggregate particles that influences the downward viscosity curves. However, the significant magnitude of the hysteresis indicates irreparable damage to the aggregates after the first sweep, suggesting that the system did not recover within the specified range before the second sweep. This reconfirms that sucrose-containing fluid gels form larger but weaker aggregates, resulting in higher viscosity with lower connectivity. The hysteresis between the upward and downward curves of viscosity, indicating reduced thixotropic behaviour, implies that these connections cannot be re-established during the downward shear rate (Moakes, Sullo, and Norton, 2015).

The corresponding frequency sweep results are shown in Figure 7. The graph displays the storage ($G'$) and loss ($G''$) moduli as a function of frequency at a constant strain (γ = 0.05%). This was performed to further characterize the

mechanical response under small oscillation strain, which covers the range of non-destructive deformations, and to describe their time-dependent behaviour.

The moduli of the fluid gels show a slight rise with increasing frequency, linked to faster particle movement at higher frequencies (Ghebremedhin, Seiffert, and Vilgis, 2021). As densely packed gel particles are confined in a cage, the linear rise in both moduli is attributed to particle motion, taking into account difference in structure and size distribution (Figures 2, 3). The rise in storage modulus with increasing frequency is less pronounced when the sucrose concentration is reduced. This indicates that the sucrose free sample is less frequency dependent, followed by the fluid gels with 10 wt%, 20 wt%, and finally 30 wt% sucrose. The lower frequency dependence can be explained by the discrete gel particles with a narrow size distribution, leading to their dense packing and higher percolation. This applies in particular to the 0 wt% but also to the 10 wt% sucrose fluid gels. Conversely, this is not the case for the fluid gels containing 20 wt% and 30 wt% sucrose, where the larger aggregates have less continuous connectivity and a weaker network, indicating that the cross-links are incoherently weaker and less ordered. In addition, the contribution of the viscosity of the sugar solution between the particles becomes more significant at higher concentrations, limiting the movement of the particles with the dense core and the hairy parts at the periphery. Therefore, this effect is less relevant when the sucrose concentration is reduced.

The increase in loss modulus ($G''$) with the frequency can be attributed to the specific structure of the particle surface. As seen in the micrographs in Figure 2, the "hairy" structural components decrease with increasing sucrose concentration. This results in a systematically more pronounced $G''$ increases starting at the angular frequency ($\omega_c$) (as indicated by the dashed lines) for the fluid gels with 0 wt% sucrose concentration, followed by 10 wt% sucrose fluid gel and so on (Ghebremedhin, Seiffert, and Vilgis, 2021; 2022). The delayed rise in loss modulus with increasing sucrose concentration can also be attributed to the larger aggregates in fluid gel particles, which move slower due to molecular weight and respond on slower time scales, requiring a higher frequency to respond properly. The observed increase in loss modulus ($G''$) at very low frequencies is attributed to the incoherently weak network of larger aggregate clusters, which are more prone to rupture. This aligns with the decrease in storage modulus ($G'$) with increasing sucrose concentration.

All rheological measurements confirmed that increasing sucrose content in fluid gels leads to the formation of larger but weaker aggregate clusters, as evidenced by the data in Figure 7 and the decreased storage ($G'$) moduli. The flow sweep exhibits the highest viscosity for the 30 wt% sucrose fluid gel, particularly pronounced at medium shear rates (5 $s^{-1}$–50 $s^{-1}$), suggesting the presence of large particle aggregates sliding against each other. This is further supported by the humps at large oscillations in the amplitude sweeps (Figure 4). Although it might be assumed that the fluid gel containing 30 wt% sucrose would show the highest moduli in the amplitude sweep and frequency sweep measurements due to the largest aggregates, our observations contradict this. Fluid gels are formed with a less discrete particle size distribution and a less densely packed core with loosely connected aggregate domains. Consequently, larger cluster of aggregate are expected to form after the formation of gel particles with a size of approximately 100 µm size is complete.

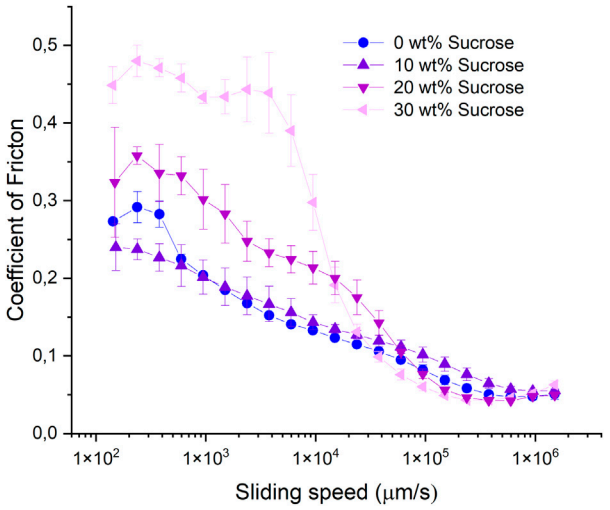


FIGURE 8
Stribeck curves at a normal load of 3 N for 1 wt% agarose fluid gels with different sucrose concentrations.

## 3.4 Tribology

Lubrication measurements were carried out to investigate the coefficient of friction of the agarose fluid gels as a function of sucrose content. Here, the lubrication between interacting surfaces and the behaviour of the fluid gels in a thin layer were investigated using tribology tests (Stokes, Boehm, and Baier, 2013). Our findings support those obtained from previous bulk examinations. Figure 8 shows the Stribeck curves with the friction coefficient as a function of the sliding speed conducted from 100 to 1,000,000 µm/s.

While the fluid gels show different overall curves, they share some common characteristics that can be related to their microstructure. All samples show an increased coefficient of friction at lower sliding speeds in the boundary regime, except for the 10 wt% sucrose sample. This is generally due to exclusion of large particles from the narrow gap between the contact surfaces, which reduces lubrication and increases contact between the plate and spheres, thereby raising friction (Baier et al., 2009; Gabriele, Spyropoulos, and Norton, 2010; Fernández Farrés and Norton, 2015). However, the peak in the friction coefficient between 2 × $10^2$ and 4 × $10^2$ µm/s can be ascribed to the entrainment of a few particles small enough to enter the small gap between the two surfaces (Gabriele et al., 2010).

At sliding speeds above 3 × $10^2$ µm/s, the coefficient of friction decreases for all samples in the mixed regime. In this regime, a thin layer of fluid gel particles separates the surfaces, thickened by bulk entrainment, leading to minimal surface contact. This improves lubrication, resulting in lower friction coefficients. However, as the sliding speed continues to increase, a point is reached where the decrease in friction stops, and for the fluid gel containing 30 wt% sucrose, friction increases slightly. In this hydrodynamic regime, the

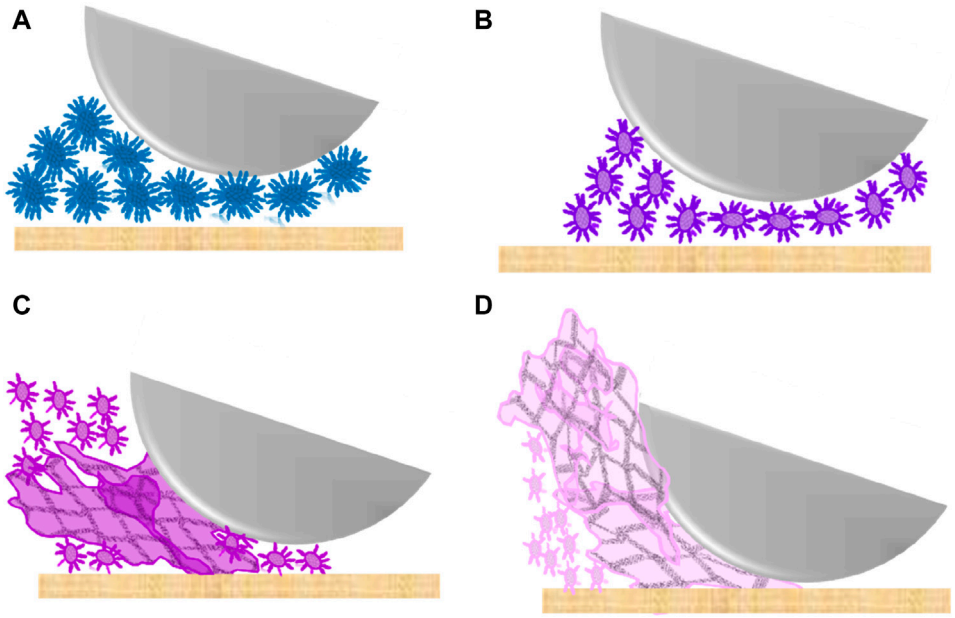


FIGURE 9
Schematic illustration of the proposed behaviour of 1 wt% agarose fluid gels with different sucrose concentration **(A)** 0 wt%, **(B)** 10 wt%, **(C)** 20 wt% and **(D)** 30 wt% sucrose, in the boundary regime of a Stribeck curve between the two surfaces (stainless steel ball and silicon sheet).

friction coefficient and the separation distance between surfaces increases as the entrainment speed of the fluid gel lubrication rises. This is due to the hydrodynamic pressure generated by the flow of the lubricant (Baier et al., 2009; Shewan, Pradal, and Stokes, 2019).

Notably, the fluid gel containing 10 wt% sucrose exhibits the lowest coefficient of friction in the boundary regime due to the smaller particles and weaker, less hairy surfaces compared to the 0 wt% sucrose fluid gel (see Figures 2, 3, 5). The higher friction of the sucrose-free samples can be attributed to larger particles containing more pronounced hairy surfaces (see Figures 3, 5A), which increase the interaction between the particles and result in higher friction coefficients. The increase and maximum friction in the boundary regime are influenced by the micro particle entrainment in the gap between the surfaces (as illustrated in Figure 9). These larger particles also contribute to a lower coefficient of friction in the mixed regime of the 0 wt% sucrose fluid gel (Figure 9A) compared to the 10 wt% sucrose fluid gel (Figure 9B). This is because larger particles increase the separation between the two surfaces, resulting in reduced contact between them (Rudge et al., 2020). This effect is especially evident at the higher sliding speed when the lubrication flow starts and the thin layer samples thickened by entrainment, causing minimal surface contact by separating them from each other.

The highest coefficient of friction in the boundary regime is observed for the agarose fluid gels with 30 wt% sucrose, attributed to the presence of additional larger aggregates (Figure 3). The exclusion of these aggregates from the narrow gap between the two contact surfaces results in an accumulation of particles around the contact region, preventing smaller particles from being entrained (illustrated in Figure 9D). This leads to high friction due to poor lubrication and nearly dry contact. The extended boundary regime may also be due to the build-up of large aggregates, requiring faster sliding speeds for these larger aggregates to enter the gap. However, the steep drop in friction could be explained by the rupture of the weaker larger clusters at increasing sliding speed. These smaller ruptured fragments are able to enter the gap with the lubricant flow. Furthermore, Fernandez et al. (2015) found that agar fluid gels with co-solutes have larger and softer particles that are unable to separate the two surfaces due to their low elasticity, resulting in a higher friction coefficient in the boundary regime (Fernandez et al., 2015). This is consistent with the present result, indicating larger but weaker network structures at higher sucrose concentrations. The friction coefficient decreases sharply in the mixed regime as more larger aggregates enter the gap with higher sliding speeds, resulting in the lower friction at a sliding speed of around $4 \times 10^4$ and $2 \times 10^5$ μm/s.

In the case of the 20 wt% sucrose fluid gel, a friction peak appears in the boundary region at the same particle entrainment speed as the other fluid gels. Particle size measurements revealed larger aggregates, although smaller than those in the 30 wt% sucrose fluid gels, resulting in lower friction coefficients (illustrated in Figure 9C). In addition, the friction gradually decreases as the sliding speed increases. Although the reduction is less pronounced compared to the 30 wt% sample, it remains steeper than for the other fluid gels. This behaviour is attributed to the presence of intermediate larger aggregates that can enter the gap and keep the surfaces apart.

## 3.5 Effect of the different solving order of agarose and sucrose on fluid gel properties

Using an alternative preparation method, 20 wt% sucrose was first dissolved in Milli-Q water, followed by the addition of

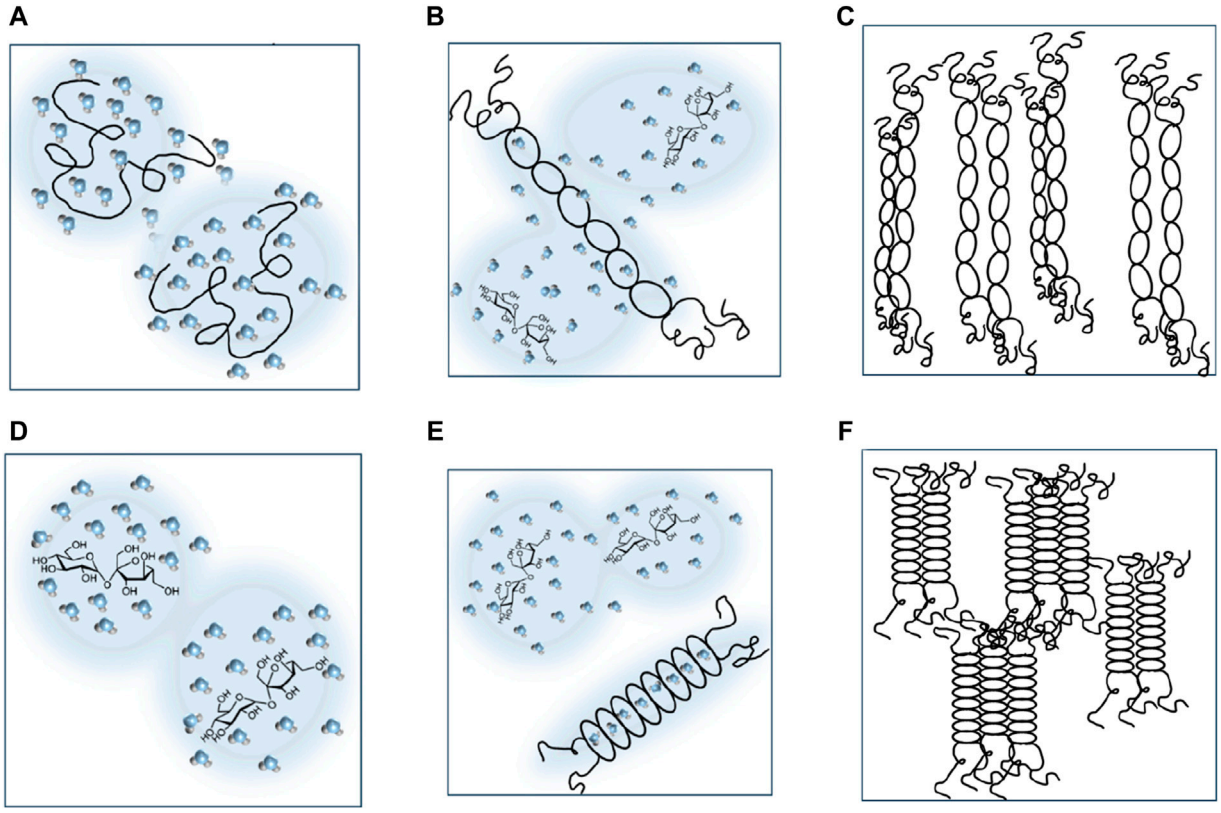


FIGURE 10
Schematic model illustrating the effect of the different order of dissolution of agarose and sucrose on the network structure of the fluid gels. Fig **(A)** shows the preparation in which agarose is dissolved first, followed by the addition of sucrose, which leads to competition between agarose and sucrose for H-bond formation with water **(B)**. This results in a lack of water for the cavity, crucial for double helix formation and their aggregation. Consequently, fewer cross-links are formed, resulting in a weak network structure **(C)**. When sucrose is first dissolved and fully hydrated **(D)**, this reduces the availability of water for the agarose chain during cooling. The exclusion of fully hydrated sucrose leads to an increased local concentration of agarose within its phase **(E)** and the formation of a closed mesh network due to increased cross-linking **(F)**.

agarose. This approach aims to compare how the order of dissolution of sucrose and agarose influences the behaviour of fluid gels and their preparation. The results are discussed in this chapter and corresponding graphs are provided in the Supplementary Material.

The viscosity profile of the 1 wt% agarose fluid gel with 20 wt% sucrose, prepared using the alternative method, is shown in Supplementary Figure S1. Similar trend can be observed, but with an earlier viscosity increase in both temperature regimes, 85°C–40°C (i) and 40°C–25°C (ii). Microscopic images in Supplementary Figure S2 show that the alternative preparation (Supplementary Figure S2B) results in particles with homogenously smaller sizes compared to the standard preparation (Supplementary Figure S2A). This was corroborated by particle size measurements (see Supplementary Figure S3), which revealed a decrease in mean particle size for the alternatively prepared fluid gel. Amplitude sweep measurements showed an increase in $G'$ for the alternatively preparation (shown in Supplementary Figure S4). This can be explained by enhanced particle interaction between smaller particles, resulting in more interconnected network due to the increased packing density (Ghebremedhin, Seiffert, and Vilgis, 2021). Frequency sweep tests (Supplementary Figure S6) reveal similar trends for storage ($G'$) and loss ($G''$) moduli, with the alternative preparation showing higher storage modulus ($G'$) values. The homogenously smaller microgel particles result in a slight increase in shear viscosity (shown in Supplementary Figure S5A, B). This observation align with the explanation for the increase in the storage ($G'$) modulus in the amplitude sweep measurements (see Supplementary Figure S4). Moreover, the Stribeck curves of the tribological measurements (see. Supplementary Figure S7) display a lower coefficient of friction for the alternatively prepared fluid gel in the boundary and mixed regime. This is due to the higher particle elasticity and the fact that smaller gel particles result in a more interconnected network, denser packing and higher percolation.

A molecular explanation for the increase in storage modulus ($G'$) relies on the formation of strong and stable hydrogen bonds between sucrose and water molecules. This reduced availability of water for agarose chains leads to the formation of a closed-meshed network. The prior complete dissolution of sucrose, and thus its fully formed hydration shell, results in the absence of sucrose molecules that would otherwise interfere with the helix formation and aggregation of agarose chains. Consequently, the storage modulus increases due to the exclusion of completely hydrated sucrose, leading to an increased local concentration of agarose within its phase.

As the hydration number of sucrose decreases with temperature, this temperature dependence may also be relevant to the various preparation methods and the resulting fluid gels (Gharsallaoui et al., 2008). This is because higher temperatures weaken the hydrogen bonds between water and sucrose molecules, leading to a reduction in the hydration number (Starzak, Peacock, and Mathlouthi, 2000; Starzak and Mathlouthi, 2006; Zhao, Ma, and Yang, 2015). The weakening of the hydrogen bond network at higher temperatures accounts for the expected changes (Zhao, Ma, and Yang, 2015).

This suggests that for the alternative fluid gel preparation when sucrose is first dissolved at ambient temperature, the subsequent high temperature used to initiate gelation has a lesser impact on its hydration number compared to the preparation when sucrose is added to the heated biopolymer solution. In the former, agarose is added to a system with less available free water, which increases the elasticity through local concentration. Consequently, depending on whether sucrose is first dissolved in water or agarose, it changes their interaction and influences the association of the agarose chains and, thus their gelation process during fluid gel preparation. To illustrate the different dissolution orders, a schematic model is shown in Figure 10. However, as mentioned in the introduction, the sol-gel transition, and thus the transition from coil to helix of the agarose chains, exists in multiple of hierarchical structures and appears to be complex. Recent studies on agarose-based fluid gels have successfully revealed thick bundles with helical assembly at the periphery of these particle surfaces using atomic force microscopy, and were discussed in detail (Ghebremedhin, Seiffert, and Vilgis, 2022). It was clearly shown that the associated helices assemble into a multitude of helices showing thick strands that change with agarose concentration. The height profile allowed clear visualisation and distinction of individual strands, showing a higher ordered aggregate at higher agarose concentrations. Therefore, based on these findings and our results on macroscopic rheological properties, supported by publications on microscopic length scales discussed throughout this work, Figure 10 is a simplified representation. However, this model provides crucial insights into the effect of sucrose on the resulting fluid gels.

Figure 10 summarizes the initial high entropic coil state and the final gel state according to the present literature. In contrast to charged systems, as discussed in Schefer, Adamcik, and Mezzenga (2014), Schefer et al. (2015a), Schefer, Usov, and Mezzenga (2015b), Diener et al. (2019), (2020), Tavagnacco et al. (2023) for carrageenan and gellan, where different intermediate states are possible during gelation as long as ions (salts) are added, for uncharged, polar agarose, such intermediate states as single helices have not been reported in the literature so far. The gelation process is likely initiated through double helices. A reason for this could be that highly flexible agarose chains in good solvent (water) are entropy and excluded volume dominated, and the polar and hydrogen bonding interactions are too weak to overcome the required entropy loss for complex secondary structures. The addition of sucrose mainly changes the apparent water concentration to first order. Still, the short-range dipolar and hydrogen bonds are seemingly not strong enough to reduce the entropy of single chains to fold into an intramolecular double helix with a hairpin-like structure.

## 4 Conclusion

In this work, we have investigated the effect of sucrose addition on the physical-chemical properties of agarose fluid gels, with the aim of relating the resulting structural changes to the rheological and tribological properties.

Based on the current findings, it appears that the presence of sucrose affects the interplay between gelation and breakup during shear. As a result, gelation is hindered by the impaired diffusion of agarose chains, leading to less defined and discrete gel particles with a broader size distribution and larger aggregates, characterized by weaker and less stable network structures. Roughly speaking, the addition of sucrose has two main effects: First, the “hairy” particles become slightly smaller with increasing viscosity as the sucrose concentration increases. Second, the reduced availability of water to stabilise the agarose double helix allows for the formation of larger and less stable gel particles with increasing sucrose concentration. These changes in network structure could be related to rheological and lubrication properties. It was found that increasing the sucrose content, which leads to reduced connectivity between the larger aggregate particles, results in a decrease in storage ($G'$) moduli but an increase in viscosity, as shown by the flow sweep test. These larger aggregates were responsible for the higher coefficient of friction in the boundary regime as they were excluded from the narrow gap preventing the smaller particles from being entrained between the surfaces up to a certain sliding speed.

Furthermore, the interaction between sugar and water molecules in hydrocolloid solutions is also primarily entropy-driven. Whether this effect is particularly pronounced when sucrose or agarose is dissolved in advance requires clarification. Therefore, aspects influencing entropic effects, including molecular flexibility, conformational changes, and solvent effects, need to be considered. The impact of dissolving sucrose and agarose in different orders on the changes in the molecular conformation of agarose was discussed in detail. The binding of sugar molecules with water in their hydration shell reduces the availability of free water surrounding the agarose polymers. This, in turn, leads to stronger interactions between the agarose chains when sucrose is first dissolved and may promote the formation of helical structures, due to locally increased concentration. However, it can be concluded that the interaction between the agarose and sucrose molecules is primarily indirect, involving hydrogen bonding, which has a noticeable impact on the fluid gel network. It can be suggested that the addition of sucrose influences the rheological and mechanical properties by affecting the hydration shell surrounding the agarose molecules during the gelation process. This consequent change in the hydration environment is considered to be a key factor in the observed changes in gel properties. Overall, the findings of this study demonstrate the ability to modify edible soft matter systems to alter textural properties for further potential applications. Additionally, they provide a deeper

understanding of the complex interactions within fluid hydrogels.

## Data availability statement

The raw data supporting the conclusion of this article will be made available by the authors, without undue reservation.

## Author contributions

MG: Conceptualization, Investigation, Methodology, Validation, Visualization, Writing–original draft, Writing–review and editing. SS: Conceptualization, Supervision, Writing–review and editing. TV: Conceptualization, Supervision, Writing–review and editing, Writing–original draft, Visualization.

## Funding

The author(s) declare that no financial support was received for the research, authorship, and/or publication of this article.

## Acknowledgments

The authors would like to thank Dr. Kaloian Koynov and especially Andreas Hanewald for the technical support during rheology and tribology experiments. Furthermore, we thank the members of the MPIP soft matter food science group for fruitful discussion and proofreading the manuscript.

## Conflict of interest

The authors declare that the research was conducted in the absence of any commercial or financial relationships that could be construed as a potential conflict of interest.

The author(s) declared that they were an editorial board member of Frontiers, at the time of submission. This had no impact on the peer review process and the final decision.

## Publisher's note



## Supplementary material

The Supplementary Material for this article can be found online at: https://www.frontiersin.org/articles/10.3389/frsfm.2024.1363898/full#supplementary-material

## References

Ablett, S., Lillford, P. J., Baghdadi, S. M. A., and Derbyshire, W. (1978). Nuclear magnetic resonance investigations of polysaccharide films, sols, and gels. *J. Colloid Interface Sci.* 67 (2), 355–377. doi:10.1016/0021-9797(78)90020-6

Arnott, S., Fulmer, A., Scott, W., Dea, I., Moorhouse, R., and Rees, D. (1974). The agarose double helix and its function in agarose gel structure. *J. Mol. Biol.* 90 (2), 269–284. doi:10.1016/0022-2836(74)90372-6

Baier, S., Elmore, D., Guthrie, B., Lindgren, T., Smith, S., Steinbach, A., et al. (2009). "A new tribology device for assessing mouthfeel attributes of foods," in *5th International Symposium on Food Structure and Rheology*, 432–435. (ETH Zurich: Switzerland).

De Carvalho, W., and Djabourov, M. (1997). Physical gelation under shear for gelatin gels. *Rheol. Acta* 36 (6), 591–609. doi:10.1007/s003970050074

Deszczynski, M., Kasapis, S., MacNaughton, W., and Mitchell, J. R. (2003a). Effect of sugars on the mechanical and thermal properties of agarose gels. *Food Hydrocoll.* 17 (6), 793–799. doi:10.1016/s0268-005x(03)00100-0

Deszczynski, M., Kasapis, S., and Mitchell, J. R. (2003b). Rheological investigation of the structural properties and aging effects in the agarose/Co-solute mixture. *Carbohydr. Polym.* 53, 85–93. doi:10.1016/s0144-8617(02)00327-2

Diener, M., Adamcik, J., Bergfreund, J., Catalini, S., Fischer, P., and Mezzenga, R. (2020). Rigid, fibrillar quaternary structures induced by divalent ions in a carboxylated linear polysaccharide. *ACS Macro Lett.* 9 (1), 115–121. doi:10.1021/acsmacrolett.9b00824

Diener, M., Adamcik, J., Sánchez-Ferrer, A., Jaedig, F., Schefer, L., and Mezzenga, R. (2019). Primary, secondary, tertiary and quaternary structure levels in linear polysaccharides: from random coil, to single helix to supramolecular assembly. *Biomacromolecules* 20 (4), 1731–1739. doi:10.1021/acs.biomac.9b00087

Doi, M., and Edwards, S. F. (1988). *The theory of polymer dynamics*. Vol. 73. Oxford, United Kingdom: Oxford University Press.

Donley, G. J., Singh, P. K., Shetty, A., and Rogers, S. A. (2020). Elucidating the G? Overshoot in soft materials with a yield transition via a time-resolved experimental strain decomposition. *Proc. Natl. Acad. Sci. U. S. A.* 117 (36), 21945–21952. doi:10.1073/pnas.2003869117

Ellis, A. L., Mills, T. B., Norton, I. T., and Norton-Welch, A. (2019). The effect of sugars on agar fluid gels and the stabilisation of their foams. *Food Hydrocoll.* 87, 371–381. August 2018. doi:10.1016/j.foodhyd.2018.08.027

Farrés, Fernández, I., Moakes, R. J. A., and Norton, I. T. (2014). Food hydrocolloids designing biopolymer fluid gels: a microstructural approach. *Food Hydrocoll.* 42, 362–372. doi:10.1016/j.foodhyd.2014.03.014

Fernández Farrés, I., and Norton, I. T. (2015). The influence of Co-solutes on tribology of agar fluid gels. *Food Hydrocoll.* 45, 186–195. doi:10.1016/j.foodhyd.2014.11.014

Fittolani, G., Seeberger, P. H., and Delbianco, M. (2020). Helical polysaccharides. *Peptide Sci.* 112 (1). doi:10.1002/pep2.24124

Frith, W. J., Garijo, X., Foster, T. J., and Norton, I. T. (2002). Microstructural origins of the rheology of fluid gels. *Special publication-royal society of chemistry* 278, 95–103.

Gabriele, A., Spyropoulos, F., and Norton, I. T. (2010). A conceptual model for fluid gel lubrication. *Soft Matter* 6 (17), 4205–4213. doi:10.1039/c001907k

Gharsallaoui, A., Rogé, B., Génotelle, J., and Mohamed, M. (2008). Relationships between hydration number, water activity and density of aqueous sugar solutions. *Food Chem.* 106, 1443–1453. 4 SPEC. ISS. doi:10.1016/j.foodchem.2007.02.047

Ghebremedhin, M., Seiffert, S., and Vilgis, T. A. (2021). Physics of agarose fluid gels: rheological properties and microstructure. *Curr. Res. Food Sci.* 4, 436–448. December 2020. doi:10.1016/j.crfs.2021.06.003

Ghebremedhin, M., Seiffert, S., and Vilgis, T. A. (2022). Molecular behavior of fluid gels - the crucial role of edges and particle surface in macroscopic properties. *Food Funct.* 13 (13), 6902–6922. doi:10.1039/d2fo00102k

He, Qi, Bramante, F., Davies, A., Elleman, C., Fourtouni, K., and Wolf, B. (2018). Material properties of *ex vivo* milk chocolate boluses examined in relation to texture perception. *Food Funct.* 9 (6), 3532–3546. doi:10.1039/c8fo00548f

Hédoux, A., Willart, J. F., Ionov, R., Affouard, F., Guinet, Y., Paccou, L., et al. (2006). Analysis of sugar bioprotective mechanisms on the thermal denaturation of lysozyme from Raman scattering and differential scanning calorimetry investigations. *J. Phys. Chem. B* 110 (45), 22886–22893. doi:10.1021/jp061568i

Imeson, A. (2009). 3 agar. *Food stabilisers, Thick. gelling agents* 31.

Kasapis, S., Al-Marhoobi, I. M., Deszczynski, M., Mitchell, J. R., and Abeysekera, R. (2003). Gelatin vs polysaccharide in mixture with sugar. *Biomacromolecules* 4 (5), 1142–1149. doi:10.1021/bm0201237

Laiho, S., Williams, R. P., Poelman, A., Appelqvist, I., and Logan, A. (2017). Effect of whey protein phase volume on the tribology, rheology and sensory properties of fat-free stirred yoghurts. *Food Hydrocoll.* 67, 166–177. doi:10.1016/j.foodhyd.2017.01.017

Lee, S. L., Debenedetti, P. G., and Errington, J. R. (2005). A computational study of hydration, solution structure, and dynamics in dilute carbohydrate solutions. *J. Chem. Phys.* 122 (20), 204511. doi:10.1063/1.1917745

Lerbret, A., Affouard, F., Bordat, P., Hédoux, A., Guinet, Y., and Descamps, M. (2011). Slowing down of water dynamics in disaccharide aqueous solutions. *J. Non-Crystalline Solids* 357 (2), 695–699. doi:10.1016/j.jnoncrysol.2010.05.092

Lerbret, A., Bordat, P., Affouard, F., Hédoux, A., Guinet, Y., and Descamps, M. (2007). How do trehalose, maltose, and sucrose influence some structural and dynamical properties of lysozyme? Insight from molecular dynamics simulations. *J. Phys. Chem. B* 111 (31), 9410–9420. doi:10.1021/jp071946z

Martínez-Sanz, M., Ström, A., Lopez-Sanchez, P., Knutsen, S. H., Ballance, S., Zobel, H. K., et al. (2020). Advanced structural characterisation of agar-based hydrogels: rheological and small angle scattering studies. *Carbohydr. Polym.* 236, 115655. February. doi:10.1016/j.carbpol.2019.115655

Maurer, S., Junghans, A., and Vilgis, T. A. (2012). Impact of xanthan gum, sucrose and fructose on the viscoelastic properties of agarose hydrogels. *Food Hydrocoll.* 29 (2), 298–307. doi:10.1016/j.foodhyd.2012.03.002

Moakes, R. J. A., Sullo, A., and Norton, I. T. (2015). Preparation and characterisation of whey protein fluid gels: the effects of shear and thermal history. *Food Hydrocoll.* 45, 227–235. doi:10.1016/j.foodhyd.2014.11.024

Nguyen, P. T. M., Kravchuk, O., Bhandari, B., and Prakash, S. (2017). Effect of different hydrocolloids on texture, rheology, tribology and sensory perception of texture and mouthfeel of low-fat pot-set yoghurt. *Food Hydrocoll.* 72, 90–104. doi:10.1016/j.foodhyd.2017.05.035

Nishinari, K., Watase, M., Kohyama, K., Nishinari, N., Oakenfull, D., Koide, S., et al. (1992). The effect of sucrose on the thermo-reversible gel-sol transition in agarose and gelatin. *Polym. J.* 24 (9), 871–877. doi:10.1295/polymj.24.871

Nordqvist, D., and Vilgis, T. A. (2011). Rheological study of the gelation process of agarose-based solutions. *Food Biophys.* 6, 450–460. doi:10.1007/s11483-011-9225-0

Normand, V., Aymard, P., Lootens, D. L., Amici, E., Plucknett, K. P., and Frith, W. J. (2003). Effect of sucrose on agarose gels mechanical behaviour. *Carbohydr. Polym.* 54 (1), 83–95. doi:10.1016/s0144-8617(03)00153-x

Normand, V., Lootens, D. L., Amici, E., Plucknett, K. P., and Aymard, P. (2000). New insight into agarose gel mechanical properties. *Biomacromolecules* 1 (4), 730–738. doi:10.1021/bm005583j

Norton, I. T., Jarvis, D. A., and Foster, T. J. (1999). A molecular model for the formation and properties of fluid gels. *Int. J. Biol. Macromol.* 26 (4), 255–261. doi:10.1016/s0141-8130(99)00091-4

Nussinovitch, A. (1997). *Hydrocolloid applications: gum technology in the food and other industries*. Springer.

Olsson, C., and Jan, S. (2020). Structural comparison between sucrose and trehalose in aqueous solution. *J. Phys. Chem. B* 124 (15), 3074–3082. doi:10.1021/acs.jpcb.9b09701

Parthasarathy, M., and Klingenberg, D. J. (1999). Large amplitude oscillatory shear of ER suspensions. *J. Newt. Fluid Mech.* 81 (1–2), 83–104. doi:10.1016/s0377-0257(98)00096-2

Rudge, R. E. D., Jesse, P. M. V.De S., Dijksman, J. A., and Scholten, E. (2020). Uncovering friction dynamics using hydrogel particles as soft ball bearings. *Soft Matter* 16 (15), 3821–3831. doi:10.1039/D0SM00080A

Russ, N., Zielbauer, B. I., Koynov, K., and Vilgis, T. A. (2013). Influence of nongelling hydrocolloids on the gelation of agarose. *Biomacromolecules* 14 (11), 4116–4124. doi:10.1021/bm4012776

Russ, N., Zielbauer, B. I., and Vilgis, T. A. (2014). Impact of sucrose and trehalose on different agarose-hydrocolloid systems. *Food Hydrocoll.* 41, 44–52. doi:10.1016/j.foodhyd.2014.03.020

Schefer, L., Adamcik, J., Diener, M., and Mezzenga, R. (2015a). Supramolecular chiral self-assembly and supercoiling behavior of carrageenans at varying salt conditions. *Nanoscale* 7 (39), 16182–16188. doi:10.1039/c5nr04525h

Schefer, L., Adamcik, J., and Mezzenga, R. (2014). Unravelling secondary structure changes on individual anionic polysaccharide chains by atomic force microscopy. *Angew. Chem. - Int. Ed.* 53 (21), 5376–5379. doi:10.1002/anie.201402855

Schefer, L., Usov, I., and Mezzenga, R. (2015b). Anomalous stiffening and ion-induced coil-helix transition of carrageenans under monovalent salt conditions. *Biomacromolecules* 16 (3), 985–991. doi:10.1021/bm501874k

Shewan, H. M., Pradal, C., and Stokes, J. R. (2019). Tribology and its growing use toward the study of food oral processing and sensory perception. *J. Texture Stud.* 51, 7–22. May. doi:10.1111/jtxs.12452

Shimizu, S., and Matubayasi, N. (2014). *Gelation: the role of sugars and polyols on gelatin and agarose*.

Sim, H. G., Ahn, K. H., and Lee, S. J. (2003). Three-dimensional dynamics simulation of electrorheological fluids under large amplitude oscillatory shear flow. *J. Rheology* 47 (4), 879–895. doi:10.1122/1.1582854

Starzak, M., and Mohamed, M. (2006). Temperature dependence of water activity in aqueous solutions of sucrose. *Food Chem.* 96 (3), 346–370. doi:10.1016/j.foodchem.2005.02.052

Starzak, M., Peacock, S. D., and Mathlouthi, M. (2000). Hydration number and water activity models for the sucrose-water system: a critical review. *Crit. Rev. Food Sci. Nutr.* 40 (4), 327–367. doi:10.1080/10408690091189185

Stokes, J. R., Boehm, M. W., and Baier, S. K. (2013). Oral processing, texture and mouthfeel: from rheology to tribology and beyond. *Curr. Opin. Colloid Interface Sci.* 18 (4), 349–359. doi:10.1016/j.cocis.2013.04.010

Tako, M., Teruya, T., Tamaki, Y., Uechi, K., and Konishi, T. (2021). Molecular origin for strong agarose gels: multi-stranded hydrogen bonding molecular origin for strong agarose gels: multi-stranded hydrogen bonding. *J. Polym. Biopolymer Phys. Chem.* 9 (1), 13–19. doi:10.12691/jpbpc-9-1-2

Tas, O., Ertugrul, U., Grunin, L., and Oztop, M. H. (2022). Investigation of the hydration behavior of different sugars by time domain-NMR. *Foods* 11 (8), 1148. doi:10.3390/foods11081148

Tavagnacco, L., Chiessi, E., Severini, L., Franco, S., Buratti, E., Capocefalo, A., et al. (2023). Molecular origin of the two-step mechanism of gellan aggregation. *Sci. Adv.* 9 (10), 1–11. doi:10.1126/sciadv.adg4392

Tsenoglou, C. (1990). Scaling concepts in suspension rheology. *J. Rheology* 34 (1), 15–24. doi:10.1122/1.550120

Vilgis, T. A. (2015a). Gels: model systems for soft matter food physics. *Curr. Opin. Food Sci.* 3, 71–84. doi:10.1016/j.cofs.2015.05.009

Watase, M., Kohyama, K., and Nishinari, I. L. (1992). Effects of sugars and polyols on the gel-sol transition of agarose by differential scanning calorimetry. *Adv. Exp. Med. Biol.* 206, 163–173. doi:10.1016/0040-6031(92)85294-6

Watase, M., Nishinari, K., and Hatakeyama, T. (1988). DSC study on properties of water in concentrated agarose gels. *Food Hydrocoll.* 2 (6), 427–438. doi:10.1016/s0268-005x(88)80043-2

Watase, M., Nishinari, K., Williams, P. A., and Phillips, G. O. (1990). Agarose gels: effect of sucrose, glucose, urea, and guanidine hydrochloride on the rheological and thermal properties *. *J. Agric. Food Chem.* 38, 1181–1187. doi:10.1021/jf00095a005

Williams, P. A., Day, D., Langdon, M., Phillips, G., and Nishinari, K. (1991). Synergistic interaction of xanthan gum with glucomannans and galactomannans. *Top. Catal.* 4 (6), 489–493. doi:10.1016/s0268-005x(09)80199-9

Wolf, B., Frith, W. J., Singleton, S., Tassieri, M., and Norton, I. T. (2001). Shear behaviour of biopolymer suspensions with spheroidal and cylindrical particles. *Rheol. Acta* 40 (3), 238–247. doi:10.1007/s003970000133

Wyss, H. M., Miyazaki, K., Mattsson, J., Hu, Z., Reichman, D. R., and Weitz, D. A. (2007). Strain-rate frequency superposition: a rheological probe of structural relaxation in soft materials. *Phys. Rev. Lett.* 98 (23), 238303. doi:10.1103/physrevlett.98.238303

Xiong, J. Y., Narayanan, J., Liu, X. Y., Chong, T. K., Chen, S. B., and Chung, T. S. (2005). Topology evolution and gelation mechanism of agarose gel. *J. Phys. Chem. B* 109 (12), 5638–5643. doi:10.1021/jp044473u

Yang, K., Wang, Z., Brenner, T., Kikuzaki, H., Fang, Y., and Nishinari, K. (2015). Sucrose release from agar gels: effects of dissolution order and the network inhomogeneity. *Food Hydrocoll.* 43, 100–106. doi:10.1016/j.foodhyd.2014.05.005

Zhao, L., Ma, K., and Yang, Zi (2015). Changes of water hydrogen bond network with different externalities. *Int. J. Mol. Sci.* 16 (4), 8454–8489. doi:10.3390/ijms16048454

Zhou, J. Z. Q., Uhlherr, P. H. T., and Luo, F. T. (1995). Yield stress and maximum packing fraction of concentrated suspensions. *Rheol. Acta* 34 (6), 544–561. doi:10.1007/bf00712315

**Electronic Supplementary Information**

# Effects of sugar molecules on the rheological and tribological properties and on the microstructure of agarose-based fluid gels

Marta Ghebremedhin[1], Sebastian Seiffert[2], Thomas A. Vilgis[1]

[1]Max Planck Institute for Polymer Research, Ackermannweg 10, 55128 Mainz, Germany

[2]Department of Chemistry, Johannes Gutenberg University Mainz, Duesbergweg 10-14, 55128 Mainz, Germany

E-mail: ghebre@mpip-mainz.mpg.de (M. Ghebremedhin), vilgis@mpip-mainz.mpg.de (T. A. Vilgis)

## S1 Materials and methods

### S1.1 Preparation of quiescently cooled gels

To verify the effect of sucrose on the storage and loss modulus of the prepared fluid gels, they were compared with the quiescently cooled gels using amplitude sweep measurements (see Fig. S.8). Therefore, disposable aluminium plates with a diameter of 25 mm and a height of 3 mm, and Teflon molds with an inner diameter of 25 mm and a height of 6 mm were used to prepare the quiescent cooled agarose gels. The hot agarose solutions with the appropriate sucrose concentration were pipetted into the Teflon mold and evenly distributed with a razor blade to produce the gels of defined height and diameter. The gels were then allowed to cool to room temperature before hardening overnight in a refrigerator at 4 °C. To reduce water evaporation, the molds were covered with disposable weighing dishes with greased edges to ensure an airtight seal. The next day, the molds were carefully removed, and the samples were allowed to reach room temperature before measurement.

# S2. Results

## S2.1 Gelation under shear

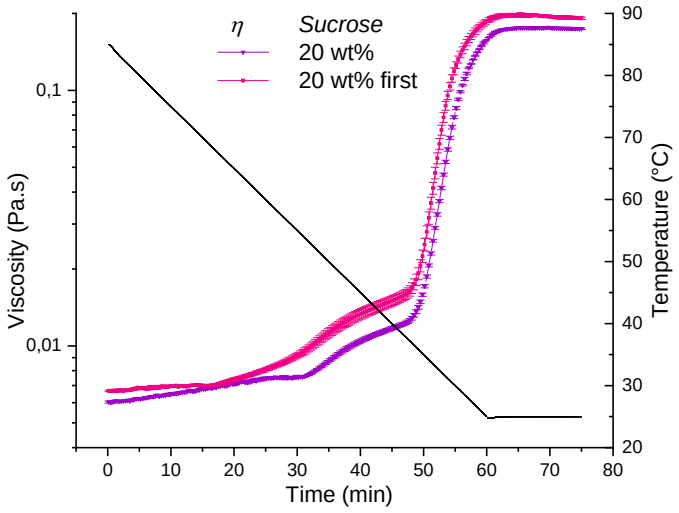


*Fig. S1. Viscosity profile during the production of 1 wt% agarose fluid gel with 20 wt% sucrose using different preparation methods. In the usual method, agarose was first dissolved in water, followed by the addition of sucrose. Conversely, in the alternative method, sucrose was first dissolved, and then agarose was added to the sucrose solution (20 wt% first). Samples were subjected to a constant applied shear rate of 400 s-1, cooled from 85 °C to 25 °C at 1 °C/min, and held at 25 °C for 15 min.*

## S2.2 Micrograph of fluid gels

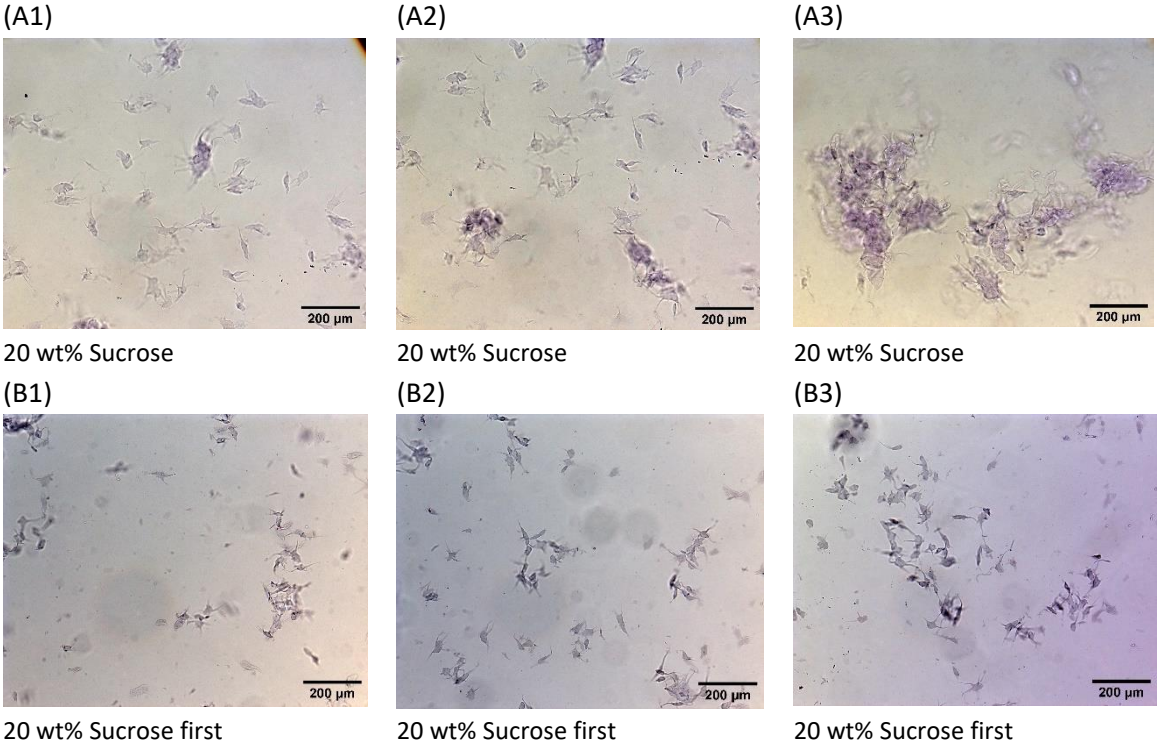


*Fig. S2. Light microscopy images of 1 wt% agarose fluid gel particles with 20 wt% sucrose. (a) Using the usual method, where agarose was first dissolved in water and then sucrose was added. (b) Using the alternative method, where sucrose was first dissolved, and then agarose was added to the sucrose solution.*

## S2.3 Particle size of fluid gels

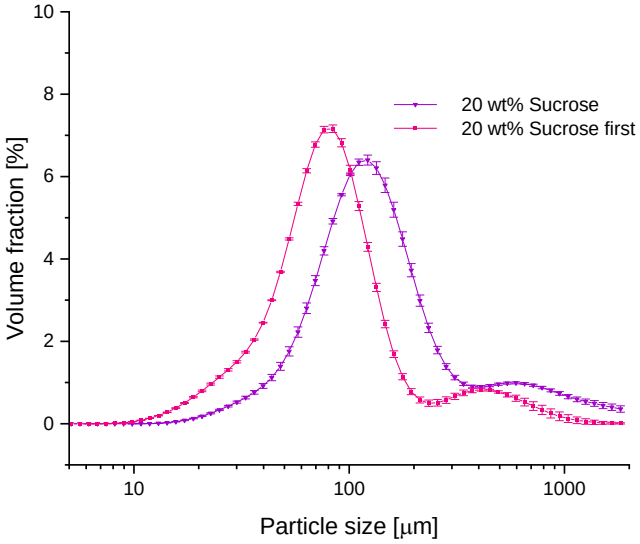


*Fig. S3 . Particle size distribution of 1 wt% agarsoe fluid ge particlel with 20 wt% sucrose concentration. Using the usual method, where agarose was first dissolved in water and then sucrose was added. And using the alternative method, where sucrose was first dissolved (20 wt% first), and then agarose was added to the sucrose solution.*

## S2.4 Rheological properties

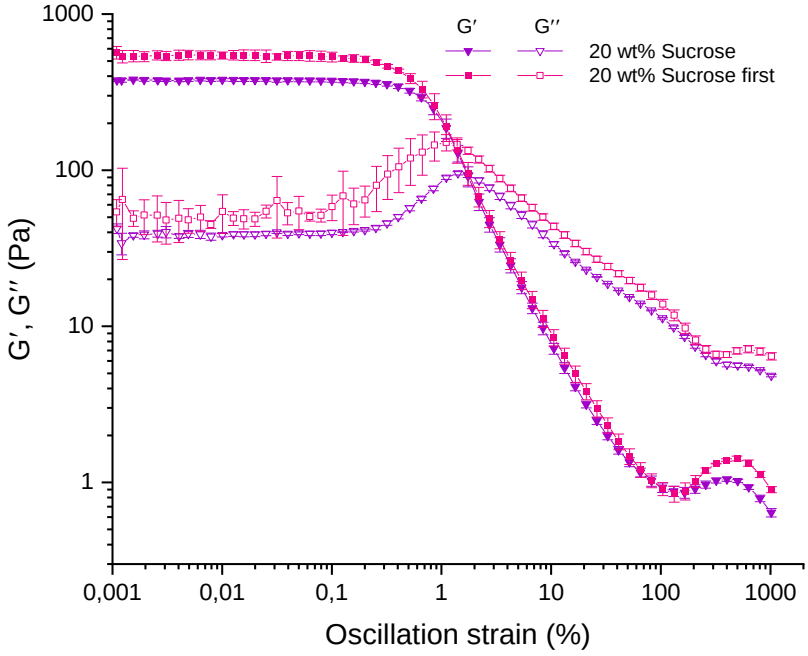


*Fig. S4. Amplitude sweep measurements of 1 wt% agarose fluid gel with 20 wt% sucrose. For the fluid gel prepared with the usual method, agarose was first dissolved in water and then sucrose was added. For and the alternative method, sucrose was first dissolved, and then agarose was added to the sucrose solution.*

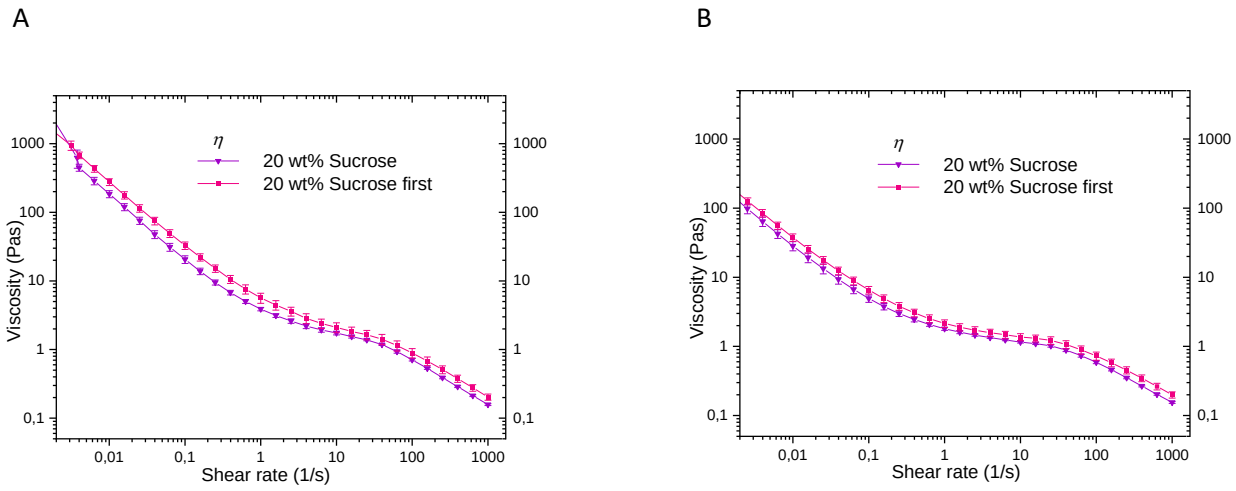


*Fig. S5. Flow sweep test. Flow behavior of 1 wt% agarose fluid gels with 20 wt% sucrose concentrations, showing ramp up (a) and ramp down (b) viscosity profiles. For the fluid gel prepared by the usual method of first dissolving agarose in water and then adding sucrose, and for the fluid gel prepared by the alternative method of first dissolving sucrose and then adding agarose to the sucrose solution.*

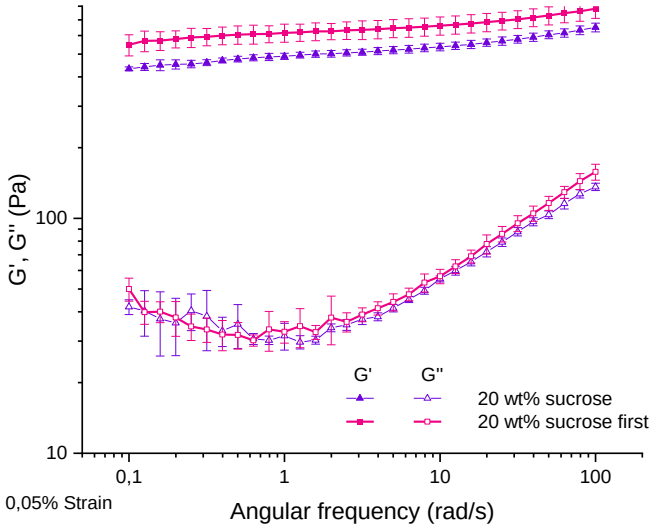


*Fig. S6. Frequency sweep test. Frequency dependence of storage moduli G′(filled symbols) and loss moduli G″(empty symbols) at a constant strain ($\gamma = 0.05$ %) and temperature ($T = 25$ °C) of 1 wt% agarose fluid gel with 20 wt% sucrose. For the fluid gel prepared by the usual method of first dissolving agarose in water and then adding sucrose, and the for the fluid gel prepared by the alternative method of first dissolving sucrose and then adding agarose to the sucrose solution. The dashed lines indicate the angular frequency ($\omega_c$) where G″starts to increase for the respective concentrations.*

## S2.5 Tribology

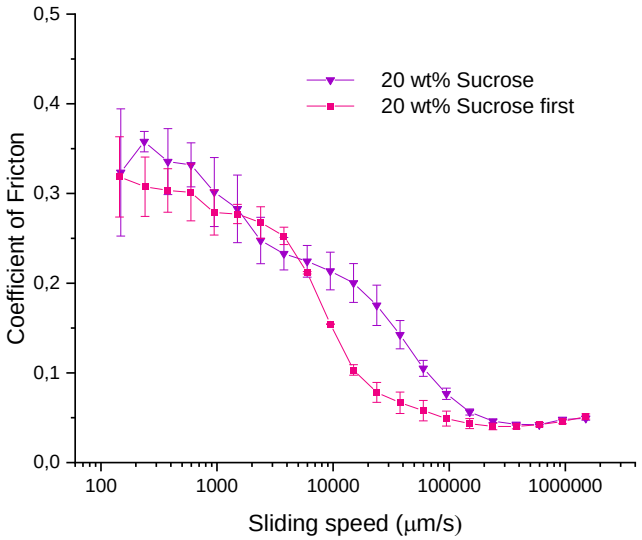


*Fig. S7. Stribeck curves at a normal load of 3 N for 1 wt% agarose fluid gels with 20 wt% sucrose. For fluid gels prepared by the usual method of first dissolving agarose in water and then adding sucrose, and for the fluid gel prepared by the alternative method of first dissolving sucrose and then adding agarose.*

## S2.6 Sucrose effect on quiescently cooled gels

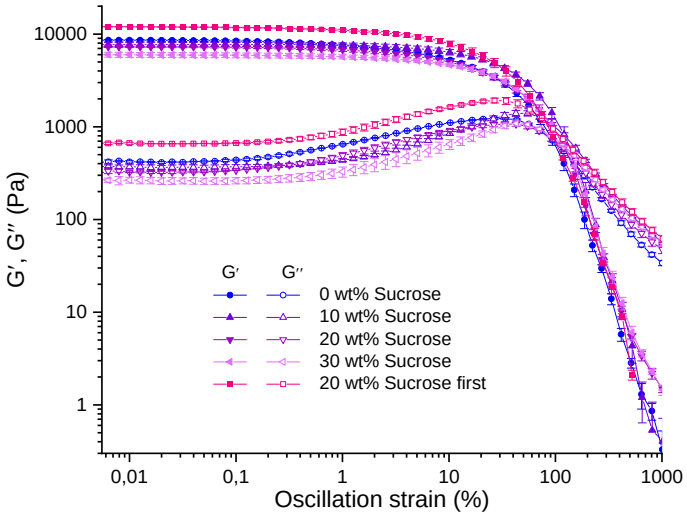


*Fig. S8. Amplitude sweep tests for the gels prepared under quiescent conditions of 1 wt% agarose gels with different sucrose concentrations. For the 20 wt% sucrose gel prepared using the alternative method of first dissolving sucrose and then adding agarose to the sucrose solution, and for the remaining concentrations using the usual method of first dissolving agarose in water and then adding sucrose.*

# 8 Appendix

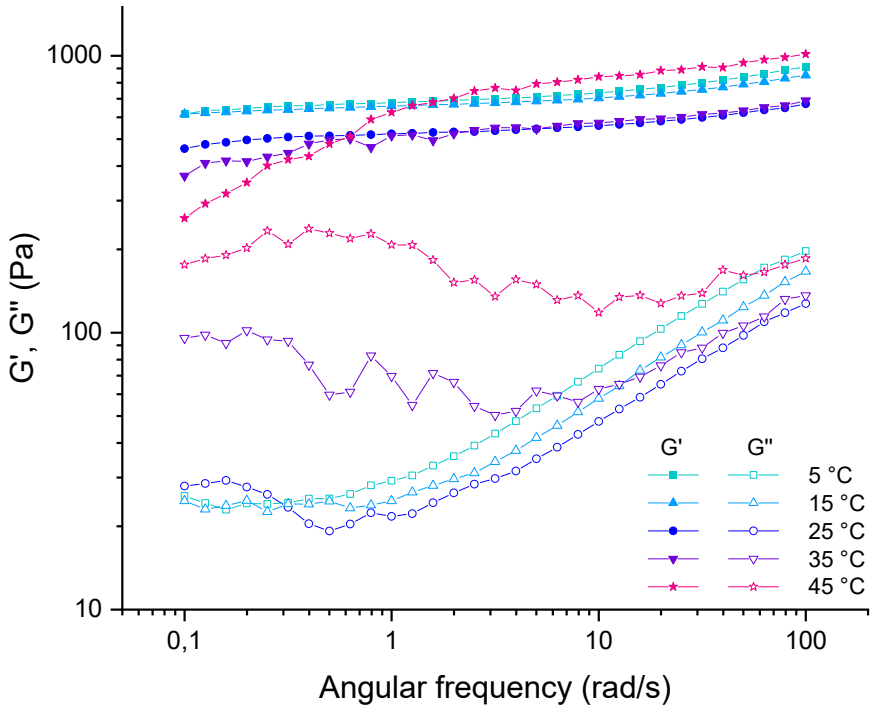


*Fig. A22. Frequency dependence of storage modulus G′(filled symbols) and loss moduli G″(empty symbols) at a constant strain (γ = 0.05 %) at different temperatures (5 °C, 15°C, 25°C, 35°C and 45°C) for 1 wt% agarose fluid gel.*

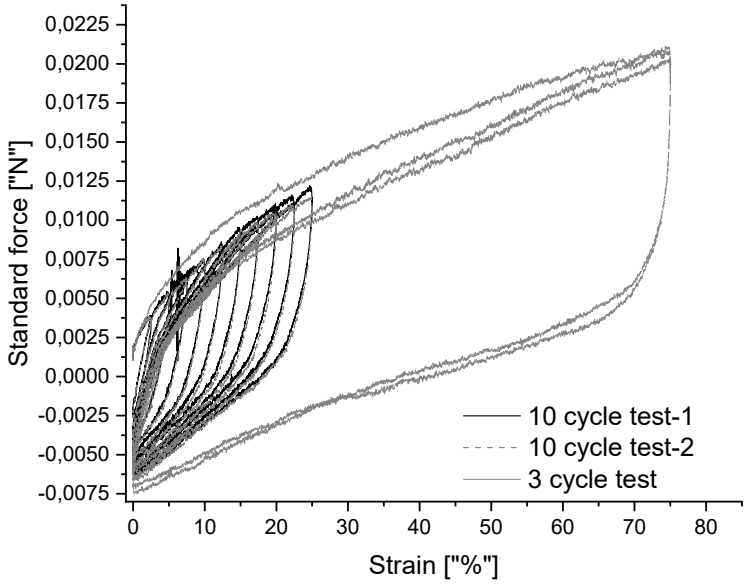


*Fig. A23. Texture analysis of 0.5 wt% agarose fluid gel: comparison of multiple force-strain curves from a 10 cycle test with gradual strain increase of 2.5% per cycle and three-cycle test with a maximum strain of 75%. Test speed: 10 mm/min.*

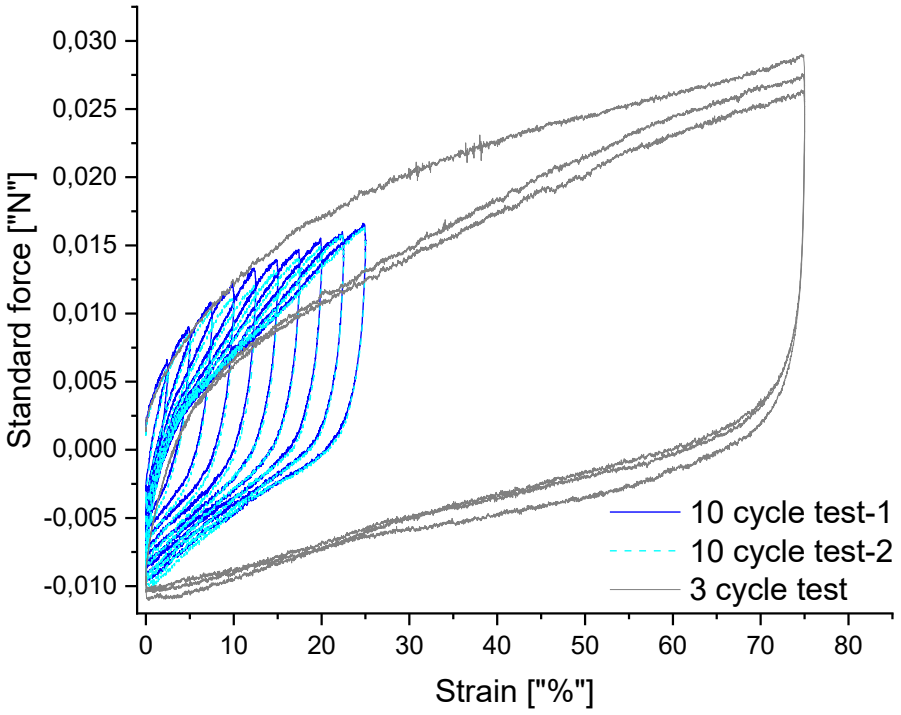


*Fig. A24. Texture analysis of 1 wt% agarose fluid gel: comparison of multiple force-strain curves from a 10 cycle test with gradual strain increase of 2.5% per cycle and three-cycle test with a maximum strain of 75%. Test speed: 10 mm/min.*

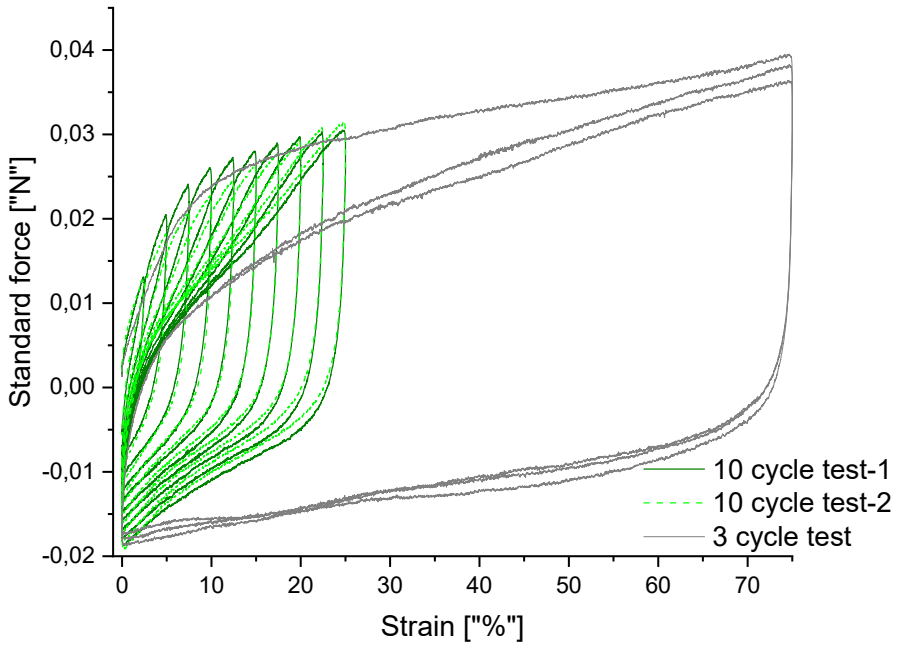


*Fig. A25. Texture analysis of 2 wt% agarose fluid gel: comparison of multiple force-strain curves from a 10 cycle test with gradual strain increase of 2.5% per cycle and three-cycle test with a maximum strain of 75%. Test speed: 10 mm/min.*

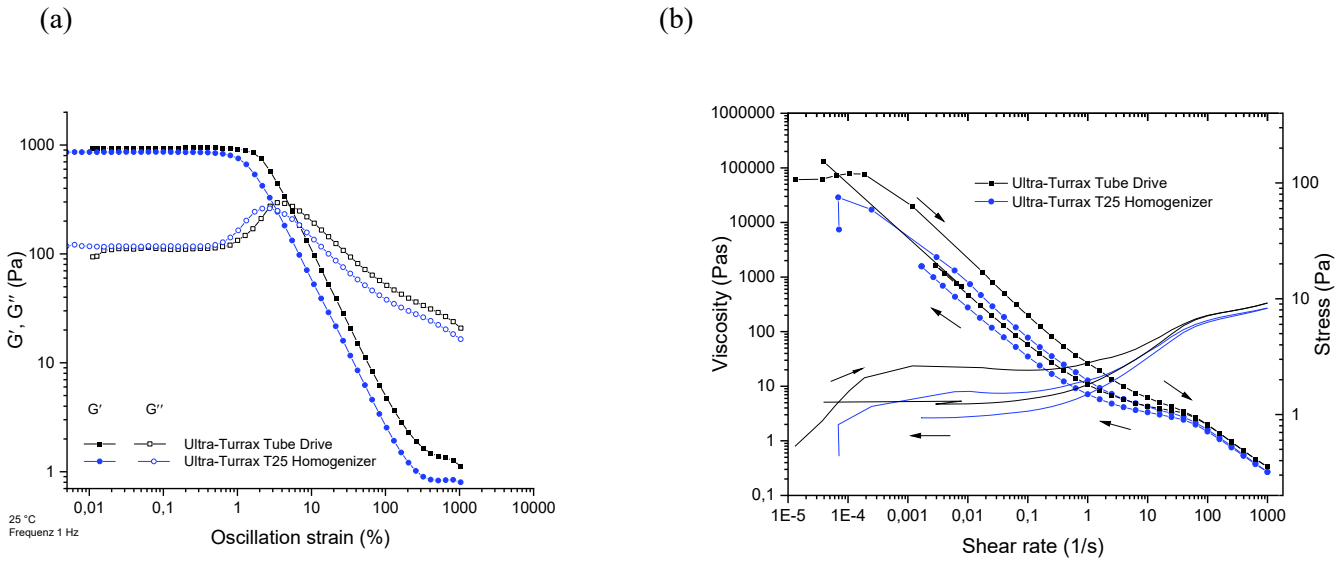


*Fig. A26. (a) Amplitude sweep measurement of 1 wt% agarose fluid gels sheared after gelation, prepared using different equipment: Ultra Turrax Tube Drive and Ultra Turrax T25 Homogenizer. (b) Flow sweep measurements of the same differently prepared fluid gels, showing viscosity profiles during rump up and rump down.*

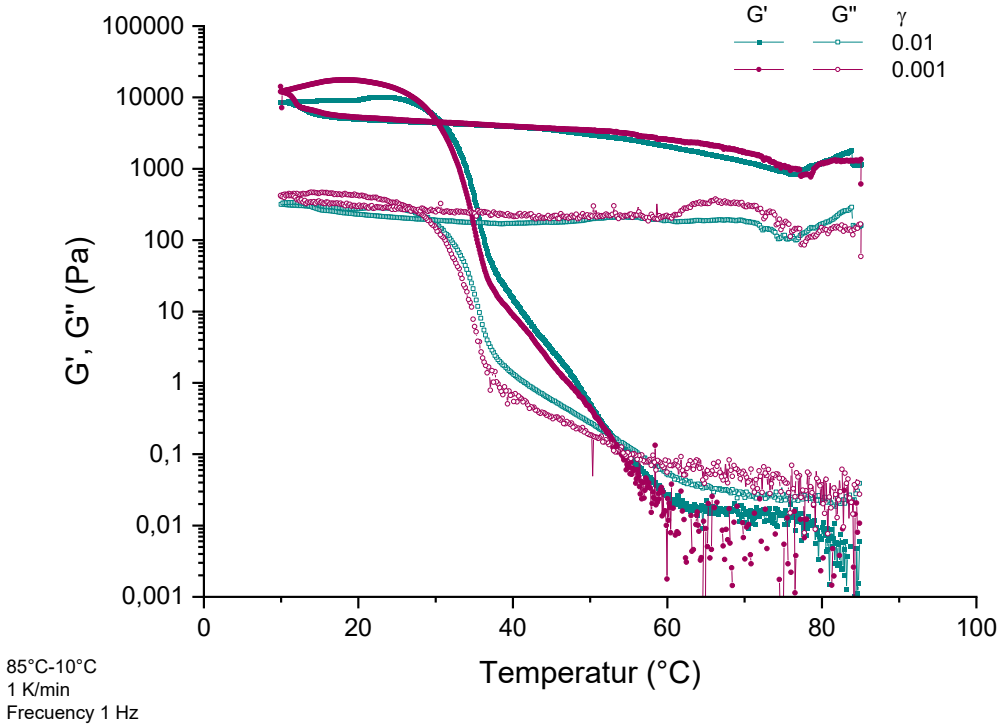


*Fig. A27. Temperature dependent oscillation measurements of 1 wt% agarose. Agarose solution in its heated sol-state was cooled down from 85°C to 10 °C and reheated to 85°C at a rate of 1 K/min under constant strain (γ= 0.01% and 0.001%). The measurements demonstrate a pronounced thermal hysteresis.*

(a) (b)

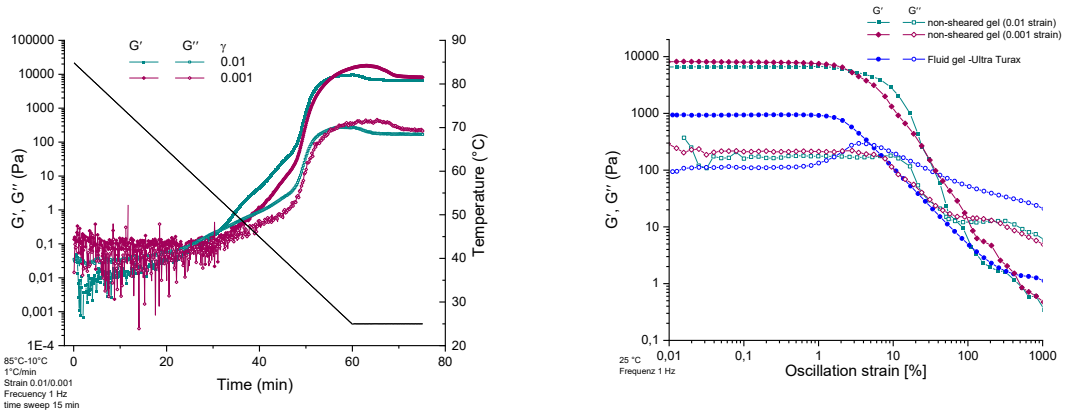


*Fig. A28. (a)Temperature dependent oscillation measurements of 1 wt% agarose. The agarose solution, in its heated sol state, was cooled from 85°C to 25 °C at a rate of 1 K/min under constant strain (γ= 0.01% and 0.001%), followed by a time sweep for 15 min. (b) An amplitude swep was subsequent performed on the same samples at a constant frequency (f = 1 Hz) and temperature (T = 25 °C). The amplitude sweep test includes also a comparison between the non-sheared 1 wt% agarose gel and the 1 wt% agarose fluid gel prepared using the Ultr-Turrax Tube Drive.*

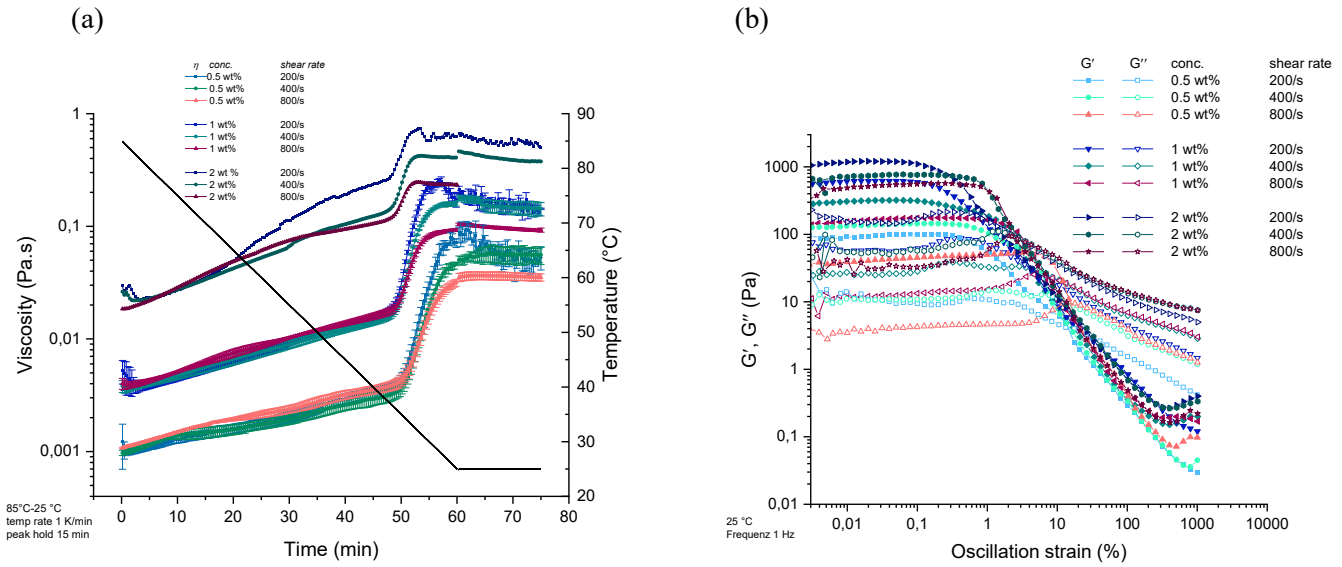


*Fig. A29. (a) Gelation under shear using parallel-plate geometry. Viscosity profiles of 0.5 wt%, 1 wt% and 2 wt% agarose fluid gels produced under different applied shear rates (200 $s^{-1}$, 400 $s^{-1}$ and 800 $s^{-1}$). The samples were subjected to constant shear rate while cooling from 85 °C to 25 °C at 1 K/min, followed by 15 min holding at 25 °C. Higher viscosity at 25 °C can be observe for fluid gels produced with higher agarose concentrations and at lower shear rates. (b) Amplitude sweep test of the corresponding agarose fluid gels (measured in the same geometry used during fluid gel production) at constant frequency (f = 1 Hz) and temperature (T = 25 °C), showing increased storage (G′) and loss (G″) moduli for samples with higher concentrations and produced at lower shear rates.*

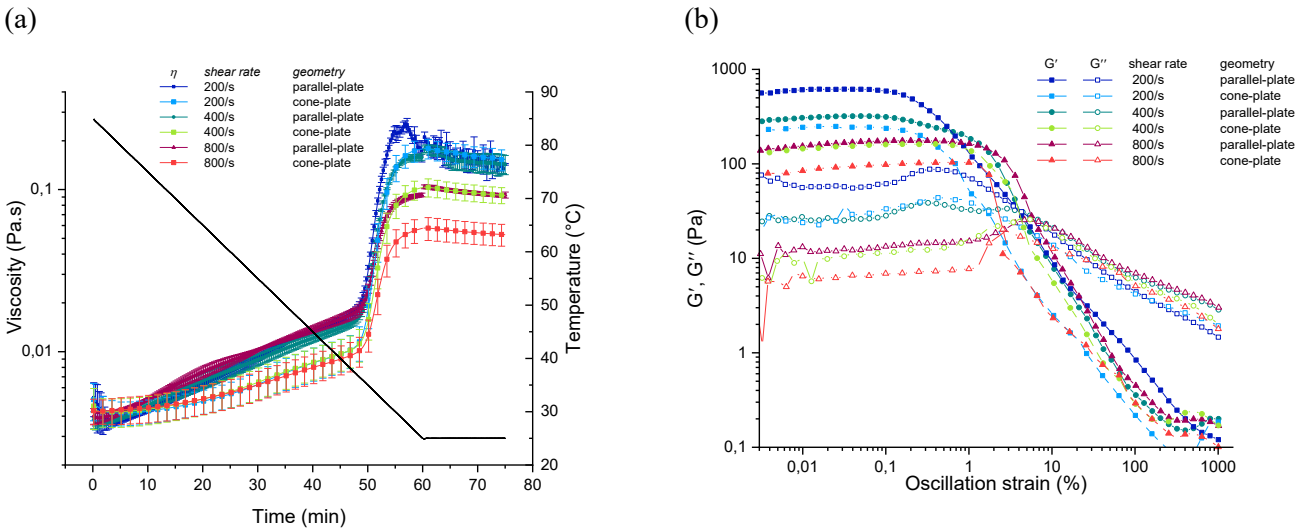


*Fig. A30. (a) Gelation under shear in parallel-plate versus cone-plate geometry. Viscosity profile of 1 wt% agarose fluid gels produced under different applied shear rate and geometries. The samples were subjected to constant shear rate while cooling from 85 °C to 25 °C at 1 K/min, followed by 15 min holding at 25 °C. Higher viscosity at 25 °C can be observe for fluid gels produced in the parallel-plate geometry compared to cone-plate, and viscosity increased with lower shear rate. (b) Amplitude sweep test of the corresponding agarose fluid gels (measured in the same geometry used during fluid gel production) at constant frequency (f = 1 Hz) and temperature (T = 25 °C), showing increased storage (G′) and loss (G″) moduli for samples produced at lower shear rates and with parallel-plate geometry.*

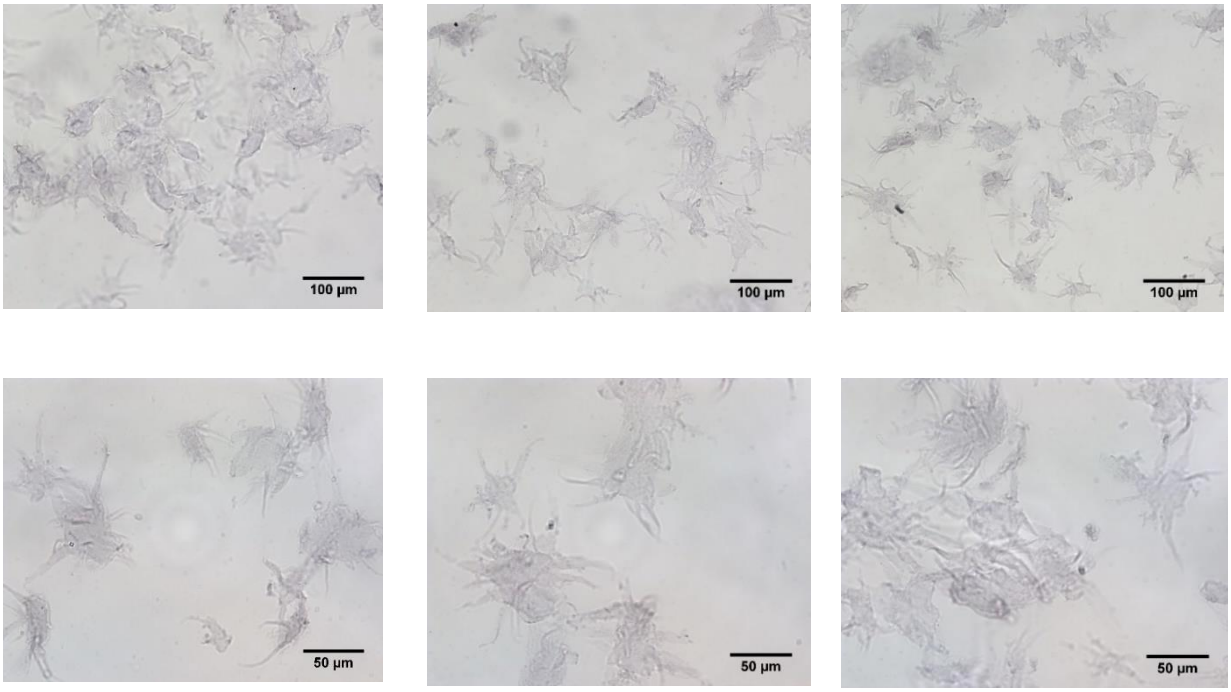


*Fig. A31. Microscopy images of 0.5 wt% agarose fluid gel particles stained with toluidine blue. The sample was prepared using parallel-plate geometry at a constant shear rate of 400 $s^{-1}$, cooled from 85 °C to 25 °C at 1 K/min, and held at 25 °C for 15 min.*

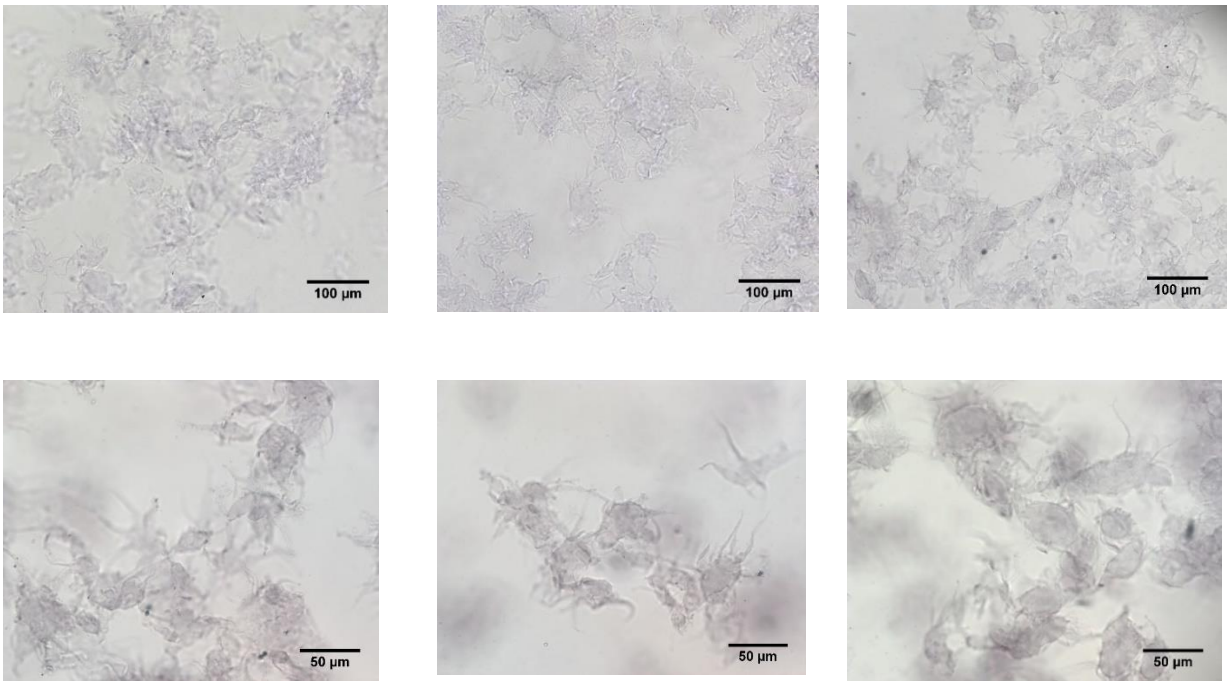


*Fig. A32. Microscopy images of 0.5 wt% agarose fluid gel particles stained with toluidine blue. The sample was prepared using cone-plate geometry at a constant shear rate of 400 $s^{-1}$, cooled from 85 °C to 25 °C at 1 K/min, and held at 25 °C for 15 min.*

(a) (b)

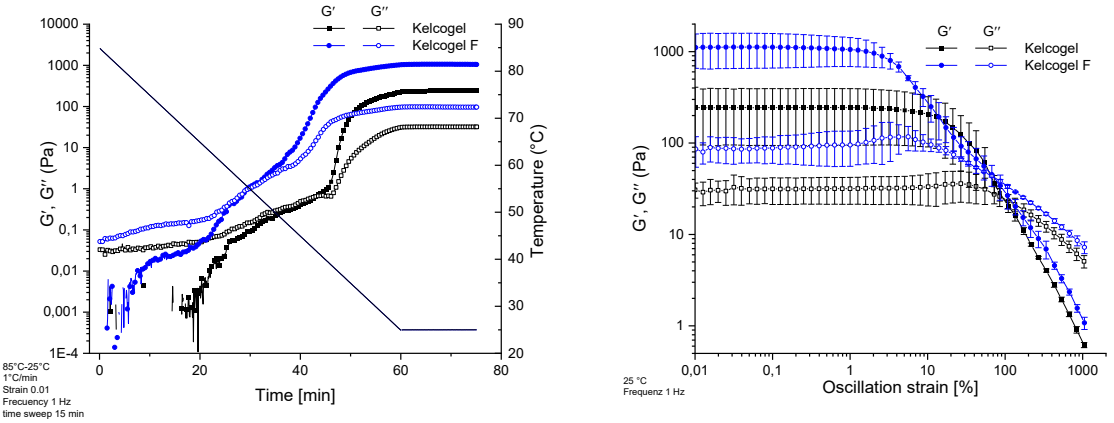


*Fig. A33. (a)Temperature dependent oscillation measurements for different types of 1 wt% gellan gum, anegative charged polysaccharide. High-acyl gellan gum (Kelgo) forms soft, elastic gels, whereas low-acyl gellan gum (Kelgo F) forms firm and brittle gel. The gellan gum solutions, in their heated sol state, were cooled from 85°C to 25 °C at a rate of 1 K/min under constant strain (γ= 0.01%), followed by a time sweep for 15 min. (b) Amplitude sweeps were subsequent performed on the same samples at a constant frequency (f = 1 Hz) and temperature (T = 25 °C).*

(a) (b)

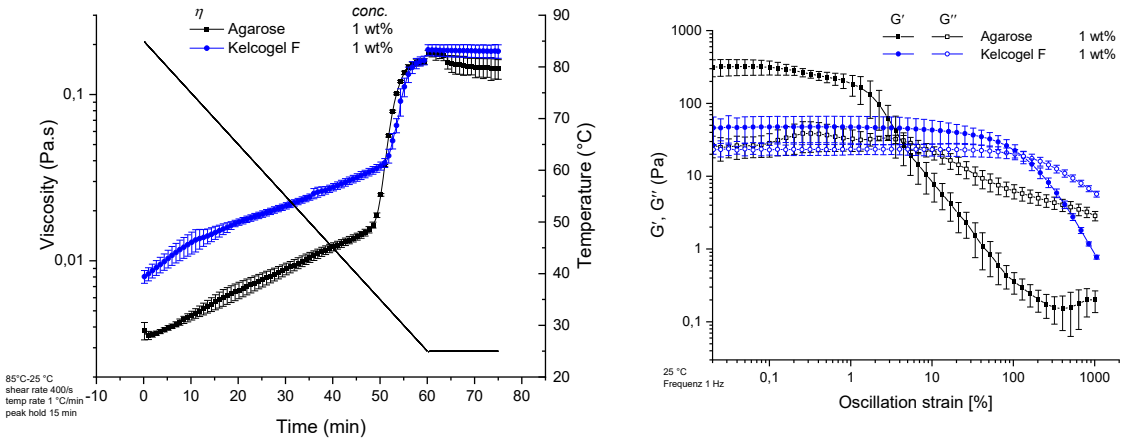


*Fig. A34. (a) Gelation under shear using parallel-plate geometry. Viscosity profiles of 1 wt% agarose and 1 wt% low-acyl gellan gum (Kelgogel F) fluid gels produced under an applied shear rate of 400 $s^{-1}$. The samples were subjected to a constant shear rate while cooling from 85 °C to 25 °C at 1 K/min, followed by 15 min holding at 25 °C. Higher viscosity curve can be observed for low-acyl gellan at higher temperatures until the sharp increase in viscosity, indicating the gelation temperature of the polysaccharide. (b) Amplitude sweep test of the corresponding fluid gels (measured in the same geometry used during fluid gel production) at constant frequency (f = 1 Hz) and temperature (T = 25 °C), showing higher storage (G′) and loss (G″) moduli for agarose fluid gel.*

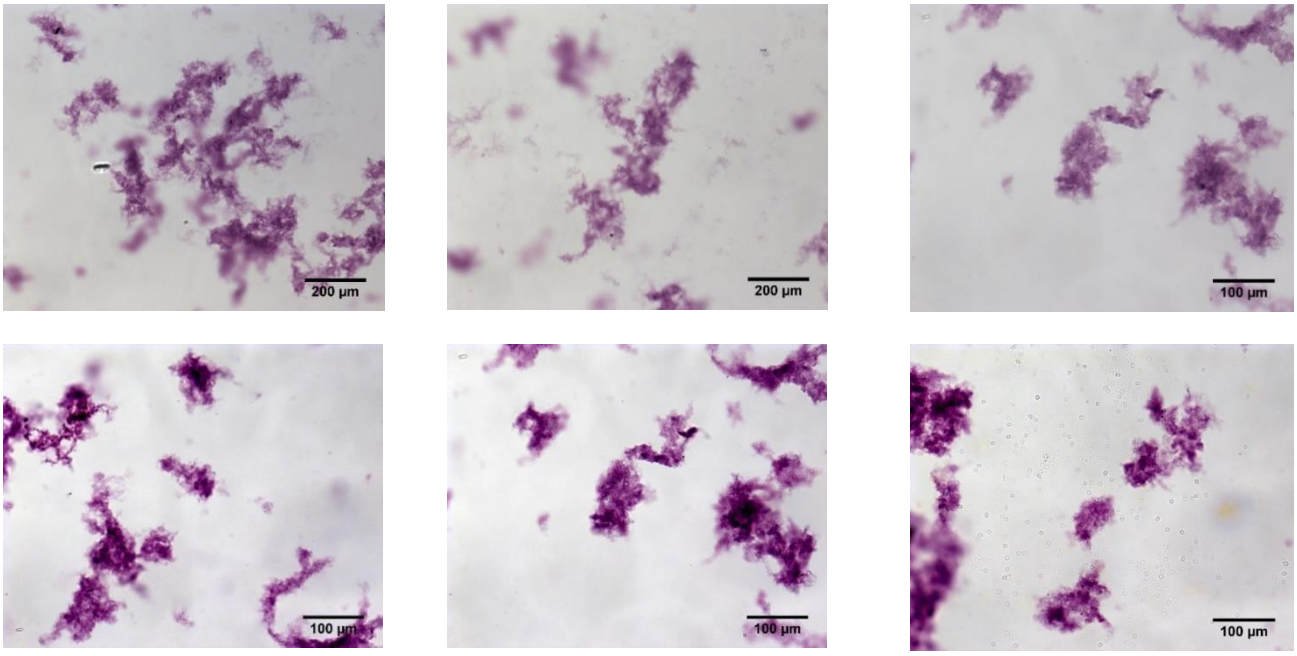


*Fig. A35. Microscopy images of 1 wt% low-acyl gellan gum (Kelgogel F) fluid gel particles stained with toluidine blue. The sample was prepared using parallel-plate geometry at a constant shear rate of 400 $s^{-1}$, cooled from 85 °C to 25 °C at 1 K/min, and held at 25 °C for 15 min.*